2021

Quantifying the Impacts of Land Use, Management and Climate Change on Water Resources in Missouri River Basin

Arun Bawa
South Dakota State University

QUANTIFYING THE IMPACTS OF LAND USE, MANAGEMENT AND CLIMATE

CHANGE ON WATER RESOURCES IN MISSOURI RIVER BASIN

BY

ARUN BAWA

A dissertation submitted in partial fulfillment of the requirements for the

Doctor of Philosophy

Major in Agricultural, Biosystems and Mechanical Engineering

South Dakota State University

2021

DISSERTATION ACCEPTANCE PAGE

Arun Bawa

This dissertation is approved as a creditable and independent investigation by a candidate

for the Doctor of Philosophy degree and is acceptable for meeting the dissertation

requirements for this degree. Acceptance of this does not imply that the conclusions

reached by the candidate are necessarily the conclusions of the major department.

Sandeep Kumar
Advisor   Date

Van Kelley
Department Head   Date

Nicole Lounsbery, PhD
Director, Graduate School   Date

ACKNOWLEDGEMENTS

I dedicate this research to the love and support of my family throughout my pursuit of this degree. A tremendous amount of respect and gratitude to my father: Lakhvinder Dass for his support and continuous guidance in life, to my loving mother: Ravinder Kaur for her enduring counsel and reassurance, to my sister: Chanchal Bawa, brother: Harsh Bawa, and grandfather: Late Resham Dass for always keeping my spirits up as I composed my dissertation. I also thank my friends, Jagmeet Singh, Bhupinder S. Gill, Amit Arora, Kanwaljot Singh, Tarun Bansal, Nitesh Godara, Anquish Kumar, Amandeep Kamboj, Ajay Gupta, Benjamin Brockmueller, Debankur Sanyal, Palavi, Abhinav Sharma, Dilkaran Singh, Teerath S. Rai, Mahtab, and Ruchika for never-ending support and encouragement.

Place: Brookings, SD   (Arun Bawa)

Date: March 26, 2021

TABLE OF CONTENTS

ABBREVIATIONS

r^2	coefficient of determination
CC	cover crop
GCM	general circulation model
ICL	integrated crop-livestock systems
NCC	no cover crop
RCP	representative concentration pathway
RMSE	root mean square error
SHS	soil health score
SOM	soil organic matter
SSEBop	Operational Simplified Surface Energy Balance
SWAT	Soil and Water Assessment Tool
T_c	cold temperature
T_h	hot temperature
TN	total nitrogen
TP	total phosphorous
T_s	land surface temperature
WBET	water balance evapotranspiration
WEOC	water-extractable organic carbon
WEON	water-extractable organic nitrogen
WETC	water-extractable total carbon
WETN	water-extractable total nitrogen
WQ	water quality

LIST OF FIGURES

LIST OF TABLES

ABSTRACT

QUANTIFYING THE IMPACTS OF LAND USE, MANAGEMENT AND CLIMATE
CHANGE ON WATER RESOURCES IN MISSOURI RIVER BASIN
ARUN BAWA

2021

A location-specific evaluation of hydrological landscape responses concerning past and

projected climate and land use land cover (LULC) changes can provide a powerful

intellectual basis for developing efficient and profitable agroecosystems, and overcoming

uncertain and detrimental consequences of LULC and climate shifts. This dissertation

assessed the impacts of land use, management, and climate change on water resources in

the Missouri River Basin (MRB) through four specific studies that included: (i) to study

the responses of leached nutrient concentrations and soil health to winter rye cover crop

(CC) under no-till corn (*Zea mays* L.)-soybean [*Glycine max* (L.) Merr.] rotation, (ii) to

simulate hydrological responses of integrated crop-livestock (ICL) system under

projected climate changes in an agricultural watershed, (iii) to evaluate the hydrological

landscape responses in relation to past (1986-2018) LULC and climate shifts across

South Dakota (SD), and (iv) to evaluate the hydrological landscape responses in relation

to past (1986-2018) LULC and climate shifts across MRB.

Cover cropping has been promoted for the ecological agricultural intensification,

however, the vulnerability of CC establishment and expected soil health and water

quality benefits under short and cold growing periods for CC are of concerns among

producers in the northern Great Plains (NGP) region. Thus, a field experiment from 2017

to 2020 was conducted to assess the impacts of winter rye (*Secale cereale* L.) CC on soil

health and water quality parameters under a no-till corn-soybean rotation at Southeast

Research Farm (SERF), Beresford, SD. Interestingly, the study site faced one dry (2020) and two abnormally wet (2018 and 2019) years which received 31% lower (2020), and 31% (2018) and 23% (2019) higher precipitation, respectively, than the annual average (1953-2019). Data showed that biomass of the rye CC was 251 kg ha^{-1} in 2018, 1213 kg ha^{-1} in 2019, and 147 kg ha^{-1} in 2020, coinciding with contrasting growing degree days i.e., 1458, 2042, 794, respectively, as a consequence of variable weather conditions. Cover cropping did not impact water quality for the majority of the study period. However, a significant reduction in leached nitrate (~19-20%) and total nitrogen (TN) (~8.5-16%) concentrations were found only in 2019, pertaining to sequestered 18.8 kg N ha^{-1}. Rye CC showed 13 and 11% significantly higher microbially active carbon and water-extractable organic nitrogen, respectively, than the control (No CC) treatment. The non-significant impacts on soil health indicators due to winter rye showed that study duration (3 years) may not be sufficient to see the beneficial impacts of cover crop on soils. However, significant reductions in leached nitrate and TN concentrations for one (2019) out of three study years suggest that well-established rye CC (biomass = 1213 kg ha^{-1}; which was 4.8 and 8.3 times higher than that in 2018 and 2020) has the potential of reducing nutrient leaching and enhancing soil health for the study region.

The ICL systems, when well managed properly, have beneficial impacts on soils and water yield, however, very limited studies are available due to the complexity of these integrated systems. Thus, a simulation study was conducted to assess the hydrological impacts of long-term implementation of ICL systems at watershed scale with the projected climate scenarios on water yield using the Soil and Water Assessment Tool (SWAT) model over two time periods [i.e. Near Future (2021-2050) and Far Future

(2070-2099)]. This study was conducted in three phases over Skunk Creek Watershed (SCW), SD, USA. In phase I, the impact of long-term ICL system implementation (1976-2005; 30 years) on soil hydrology was evaluated. Phase II and phase III evaluated the impacts of projected climate changes under existing land cover and ICL system, respectively. Outcomes of phase I showed a significant decrease in water yield and surface runoff. Phase II showed the susceptibility of SCW to extreme events such as floods and waterlogging during spring, and droughts during summers under the projected climate changes. Phase III showed the reduction in water yield and surface runoff due to the ICL system and minimizing the induced detrimental impacts only due to climate change.

Evapotranspiration (ET) plays a significant role in crop growth and development, therefore, an accurate estimation of ET is very important for water use and availability. The past hydrological landscape responses were studied using well-validated ($r^2 = 0.91$, PBIAS= -4%, and %RMSE = 11.8%) actual evapotranspiration (ETa) time-series (1986-2018) estimations. The developed ETa products were further used to understand the crop water-use (CWU) characteristics and existing historic mono-directional (increasing or decreasing) trends across the SD and MRB regions. Spatial variability of the Operational Simplified Surface Energy Balance (SSEBop) model- and Landsat-based ETa estimations showed strong correspondence with land cover and climate across the basin. The drier foothills in northwestern MRB, dominated by grassland/shrubland, showed lower ETa (< 400 mm/year), whereas, cropland dominated regions in lower semi-humid MRB and forested headwater exhibited higher ETa (> 500 mm/year). For the SD region, Mann Kendall trend analysis revealed an absence of a significant trend in annual CWU at a

regional scale due to the combined impact of varying weather conditions, and the presence of both increasing (12%) and decreasing (9%) CWU trends over a substantial portion at the pixel-scale. Whereas, for the MRB, summer season CWU trend analysis revealed a significant increasing trend at the regional-scale with 30% MRB cropland pixels under a significant increasing trend at pixel-scale. The existing increasing trends can be explained by the shift in agricultural practices, increased irrigated cropland area, higher productions, moisture regime shifts, and decreased risk of farming in the dry areas. Moreover, the decreasing trend pixels could be the result of the dynamic conversion of wetlands to croplands, decreased and improved irrigation and water management practices in the region. Overall, both studies highlight the potential of Landsat imagery and remote sensing-based ETa modeling approaches in generating historical time-series ETa maps over a wide range of elevation, vegetation, and climate.

CHAPTER 1

INTRODUCTION

Land use land cover (LULC) and climate impact water resources. The LULC and

climate are the major drivers and determinant factors for global energy and hydrological

processes. The synergistic impacts of both can significantly affect hydrology, water

resources, and agriculture (Choi 2008). Recent studies suggest that the intense LULC and

climate changes influence local, regional, and global environment (Sleeter et al. 2013;

Jha, Gassman, and Panagopoulos 2015) and ecosystem services (DeFries, Foley, and

Asner 2004; Huntington et al. 2009). For example, increased atmospheric water demands

and warmer surface temperature due to more available heat in the atmosphere can result

in decreased soil moisture that increases the probability of drought conditions (Burkett et

al. 2013). Scientists have predicted an increase in heat waves, heavy precipitation, and

stress over water resources in semiarid regions of North America (IPCC 2007).

Freshwater ecosystems are vital for a nation's socioeconomic status, environmental

sustainability, quality of life, and public health (Murdoch, Baron, and Miller 2000).

Missouri River Basin (MRB) is an important global food-producing region, which

is responsible for approximately half of the nation's wheat production (Wise et al. 2018;

Mehta, Rosenberg, and Mendoza 2011). Water resources of the MRB are vulnerable to

variable climate, water demand (high consumptive demand or low supply), groundwater,

and streamflow (Gleick and Waggoner 1990). The recurring droughts and floods

fluctuate the vulnerability of the basin and are of concern for the MRB (Mehta,

Rosenberg, and Mendoza 2011). The vulnerability of the basin and recurring long

drought periods (1950s, 1980s, 2002-2006) in the MRB has caused tension between

upstream and downstream users, and between senior and junior water rights in the past (Mehta, Rosenberg, and Mendoza 2011). These tensions seem to be intensified under the projected climate and LULC scenarios. The decreased precipitation and streamflow during the summer months (Qiao et al. 2014), earlier snowmelt due to the increased spring temperature (Barnhart et al. 2016), and agricultural intensification (Claassen 2011) will further escalate the tension between the MRB water users and may be detrimental to agricultural production.

The LULC and climate changes pose direct challenges for natural resources, including water and soil at local and regional levels (Terando et al. 2020; Burkett et al. 2013). Researchers are promoting ecological agricultural intensification considering future food security goals to overcome uncertain and detrimental consequences of LULC and climate shifts. A recent focus is on the adoption of conservation practices and increased agricultural diversification (Singh 2020; McDaniel, Tiemann, and Grandy 2014) to guide LULC changes, driven by climate changes, toward sustainable agricultural development. Cover cropping (Brockmueller 2020) and integrated crop-livestock (ICL) (Pérez-Gutiérrez and Kumar 2019) practices are among the most promoted and adopted conservation practices in the Midwest and northern Great Plains (NGP) regions. Cover crops (CC) are promoted to enhance soil health which in turn increases the water storage and improves the resilience to droughts, floods, and extreme weather conditions (Basche and DeLonge 2017; McDaniel, Tiemann, and Grandy 2014). Cover cropping is also widely addressed for removing residual nutrients from the soil profile by increasing the uptake demands during the off-season (Strock, Porter, and Russelle 2004) and reducing detrimental impacts of adopting subsurface drainage management practices (Drury et al.

2014). The ICL systems are also widely adopted environmentally favorable alternatives to the traditional cropping systems of the Midwest and NGP regions (Pérez-Gutiérrez and Kumar 2019). Cover cropping and ICL play a considerable role in enhancing soil health indicators such as organic matter, nutrient cycling, reduced runoff and higher water infiltration (Pérez-Gutiérrez and Kumar 2019; Sulc and Tracy 2007; Basche and DeLonge 2017). Increased soil organic matter and soil health can improve the efficiency of N and P nutrients cycling and lower the eutrophication of aquatic ecosystems (Zimnicki et al. 2020). Faust et al. (2018) studied the influences of ICL systems under 30-min rainfall simulation on water quality, and observed significant alteration in nutrient concentrations in generated surface runoff. Constantin et al. (2010) studied the long-term impact of adopting cover crop, no-till, and reduced nitrogen fertilization on leached N concentrations and found cover crop as the most efficient and long-term effective practive to reduce N leaching by 36 to 62%. Although a growing body of research highlights the agricultural, environmental, and economic benefits of cover cropping and ICL systems, however, there are limited studies conducted in MRB to highlight the benefits of these conservation practices on soil health and water quantity and quality. Hence, further research is required for a better understanding of location-specific interactions among LULC, climate, and hydrological responses that can lead to the sustainable and effective management of water resources. These interactions are of utmost important to stakeholders, watershed managers, and policymakers to better identify where these conservation practices can be implemented to preserve water quantity and quality and other associated ecosystem services.

Predicting future changes in hydrological responses and influences on the quantity and quality of water resources due to climate and LULC shifts require the development and application of hydrological models (Burkett et al. 2013). Future scenario-based models can provide a representative dataset and interpretive framework for assessing potential impacts of changes in population, land use, climate, and management practices on future water availability. The availability of simulation models such as the Soil and Water Assessment Tool (SWAT) has provided a platform to study the relative response of the hydrologic system (for example, infiltration, runoff, and water yield) to specific land covers while incorporating projected climate scenarios.

While studying the influences of future climate scenarios is critical to the success of ecological intensification of agriculture, exploring hydrological landscape responses concerning past climate and LULC changes provide a powerful intellectual basis for developing efficient and profitable agroecosystems. An evaluation of past hydrological responses to changing LULC and climate can assist in distinguishing natural and human influences on water resources. A review of historical landscape responses such as evapotranspiration (ET) along with existing trends provides a decision support toolkit for planning water management, water rights, and water resource allocation and minimizing the basin/watershed water supply vulnerability during extreme events (Senay et al. 2017). The moderate spatial resolution (30 m) and available relatively long record of Landsat images in combination with ET models such as the Operational Simplified Surface Energy Balance model (SSEBop) provide an upper edge to study the historical water use dynamics at field scale and to update the historical water use records. An evaluation of past and future hydrological responses under changing LULC and climate

in conjunction with conservation practices-associated concerns is required for an
ecological nature of future changes. While modeling frameworks can help in an
intellectual basis for past, present, and future interactions among LULC, climate, and
hydrological processes, the field studies assist in developing fundamental knowledge and
capturing the crucial elements of the vulnerability of conservation practices.

The increased knowledge of rapid and unpredictable global change has generated a
growing demand for information about the essence of forthcoming changes and how to
respond effectively among the public, policymakers, and resource managers (Burkett et
al. 2013). There is also a consensus about the integration of landscape- and regional-level
partnerships of science and management to diminish future detrimental environmental
changes.

Study Objectives

The goal of this research was to quantify the impacts of land use, management, and
climate change on water resources in the Missouri River Basin. The study objectives
were achieved using field-trial as well as modeling frameworks. This dissertation
evaluated several indicators across various spatial and temporal scales through the
following mentioned studies:

Study 1. The study was entitled "Responses of leached nutrient concentrations and soil
health to winter rye cover crop under no-till corn-soybean rotation". The
specific objectives of the study are to (i) assess the impacts of winter rye CC
and NCC on soil health indicators (e.g, soil organic matter, soil respiration,
water-extractable total nitrogen, water-extractable organic nitrogen, water-
extractable total carbon, nitrate, ammonium, inorganic nitrogen, total

phosphorus, inorganic phosphorus, microbially active carbon, soil health score, and plant available nutrients) parameters, and (ii) assess the impacts of winter rye CC on water quality parameters (e.g., nitrate-N, ammonia-N, and total nitrogen).

Study 2. The study was entitled "Simulating hydrological responses of integrated crop-livestock systems under future climate changes in an agricultural watershed" with the specific objective is to analyze the potential impacts of long-term usage of ICL systems under future climate scenarios on water yield and its hydrological components (i.e., surface runoff, lateral flow) along with evapotranspiration using the Soil and Water Assessment Tool (SWAT).

Study 3. The study was entitled "Regional crop water use assessment using Landsat-derived evapotranspiration across South Dakota" with the specific objective is to characterize annual crop water-use dynamics and trends across the eastern and western regions of SD using Landsat imagery and SSEBop model-derived ETa estimations from 1986-2018 (33 years).

Study 4. The study was entitled "Landsat-derived evapotranspiration for long-term (1986-2018) crop water use assessment across the Missouri River Basin" with the specific objective is to quantify and characterize historical (1986-2018; 33 years) summer season crop water-use (CWU-Su) dynamics and CWU-Su trends across the Missouri River Basin.

All four studies were written independently in the format of journal manuscripts for publication purposes. To date, Study 2 is published in *Journal of American Water Resources Association (JAWRA)* and Study 3 is published in *Hydrological Processes*.

References

Barnhart, T. B., Molotch, N. P., Livneh, B., Harpold, A. A., Knowles, J. F., & Schneider, D. (2016). Snowmelt rate dictates streamflow. Geophysical Research Letters, 43(15), 8006-8016.

Basche, A., & DeLonge, M. (2017). The impact of continuous living cover on soil hydrologic properties: A meta-analysis. Soil Science Society of America Journal, 81(5), 1179-1190.

Brockmueller, B. (2020). Management implications of a rye cover crop on nutrient cycling and soybean production in southeast South Dakota: Focus on rye seeding rates and termination timing. Electronic Theses and Dissertations. 4094. https://openprairie.sdstate.edu/etd/4094.

Burkett, V., Kirtland, D. A., Taylor, I. L., Belnap, J., Cronin, T. M., Dettinger, M. D., . . . Milly, P. C. (2013). U.S. Geological Survey Climate and Land Use Change Science Strategy--a Framework for Understanding and Responding to Global Change: US Department of the Interior, U.S. Geological Survey Circular 1383–A, 43 p.

Choi, W. (2008). Catchment-scale hydrological response to climate-land-use combined scenarios: A case study for the Kishwaukee River Basin, Illinois. Physical Geography, 29(1), 79-99.

Claassen, R. L. (2011). Grassland to cropland conversion in the Northern Plains: the role of crop insurance, commodity, and disaster programs (No. 120): *DIANE Publishing*.

DeFries, R. S., Foley, J. A., & Asner, G. P. (2004). Land-use choices: Balancing human needs and ecosystem function. Frontiers in Ecology and the Environment, 2(5), 249-257.

Drury, C., Tan, C., Welacky, T., Reynolds, W., Zhang, T., Oloya, T., . . . Gaynor, J. (2014). Reducing nitrate loss in tile drainage water with cover crops and water-table management systems. Journal of Environmental Quality, 43(2), 587-598.

Gleick, P. H., & Waggoner, P. E. (1990). Climate Change and US Water Resources. Vulnerability of Water Systems, PE Waggoner (Editor). *Wiley Interscience*, New York, 223-240.

Huntington, T. G., Richardson, A. D., McGuire, K. J., & Hayhoe, K. (2009). Climate and hydrological changes in the northeastern United States: recent trends and implications for forested and aquatic ecosystems. Canadian Journal of Forest Research, 39(2), 199-212.

Jha, M. K., Gassman, P. W., & Panagopoulos, Y. (2015). Regional changes in nitrate loadings in the Upper Mississippi River Basin under predicted mid-century climate. Regional Environmental Change, 15(3), 449-460.

McDaniel, M., Tiemann, L., & Grandy, A. (2014). Does agricultural crop diversity enhance soil microbial biomass and organic matter dynamics? A meta-analysis. Ecological Applications, 24(3), 560-570.

Mehta, V. M., Rosenberg, N. J., & Mendoza, K. (2011). Simulated Impacts of Three Decadal Climate Variability Phenomena on Water Yields in the Missouri River Basin 1. JAWRA Journal of the American Water Resources Association, 47(1), 126-135.

Murdoch, P. S., Baron, J. S., & Miller, T. L. (2000). Potential effects of climate change on surface-water quality in North America 1. JAWRA Journal of the American Water Resources Association, 36(2), 347-366.

Pérez-Gutiérrez, J. D., & Kumar, S. (2019). Simulating the influence of integrated crop-livestock systems on water yield at watershed scale. Journal of environmental management, 239, 385-394.

Qiao, L., Pan, Z., Herrmann, R. B., & Hong, Y. (2014). Hydrological variability and uncertainty of lower Missouri River basin under changing climate. JAWRA Journal of the American Water Resources Association, 50(1), 246-260.

Senay, G. B., Schauer, M., Friedrichs, M., Velpuri, N. M., & Singh, R. K. (2017). Satellite-based water use dynamics using historical Landsat data (1984–2014) in the southwestern United States. Remote Sensing of Environment, 202, 98-112.

Singh, J. (2020). Crop rotations, tillage and cover crops influences on soil health, greenhouse gas emissions and farm profitability. Electronic Theses and Dissertations. 4084. https://openprairie.sdstate.edu/etd/4084.

Sleeter, B. M., Sohl, T. L., Loveland, T. R., Auch, R. F., Acevedo, W., Drummond, M. A., . . . Stehman, S. V. (2013). Land-cover change in the conterminous United States from 1973 to 2000. Global Environmental Change, 23(4), 733-748.

Strock, J. S., Porter, P. M., & Russelle, M. (2004). Cover cropping to reduce nitrate loss through subsurface drainage in the northern US Corn Belt. Journal of Environmental Quality, 33(3), 1010-1016.

Sulc, R. M., & Tracy, B. F. (2007). I ntegrated Crop–Livestock Systems in the U.S. Corn Belt. Agronomy Journal, 99: 335-345. https://doi.org/10.2134/agronj2006.0086.

Terando, A., Reidmiller, D., Hostetler, S. W., Littell, J. S., Beard Jr, T. D., Weiskopf, S. R., . . . Plumlee, G. S. (2020). Using Information from Global Climate Models to Inform Policymaking: The Role of the US Geological Survey: US Department of the Interior, US Geological Survey.

Wise, E. K., Woodhouse, C. A., McCabe, G. J., Pederson, G. T., & St-Jacques, J.-M. (2018). Hydroclimatology of the Missouri River Basin. Journal of Hydrometeorology, 19(1), 161-182.

CHAPTER 2

LITERATURE REVIEW

2.1.   Land-use Change Impacts on Hydrology and Water Quality

Land use land cover (LULC) change is defined by Verma et al. (2020) as "*a change in certain continuous characteristics of the land such as vegetation type, soil properties, and so on, whereas land-use change consists of an alteration in the way certain area of land is being used or managed by humans*". Many anthropogenic and natural causes, dating back a century or more, have changed land management practices. The LULC and changes in farmland management that occurred as a result of the Dust Bowl are the biggest examples of natural causes. The economic impacts, fatalities, soil erosion, dust storms, personal hardships, and distress migration due to the multi-drought years of the 1930s triggered farmland management practices and governmental policies focusing on adopting soil conservation, improved tillage technologies, and advanced irrigation practices (McLeman et al., 2014). Increased demand for food supply with increasing population can amplify LULC changes. The LULC change influences the hydrologic system involving alternations in water infiltration, interception, soil storage, and evapotranspiration which lead to changes in surface runoff and streamflow impacting both drought and flood frequencies (Legesse et al., 2003; Paul, 2016; Zhang and Schilling, 2006). Understanding the LULC impacts on regional hydrologic cycles of various spatial and temporal scales is vital to the management of land use, water resources, and sustainable socio-economical development. For example, intensification and expansion of farming to meet future food demands require sufficient water supplies to ensure the survival of crops and livestock (McNeill et al., 2017), which in turn, could

increase stress over water resources. The LULC impacts on hydrology and water quality

have been mentioned below in different headings:

2.1.1. Evapotranspiration

Evapotranspiration (ET), groundwater recharge, and runoff are the most affected

hydrological processes by LULC (Batelaan et al., 2003). Senay et al. (2019a) defined ET

as "*the hydrological process that converts liquid water on the soil-vegetative surface into

atmospheric vapor*". The ET involves the soil-plant-atmosphere interaction (Senay et al.,

2017) and is a combination of two processes, namely evaporation and transpiration. The

evaporation component includes water losses from the surface of plants and soil,

whereas, transpiration includes water losses through the plant stomata. Therefore, ET is

heavily influenced by land characteristics. Different land cover converts water into

atmospheric vapors at different ET change rates. Land cover density controls leaf area

index, canopy resistance, and precipitation interception. For example, perennial grassland

provides dense vegetation and a higher leaf area index than the cropland and executes

higher ET. Similar results were observed for Midwestern USA (Schilling et al., 2008)

where ET decreased due to the agricultural shift from mixed perennial and annual

cropping systems to primarily annual crops. In a study over 5 river basins of India, Das et

al. (2018) found LAI as the most sensitive parameter to alter water balance among the

other vegetation parameters. The study also observed a decreased canopy cover for

transpiration and interception governed by deforestation, urbanization, and cropland

expansions that in turn contributed to decreased ET. Bawa et al. (2021b) also reported an

increase in annual ET in South Dakota, USA due to the shift of agricultural practices

from low biomass crops to high biomass crops. Forested areas generally provide low

albedo, deep roots, and permanent covers that promote ET. Baker and Miller (2013) simulated the hydrological responses under 17 years of LULC changes and observed reductions in average annual ET due to a decrease in forested areas. Urbanization reduces transpiration but could increase evaporation. Many studies (e.g., Rose and Peters, 2001; Roy et al., 2009) related the urban expansion with a decreased ET in the study watersheds.

2.1.2. Soil Moisture and Groundwater

The LULC is a catchment phenomenon that greatly influences the hydrological processes (Das et al., 2018). Even after the potential scale of LULC impacts on subsurface components (soil moisture and groundwater), these impacts are not well recognized (Scanlon et al., 2005). Previous studies (e.g., Defries et al., 2002; Lawrence et al., 2010; Seneviratne et al., 2010) highlighted concerns about the consequences of LULC changes on hydrological cycles involving groundwater depletion, soil moisture alterations, streamflow alteration, and flood intensification. Soil moisture is a controlling variable for plant transpiration and photosynthesis (Seneviratne et al., 2010). Therefore, land characteristics influence soil moisture and are important to understand to conserve soil moisture and increase groundwater recharge. Producers around the globe are adopting different conservation practices such as no-till (Lahmar, 2010), crop diversity (Hobbs et al., 2008), and cover crops (Dinnes et al., 2002) to conserve soil moisture and increase soil moisture-holding capacities.

Land cover and soil hydrologic property determine the partitioning of precipitation into the surface runoff, infiltration, soil water holding capacity, and groundwater recharge. Land cover can significantly alter precipitation partitioning affecting soil

moisture and groundwater. The influence of vegetative cover on soil moisture contents is questionable (Chen et al., 2009). For example, on one hand, vegetation cover can lower soil moisture losses through transpiration and rainfall interception (Bublinec, 1971), whereas, on the other hand, shading of vegetation cover can also reduce the evaporation loss (Tallaksen, 1993). Scanlon et al. (2005) discussed vegetation as one of the controlling parameters for soil water and groundwater recharge. Changing the vegetation type alters key vegetation parameters that influence soil moisture and recharge such as wilting point, transpiration rate, root depth, and fractional canopy coverage. Natural rangeland vegetation has a low matric potential (Smith et al., 2012). Changing natural rangeland to a higher matric potential agricultural land could increase the groundwater recharge (Scanlon et al., 2005). Conversion of rangeland to agricultural land with increased surface irrigation practices enhances the amount of water to the system subsequently increasing groundwater recharge (Roark, 1998). While reducing vegetation cover to zero, fallow systems have the potential to increase groundwater recharge as observed in the Northern Great Plains, USA (Miller et al., 1981). Reduced percolation, baseflow (Nie et al., 2011), and groundwater recharge (Jobbágy and Jackson, 2004) were observed by replacing shallow-rooted grasses with deep-rooted woodlands and trees. Locatelli and Vignola (2009) demonstrated changes in groundwater recharge due to reduced baseflow resulting from forestation in sub-tropical environments.

2.1.3. Surface Runoff and Water Yield

The LULC changes are often linked with alteration in the quantity and quality of water resources (Giri and Qiu, 2016). From the hydrological perspective, the LULC changes can have a profound effect on watershed hydrology by changing soil

characteristics, vegetation cover, and surface roughness which subsequently alter runoff and water yield. The LULC changes are well recognized as one of the critical factors changing runoff and streamflow characteristics (Chang, 2007). Runoff characteristics involve the timing and magnitude of the surface runoff. Changes in the timing of surface runoff not only alter the magnitude of floods but also impact flooding frequency. Water yield alteration includes the combined impact of surface runoff and lateral flow. The above discussed LULC impacts on infiltration, percolation, and groundwater recharge affect the lateral flow. Therefore, LULC changes are indirectly linked to the water yield alterations. The LULC impact for surface runoff can also be explained by the changes in precipitation partitioning. Higher losses through ET under a forested area with permanent cover could reduce surface runoff, whereas, decreased or zero infiltration under impervious covers can increase surface runoff. Considerable deforestation leads to reduced ET due to reduced leaf area index and rooting depths, which in turn, amplify surface runoff (Calder, 1992; Das et al., 2018). Baker and Miller (2013) stated that the "*conversion of natural landscapes for agricultural and urban uses often influences soil integrity, nutrient fluxes, and native species assemblages*". Such changes lead to alterations in hydrology by changing the interception rates, infiltration rates, ET, and groundwater recharge, leading to changes in surface runoff characteristics. Ahiablame et al. (2017a) observed the changes in baseflow due to decreased grassland and increased agricultural land in the Missouri River basin. Baker and Miller (2013) observed an increase in surface runoff and a decrease in groundwater recharge, resulting from the conversion of the forested area into an agricultural area.

2.1.4. Water Quality

Land cover plays a vital role in the generation of water pollution (Giri and Qiu, 2016). Increased population has triggered the LULC changes primarily due to housing and food. The LULC changes modify the flow behavior of the landscape that may alter the water quality. Increased impervious surface/urbanization increases surface runoff which provides an additional pathway for transportation of pollution from landscape to waterbodies (Wilson and Weng, 2010). The conversion of the natural landscape to agricultural land can increase non-point source pollution. Grassland conversion to agricultural land increases agricultural activities such as fertilization, manure, pesticide, and herbicide applications, that are carried through runoff and pollute the nearby surface-/ground-water resources. Changing land cover (such as crop diversification and cover cropping) is also adopted and promoted in the agricultural system to control water pollution. For example, changing the fallow system during the non-growing season by adopting cover crops has reduced the agricultural nutrient and sediment loads to water bodies in the northern Great Plains ecoregions of North America (Faust et al., 2018; Faust et al., 2020).

2.2. Climate Change Impacts on Hydrology and Water Quality

Climate is another major factor affecting the hydrological responses of the landscape. Climate shifts often amplify the hydrological impacts of LULC changes (Ahiablame et al., 2017a). Changes in natural systems are the strongest and the most comprehensive pieces of evidence of climate change impacts. A global temperature increase may lead to the intensification of the hydrological cycle by changing precipitation amounts, evapotranspiration rates, and snowmelt periods (Stagl et al., 2014;

Van Vliet and Zwolsman, 2008). Many studies (e.g., Field, 2014; Xu et al., 2013) highlighted the growing concerns of potential adverse impacts of global climate and LULC changes on water resources. Climatic changes are often linked to declining biodiversity (Gregory et al., 2009), influences in hydrology and water resources (Clifton et al., 2018; De Wit and Stankiewicz, 2006), and other ecosystem damages (Walther et al., 2002). Observed past climate changes revealed an increase in the frequency of extreme events since the early 20th century (NOAA, 2016), characterized by an increase in temperature, precipitation, and atmospheric greenhouse gas concentrations (Huntington et al., 2009). Huang et al. (2015) studied the impacts of changing climate on floods and droughts in Germany and observed more significant changes in hydrological extreme events deviating from the mean conditions. Altered precipitation can cause variations in surface runoff, magnitude and timing of water yield and floods (Clifton et al., 2018) that in turn will affect vegetation (Adams et al., 2012) and water supply (Vose et al., 2016). Whereas, a warmer climate can trigger the chain reaction in the hydrological cycle by altering ET and directly affecting the regional natural ecosystems, agriculture, and water resources (Clifton et al., 2018).

According to the Fourth National Climate Assessment report (USGCRP, 2018), the Midwestern USA is becoming more vulnerable to climate change impacts such as drought, floods, and extreme heatwaves. Researchers have conducted many hydro-climatological studies to evaluate the climate change impacts (especially increased air temperatures) on regional hydrological cycles in the Midwest and Great Plains (e.g., Ahiablame et al., 2017b; Changnon and Kunkel, 1995; Chien et al., 2013; Gautam et al., 2018). These studies demonstrated earlier snowmelts and increased annual ET due to

increased spring temperatures caused by changing climate. Early spring snowmelt could cause increased floods during spring in the region. A decreasing trend in projected summer precipitations (USGCRP, 2018) was also observed that could reduce surface runoff and streamflow during summers. Climate change impacts on hydrology are listed below as:

2.2.1. Evapotranspiration

The impacts of climate change on hydrological processes will be intensified under the projected changes during the coming century (IPCC, 2007). Solar radiation and air temperature supply energy required for the ET process. Soil moisture is another controlling factor for the ET process and depends on precipitation amounts. Atmospheric demand is directly related to temperature. Therefore, changes in precipitation amounts and air temperatures can cause variation in the ET amounts. Researchers used various models and developed a relationship between climate and ET: lower annual precipitation with decreased ET (Ficklin et al., 2013; Neupane and Kumar, 2015), increased temperature with elevated atmospheric demands resulting in an increased ET (Bawa et al., 2021b; Ficklin et al., 2013; Senay, 2019), lower temperature and higher humidity with reduced ET in dry seasons (Guo et al., 2008), and increased temperature and precipitation with increased ET (Zhang et al., 2016). The combined impact of temperature and precipitation can amplify or neutralize the ET alterations. For example, temperature increases can augment the atmospheric demand, whereas, decreased precipitation amounts lower the soil moisture availability of evaporation and transpiration (Allen et al., 1998). Ficklin et al. (2013) stated that the increased temperature and

decreased precipitation might result in an overall increase in ET under the projected climate changes in California.

2.2.2. Surface Runoff and Water Yield

Precipitation is the main cause of variability in available water (Novotny and Stefan, 2007). Available water is the remaining amount of precipitated water after ET losses and contribute to surface runoff and water yield (Oki and Kanae, 2006). Changing precipitation and ET losses (via temperature change) can cause variation in available water. Therefore, a changing climate could alter the surface runoff and water yield by altering available water. Climate change affects low and high streamflow. Streamflow sensitivity to temperature was the most pronounced during the summer and fall seasons (DeWalle et al., 2000). DeWalle et al. (2000) reported that an increase in summer temperature reduces the streamflow, while an increase in winter temperature might slightly reduce or increase the streamflow in the Northeast, North-Central, Western, and Southern regions of the United States. They also studied the sensitivity of high and low streamflow conditions to precipitation and reported significant alteration in the streamflow with the variations in precipitation amounts. In this study, high streamflow conditions were found to be sensitive to precipitation while low flow conditions were found to be sensitive to temperature. Similar impacts of climate change on base flow conditions were observed for the water channels in the Missouri River Basin (Ahiablame et al., 2017a).

Climate change influences snowmelt dynamics. Increased temperature affects the timing and rate of snowmelt, leading to changes in snowpack volume (Hamlet et al., 2005), seasonal surface runoff, and streamflow (Hamlet et al., 2013). Ficklin et al. (2013)

observed a shift in the timing of peak streamflow as a consequence of early snowmelt due to the increased spring temperature. Early snowmelt, increased temperature, and decreased summer precipitation could also lead to drier streams in summer (Ficklin et al., 2013; Hay and Todey, 2011). Novotny and Stefan (2007) reported an earlier surface runoff generation from snowmelt at the rate of 0.3 days per year because of increased temperature during 1964-2000 for three river channels in Minnesota. This study also observed an increase in peak flows, a higher number of days with high flow, and an increase in summer and winter baseflow due to increased summer precipitation and more frequent snowmelt events during winters (via increased temperature). Many other studies have also revealed the impact of climate change on streamflow such as increased streamflow in the Wolf Bay watershed (via. increased temperature and precipitation; Wang et al., 2014), decreased annual streamflow in the Mono Lake basin (via. increased temperature; Ficklin et al., 2013), and increased streamflow due to increased precipitation and reduced ET losses (Oki and Kanae, 2006).

2.2.3. Water Quality

As discussed above, modifications in flow behavior of the landscape due to changes in the LULC, climate, or a combined impact of both may alter water quality. Increased precipitation raises surface runoff that in turn increases the transportation of pollution from landscape to waterbodies. For example, increased precipitation in the northwestern Corn Belt resulted in an intensification of subsurface drainage practices (Hay and Todey, 2011). These subsurface drainage practices are the major pathways for agricultural nutrients to leave the field through leaching, thereby impairing the water quality of downstream surface water resources.

2.3. Management Impacts on Hydrology and Water Quality

Management practices include structural and nonstructural practices. Structural management practices include tillage, vegetative filter strips, subsurface drainage practices, whereas, nonstructural practices include such as crop diversification, cover cropping, and legume cropping, integrated crop-livestock systems. The management practices are adopted to improve soil physical, chemical, and biological properties. Changes in soil physical properties lead to the alteration in soil hydrological processes. For example, adopting crop diversification can improve soil pore characteristics and aggregate stability (Alhameid et al., 2020; Bansal et al., 2020), which in turn increases hydraulic conductivity and soil water holding capacity. Subsurface drainage practices are adopted over waterlogged or high water table soils to improve the water drainage process in the soil (Fraser and Fleming, 2001). Adopting conservation tillage such as no-till can alter infiltration, ET, groundwater recharge, and surface runoff (Leduc et al., 2001; Singh, 2020). Pérez-Gutiérrez and Kumar (2019) simulated the hydrological influences of integrated crop-livestock (ICL) systems and observed a decrease in the surface runoff with an increase in lateral flow. Faust et al. (2018) studied water quality influences of ICL systems under 30-min rainfall simulation and observed significant alteration in nutrient concentrations in generated surface runoff. Cover cropping management practices are widely accepted to enhance soil health and water quality. Constantin et al. (2010) studied the long-term impact of adopting cover crop, no-till, and reduced nitrogen fertilization on leached N concentrations and found the cover crop practices as the most efficient and long-term effective method to reduce N leaching by 36 to 62%. In this

section, the impacts of three management practices (subsurface drainage, cover crops,

and ICL systems) on water quality were discussed as follows:

2.3.1. Subsurface Drainage Practices

Excess water and high water table increase the risk of agricultural production in

poorly drained soils. Subsurface drainage removes the excess water from the soil and

promotes deep root growth and prevents the roots from sinking in too much water.

Excess water removal provides the necessary aeration and mineral provision within the

soil profile required for proper crop root growth (Ghane, 2018). The upper Midwest has

an abundance of such highly productive but poorly drained soils. Improved drainage

minimizes soil compaction and supports the conditions for seedbed establishment and

germination due to the warmer temperatures. Excess water removal also benefits the soil

structure by better aeration and microbial activities, improved soil porosity, and better

tilth (Fraser and Fleming 2001).

Subsurface drainage practices have frequently faced controversy. While widely

implemented throughout North America to keep soils free of excess water to ensure

optimal crop growth, the subsurface drainage systems are also a major pathway for

nutrients (especially the dissolved form of nitrogen, N and phosphorus, P) to leave from

the agricultural fields. The increased demand for food, feed, and bioenergy has increased

the use of fertilizers in fields leading to a buildup of residual nutrients in the crop root

zone after the harvest (Drury et al., 2014). Nutrients washed off from the fields reach the

Missouri River and Mississippi river basins downstream river networks, which in turn

enrich the northern Gulf of Mexico's waters. Elevated nutrient levels in the Gulf's waters

contribute to the occurrence of a hypoxic zone that triggers serious and undesirable environmental effects.

Subsurface drainage may have positive impacts on water quality by reducing the surface runoff, peak runoff rate, and reducing the soil erosion from the field. Around 16-65% of sediment loss by water erosion can be reduced by adopting subsurface drainage practices (Zucker and Brown, 1998). The reduction in sediment losses might result in reducing the phosphorous (P) load as well. Sims et al. (1998) reviewed 21 studies related to P concentrations in the subsurface drainage discharge. Most of the studies supported the lower sediment and P losses through subsurface drainage as compared to the surface drainage. However, significant P concentrations were still found to be delivered by the subsurface drainage in dissolved forms. Smith et al. (2015) studied P transportation through the subsurface drain and surface runoff from the Midwestern US to Lake Erie. The study found that 49% of soluble P and 48% of total P losses occurred through the subsurface drainage systems often exceeding the P loading to water resources. As a result, Lake Erie is facing a pervasive problem of algal bloom for the last one and a half-decade. Subsurface drain-related water quality issues are raising environmental concerns and attracting the attention of environmental protection agencies. The negative impacts of subsurface drainage are unavoidable. It is important to couple subsurface drainage practices with the best management practices for an ecologically improved drainage approach.

2.3.2. Cover Cropping

Cover cropping influences many aspects of the hydrological cycle such as ET (Dabney, 1998), water infiltration (Folorunso et al., 1992), runoff (Dabney, 1998), and

soil erosion (Dabney et al., 2001; Liu et al., 2019). Cover crop provides a living ground cover during the off-season (Hartwig and Ammon, 2002) that increases ET and utilizes residual nutrients from the fields. A growing body of research suggests that CCs can contribute to physical, biological, and chemical transformations in soil that in-turn can increase water storage, improve resilience to droughts, floods, and extreme weather conditions (Basche and DeLonge, 2017; McDaniel et al., 2014; Sanyal and Wolthuizen, 2021).

Cover cropping during the winter prior to cash crop planting removes the water and residual nutrients from the soil profile by increasing the uptake demands during the off-season (Strock, Porter, and Russelle 2004). In a meta-analysis of 69 studies across the United States, Tonitto et al. (2006) found that reduction in nitrate leaching due to cover crop was related to its biomass production. This study reported the potential of non-legume CC to accumulate 20 to 60 kg N ha^{-1} post-harvest N uptake and a 40-70% nitrate leaching reduction. However, the benefits of winter cover crops in reducing nutrient leaching and enhancing soil health are limited in the NGP region due to the short and cold growing period of cover crops (Dinnes et al., 2002). Therefore, cold-tolerant species such as winter rye have been suggested by previous studies for the NGP and Corn Belt regions (Christianson et al., 2012; Snapp et al., 2005). Kaspar et al. (2007) examined the effect of rye cover crop nitrate load in tile drainage under a corn-soybean rotation and reported a 48% and 26% reduction in nitrate concentration for corn and soybean, respectively, over the 5-year study period. Drury et al. (2014) observed that CC enhanced the crop yields under a controlled drainage system which reduced the nitrate losses by 47%.

2.3.3. Integrated Crop-Livestock System

Integrated crop-livestock (ICL) systems are being promoted as an eco-friendly and cost-effective production system in the Midwest, USA to replace the traditional production systems such as corn-soybean rotations. Management practices such as grazing can significantly alter soil physical properties (Drewry et al., 2008; Liebig et al., 2014), and hence the soil hydrological characteristics. Grazing livestock can cause soil compaction and increase surface roughness (Clark et al., 2004). Therefore, various factors such as the number and type of animals, grazing period, soil moisture content, and soil texture need to be considered to study the grazing impacts on soil hydraulic properties (Bilotta et al., 2007). Heavy grazing practices could result in soil compaction and increased bulk density. These properties disturb the pore structure of soil and subsequently alter soil hydrological characteristics. In a review study, Sulc and Tracy (2007) summarized the potential effects of introducing diversification in the agricultural systems through grazing operations across the U.S. Corn Belt. They reported that animal traffic compactions and detrimental crop yields can be avoided by restricting the grazing periods to only when soil is dry and frozen. In a simulation study, Pérez-Gutiérrez and Kumar (2019) and Bawa et al. (2021a) found that introducing long-term grazing in a cropping system may improve storage and transit of water in the soil which subsequently can reduce surface runoff and water yield at a watershed scale. Kumar et al. (2010) and Liebig et al. (2014) documented decreased infiltration as a consequence of increased soil compaction under heavy grazing.

2.4. Climate Projection Models

Climate has a profound impact on hydrology. Human-induced climate change is a rising matter of concern (IPCC 2001). The Intergovernmental Panel on Climate Change (IPCC) has presented reports, starting from the 1990s, showing scientific evidence for human-induced climate change. Human-induced climate change research has been well recognized since the 1980s by focusing on the development of numerical General Circulation Models (GCMs). These numerical models are the most readily available and advanced tools representing Earth's climate in response to changing atmospheric composition (Gautam, 2018). The increasing concentration of greenhouse gases (GHGs) in the atmosphere because of anthropogenic activities affects the radiative forces in Earth's environment, which alters temperature and precipitation patterns (Pachauri et al., 2014; Solomon et al., 2007). Depending upon which GHGs emissions and mitigation scenarios are adopted, radiative forcing is projected to be between 2.5 W/m^2 to 9 W/m^2 or higher by 2100 (Fisher et al., 2007). The IPCC assessment reports, based on the radiative forcing, projected an increase of 0.3 to 4.8°C in the mean surface temperature by the end of the 21st century (Van Vuuren et al., 2011a).

The IPCC is an intergovernmental body of the United Nations that provides the state of scientific, technical, and socio-economic knowledge on human-induced climate change by identifying the agreements in the scientific community on climate change topics. The IPCC has published five assessment reports (first, 1990; second, 1995; third, 2001; fourth, 2007; fifth, 2013) and provided long-term climate scenarios focusing on climate change driving forces (e.g., demographic development, socio-economic development, and technological change). These climate change scenarios are widely used

in climate change analysis including assessments of impacts, adaption, and mitigation (Nakicenovic et al., 2000). The projected climate scenarios have evolved over the period. For example, the spatial resolution has improved from 500 km^2 (first assessment report) to 87.5 km^2 (fifth assessment report).

The fifth phase of the Coupled Model Intercomparison Project (CMIP5) by IPCC provided new representative concentration pathways (RCP) based on total radiative forcing by the end of the 21st century with remarkable information about climate parameters at a very fine spatial resolution (Collins et al., 2013). IPCC's fifth assessment report (AR5; IPCC 2014) consists of four RCPs based on the radiative forcing in the year 2100.

RCP 2.6: RCP 2.6 is the "most stringent" of the four RCPs (Masui et al., 2011). It represents a low emission and radiative forcing (2.6 W/m^2 in 2100) scenario. It is a mitigation scenario that requires substantial changes in GHGs emissions (70% reduction from 2010 to 2100) and limits the increase of global mean temperature to 2°C by 2100 (Van Vuuren et al., 2011b).

RCP 4.5: RCP 4.5 represents a stabilization scenario and assumes that "climate policies are invoked to achieve the goal of limiting emissions and radiative forcing" (Thomson et al., 2011). It is a long-term climate system response scenario that aims to achieve stable radiative forcing (4.5 W/m^2) in 2100 without ever exceeding that value (Thomson et al., 2011).

RCP 6.0: RCP 6.0 represents a climate-policy intervention scenario that requires explicit policies designed to reduce GHGs emissions and limit radiative forcing to 6.0 W/m^2 in the year 2100. It is also a stabilization scenario. The global mean temperature is expected

to increase by 4.9°C by 2100 under this scenario with a carbon dioxide concentration of 850 ppm (Masui et al., 2011).

RCP 8.5: RCP 8.5 corresponds to a scenario of comparatively high GHGs emissions (Riahi et al., 2011). It represents a baseline scenario with its "no climate policy" assumption (Masui et al., 2011). It is a high GHG emission pathway leading to a radiative forcing of 8.5 W/m^2 in 2100.

2.4.1. Climate Bias Corrections

The availability of projected climate data and scenario-based hydrological modeling approaches provide an opportunity to quantify the climate change impacts and understand possible scenarios to minimize resulting negative impacts. However, the climate projections are still associated with biases due to their coarse resolution that involves spatial averaging (Gautam, 2018). Associated biases with the GCM are a major challenge to simulate and analyze climate change impacts on water quantity and water quality at multiple scales. Biases lead to uncertainty in the impact assessment. The uncertainty in the projected climate data depends on the scale of operation. Although the available climate projection data from CMIP5-Bias-corrected Constructed Analog (BCCA) archive are bias-corrected and downscaled, it could be still associated with the biases. The CMIP5-BCCA simulated precipitation data contains two major limitations: numerous drizzle days and underestimated extreme events. Therefore, previous researchers (e.g., Gautam, 2018; Shrestha et al., 2019) have suggested an additional bias correction by adjusting GCM outputs, basically for precipitation and temperature. Gautam et al. (2018) suggested bias correction using modified quantile mapping techniques for precipitation data and delta methods for temperature data. The multi-

model ensembled modeling approach is another method suggested to minimize the predictive error associated with individual GCMs (Pierce et al., 2009).

2.5. Process-based Models

Process-based models are useful tools for assessing the impacts of LULC, climate, and management changes on hydrologic components. The purpose of modeling approaches is to represent complex processes in a simplified way. Models provide cost-effective approaches to evaluate the movement of water and the fate of nutrients across complex land surfaces under given weather conditions (Bawa et al., 2021b). Simulation models provide an additional tool to assess the impacts of alternate management systems (Dabney et al., 2001) and future climate projections. Semi-distributed hydrologic models such as SWAT (Neitsch et al., 2011), EPIC, APEX (Gassman et al., 2009)   divide the watershed into sub-basins and calculate flow contribution from separated sub-basins.

2.5.1. Soil and Water Assessment Tool (SWAT)

The Soil and Water Assessment Tool (SWAT) is an intensively widely used hydrological model to study the impacts of land management practices on hydrology and water quality at the watershed scale over long time-periods (Arnold et al. 2013). SWAT is a process-based, semi-distributed, daily time-step, basin-scale hydrological simulation model (Santhi et al., 2001). SWAT is one of the most widely used hydrological simulation models to assess LULC change (Baker and Miller, 2013; Schilling et al., 2008), climate change (Mehta et al., 2016), and alternative management practices (Dabney et al., 2001) impact on hydrological components (Ficklin et al., 2013; Neupane and Kumar, 2015), crop productions (Panagopoulos et al., 2014), and nutrient fate (Jha et al., 2015; Panagopoulos et al., 2014).

The components of SWAT include climate, hydrology, soil temperatures, plant growth, nutrient and pesticide fate, management practices, carbon cycling, erosion, and sedimentation. This model comprises two modeling phases: land phase modeling and water balance modeling (Neitsch et al. 2011). Land phase modeling delineates the watershed of interest and divides it into sub-watersheds based on a required threshold area. These sub-watersheds are further partitioned into small hydrologic response units (HRU) which are a unique combination of land cover, soil type, and slope. The HRU represents the homogenous land cover, soil, and topography that better explains the heterogeneity of the watershed. After the land phase modeling, SWAT considers several physical processes including surface and subsurface runoff, infiltration, evapotranspiration, soil storage, and groundwater recharge. Then, it applies a water balance in the soil profile to simulate the in-land hydrological cycle at the HRU scale (Arnold et al. 2012).

2.5.2. Operational Simplified Surface Energy Balance (SSEBop)

Direct ET measurements using vapor transfer or lysimeter water balance approaches are limited to field-scale. Remotely sensed images and emerging energy balance techniques have enabled ET estimations at various spatial- (field scale to global scale) and temporal- scales (daily/seasonal/annual) (Lurtz et al., 2020; Velpuri et al., 2020; Yang et al., 2020). However, accurate ET estimations using satellite remote sensing techniques are still a challenge as a result of the numerous assumptions and complex factors such as radiations, temperature, vapor-pressure deficit, sensible heat, and ground heat fluxes that must be considered (Ji, Senay, Velpuri, & Kagone, 2019; Velpuri, Senay, Singh, Bohms, & Verdin, 2013).

Satellite-based ET estimation approaches are prone to various uncertainties introduced by input data quality, cloud contamination, and an unequal number of images over different years. The SSEBop model is a relatively simplified model to estimate the ET using satellite images (de Andrade et al., 2021). The SSEBop model uses a pre-defined dT parameter to define the "wet" and "dry" conditions for each pixel (Senay et al., 2013). Wet conditions refer to the cold temperature (in case of no sensible heat flux) and dry conditions refer to the hot temperature (in case of no latent heat flux), used to estimate the ET fraction (ET_f) in combination with land surface temperature. Another innovative approach of scene-based c-factor in the SSEBop modeling approach minimizes the potential difference in land surface temperature calibration among different satellite sensors such as Landsat 5,7, and 8 (Senay et al., 2019b). This innovative parameterization procedure for limiting extreme surface temperature conditions helps the model to eliminate all complex calculations to solve energy balance terms and provides a simple energy balance approach to obtain the ET_f. This model requires low input model drivers and parameters, hence limiting complexity and uncertainties introduced by input data quality and model parameterization (Bawa et al., 2021b; Ji et al., 2019). Generally, less complex models are assumed to compromise accuracy by eliminating less important processes. Chen et al. (2016) compared the SSEBop estimated ET with ET estimations at 42 Ameriflux tower sites and reported a satisfactory performance of the SSEBop model for the ET estimations. Model evaluation statistics of other studies across the world that include, for instance, USA (Senay et al., 2019a; Singh et al., 2020; Velpuri et al., 2020), Brazil (Dias Lopes et al., 2019; Paula et al., 2019), China (Jin et al., 2019), India (Sharma and Tare, 2018), West Africa

(Dembélé et al., 2020), East Africa (Alemayehu et al., 2017) and others support the reliability of the SSEBop ET estimations. These studies also reflect the robustness of the SSEBop model to quantify ETa over a wide range of vegetation types, climate, and water availability.

2.6. Summary of Literature Review and Research Gaps

This review summarized the impacts of LULC, climate, and management practices changes on the components of the hydrological cycle. However, LULC- and location-specific data are still required among trending conservation practices for improved water resource management. Researchers are promoting various conservation practices for sustainable production. These practices such as ICL systems and cover cropping (the focus of our current research) have been suggested to create a win-win scenario for both agricultural production and soil and water conservation. The success of these conservation practices under future climatic changes is critical to meet food security goals and protecting the environment.

From this literature review, it is well documented that ICL systems and cover cropping provide benefits including enhanced soil health, resilience, and fertility as well as agricultural diversification and production. Cover crops if used in conjunction with conservation tillage such as no-till can cause a synergistic effect on the environment and agricultural economy by enhancing soil fertility, suppressing weed growth, and reducing agricultural nutrient losses. However, the vulnerability of cover crops establishment and expected soil health and water quality benefits under the short and cold cover crop growing periods are of major concern among producers in the Northern Great Plains

(NGP) regions. Therefore, cover crops those are suitable in the short growing period under colder regions of NGP needs further research.

Integration of crops with livestock is another trending conservation practice that has gained popularity in the NGP and Midwest regions to promote agricultural diversification, soil productivity, and environmental quality. While literature highlights the environmental and economic benefits of ICL systems, there are limited studies to address the generalized concerns about the detrimental impacts of ICL systems on soil hydrological properties. Knowledge of hydrological responses with soil physical properties under ICL systems can help in making future land-use management decisions and improving agricultural production with economic decision support. Therefore, there is a need to explore the relative hydrological impact of implementing favorable agricultural practices such as ICL systems in a changing climate for an improved understanding of hydrological responses. Additionally, process-based models can be useful tools to understand the long-term benefits of these cover crops and integrated crop-livestock systems in the NGP regions.

While studying the influences of future climate scenarios is critical to the success of ecological intensification of agriculture, exploring hydrological landscape responses in relation to past climate and LULC changes is essential for developing an efficient and profitable agroecosystem. An evaluation of past hydrological responses to changing LULC and climate can assist in distinguishing natural and anthropogenic changes in water resources. Historical landscape responses such as ET along with existing trends provide a decision support toolkit for future policies. Hence, additional research is required to understand location-specific interactions between LULC, climate, and

hydrological landscape responses that can lead to the sustainable and effective

management of water resources. These interactions are of utmost importance to

stakeholders, watershed managers, and policymakers to better identify where these

conservation practices can be implemented to preserve water quantity and quality with

other ecosystem services.

References

Adams, H. D., Luce, C. H., Breshears, D. D., Allen, C. D., Weiler, M., Hale, V. C., . . . Huxman, T. E. (2012). Ecohydrological consequences of drought-and infestation-triggered tree die-off: insights and hypotheses. Ecohydrology, 5(2), 145-159.

Ahiablame, L., Sheshukov, A. Y., Rahmani, V., & Moriasi, D. (2017). Annual baseflow variations as influenced by climate variability and agricultural land use change in the Missouri River Basin. Journal of Hydrology, 551, 188-202.

Ahiablame, L., Sinha, T., Paul, M., Ji, J.-H., & Rajib, A. (2017). Streamflow response to potential land use and climate changes in the James River watershed, Upper Midwest United States. Journal of Hydrology: Regional Studies, 14, 150-166.

Alemayehu, T., Griensven, A. v., Senay, G. B., & Bauwens, W. (2017). Evapotranspiration mapping in a heterogeneous landscape using remote sensing and global weather datasets: Application to the Mara Basin, East Africa. Remote Sensing, 9(4), 390.

Alhameid, A., Singh, J., Sekaran, U., Ozlu, E., Kumar, S., & Singh, S. (2020). Crop rotational diversity impacts soil physical and hydrological properties under long-term no-and conventional-till soils. Soil Research, 58(1), 84-94.

Allen, R. G., Pereira, L. S., Raes, D., & Smith, M. (1998). Crop evapotranspiration-Guidelines for computing crop water requirements-FAO Irrigation and drainage paper 56. Fao, Rome, 300(9), D05109.

Baker, T. J., & Miller, S. N. (2013). Using the Soil and Water Assessment Tool (SWAT) to assess land use impact on water resources in an East African watershed. Journal of Hydrology, 486, 100-111.

Bansal, S., Yin, X., Savoy, H. J., Jagadamma, S., Lee, J., & Sykes, V. (2020). Long-term influence of phosphorus fertilization on organic carbon and nitrogen in soil aggregates under no-till corn–wheat–soybean rotations. Agronomy Journal, 112(4), 2519-2534.

Basche, A., & DeLonge, M. (2017). The impact of continuous living cover on soil hydrologic properties: A meta-analysis. Soil Science Society of America Journal, 81(5), 1179-1190.

Batelaan, O., De Smedt, F., & Triest, L. (2003). Regional groundwater discharge: phreatophyte mapping, groundwater modelling and impact analysis of land-use change. Journal of Hydrology, 275(1-2), 86-108.

Bawa, A., Pérez-Gutiérrez, J. D., & Kumar, S. (2021a). Simulating Hydrological Responses of Integrated Crop-Livestock Systems under Future Climate Changes in an Agricultural Watershed. JAWRA Journal of the American Water Resources Association. https://doi.org/10.1111/1752-1688.12908.

Bawa, A., Senay, G. B., & Kumar, S. (2021b). Regional crop water use assessment using Landsat-derived evapotranspiration. Hydrological Processes, 35(1), e14015. doi:10.1002/hyp.14015

Bilotta, G., Brazier, R., & Haygarth, P. (2007). The impacts of grazing animals on the quality of soils, vegetation, and surface waters in intensively managed grasslands. Advances in Agronomy, 94, 237-280.

Bublinec, E. (1971). Influence of pine forests on instant soil moisture in climatic variable years. Journal of Hydrology and Hydromechanics (Bratislava), 19(6), 622-650.

Calder, I. (1992). Hydrologic effects of land-use change: McGraw-Hill Inc.

Chang, H. (2007). Comparative streamflow characteristics in urbanizing basins in the Portland Metropolitan Area, Oregon, USA. Hydrological Processes, 21(2), 211-222.

Changnon, S. A., & Kunkel, K. E. (1995). Climate-related fluctuations in Midwestern floods during 1921–1985. Journal of Water Resources Planning Management, 121(4), 326-334.

Chen, M., Senay, G. B., Singh, R. K., & Verdin, J. P. (2016). Uncertainty analysis of the Operational Simplified Surface Energy Balance (SSEBop) model at multiple flux tower sites. Journal of Hydrology, 536, 384-399.

Chen, X., Zhang, Z., Chen, X., & Shi, P. (2009). The impact of land use and land cover changes on soil moisture and hydraulic conductivity along the karst hillslopes of southwest China. Environmental Earth Sciences, 59(4), 811-820.

Chien, H. C., Yeh, P. J. F., & Knouft, J. H. (2013). Modeling the potential impacts of climate change on streamflow in agricultural watersheds of the Midwestern United States. Journal of Hydrology, 491, 73-88. doi:10.1016/j.jhydrol.2013.03.026

Clark, J. T., Russell, J. R., Karlen, D. L., Singleton, P., Darrell Busby, W., & Peterson, B. C. (2004). Soil surface property and soybean yield response to corn stover grazing. Agronomy Journal, 96(5), 1364-1371.

Clifton, C. F., Day, K. T., Luce, C. H., Grant, G. E., Safeeq, M., Halofsky, J. E., & Staab, B. P. (2018). Effects of climate change on hydrology and water resources in the Blue Mountains, Oregon, USA. Climate Services, 10, 9-19.

Collins, M., Knutti, R., Arblaster, J., Dufresne, J.-L., Fichefet, T., Friedlingstein, P., . . . Krinner, G. (2013). Long-term climate change: projections, commitments and

irreversibility. *In Climate Change 2013*-The Physical Science Basis: Contribution of Working Group I to the Fifth Assessment Report of the Intergovernmental Panel on Climate Change (pp. 1029-1136): Cambridge University Press.

Dabney, S., Delgado, J., & Reeves, D. (2001). Using winter cover crops to improve soil and water quality. Communications in Soil Science and Plant Analysis, 32(7-8), 1221-1250.

Dabney, S. M. (1998). Cover crop impacts on watershed hydrology. Journal of Soil and Water Conservation, 53(3), 207-213.

Das, P., Behera, M. D., Patidar, N., Sahoo, B., Tripathi, P., Behera, P. R., . . . Agrawal, S. (2018). Impact of LULC change on the runoff, base flow and evapotranspiration dynamics in eastern Indian river basins during 1985–2005 using variable infiltration capacity approach. Journal of Earth System Science, 127(2), 1-19.

de Andrade, B. C. C., de Andrade Pinto, E. J., Ruhoff, A., & Senay, G. B. (2021). Remote sensing-based actual evapotranspiration assessment in a data-scarce area of Brazil: A case study of the Urucuia Aquifer System. International Journal of Applied Earth Observation and Geoinformation, 102298.

De Wit, M., & Stankiewicz, J. (2006). Changes in surface water supply across Africa with predicted climate change. science, 311(5769), 1917-1921.

Defries, R. S., Bounoua, L., & Collatz, G. J. (2002). Human modification of the landscape and surface climate in the next fifty years. Global Change Biology, 8(5), 438-458.

Dembélé, M., Ceperley, N., Zwart, S. J., Salvadore, E., Mariethoz, G., & Schaefli, B. (2020). Potential of satellite and reanalysis evaporation datasets for hydrological modelling under various model calibration strategies. Advances in Water Resources, 143, 103667.

DeWalle, D. R., Swistock, B. R., Johnson, T. E., & McGuire, K. J. (2000). Potential effects of climate change and urbanization on mean annual streamflow in the United States. Water Resources Research, 36(9), 2655-2664.

Dias Lopes, J., Neiva Rodrigues, L., Acioli Imbuzeiro, H. M., & Falco Pruski, F. (2019). Performance of SSEBop model for estimating wheat actual evapotranspiration in the Brazilian Savannah region. International Journal of Remote Sensing, 40(18), 6930-6947.

Dinnes, D. L., Karlen, D. L., Jaynes, D. B., Kaspar, T. C., Hatfield, J. L., Colvin, T. S., & Cambardella, C. A. (2002). Nitrogen management strategies to reduce nitrate leaching in tile-drained Midwestern soils. Agronomy Journal, 94(1), 153-171.

Drewry, J., Cameron, K., & Buchan, G. (2008). Pasture yield and soil physical property responses to soil compaction from treading and grazing—a review. Soil Research, 46(3), 237-256.

Drury, C., Tan, C., Welacky, T., Reynolds, W., Zhang, T., Oloya, T., . . . Gaynor, J. (2014). Reducing nitrate loss in tile drainage water with cover crops and water-table management systems. Journal of Environmental Quality, 43(2), 587-598.

Faust, D. R., Liebig, M. A., Toledo, D., Archer, D. W., Kronberg, S. L., Hendrickson, J. R., ... & Kumar, S. (2020). Water quality of an integrated crop–livestock system in the northern Great Plains. Agrosystems, Geosciences & Environment, 3(1), e20129.

Faust, D. R., Kumar, S., Archer, D. W., Hendrickson, J. R., Kronberg, S. L., & Liebig, M. A. (2018). Integrated Crop-Livestock Systems and Water Quality in the Northern Great Plains: Review of Current Practices and Future Research Needs. Journal of Environmental Quality, 47(1), 1-15.

Ficklin, D. L., Stewart, I. T., & Maurer, E. P. (2013). Effects of projected climate change on the hydrology in the Mono Lake Basin, California. Climatic Change, 116(1), 111-131.

Field, C. B. (2014). Climate change 2014–Impacts, adaptation and vulnerability: Regional aspects: Cambridge University Press.

Fisher, B., Nakicenovic, N., Alfsen, K., Corfee-Morlot, J., & Riahi, K. (2007). Issues related to mitigation in the long-term context (Chapter 3). In: *Climate Change* 2007: Mitigation. Contribution of WG III to the Fourth Assessment Report of the IPCC. Eds. Metz, B., Davidson, O.R., Bosch, P.R., Dave, R. & Meyer, L.A., Cambridge: Cambridge University Press.

Folorunso, O., Rolston, D., Prichard, T., & Loui, D. (1992). Soil surface strength and infiltration rate as affected by winter cover crops. Soil Technology, 5(3), 189-197.

Fraser, H., & Fleming, R. (2001). Environmental benefits of tile drainage: Literature review. Available at age-web. age. uiuc. edu/classes/age357/html/benefits% 20of% 20tile% 20drainage. pdf (accessed 7 Aug. 2011, verified 1 Oct. 2011). Univ. of Guelph, Guelph, ON, Canada.

Gassman, P. W., Williams, J. R., Wang, X., Saleh, A., Osei, E., Hauck, L. M., . . . Flowers, J. (2009). The Agricultural Policy Environmental EXtender (APEX) Model: An Emerging Tool for Landscape and Watershed Environmental Analyses. CARD Technical Reports. 41.

Gautam, S. (2018). Climate change impacts on hydrologic components and occurrence of drought in an agricultural watershed. (Doctoral dissertation, University of Missouri--Columbia).

Gautam, S., Costello, C., Baffaut, C., Thompson, A., Svoma, B. M., Phung, Q. A., & Sadler, E. J. (2018). Assessing Long-Term Hydrological Impact of Climate Change Using an Ensemble Approach and Comparison with Global Gridded Model-A Case Study on Goodwater Creek Experimental Watershed. Water, 10(5), 564. doi:UNSP 56410.3390/w10050564

Ghane, E. (2018). Agricultural Drainage. Extension Bulletin E3370.

Giri, S., & Qiu, Z. (2016). Understanding the relationship of land uses and water quality in twenty first century: a review. Journal of environmental management, 173, 41-48.

Gregory, R. D., Willis, S. G., Jiguet, F., Voříšek, P., Klvaňová, A., van Strien, A., . . . Green, R. E. (2009). An indicator of the impact of climatic change on European bird populations. PloS one, 4(3), e4678.

Guo, H., Hu, Q., & Jiang, T. (2008). Annual and seasonal streamflow responses to climate and land-cover changes in the Poyang Lake basin, China. Journal of Hydrology, 355(1-4), 106-122.

Hamlet, A. F., Elsner, M. M., Mauger, G. S., Lee, S.-Y., Tohver, I., & Norheim, R. A. (2013). An overview of the Columbia Basin Climate Change Scenarios Project: Approach, methods, and summary of key results. Atmosphere-ocean, 51(4), 392-415.

Hamlet, A. F., Mote, P. W., Clark, M. P., & Lettenmaier, D. P. (2005). Effects of temperature and precipitation variability on snowpack trends in the western United States. Journal of Climate, 18(21), 4545-4561.

Hartwig, N. L., & Ammon, H. U. (2002). Cover crops and living mulches. Weed science, 50(6), 688-699.

Hay, C., & Todey, D. (2011). Precipitation and evapotranspiration patterns in the northwestern corn belt and impacts on agricultural water management. Paper presented at the 2011 Louisville, Kentucky, August 7-10, 2011, St. Joseph, MI. https://elibrary.asabe.org/abstract.asp?aid=38114&t=5.

Hobbs, P. R., Sayre, K., & Gupta, R. (2008). The role of conservation agriculture in sustainable agriculture. Philosophical Transactions of the Royal Society B: Biological Sciences, 363(1491), 543-555.

Huang, S., Krysanova, V., & Hattermann, F. (2015). Projections of climate change impacts on floods and droughts in Germany using an ensemble of climate change scenarios. Regional Environmental Change, 15(3), 461-473.

Huntington, T. G., Richardson, A. D., McGuire, K. J., & Hayhoe, K. (2009). Climate and hydrological changes in the northeastern United States: recent trends and implications for forested and aquatic ecosystems. Canadian Journal of Forest Research, 39(2), 199-212.

IPCC, 2007: Climate Change 2007: The Physical Science Basis. Contribution of Working Group I to the Fourth Assessment Report of the Intergovernmental Panel on Climate Change [Solomon, S., D. Qin, M. Manning, Z. Chen, M. Marquis, K.B. Averyt, M. Tignor and H.L. Miller (eds.)]. Cambridge University Press, Cambridge, United Kingdom and New York, NY, USA, 996 pp.

IPCC, 2014: Climate Change 2014: Synthesis Report. Contribution of Working Groups I, II and III to the Fifth Assessment Report of the Intergovernmental Panel on

Climate Change [Core Writing Team, R.K. Pachauri and L.A. Meyer (eds.)]. IPCC, Geneva, Switzerland, 151 pp.

Jha, M. K., Gassman, P. W., & Panagopoulos, Y. (2015). Regional changes in nitrate loadings in the Upper Mississippi River Basin under predicted mid-century climate. Regional Environmental Change, 15(3), 449-460.

Ji, L., Senay, G. B., Velpuri, N. M., & Kagone, S. (2019). Evaluating the Temperature Difference Parameter in the SSEBop Model with Satellite-Observed Land Surface Temperature Data. Remote Sensing, 11(16), 1947.

Jin, X., Zhu, X., & Xue, Y. (2019). Satellite-based analysis of regional evapotranspiration trends in a semi-arid area. International Journal of Remote Sensing, 40(9), 3267-3288.

Jobbágy, E. G., & Jackson, R. B. (2004). Groundwater use and salinization with grassland afforestation. Global Change Biology, 10(8), 1299-1312.

Kumar, S., Anderson, S. H., Udawatta, R. P., & Gantzer, C. J. (2010). CT-measured macropores as affected by agroforestry and grass buffers for grazed pasture systems. Agroforestry systems, 79(1), 59-65.

Lahmar, R. (2010). Adoption of conservation agriculture in Europe: lessons of the KASSA project. Land use policy, 27(1), 4-10.

Lawrence, K., Sosdian, S., White, H., & Rosenthal, Y. (2010). North Atlantic climate evolution through the Plio-Pleistocene climate transitions. Earth and Planetary Science Letters, 300(3-4), 329-342.

Leduc, C., Favreau, G., & Schroeter, P. (2001). Long-term rise in a Sahelian water-table: The Continental Terminal in south-west Niger. Journal of Hydrology, 243(1-2), 43-54.

Legesse, D., Vallet-Coulomb, C., & Gasse, F. (2003). Hydrological response of a catchment to climate and land use changes in Tropical Africa: case study South Central Ethiopia. Journal of Hydrology, 275(1-2), 67-85.

Liebig, M. A., Archer, D. W., & Tanaka, D. L. (2014). Crop diversity effects on near-surface soil condition under dryland agriculture. Applied and Environmental Soil Science, 2014, 703460. doi:10.1155/2014/703460.

Liu, J., Macrae, M. L., Elliott, J. A., Baulch, H. M., Wilson, H. F., & Kleinman, P. J. (2019). Impacts of cover crops and crop residues on phosphorus losses in cold climates: A review. Journal of Environmental Quality, 48(4), 850-868.

Locatelli, B., & Vignola, R. (2009). Managing watershed services of tropical forests and plantations: Can meta-analyses help? Forest Ecology and Management, 258(9), 1864-1870.

Masui, T., Matsumoto, K., Hijioka, Y., Kinoshita, T., Nozawa, T., Ishiwatari, S., . . . Kainuma, M. (2011). An emission pathway for stabilization at 6 Wm^{-2} radiative forcing. Climatic Change, 109(1), 59-76.

McDaniel, M., Tiemann, L., & Grandy, A. (2014). Does agricultural crop diversity enhance soil microbial biomass and organic matter dynamics? A meta-analysis. Ecological Applications, 24(3), 560-570.

McLeman, R. A., Dupre, J., Ford, L. B., Ford, J., Gajewski, K., & Marchildon, G. (2014). What we learned from the Dust Bowl: lessons in science, policy, and adaptation. Population and environment, 35(4), 417-440.

McNeill, K., Macdonald, K., Singh, A., & Binns, A. D. (2017). Food and water security: analysis of integrated modeling platforms. Agricultural Water Management, 194, 100-112.

Mehta, V. M., Mendoza, K., Daggupati, P., Srinivasan, R., Rosenberg, N. J., & Deb, D. (2016). High-resolution simulations of decadal climate variability impacts on water yield in the Missouri River basin with the Soil and Water Assessment Tool (SWAT). Journal of Hydrometeorology, 17(9), 2455-2476.

Miller, M., Brown, P., Donovan, J., Bergatino, R., Sonderegger, J., & Schmidt, F. (1981). Saline seep development and control in the North American Great Plains-hydrogeological aspects. Agricultural Water Management, 4(1-3), 115-141.

Nakicenovic, N., Alcamo, J., Davis, G., Vries, B. d., Fenhann, J., Gaffin, S., . . . Kram, T. (2000). Special report on emissions scenarios. Lawrence Berkeley National Laboratory. LBNL Report #: LBNL-59940. Retrieved from https://escholarship.org/uc/item/9sz5p22f.

Neitsch, S. L., Arnold, J. G., Kiniry, J. R., & Williams, J. R. (2011). Soil and water assessment tool theoretical documentation version 2009. Texas Water Resources Institute.

Neupane, R. P., & Kumar, S. (2015). Estimating the effects of potential climate and land use changes on hydrologic processes of a large agriculture dominated watershed. Journal of Hydrology, 529, 418-429.

Nie, W., Yuan, Y., Kepner, W., Nash, M. S., Jackson, M., & Erickson, C. (2011). Assessing impacts of Landuse and Landcover changes on hydrology for the upper San Pedro watershed. Journal of Hydrology, 407(1-4), 105-114.

NOAA (National Oceanic and Atmospheric Administration). (2016). Global Climate Change Indicators. NOAA-National Centers for Environmental Information. accessed on May 10, 2016. Available at: http://www.ncdc.noaa.gov/indicators/. accessed on May 10, 2016.

Novotny, E. V., & Stefan, H. G. (2007). Stream flow in Minnesota: Indicator of climate change. Journal of Hydrology, 334(3-4), 319-333.

Oki, T., & Kanae, S. (2006). Global hydrological cycles and world water resources. science, 313(5790), 1068-1072.

Pachauri, R. K., Allen, M. R., Barros, V. R., Broome, J., Cramer, W., Christ, R., ... & van Ypserle, J. P. (2014). Climate change 2014: synthesis report. Contribution of

Working Groups I, II and III to the fifth assessment report of the Intergovernmental Panel on Climate Change (p. 151). IPCC.

Panagopoulos, Y., Gassman, P., Arritt, R., Herzmann, D., Campbell, T., Jha, M. K., . . . Arnold, J. (2014). Surface water quality and cropping systems sustainability under a changing climate in the Upper Mississippi River Basin. Journal of Soil and Water Conservation, 69(6), 483-494.

Paul, M. (2016). Impacts of land use and climate changes on hydrological processes in South Dakota Watersheds. Theses and Dissertations. Paper 1018. Theses and Dissertations. Paper 1018. https://openprairie.sdstate.edu/cgi/viewcontent.cgi?article=2018&context=etd.

Paula, A. C. P. d., Silva, C. L. d., Rodrigues, L. N., & Scherer-Warren, M. (2019). Performance of the SSEBop model in the estimation of the actual evapotranspiration of soybean and bean crops. Pesquisa Agropecuária Brasileira, 54.

Pérez-Gutiérrez, J. D., & Kumar, S. (2019). Simulating the influence of integrated crop-livestock systems on water yield at watershed scale. Journal of environmental management, 239, 385-394.

Pierce, D. W., Barnett, T. P., Santer, B. D., & Gleckler, P. J. (2009). Selecting global climate models for regional climate change studies. Proceedings of the National Academy of Sciences, 106(21), 8441-8446.

Riahi, K., Rao, S., Krey, V., Cho, C., Chirkov, V., Fischer, G., . . . Rafaj, P. (2011). RCP 8.5—A scenario of comparatively high greenhouse gas emissions. Climatic Change, 109(1), 33-57.

Roark, D. M. (1998). Quantification of Deep Percolation from Two Flood-irrigated Alfalfa Field, Roswell Basin, New Mexico (Vol. 98): US Department of the Interior, US Geological Survey.

Rose, S., & Peters, N. E. (2001). Effects of urbanization on streamflow in the Atlanta area (Georgia, USA): a comparative hydrological approach. Hydrological Processes, 15(8), 1441-1457.

Roy, A. H., Dybas, A. L., Fritz, K. M., & Lubbers, H. R. (2009). Urbanization affects the extent and hydrologic permanence of headwater streams in a midwestern US metropolitan area. Journal of the North American Benthological Society, 28(4), 911-928.

Santhi, C., Arnold, J. G., Williams, J. R., Dugas, W. A., Srinivasan, R., & Hauck, L. M. (2001). Validation of the swat model on a large rwer basin with point and nonpoint sources 1. JAWRA Journal of the American Water Resources Association, 37(5), 1169-1188.

Sanyal, D., & Wolthuizen, J. (2021). Regenerative Agriculture: Beyond Sustainability. Int J. Agri Res Env Sci, 2(1), 17-18.

Scanlon, B. R., Reedy, R. C., Stonestrom, D. A., Prudic, D. E., & Dennehy, K. F. (2005). Impact of land use and land cover change on groundwater recharge and quality in the southwestern US. Global Change Biology, 11(10), 1577-1593.

Schilling, K. E., Jha, M. K., Zhang, Y. K., Gassman, P. W., & Wolter, C. F. (2008). Impact of land use and land cover change on the water balance of a large agricultural watershed: Historical effects and future directions. Water Resources Research, 44(7).

Senay, G. (2019). Characterizing crop water use dynamics in the Central Valley of California using landsat-derived evapotranspiration. Remote Sensing, 15(11).

Senay, G. B., Bohms, S., Singh, R. K., Gowda, P. H., Velpuri, N. M., Alemu, H., & Verdin, J. P. (2013). Operational evapotranspiration mapping using remote sensing and weather datasets: A new parameterization for the SSEB approach. JAWRA Journal of the American Water Resources Association, 49(3), 577-591.

Senay, G. B., Schauer, M., Friedrichs, M., Velpuri, N. M., & Singh, R. K. (2017). Satellite-based water use dynamics using historical Landsat data (1984–2014) in the southwestern United States. Remote Sensing of Environment, 202, 98-112.

Senay, G. B., Schauer, M., Velpuri, N. M., Singh, R. K., Kagone, S., Friedrichs, M., . . . Douglas-Mankin, K. R. (2019). Long-term (1986–2015) crop water use characterization over the Upper Rio Grande Basin of United States and Mexico using Landsat-based evapotranspiration. Remote Sensing, 11(13), 1587.

Senay, G. B., Velpuri, N. M., Nagler, P. L., & Bateni, S. M. (2019). Evapotranspiration (ET): Advances in in Situ ET Measurements and Remote-Sensing-Based ET Estimation, Mapping, and Evaluation II. Paper presented at the AGU Fall Meeting 2019.

Seneviratne, S. I., Corti, T., Davin, E. L., Hirschi, M., Jaeger, E. B., Lehner, I., . . . Teuling, A. J. (2010). Investigating soil moisture–climate interactions in a changing climate: A review. Earth-Science Reviews, 99(3-4), 125-161.

Sharma, D., & Tare, V. (2018). Evapotranspiration estimation using SSEBOP method with Sentinel-2 and Landsat-8 data set. International Archives of the Photogrammetry, Remote Sensing and Spatial Information Sciences, 42, 563-566.

Shrestha, S., Sharma, S., Gupta, R., Bhattarai, R. J. I. J. o. A., & Engineering, B. (2019). Impact of global climate change on stream low flows: A case study of the great Miami river watershed, Ohio, USA. 12(1), 84-95.

Sims, J. T., Simard, R. R., & Joern, B. C. (1998). Phosphorus loss in agricultural drainage: Historical perspective and current research. Journal of Environmental Quality, 27(2), 277-293.

Singh, J. (2020). Crop Rotations, Tillage and Cover Crops Influences on Soil Health, Greenhouse Gas Emissions and Farm Profitability. Electronic Theses and Dissertations. 4084. https://openprairie.sdstate.edu/etd/4084.

Singh, R. K., Khand, K., Kagone, S., Schauer, M., Senay, G. B., & Wu, Z. (2020). A novel approach for next generation water-use mapping using Landsat and Sentinel-2 satellite data. Hydrological Sciences Journal, 65(14), 2508-2519.

Smith, D. R., King, K. W., Johnson, L., Francesconi, W., Richards, P., Baker, D., & Sharpley, A. N. (2015). Surface runoff and tile drainage transport of phosphorus in the midwestern United States. Journal of Environmental Quality, 44(2), 495-502.

Smith, S. D., Monson, R., & Anderson, J. E. (2012). Physiological Ecology of North American Desert Plants. Germany: Springer Berlin Heidelberg.

Solomon, S., Qin, D., Manning, M., Chen, Z., Marquis, M., Averyt, K., . . . Miller, H. (2007). IPCC fourth assessment report (AR4). Climate change, 374.

Stagl, J., Mayr, E., Koch, H., Hattermann, F. F., & Huang, S. (2014). Effects of climate change on the hydrological cycle in central and eastern Europe. In Managing Protected Areas in Central and Eastern Europe Under Climate Change (pp. 31-43): Springer, Dordrecht.

Sulc, R. M., & Tracy, B. F. (2007). I ntegrated Crop–Livestock Systems in the U.S. Corn Belt. Agronomy Journal, 99: 335-345. https://doi.org/10.2134/agronj2006.0086.

Tallaksen, L. (1993). Modelling land use change effects on low flows. In FRIEND (Vol. 1, 56-68).

Thomson, A. M., Calvin, K. V., Smith, S. J., Kyle, G. P., Volke, A., Patel, P., . . . Clarke, L. E. (2011). RCP4. 5: a pathway for stabilization of radiative forcing by 2100. Climatic Change, 109(1), 77-94.

Van Vliet, M., & Zwolsman, J. (2008). Impact of summer droughts on the water quality of the Meuse river. Journal of Hydrology, 353(1-2), 1-17.

Van Vuuren, D. P., Edmonds, J., Kainuma, M., Riahi, K., Thomson, A., Hibbard, K., . . . Lamarque, J.-F. (2011). The representative concentration pathways: an overview. Climatic change, 109(1-2), 5.

Van Vuuren, D. P., Stehfest, E., den Elzen, M. G., Kram, T., van Vliet, J., Deetman, S., . . . Beltran, A. M. (2011). RCP2. 6: exploring the possibility to keep global mean temperature increase below 2 C. Climatic Change, 109(1), 95-116.

Velpuri, N. M., Senay, G. B., Schauer, M., Garcia, C. A., Singh, R. K., Friedrichs, M., ... & Conlon, T. (2020). Evaluation of hydrologic impact of an irrigation curtailment program using Landsat satellite data. Hydrological Processes, 34(8), 1697-1713.

Verma, P., Singh, R., Singh, P., & Raghubanshi, A. (2020). Urban ecology–current state of research and concepts. In Urban Ecology (3-16): Elsevier.

Vose, J. M., Clark, J. S., & Luce, C. H. (2016). Introduction to drought and US forests: Impacts and potential management responses. Forest Ecology and Management, 100(380), 296-298.

Walther, G.-R., Post, E., Convey, P., Menzel, A., Parmesan, C., Beebee, T. J., . . . Bairlein, F. (2002). Ecological responses to recent climate change. Nature, 416(6879), 389-395.

Wang, R., Kalin, L., Kuang, W., & Tian, H. (2014). Individual and combined effects of land use/cover and climate change on Wolf Bay watershed streamflow in southern Alabama. Hydrological Processes, 28(22), 5530-5546.

Wilson, C., & Weng, Q. (2010). Assessing surface water quality and its relation with urban land cover changes in the Lake Calumet Area, Greater Chicago. Environmental Management, 45(5), 1096-1111.

Xu, X., Scanlon, B. R., Schilling, K., & Sun, A. (2013). Relative importance of climate and land surface changes on hydrologic changes in the US Midwest since the 1930s: Implications for biofuel production. Journal of Hydrology, 497, 110-120.

Zhang, L., Nan, Z., Yu, W., & Ge, Y. (2016). Hydrological responses to land-use change scenarios under constant and changed climatic conditions. Environmental Management, 57(2), 412-431.

Zhang, Y.-K., & Schilling, K. (2006). Increasing streamflow and baseflow in Mississippi River since the 1940 s: Effect of land use change. Journal of Hydrology, 324(1-4), 412-422.

Zucker, L. A., & Brown, L. C. (1998). Agricultural drainage: Water quality impacts and subsurface drainage studies in the Midwest (Vol. 871): Ohio State University Extension.

CHAPTER 3

RESPONSES OF LEACHED NUTRIENT CONCENTRATIONS AND SOIL HEALTH TO WINTER RYE COVER CROP UNDER NO-TILL CORN-SOYBEAN ROTATION

ABSTRACT

This study was established in 2017 under a no-till corn (*Zea mays* L.)-soybean [*Glycine max* (L.) Merr.] rotation to assess the impacts of winter rye (*Secale cereale* L.) cover crop (CC) on soil health and water quality parameters. CC was planted after crop harvest, and data was collected for three years (2017 to 2020). The study site faced one dry (2020) and two abnormally wet years (2018 and 2019) which received 31% lower (2020), and 31% (2018) and 23% (2019) higher precipitation, respectively, than the annual average (1953-2019). Data showed that rye CC biomass was 251 kg ha^{-1} in 2018, 1213 kg ha^{-1} in 2019, and 147 kg ha^{-1} in 2020, coinciding with contrasting growing degree days i.e., 1458, 2042, 794, respectively, as a consequence of variable weather conditions. Cover cropping did not affect the water quality for the majority of the study period. A significant reduction in leached nitrate (~19-20%) and total nitrogen (TN) (~8.5-16%) concentrations were found only in 2019, pertaining to sequestered 18.8 kg-N ha^{-1}. Rye CC showed 13 and 11% significantly higher microbially active carbon and water-extractable organic nitrogen, respectively, than the control treatment. The non-significant impacts on soil health indicators due to winter rye showed that study duration (3 years) may not be sufficient to see the beneficial impacts of cover crops on soils. However, significant reductions in leached nitrate and TN concentrations for one (2019) out of three study years suggest that well-established rye CC (biomass = 1213 kg ha^{-1}; which

was 4.8 and 8.3 times higher than that in 2018 and 2020) has the potential of reducing nutrient leaching and enhancing soil health for the study region.

3.1. Introduction

Subsurface drainage removes excess water from poorly drained soils to enhance trafficability, allow timely farm operations for enhanced crop production and profit (Kladivko et al., 2004; Saadat et al., 2018). However, these drainage systems produce environmental externalities by transporting a substantial nutrient load (especially the dissolved form of N and P) from agricultural fields to the adjacent ditches which contribute to water quality (WQ) issues (Kladivko et al., 2004; Saadat et al., 2018). Further, these subsurface drainage systems alter the hydrology of the landscapes and WQ of the surface water bodies (Blann et al., 2009; Fraser and Fleming, 2001). Therefore, a range of strategies has been suggested to mitigate WQ issues caused by the subsurface drainage systems. Controlled drainage, no-till, and cover crops (CCs) are the few conservation practices that are beneficial in enhancing the WQ. Controlled drainage is a structural conservation practice where drainage outlet elevation is managed to reduce drain flow volume and N loads to water bodies (Gunn et al., 2015; Williams et al., 2015). No-till systems and CCs play important roles in enhancing the WQ by conserving crop residues, improving soil health, and reducing surface runoff, all of these reduce nutrient losses.

The CCs are introduced into traditional cropping systems for their ability to provide environmental and economic benefits by enhancing soil fertility, suppressing weed growth, and reducing ammonia volatilization and nitrate leaching losses (Dinnes et al., 2002; Wyland et al., 1996). These crops provide various benefits such as supplying

nutrients to crops, supporting rapid nutrient cycling through microbial biomass, and helping to retain applied mineral fertilizer (Trujillo Cabrera, 2002). In general, CCs are planted after harvesting the main crop to reduce nutrient losses by absorbing residual nutrients. Meisinger et al. (1991) reported a decrease in nitrate concentration by 20 to 80% in leachate samples due to the presence of CC. Logsdon et al. (2002) reported that Oat (Avena sativa L.) and winter rye (Secale cereale L.) as CCs can reduce nitrate leaching by 70% in a corn (Zea mays L.)-soybean [Glycine max (L.) Merr.] rotation. The success of CC depends on the coincidence of its N release and uptake of the subsequent crop. Steenwerth and Belina (2008) reported that cover-cropped treatments had higher microbial biomass and N transformation rates, and lower soil nitrate values than without CC (controls). Thus, CCs play a considerable role in enhancing soil health indicators such as organic matter, nutrient cycling, reduced runoff, and higher water infiltration. Increased soil organic matter can improve the efficiency of N and P nutrients cycling and lower the eutrophication of aquatic ecosystems (Zimnicki et al., 2020). Previous studies (e.g., Bosch et al., 2013; Kaspar et al., 2007; Smith et al., 2015) demonstrated the importance of conservation practices such as no-till, filter strips, and CC for water quality improvement and they reported that high nitrate losses in between the crop mature and canopy development stage can be mitigated by adopting the combination of conservation practices.

Adopting CC in a cropping sequence is becoming a common practice in the upper Midwest and upper Great Plains regions for providing a range of ecosystem services (CTIC, 2017; Singer et al., 2007). However, the growing period for winter CC between harvest and spring plantation of corn or soybean is particularly limited with cooler

temperatures in these regions, causing reduced persistence and insignificant gain in cover crop biomass. Therefore, winter rye as a cover crop in these conditions can be promising in enhancing soil health and water quality. Snapp et al. (2005) suggested rye as the most promising cover crop for winter niches because of its winter hardiness. A thick, fibrous root system and prolific growth provide winter rye an exceptional ability to take up the residual N from the soil system. After the termination of winter rye during the spring period, the breakdown of rye residue cycles organically bound N into soil organic matter which is released over time as inorganic N through microbially mediated processes (Ruffo et al., 2004).

Soil health and water quality benefits from CC are highly dependent on the successful establishment and biomass production of the CC (Strock et al., 2004). Although previous studies (e.g., Bergtold et al., 2017; Snapp et al., 2005) highlighted the environmental and agroeconomic benefits of CC, yet the influence of short CC growing period on soil health and water quality under corn-soybean rotations in regions with year-to-year climate variability needs further research. In addition, the influence of uncontrollable management factors (climate and soil type) on controllable factors (management decisions) on winter rye CC establishment still needs exploration. Limited studies have been conducted in the Northern Great Plains (NGP) region of the USA those focused on assessing the impacts of winter rye CC under no-till corn-soybean rotation system on soil health and water quality. Therefore, this study was conducted based on the hypothesis that winter rye cover cropping can significantly reduce nutrient leaching and enhance soil health compared to the no cover crop (NCC) treatment. Specific objectives of the study are to assess the impacts of winter rye CC and NCC on: (i) soil health

indicators [e.g, soil organic matter (SOM), soil respiration (CO_2-C), water-extractable total nitrogen (WETN), water-extractable organic nitrogen (WEON), water-extractable total carbon (WETC), nitrate (H3ANO3-N), ammonium (H3ANH4-N), inorganic nitrogen (H3AIN), total phosphorus (H3ATP), inorganic phosphorus (H3AIP), microbially active carbon (MAC), and (ii) water quality parameters [e.g., nitrate-N (NO_3^-), ammonia-N (NH_4^+) and total nitrogen (TN)].

3.2. Materials and Methods

3.2.1. Study Site and Treatments Details

The present study was conducted at Southeast Research Farm (SERF) of South Dakota State University, near Beresford, South Dakota (SD) (43° 03' 05" N, 96° 53' 42" W) to assess the impacts of winter rye cover crop on leached nutrient concentrations and soil health indicators. The experiment was conducted on the Egan series (Fine-silty, mixed, superactive, mesic Udic Haplustolls) and Trent series (Fine-silty, mixed, superactive, mesic Pachic Haplustolls). Soils at the field site are classified as moderately permeable silty sediments overlying on moderately slow or slow permeable glacial-till. The subsurface drainage was installed in 2013 at a depth of 180 cm with an end-of-drainage control structure with a 31 cm tall barrier set at the bottom of the structure for an effective depth of 149 cm.

The crop rotation at this site followed a corn-soybean that was managed with conventional tillage until 2011 and then changed to a no-till system in 2012. The winter rye CC was introduced in October 2017 after corn harvest and planted thereafter every year after the crop harvest under no-till corn-soybean rotation. Therefore, treatments of this study included (i) winter rye cover crops and (ii) control, no CC under no-till corn-

soybean rotation with six replications. The field experiment was divided into six blocks with alleys ranging from 23 to 42 m between each block. The alleys were cropped and managed similar to the experimental plots. Blocks were subdivided into randomly assigned CC and NCC treatments with an individual controlled drainage system for each plot. The winter rye CC ('Hazlet' rye at 56 kg ha^{-1}) was planted using a no-till drill (model 750, Deere & Company, Moline, IL). Corn (variety: Pioneer P0589AM at 77,805 seeds ha^{-1} in 2018 and 'P0421AM' at 79,072 seeds ha^{-1} in 2020 and soybean (variety: Pioneer P25A54X at 370,500 seeds ha^{-1}) were planted using a row crop planter (model NG-66-33-0, Monosem Inc., Largeasse, France) with a row width of 76.2 cm. The additional agronomic details of the site during the period (2017-2020) are given in Table 3.1.

3.2.2. Climate

The climate data were collected from South Dakota Mesonet and SERF climate stations located near the study site. The 67-year (1953-2019) average monthly temperature and precipitation information were extracted from the SERF climate station to compare the observed weather conditions during the study period. The Köppen Climate Classification at the field site is continental with warm to hot summers and cold to severely cold winters. Mean daily temperature varied between -13.9°C (January) and 29.1°C (July). The average annual rainfall is about 655 mm with 69 mm (snow water equivalent) of the annual average snowfall (South Dakota Mesonet, 2020). Around 75% of this rainfall occurs during April to September growing season, making the fields suitable for corn-soybean production without irrigation. Maximum rainfall occurrence in June (111 mm), followed by May (92 mm) over slow permeable soil makes subsurface drainage beneficial for optimized growth of crops at the field site.

3.2.3. Soil and Water Samples Collection

Soil, water, and CC biomass samples were collected to study the influence of rye CC adoption on nutrients uptake, soil health, and WQ. Water samples of leached water were collected manually in plastic bottles weekly and during major precipitation events and stored frozen at -20°C, starting from spring 2018 to fall 2020. The US Environmental Protection Agency (EPA) approved methods were used to analyze nitrate-N (NO_3^-), ammonia-N (NH_4^+), and total nitrogen (TN) concentrations in the collected water samples using the AQ1 discrete analyzer (Seal Analytical Inc., WI). Filtered water samples, using 0.45 μm cellulose membrane filter, were analyzed for the NO_3^- and NH_4^+ concentrations, whereas, TN concentrations were determined using the 50 ml digested unfiltered samples.

Soil samples were collected in spring, summer, and fall every year from every plot at 0-15 cm depth. The composited soil samples were air-dried and passed through a 2 mm sieve for soil health assessment using Haney Soil Health Test (Haney et al., 2006) at Ward Lab (Ward Laboratories, Inc.). In this test, two nutrients extraction methods (H2O; water and H3A; organic acids) were used to analyze pH, electric conductivity (EC), SOM, CO_2-C, WETN, WEON, WETC, H3ANO3-N, H3ANH4-N, H3AIN, H3ATP, H3AIP, MAC, SHS, AvailN, and AvailP. Detailed knowledge for the used extractant can be found in Haney et al. (2006).

The CO_2-C was analyzed using an infrared gas analyzer (IRGA) Li-Cor 840A (LI-COR Biosciences, Lincoln NE). The water and H3A extracts were analyzed on a Lachat 8000 flow injection analyzer (Hach Company, Loveland CO) for H3ANO3-N, H3ANH4-N, and H3APO4-P. For analyzing water-extractable organic C and total N, Teledyne-

Tekmar Torch C:N analyzer was used. Soil health score (SHS) was calculated using
equation (1) shown below to include a weighted contribution of water-extractable organic
C (WEOC) and organic N representing the overall soil health. Available N and P
represent the amount of N and P_2O_5 in the soil as kg ha^{-1}.

$$SHS = \frac{CO_2-C}{10} + \frac{WEOC}{50} + \frac{WEON}{10} \quad (1) \qquad \text{(Haney and Haney, 2015)}$$

where SHS is the soil health score, CO_2-C is the soil respiration, WEOC is the water-extractable organic carbon, and WEON is the water-extractable organic nitrogen.

3.2.4. Statistical Analysis

The effect of CC and sampling time were determined by repeated measures
analysis using the PROC GLIMMIX option of SAS 9.4 version (SAS Institute, Cary, NC)
with time considered as the repeated measure with autoregressive 1 covariance structure
to account for unevenly spaced time periods. For soil health parameter analysis (SOM,
CO_2-C, WETN, WEON, WETC, H3ANO3-N, H3ANH4, H3AIN, H3ATP, H3AIP,
MAC, SHS, AvailN, AvailP), cover crop and time were considered as fixed effects. Mean
separation was performed with SAS PDMIX using Tukey's HSD test and mean
differences were considered statistically significant at α = 0.05.

3.3.   Results and Discussion

3.3.1. Weather and Winter Rye Biomass Production

Winter rye CC establishment and residual nutrient uptake were highly dependent
on weather conditions during the fall CC planting and spring periods in regions with
below zero temperature throughout the winters (Strock et al., 2004; Tonitto et al., 2006).
Spring temperatures are important for winter rye growth and development (Brockmueller,
2020). Interestingly, the study site faced abnormal and highly variable weather conditions

during three years of the study period, especially during spring. Weather conditions during the first two years of the study (2018 and 2019) were abnormally wet which received 205 mm and 154 mm higher annual precipitation than the 67-year average, respectively (Figure 3.1). However, the last year of the study period (2020) faced dry weather conditions which received 204 mm lower precipitation (31% less) than the 67-year average. Precipitation and soil moisture content are generally the most important factors in determining a successful establishment of rye (Wilson et al., 2013).

During October 2017, the study site received 65 mm higher precipitation than the 67-year average, resulting in high soil moisture conditions during the winter rye planting period. In addition, April of the following spring faced a 5°C lower temperature than the 67-year average (i.e., 8°C), which limited the growing degree-day (GDD; 1458 GDD) accumulation for winter rye CC by the time of termination. Lower than normal spring temperatures coupled with an unusual wet weather during the CC planting period affected winter rye establishment and resulted in low biomass production and low N-uptake (Table 3.2).

The Spring 2019 year received 112 mm higher precipitation than the 67-year average, of which 66 mm occurred only during May 2019. The high soil moisture conditions during May 2019 delayed the field operations for CC termination and soybean planting, which facilitated rye CC in gaining higher GDD accumulations (2042 GDD) and growth. As a consequence, the higher biomass production (1213 kg ha^{-1}) of winter rye resulted in higher N-uptake (Table 2) than that in 2018. Christianson et al. (2012) suggested that there is no negative effect of delay in rye termination on soybean yield.

Therefore, the growing period of rye CC growth can be extended in the spring to obtain potential water quality and soil health benefits.

The year 2020 started with a dry spring, receiving 53 mm and 39 mm lower precipitation during April and May, respectively, than the 67-year average. The observed dry conditions resulted in early winter rye termination (10 days and 32 days earlier than that in 2018 and 2019, respectively) to conserve soil moisture for the next corn crop. The early termination resulted in very limited GDD accumulation and lowered biomass production (Table 3.2) with 5.8 kg ha^{-1} N uptake by the time of winter rye termination. Farsad et al. (2011) explored the impact of delay in the planting of CC on accumulated GDD, biomass production, N uptake, and N losses using a spatial modeling approach. They observed a direct correlation among GDD, winter rye CC biomass, and nutrient recovery, and suggested a GDD range between 950 and 1100 as the critical value for an adequate rye CC biomass production and nutrient recovery. These researchers also reported a dramatic reduction in N accumulation with a reduction in accumulated GDD. However, in our study, the CC biomass production and nutrient recovery were very low even after accumulating higher GDD than the critical range during the 2017-2018 growing season (Table 3.2). The CC biomass productions and accumulated GDD under these extreme weather conditions indicated vulnerability of CC establishment and expected CC services with varying weather conditions of SD.

3.3.2. Water Quality

The NO_3^- concentrations in the subsurface drainage discharge were quite variable with peaks around the timings after fertilizer application. The maximum NO_3^- concentration of 28.5 mg l^{-1} was observed for the samples collected from NCC treatment

on June 23, 2020 as a combined result of the received 63 mm cumulative precipitation during June 18-21, 2020 and the Urea Ammonium Nitrate (UAN) application (65 kg ha^{-1} as N) on June 16, 2020. The higher nitrate losses occurred during the summer months when the study site received higher precipitation than the spring and fall periods. The general trend for the observed NO$_3^-$ concentrations (for 86% of samples) was well within the limits of EPA guidelines of drinking water (i.e., 10 mg l^{-1} of N), however, the freshwater aquatic life limit (i.e., 4.7 mg l^{-1} of N) was surpassed very frequently (for 61% of samples). These limits were generally exceeded during the May and June months due to high precipitation or the fertilizer applications during these months. Overall, the monthly average NO$_3^-$ concentrations were lower than the drinking water limit (10 mg l^{-1}) except June 2018 (Figure 3.2). In a similar study, conducted in Ontario, Canada, Drury et al. (2014) found 19% and 54% of tile drainage events exceeding the drinking water guidelines and freshwater guidelines, respectively.

Cover crops, when well established, are beneficial in enhancing soil organic carbon and reducing nitrate leaching. The statistical analysis of the leached NO$_3^-$ and TN concentrations under CC and NCC treatments revealed a trend inversely proportional to the CC biomass production. The significant reductions between CC vs. NCC for the leached NO$_3^-$ concentrations were found for September 2018 (~38% reduction) and June and July 2019 (~19% and 20% reduction, respectively), whereas, significant differences for TN concentrations were observed only during 2019 (8.5% reduction in May; 13% in June, and 16% in July; Figure 3.4). The NH$_4^+$ concentrations did not show any significant differences under CC and NCC treatments throughout the study period (Figure 3.3) due to lower susceptibility to loss by leaching. A significant reduction in NO$_3^-$ and TN

concentrations were observed during 2019 under CC treatment, pertaining to good

biomass growth which sequestered 18.8 kg of N ha^{-1}. In addition, the observed lower N

concentration i.e., 1.55% in CC biomass in 2019 might have possibly resulted in a slower

release of N during the summer months. The majority of the 2018 and 2020 periods

revealed a non-significant reduction in leached NO_3^- and TN concentrations due to

limited CC biomass growth, lessened N-uptakes, and higher N concentration in biomass

(~4%). In general, high or low precipitation during fall and/or spring coupled with low

spring temperature significantly influenced the CC establishment, biomass production,

and residual N-uptake by rye CC (Table 3.2). In a meta-analysis of 69 studies across the

United States, Tonitto et al. (2006) found that reduction in nitrate leaching due to cover

crop was related to its biomass production. Tonitto et al. (2006) reported the potential of

non-legume CC for 20 to 60 kg N ha^{-1} post-harvest N uptake and 40-70% nitrate leaching

reduction.

The benefits of CCs in reducing nutrient leaching and enhancing soil health are

limited in the NGP region due to the short and cold growing period of the cover crops

(Dinnes et al., 2002). Therefore, cold-tolerant species such as winter rye have been

suggested by various researchers for the NGP and Corn Belt regions (Christianson et al.,

2012; Snapp et al., 2005). However, soil temperature values of 1.1°C and 3.3°C are

needed for winter rye germination and vegetative growth, respectively (Appelgate et al.,

2017), these conditions make it vulnerable for winter rye to establish in the NGP. Strock

et al. (2004) analyzed the 41-yr weather data in Southwestern Minnesota (weather

conditions similar to our study) and concluded that winter rye may have a 25%

probability of favorable conditions for a successful establishment, which can be helpful

for reducing the nitrate losses. Kessavalou and Walters (1997) also reported the poor establishment of winter rye for 1 out of 3 years in eastern Nebraska due to the unusual cold weather during spring. Feyereisen et al. (2006) utilized a simulation model, RyeGro to quantify the potential of rye cover crop in nitrate reduction in the northern Corn Belt. The model simulated an average 4.6 kg N ha^{-1} reduction in nitrate losses through subsurface drainage in southwestern Minnesota if planted on 30 October and terminated on 15 May.

The NO_3^- leaching was also found to be significantly reduced under CC treatment during September 2018, which was an abnormally wet month with 100 mm higher precipitation than the 67-year average. The observed higher ($p \leq 0.10$) corn yield during 2018 under CC treatment (corn yield: CC = 11.8 Mg ha^{-1}; NCC = 11.6 Mg ha^{-1}) might have lowered the residual N in the CC than the NCC treatment. Drury et al. (2014) observed similar reductions in NO_3^- leaching where CC enhanced the crop yields under a controlled drainage system, which reduced the nitrate losses by 47%. Moreover, the Haney test results for soil samples revealed significantly higher residual plant-available N (Avail N; CC = 27.7 kg N ha^{-1}; NCC = 41 kg N ha^{-1}) and NO_3^--N (CC = 4 mg kg^{-1}; NCC = 5.32 mg kg^{-1}) under NCC compared to the CC treatment.

3.3.3. Soil Health

Soil health parameters measured in the study are presented in Table 3.3 and Table 3.4. Rye CC showed 13 and 11% significantly higher MAC and WEON, respectively, than the NCC treatment. Soil respiration (CO_2-C) and SHS varied significantly for rye CC and NCC treatments over time. Rye CC and NCC treatments showed significantly higher CO_2-C of 220.03 mg kg^{-1} and 222.27 mg kg^{-1}, respectively, around the time of

corn planting in May 2020 and post N fertilization in July 2018, whereas, comparatively lower values of CO_2-C under rye CC (59.9 mg kg^{-1}) and NCC (30.5 mg kg^{-1}) were observed in December 2018. Higher values of CO_2-C in May and July are suggestive of considerable microbial existence and activity with high potential for N mineralization, whereas, lower soil respiration is indicative of slower crop residue decomposition. Soil organic matter was significantly higher (55.7 g kg^{-1}) in November 2019 compared to all other time periods, which could potentially be due to the inclusion of soybean in the rotation that can intensify C mineralization because of the introduction of crop residues with a low C:N ratio, especially after corn.

The WETN and WETC were significantly higher around rye CC termination and corn planting in May 2020, suggesting the presence of inorganic and organic N and C sources in soil. The WEON was significantly greater in May 2020 and August 2020 than all other time periods, demonstrating the presence of an easily decomposed N form by soil microbes which are released to growing plants offering the minimal possibility of loss. Additionally, WEON can be strongly influenced by changes in N levels in soil, especially after the application of N fertilizer. Moreover, soil H3ANO3-N and H3ANH4-N (~15.2 and 46.2 mg kg^{-1}) were also considerably higher in May 2020 around corn planting and UAN fertilization than all other time periods. Throughout study duration, soil P ranged between medium to high category (i.e., 13-25, medium and 26-50 mg kg^{-1}, high). Based on the calculated soil health parameters, the SHS was significantly higher in May 2020 (SHS = 26.1) than all other time periods, and the lowest overall score was observed in December 2018 (SHS = 9.77). Based on the SHS2015 (soil health score version), scores above 7 indicate good soil health (Presley, 2016). Therefore, soil health

performed significantly well despite greater variation in precipitation throughout the study period. Available N was significantly higher in May 2020 (175.6 kg ha^{-1}) than all other time periods, which includes the inorganic N measured as nitrate and ammonium and the amount of N anticipated to be released from the organic N pool by microbial activity.

Overall, the majority of soil health parameters (e.g., CO_2-C, WETN, WETC, WEON, and SHS) being considerably higher in May 2020 than the other years are largely explained by and coincided with the substantial increase in rye CC biomass (1213 kg ha^{-1}) and soybean establishment. Whereas, the lack of significant differences between rye CC and NCC can be attributed to shorter study duration (3 years), suggesting that the length of CC management is also a major factor in providing soil health benefits (Daigh et al., 2018; Nouri et al., 2020). An insignificant increase in soil health parameters was observed under CC treatment compared to the NCC (e.g. SOM, CO_2-C, SHS, AvailN, AvailP, WETC, WETN, WEON, H3ANH4-N, H3ATP, H3AIP). The results with no significant differences among rye CC and NCC are in agreement with findings that demonstrated that SHS2015 scores did not differ among 4 years of CC treatments (Bavougian et al., 2019; Chu et al., 2019; Singh et al., 2020). The soil health parameters showed that the variation in soil health was constrained by both C- and N-related parameters, indicating the complete association of soil C and N status with soil health.

3.4. Conclusions

The present study was conducted to assess the impacts of winter rye as a cover crop on soil health and water quality parameters. Unusually high or low precipitation during fall and/or spring coupled with lower spring temperatures significantly influenced

CC establishment, biomass production, and residual N-uptake by rye CC that reflect the

vulnerability of CC establishment and expected CC benefits with varying weather

conditions of SD. Observed inadequate CC biomass production during 2018 and 2020

indicated the importance of management considerations for rye CC establishment under

extreme weather conditions. Moreover, observed significant reductions in leached NO_3^-

and TN concentrations during 2019 suggested that well-established rye CC could be a

useful management tool for reducing nutrient leaching and enhancing soil health for the

SD region.

In terms of soil health parameters, higher MAC and WEON values were observed

under rye CC than the NCC treatment, which indicated enhanced soil respiration and

availability of easily decomposed and released N by soil microbes to growing plants

resulting in the minimal possibility of loss. However, to observe the positive influence of

a rye CC on soil health parameters, a study for longer can be helpful.

References

Appelgate, S.R., Lenssen, A.W., Wiedenhoeft, M.H. and Kaspar, T.C. (2017). Cover crop options and mixes for upper midwest corn–soybean systems. Agronomy Journal, 109(3): 968-984.

Bavougian, C.M., Shapiro, C.A., Stewart, Z.P. and Eskridge, K.M. (2019). Comparing Biological and Conventional Chemical Soil Tests in Long-Term Tillage, Rotation, N Rate Field Study. Soil Science Society of America Journal, 83(2): 419-428.

Bergtold, J.S., Ramsey, S., Maddy, L. and Williams, J.R. (2017). A review of economic considerations for cover crops as a conservation practice. Renewable Agriculture and Food Systems, 34(1): 62-76.

Blann, K.L., Anderson, J.L., Sands, G.R. and Vondracek, B. (2009). Effects of agricultural drainage on aquatic ecosystems: a review. Critical reviews in environmental science and technology, 39(11): 909-1001.

Bosch, N.S., Allan, J.D., Selegean, J.P. and Scavia, D. (2013). Scenario-testing of agricultural best management practices in Lake Erie watersheds. Journal of Great Lakes Research, 39(3): 429-436.

Brockmueller, B. (2020). Management implications of a rye cover crop on nutrient cycling and soybean production in southeast South Dakota: focus on rye seeding rates and termination timing. Electronic Theses and Dissertations. 4094. https://openprairie.sdstate.edu/etd/4094.

Christianson, L., Castellano, M. and Helmers, M. (2012). Nitrogen and phosphorus balances in Iowa cropping systems: sustaining Iowa's soil resource, Proceedings of the Integrated Crop Management Conference. Iowa State University Extension Ames, IA.

Chu, M., Singh, S., Walker, F. R., Eash, N. S., Buschermohle, M. J., Duncan, L. A., & Jagadamma, S. (2019). Soil health and soil fertility assessment by the haney soil health test in an agricultural soil in west Tennessee. Communications in Soil Science and Plant Analysis, 50(9), 1123-1131.

CTIC (2017). SARE Annual Report 2016-2017 Cover Crop Survey. Joint publication of the Conservation Technology Information Center, the North Central Region Sustainable Agriculture Research and Education Program, and the American Seed Trade Association.

Daigh, A. L., Dick, W. A., Helmers, M. J., Lal, R., Lauer, J. G., Nafziger, E., ... & Cruse, R. (2018). Yields and yield stability of no-till and chisel-plow fields in the Midwestern US Corn Belt. Field Crops Research, 218, 243-253.

Dinnes, D. L., Karlen, D. L., Jaynes, D. B., Kaspar, T. C., Hatfield, J. L., Colvin, T. S., & Cambardella, C. A. (2002). Nitrogen management strategies to reduce nitrate leaching in tile-drained Midwestern soils. Agronomy journal, 94(1), 153-171.

Drury, C. F., Tan, C. S., Welacky, T. W., Reynolds, W. D., Zhang, T. Q., Oloya, T. O., ... & Gaynor, J. D. (2014). Reducing nitrate loss in tile drainage water with cover crops and water-table management systems. Journal of Environmental Quality, 43(2), 587-598.

Farsad, A., Randhir, T.O., Herbert, S.J. and Hashemi, M. (2011). Spatial modeling of critical planting date for winter rye cover crop to enhance nutrient recovery. Agronomy journal, 103(4): 1252-1257.

Feyereisen, G., Wilson, B.N., Sands, G.R., Strock, J.S. and Porter, P.M. (2006). Potential for a rye cover crop to reduce nitrate loss in southwestern Minnesota. Agronomy Journal, 98(6): 1416-1426.

Fraser, H. and Fleming, R. (2001). Environmental benefits of tile drainage: Literature review. Available at age-web. age. uiuc. edu/classes/age357/html/benefits% 20of% 20tile% 20drainage. pdf (accessed 7 Aug. 2011, verified 1 Oct. 2011). Univ. of Guelph, Guelph, ON, Canada.

Gunn, K. M., Fausey, N. R., Shang, Y., Shedekar, V. S., Ghane, E., Wahl, M. D., & Brown, L. C. (2015). Subsurface drainage volume reduction with drainage water management: Case studies in Ohio, USA. Agricultural water management, 149, 131-142.

Haney, R., Haney, E., Hossner, L. and Arnold, J. (2006). Development of a new soil extractant for simultaneous phosphorus, ammonium, and nitrate analysis. Communications in Soil Science and Plant Analysis, 37(11-12): 1511-1523.

Haney, R.L. and Haney, E.B. (2015). Estimating potential nitrogen mineralisation using the Solvita soil respiration system. Open Journal of Soil Science, 5(12): 319.

Kaspar, T., Jaynes, D., Parkin, T., & Moorman, T. (2007). Rye cover crop and gamagrass strip effects on NO3 concentration and load in tile drainage. Journal of Environmental Quality, 36(5), 1503-1511.

Kessavalou, A., & Walters, D. T. (1997). Winter rye as a cover crop following soybean under conservation tillage. Agronomy Journal, 89(1), 68-74.

Kladivko, E., Frankenberger, J., Jaynes, D., Meek, D., Jenkinson, B., & Fausey, N. (2004). Nitrate leaching to subsurface drains as affected by drain spacing and changes in crop production system. Journal of Environmental Quality, 33(5), 1803-1813.

Logsdon, S., Kaspar, T. C., Meek, D. W., & Prueger, J. H. (2002). Nitrate leaching as influenced by cover crops in large soil monoliths. Agronomy Journal, 94(4), 807-814.

Meisinger, J., Hargrove, W., Mikkelsen, R., Williams, J., & Benson, V. (1991). Effects of cover crops on groundwater quality. Cover crops for clean water, 57-68.

Nouri, A., Lee, J., Yoder, D. C., Jagadamma, S., Walker, F. R., Yin, X., & Arelli, P. (2020). Management duration controls the synergistic effect of tillage, cover crop, and nitrogen rate on cotton yield and yield stability. Agriculture, ecosystems & environment, 301, 107007.

Presley, D. (2016). Effects of flue gas desulfurization gypsum on crop yield and soil properties in Kansas. Kansas Agricultural Experiment Station Research Reports, 2(5), 3.

Ruffo, M. L., Bullock, D. G., & Bollero, G. A. (2004). Soybean yield as affected by biomass and nitrogen uptake of cereal rye in winter cover crop rotations. Agronomy Journal, 96(3), 800-805.

Saadat, S., Bowling, L., Frankenberger, J., & Kladivko, E. (2018). Nitrate and phosphorus transport through subsurface drains under free and controlled drainage. Water research, 142, 196-207.

Singer, J., Nusser, S., & Alf, C. (2007). Are cover crops being used in the US corn belt? Journal of Soil and Water Conservation, 62(5), 353-358.

Singh, S., Nouri, A., Singh, S., Anapalli, S., Lee, J., Arelli, P., & Jagadamma, S. (2020). Soil organic carbon and aggregation in response to thirty-nine years of tillage management in the southeastern US. Soil and Tillage Research, 197, 104523.

Smith, D. R., Francesconi, W., Livingston, S. J., & Huang, C.-h. (2015). Phosphorus losses from monitored fields with conservation practices in the Lake Erie Basin, USA. Ambio, 44(2), 319-331.

Snapp, S., Swinton, S., Labarta, R., Mutch, D., Black, J., Leep, R., . . . O'neil, K. (2005). Evaluating cover crops for benefits, costs and performance within cropping system niches. Agronomy Journal, 97(1), 322-332.

Steenwerth, K., & Belina, K. (2008). Cover crops and cultivation: Impacts on soil N dynamics and microbiological function in a Mediterranean vineyard agroecosystem. Applied Soil Ecology, 40(2), 370-380.

Strock, J. S., Porter, P. M., & Russelle, M. (2004). Cover cropping to reduce nitrate loss through subsurface drainage in the northern US Corn Belt. Journal of Environmental Quality, 33(3), 1010-1016.

Tonitto, C., David, M., & Drinkwater, L. (2006). Replacing bare fallows with cover crops in fertilizer-intensive cropping systems: A meta-analysis of crop yield and N dynamics. Agriculture, ecosystems & environment, 112(1), 58-72.

Trujillo Cabrera, L. (2002). Fluxos de nutrientes em solo de pastagem abandonada sob adubação orgânica e mineral na Amazônia Central.

Wilson, M. L., Baker, J. M., & Allan, D. L. (2013). Factors affecting successful establishment of aerially seeded winter rye. Agronomy Journal, 105(6), 1868-1877.

Wyland, L., Jackson, L., Chaney, W., Klonsky, K., Koike, S., & Kimple, B. (1996). Winter cover crops in a vegetable cropping system: Impacts on nitrate leaching, soil water, crop yield, pests and management costs. Agriculture, ecosystems & environment, 59(1-2), 1-17.

Zimnicki, T., Boring, T., Evenson, G., Kalcic, M., Karlen, D. L., Wilson, R. S., . . . Blesh, J. (2020). On quantifying water quality benefits of healthy soils. BioScience, 70(4), 343-352.

Table 3.1. Detailed agronomic information adopted during the study period.

Operations	2017-2018	2018-2019	2019-2020
CC Planted	10/24/2017	10/22/2018	10/24/2019
CC Sprayed Out	05/16/2018: before planting corn	06/08/2019: after Soybean planting	05/06/2020
Crop Planted	05/17/2018: Corn	06/05/2019: Soybean	05/07/2020: Corn
Fertilization	05/16/2018: UREA at 46.5 kg/ha as N, AMS 45 kg/ha using commercial spreader	-	04/07/2020: UREA at 90 kg/ha as N using commercial spreader
	05/17/2018: UAN surface band at planting; 56 kg/ha N	-	
	06/25/2018: UAN sidedress at 140 l/ha (51 kg/ha as N)	-	6/16/2020: UAN sidedress at 187 l/ha (65 kg/ha as N)
Harvest	10/17/2018	10/18/2019	10/13/2020

Note: CC, Cover Crop; UAN, Urea Ammonium Nitrate

Table 3.2. Winter rye cover crop achieved growing degree days, biomass production, and nitrogen concentration during the study period for 2017 through 2020.

Year	Growing Degree Days	CC[†] Biomass kg ha^{-1}	N-concentration %	N-uptake kg ha^{-1}
2017-2018	1458	251	4	10
2018-2019	2042	1213	1.55	18.8
2019-2020	794	147	4	5.8

[†]CC, Cover Crop; N, Nitrogen

Table 3.3. Haney soil health indicators as influenced by cover crop (CC) and no cover crop (NCC) treatments.

Treatment	Soil parameters				
	SOM† (%)	MAC (%)	AvailN (kg ha^{-1} N)	AvailP (kg ha^{-1} P$_2$O$_5$)	WETN (mg kg^{-1})
NCC	4.73	56.17^b	77.16	45.07	29.16
CC	4.82	63.49^a	79.82	52.52	29.27
			p-value		
Treatment	0.2643	0.044*	0.594	0.487	0.9152
Time	<0.0001	<0.0001	<0.0001	0.0001	<0.0001
Treatment X Time	0.9643	0.213	0.191	0.633	0.4688

†SOM, soil organic matter; MAC, microbially active carbon; AvailN, available nitrogen; AvailP, available phosphorus; WETN, water-extractable total nitrogen.

*Significant at p ≤ 0.05.

Table 3.4. H3A-extractable Haney soil health indicators as influenced by cover crop (CC) and no cover crop (NCC) treatments.

Treatment	Soil parameters				
	H3ANO3-N[†]	H3ANH4-N	H3AIN	H3ATP	H3AIP
	—————————— (mg kg^{-1}) ——————————				
NCC	5.28	17.81	23.09	3.923	13.046
CC	5.17	16.99	22.17	3.925	15.14
	p-value				
Treatment	0.76	0.7381	0.6912	0.5216	0.562
Time	<0.0001	<0.0001	<0.0001	0.0002	0.0005
Treatment X Time	0.298	0.1754	0.229	0.597	0.507

[†]H3ANO3-N, nitrate; H3ANH4-N, ammonium, H3AIN, inorganic nitrogen, H3ATP, total phosphorus, H3AIP, inorganic phosphorus.

Table 3.5. Haney soil health score in response to cover crop (CC) and no cover crop (NCC) treatments.

Treatment	CO_2-C[†]	WETC	WEON	SHS
	——— (mg kg^{-1}) ———			
NCC	133	238.1	15.22[b]	17.09
CC	147.07	237.8	16.9[a]	18.55
	p-value			
Treatment	0.2711	0.9725	0.0198*	0.14
Time	<0.0001	<0.0001	<0.0001	<0.0001
Treatment X Time	0.0489	0.162	0.76	0.059

[†]CO_2-C, soil respiration; WETC, water-extractable total carbon; WEON, water-extractable organic nitrogen; SHS, Soil health score.
*Significant at $p \leq 0.05$.
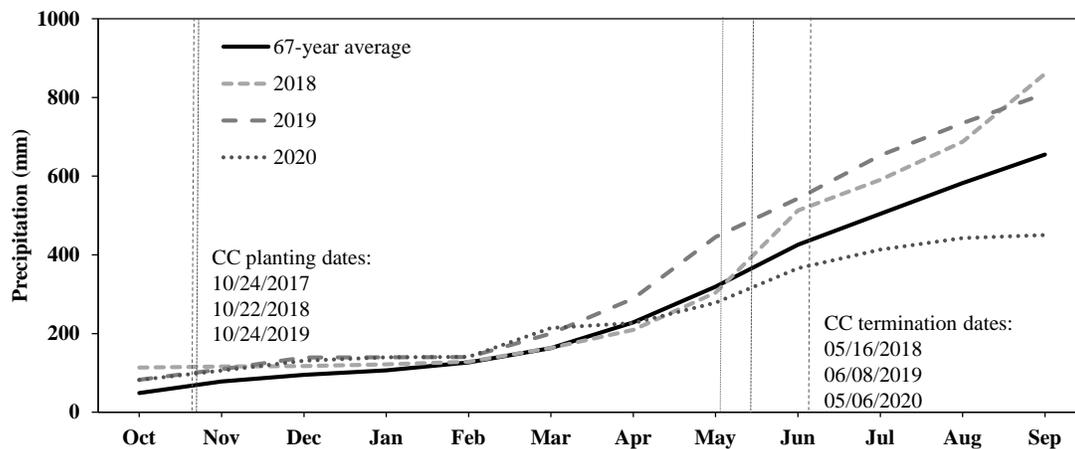
Fig. 3.1. Monthly cumulative precipitation (2018-2020) with 67-year (1953-2019) monthly average values at Southeast Research Farm, Beresford, South Dakota. Plotted as the hydrologic year (October to September). (Note: CC, cover crop).
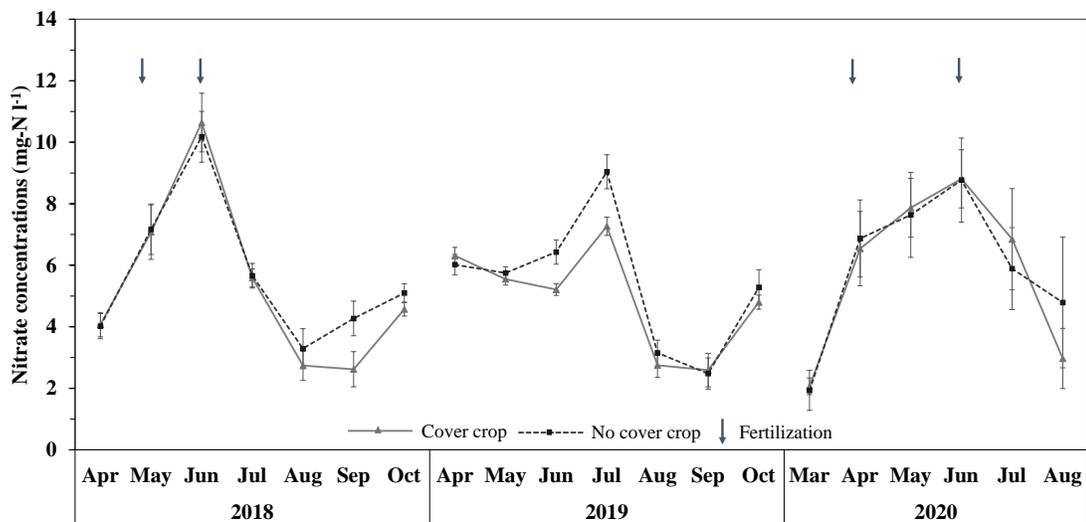
Fig. 3.2. Average monthly nitrate-N losses from 2018 through 2020 through the subsurface drainage under cover crop and no cover crop treatments. The bars show standard errors and inverted arrows indicate the fertilization events.
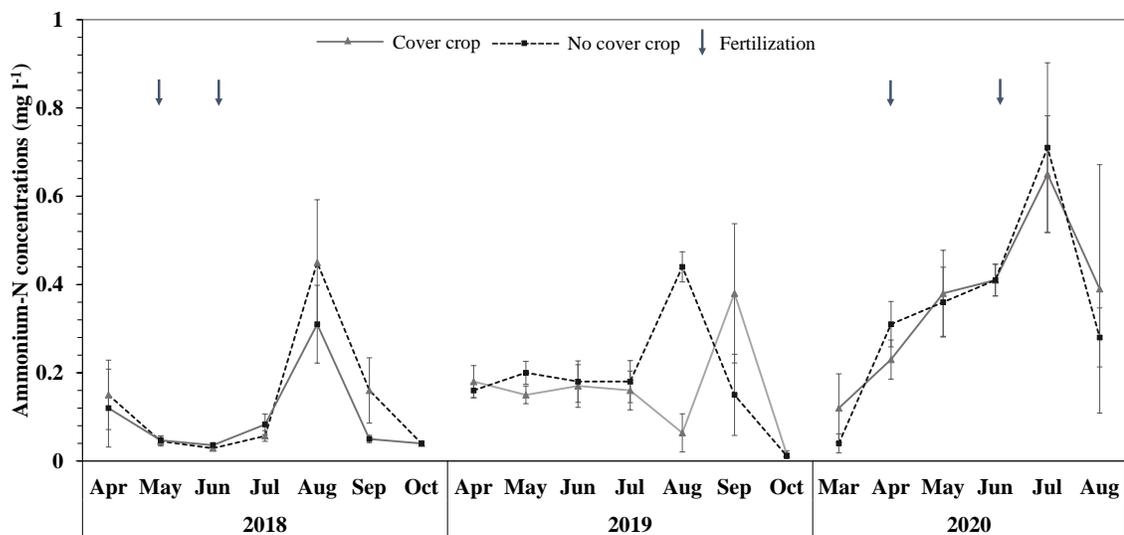
Fig. 3.3. Average monthly ammonium-N losses from 2018 through 2020 through the subsurface drainage under cover crop and no cover crop treatments. The bars show the standard errors and inverted arrows indicate the fertilization events.
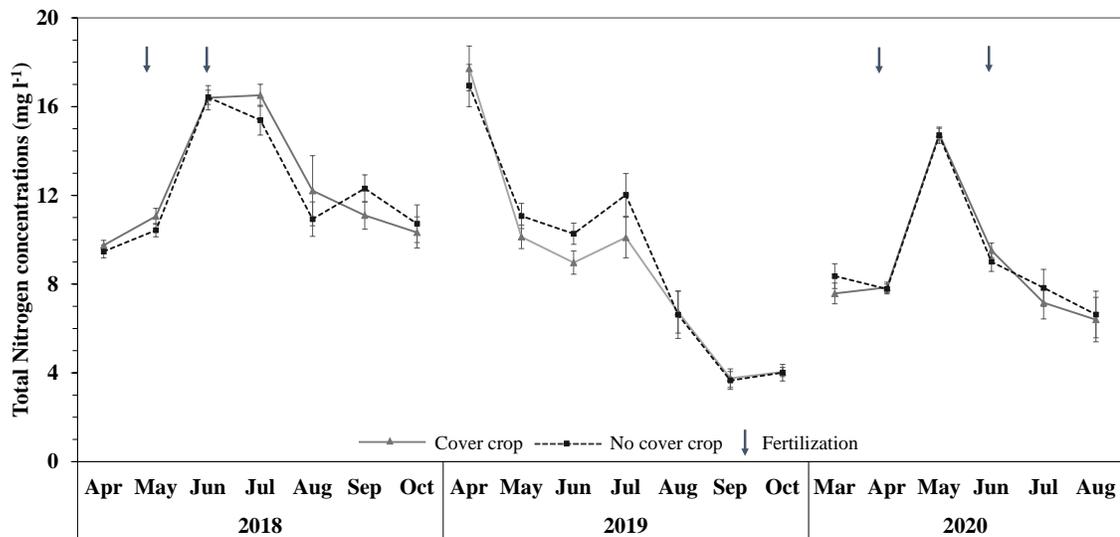
Fig. 3.4. Average monthly total nitrogen losses from 2018 through 2020 through the subsurface drainage under cover crop and no cover crop treatments. The bars show standard errors and inverted arrows indicate the fertilization events.

CHAPTER 4

SIMULATING HYDROLOGICAL RESPONSES OF INTEGRATED CROP-LIVESTOCK SYSTEMS UNDER FUTURE CLIMATE CHANGES IN AN AGRICULTURAL WATERSHED

ABSTRACT

Land use land cover (LULC) and climate are the determinant factors for the soil water balance. The combined effect of LULC and climate change is of great importance for effective water resources planning and management. This study assessed the hydrological impact of long-term implementation of integrated crop-livestock (ICL) system with the projected climate scenarios on water yield using the Soil and Water Assessment Tool (SWAT) model over two time periods [*i.e.* Near Future (2021-2050) and Far Future (2070-2099)]. This study was conducted in three phases over Skunk Creek watershed (SCW), South Dakota, USA. In phase I, the impact of long-term ICL system implementation (1976-2005; 30 years) on soil hydrology was evaluated. Phase II and phase III evaluated the impacts of projected climate changes under existing land cover and ICL system, respectively. Outcomes of phase I showed a significant decrease in water yield and surface runoff. Phase II showed the susceptibility of SCW to extreme events such as floods and waterlogging during spring, and droughts during summers under the projected climate changes. Phase III showed the reduction in water yield and surface runoff due to the ICL system and minimizing the induced detrimental impacts only due to climate change. This study provides a perspective on the possible impacts of the ICL system to mitigate the hydrological alteration due to climate change.

4.1. Introduction

High concentration of greenhouse gases (GHGs) in the atmosphere due to anthropogenic activities affects the radiative forces in Earth's environment, which alters temperature and precipitation patterns (Solomon et al. 2007; Pachauri et al. 2014). According to Fisher et al. (2007), radiative forcing in 2100 could be found from 2.5 W/m^2 to 9 W/m^2 or higher, depending upon what GHGs emissions and mitigation scenarios are being simulated. Intergovernmental Panel on Climate Change (IPCC) reported an increase of 0.3 to 4.8°C in the mean surface temperature, based on the radiative forcing, by the end of 21st century (Van Vuuren et al. 2011). Over the last few decades, studies linked climate shifts and their impacts on the hydrological cycle, economy, ecology, and biodiversity at regional and global scales (Field 2014; El-Khoury et al. 2015; Ficklin et al. 2009; Groisman et al. 2001). Changes in natural systems are the strongest and the most comprehensive pieces of evidence of the climate change impacts. A global temperature increase may lead to the intensification of the hydrological cycle by changing precipitation amounts, evapotranspiration rates, and snowmelt periods (Stagl et al. 2014; Van Vliet and Zwolsman 2008, Bawa et al. 2021). According to the Fourth National Climate Assessment report (USGCRP, 2018), the Midwest USA is becoming more vulnerable to climate change impacts such as drought, floods, and extreme heatwaves. Many hydro-climatological studies have been conducted to understand the impacts of increased air temperatures on regional hydrological cycles in the Midwest and Great Plains (Changnon and Kunkel 1995; Chien et al. 2013; Ahiablame et al. 2017; Gautam et al. 2018). These studies demonstrated earlier snowmelts due to increased spring temperatures, decreased summer precipitations, and increased annual

evapotranspiration (ET) caused by changing climate. Subsequently, there will be reduced availability of water during summer and increased floods during spring in the region. These studies emphasized the need for early development of land-use and management of water resources to mitigate and better respond to climate change and its associated consequences. The fifth phase of the Coupled Model Intercomparison Project (CMIP5) by IPCC provided new representative concentration pathways (RCP) based on total radiative forcing by the end of the 21st century with remarkable information about climate parameters at a very fine spatial resolution (Collins et al. 2013). The availability of projected climate data and scenario-based hydrological modeling approaches provide an opportunity to quantify the climate change impacts and understand possible scenarios to minimize resulting negative impacts.

In addition to climate, land use and land cover (LULC) is another determinant factor for water balance. Increasing demand for food supply with increasing population can amplify these impacts by changes in LULC. Intensification and expansion of farming to meet future food demands need sufficient water supplies to ensure the survival of crops and livestock (McNeill et al. 2017). LULC plays a vital role in increasing or decreasing the drainage density and storing the water into the soil (de Wit and Stankiewicz 2006). Agricultural practices with high production and low adverse environmental impacts such as integrated crop-livestock (ICL) systems are being promoted as an eco-friendly and cost-effective production system in Midwest, USA to replace the traditional production systems (Pérez-Gutiérrez and Kumar 2019). However, the potential effects of ICL systems on hydrological cycles have not been fully evaluated. In a simulation study, Pérez-Gutiérrez and Kumar (2019) found that introducing grazing for long-term in a

cropping system may improve the storage and transit system of water in the soil and subsequently reduce surface runoff and water yield at a watershed scale.

Land management practices such as grazing can significantly alter soil physical properties (Drewry et al. 2008; Taghizadeh-Mehrjardi et al. 2019; Liebig et al. 2004), and hence the water yield. Grazing impacts on soil hydraulic properties depend on various factors such as type of animal, the number of animals, grazing period, soil moisture content, and soil texture (Bilotta et al. 2007; Pulido et al. 2018). Sulc and Tracy (2007) summarized the potential effects of introducing diversification in the agricultural systems through grazing operations across the U.S. Corn Belt. They reported that animal traffic compactions and detrimental crop yields can be avoided by restricting the grazing operation periods when soil is dry and frozen. While fields under heavy grazing experience increased bulk density and soil compression with reduced infiltration (Liebig et al. 2014; Kumar et al. 2010), the lightly grazed fields under dry and frozen soil may not introduce any significant changes in soil physical properties. Knowledge of hydrological responses with soil physical properties under ICL systems can help in making future land-use management decisions and improving agricultural production with economic decision support. Therefore, understanding the relative hydrological impact of implementing favorable agricultural practices such as ICL systems in a changing climate can lead to the sustainable and effective management of water resources. The success of this management is critical to meet future food security goals and protecting the environment.

The objective of this study is to analyze the potential impacts of long-term usage of ICL system under future climate scenarios on water yield and its hydrological

components (*i.e.,* surface runoff, lateral flow) along with ET using the Soil and Water

Assessment Tool (SWAT).

4.2. Materials and Methods

4.2.1. Study Area

Skunk Creek is a watershed of the Big Sioux River basin and is located in the

southeast portion of South Dakota with approximately 1,606 km^2 of the drainage area

(Figure 4.1). This agriculture dominated watershed has a relatively flat landscape ranging

from 427 m to 572 m. Based on the 2008 cropland data layer (USDA NASS Cropland

Data Layer, 2018), the major land uses over the watershed are corn (*Zea mays* L.; 38%),

soybean (*Glycine max* (L.) Merr.; 27%) and pasture (26%). Most of the producers in the

watershed adopt a two-year corn-soybean crop rotation. Besides that crop residue

management conservation practices (no-till or other conservation tillage system) are

mostly adopted considering major resource concerns such as water and wind erosion, soil

moisture losses, and maintaining soil quality. The watershed area contains highly

productive glaciated soils mainly belonging to hydrologic soil group B (~70.3%).

Environmental Protection Agency has designated the Skunk Creek as an important source

of irrigation water, fishing and wildlife, and other recreational activities in the area

(South Dakota surface water quality assessment report, 2020). The average annual

rainfall in the watershed is 669 mm with an average annual snowfall of 1120 mm, and the

daily air temperature varies between -14°C (minimum temperature observed in January)

to 29°C (maximum temperature observed in July) (South Dakota Mesonet, 2020).

4.2.2. SWAT- Hydrological Model

SWAT is one of the most widely used hydrological models to study the impacts of land management practices on hydrology and water quality at the watershed scale over long time-periods (Arnold et al. 2013). SWAT comprises two modeling phases: land phase modeling and water balance modeling (Neitsch et al. 2011). Land phase modeling delineates the watershed of interest and divides it into sub-watersheds based on a required threshold area. These sub-watersheds are further partitioned into small hydrologic response units, which are a unique combination of land cover, soil type, and slope. After the land phase modeling, SWAT considers several physical processes including surface and subsurface runoff, infiltration, evapotranspiration, soil storage, and groundwater recharge. Then, it applies a water balance in the soil profile to simulate the in-land hydrological cycle (Arnold et al. 2012). The water balance equation used by SWAT for simulation of the hydrological cycle is:

$$SW_t = SW_0 + \sum_{i=1}^{t} (R_{day} - Q_{surf} - E_a - w_{seep} - Q_{gw})$$

(1)

where SW_t is soil water content (mm) after time t, SW_0 is initial soil water content (mm) on day i, R_{day} is the precipitation amount (mm) on day i, Q_{surf} is the surface runoff amount (mm) on day i, E_a is the evapotranspiration amount (mm) on day i, w_{seep} is water entering amount (mm) to the vadose zone of soil profile on day i, Q_{gw} is the return flow amount (mm) on day i and t is time in days. The Soil Conservation Service curve number (CN) method (Cronshey et al. 1985) is used to estimate surface runoff. This method considers the parameters which control the hydrological cycle such as land use and soil information with moisture and energy inputs from climate data to calculate the curve number, initial and maximum surface storage, and surface runoff (Neitsch et al. 2011).

4.2.3. SWAT Input Data

The SWAT model for the Skunk creek watershed was built using the ArcSWAT 2012 version. The major inputs required for setting up the model include digital elevation model (DEM), soil data, land cover data, and climate datasets. A DEM with 30m spatial resolution for the year 2008 obtained from U.S. Geological Survey- National Elevation Dataset (USGS-NED) (Archuleta et al. 2017) was used to delineate the watershed and define the stream network within the watershed while considering its outlet at 43.53°N and 96.79°W. SWAT partitioned the watershed into 75 sub-basins with the given threshold area of 1000 ha. A soil map extracted from the Soil Survey Geographical Database (SSURGO) through the U.S. Department of Agriculture - Natural Resources Conservation Service (USDA - NRCS) and the cropland data layer (CDL) of a 30m spatial resolution for the year 2008 obtained from the USDA- National Agricultural Statistics Service (USDA-NASS) was used for the further partition of sub-basins into 2510 hydrological response units (HRUs). The 2008 cropland data layer was the earliest available layer for the region. Subbasin area thresholds of 5, 10, and 10% for land use, soil, and slope, respectively, were used to simplify spatial complexity of watershed by avoiding minor land uses, soil, and slope ranges and redistributing those to the simulated HRUs.

For the baseline scenario, daily-observed climate data including precipitation, minimum and maximum temperature for four stations that fall within and nearby the Skunk Creek watershed were used as the fourth main input for the model. The daily weather data for years 1971–2005 were acquired from NOAA's (National Oceanic and Atmospheric Administration) National Centers for Environmental Information (NCEI)

and USDA-Grassland Soil and Water Research Laboratory datasets. The SWAT weather generator internally estimated additional climate information, including relative humidity, wind speed, and solar radiation.

To assess the potential impacts of future climate scenarios, climate projection data from CMIP5- Bias-corrected Constructed Analog (BCCA) was used. The data include new Global Circulation Models (GCMs) and provide bias-corrected and downscaled data to a spatial resolution of 12 km. The key variable for the GCMs in CMIP5 is projected greenhouse gas emissions and its concentrations in the atmosphere, based on which the IPCC constructed four RCPs to replace the previous emission scenarios. Ruane and McDermid (2017) discussed an approach (Representative Temperature and Precipitation GCM Subsetting Approach) to select a subset of GCMs and avoid the computational complexity introduced by using the full ensemble GCMs. The approach suggests a quantitative selection (cool/wet, cool/dry, middle, hot/wet, and hot/dry) of GCMs. The study considered four GCMs models to capture the variability and to cancel out the model biases induced in the climate data. The considered four GCMs belongs to two climate modeling groups (Table 4.2). Among the selected GCMs, two GCMs are associated with higher simulated precipitation and the other two models with lower simulated precipitation. An additional bias correction approach (explained in the "climate data and bias correction method" section) was used to further remove the associated temperature and precipitation biases. The BCCA downscaled climate data for four RCPs from four GCMs were obtained from downscaled CMIP3 and CMIP5 climate and hydrology projections archive (Pachauri et al. 2014; Maurer et al. 2007; Brekke et al. 2013) which resulted in 16 unique climate projection datasets for the study. The climate

data at Brekke et al. (2013) archive was bias-corrected and downscaled using the climate data from Livneh et al. (2013) as a training set. Predicted carbon dioxide (CO_2) levels with respect to each GCM, RCP, and simulation period was also considered accounting for the impact of CO_2 changes on plant growth and ultimately on evapotranspiration and hydrological cycle. The Penman-Monteith method incorporated in the SWAT model was used to estimate potential evapotranspiration as this method accounts for the CO_2 changes with other climate changes (Neitsch et al. 2011).

4.2.4. SWAT Model Setup, Calibration, and Validation

The baseline scenario was assembled using NASS-2008 land use and NOAA climate data for the period of 1976-2005 with 5-years (1971-1975) warm-up period. All the simulated scenarios were constructed regarding the baseline model. As recommended by Ahiablame et al. (2017), the execution decision for the calibration should be based upon the intended level of analysis and objectives of the study. As the goal for this study was the long-term impacts of climate and ICL system on water yield, streamflow from a single outlet can be used for calibration rather than using a relatively rigorous multi-scale calibration approach. The model was calibrated and validated using mean monthly-observed streamflow from USGS gauge station - 06481500 located at the outlet of the delineated Skunk Creek watershed. The calibration and sensitivity analysis were performed using the SWAT Calibration Uncertainty Programs (SWAT-CUP) tool (Abbaspour 2013). An automatic parameter optimization using Sequential Uncertainty Fitting version 2 (SUFI-2) optimization algorithm was used for sensitivity analysis and to fine-tune the calibration parameters. The calibration and validation periods, calibration parameters, and their initial ranges were selected from existing literature on Skunk Creek

watershed and nearby watersheds (Mehan et al. 2016; Neupane and Kumar 2015; Paul, Rajib, and Ahiablame 2017; Pérez-Gutiérrez and Kumar 2019; Ahiablame et al. 2017). After sensitive analysis using the one-at-a-time approach, 23 parameters were finalized to perform a calibration.

A combination of subjective and objective techniques was used to check the agreement of simulated data with the corresponding observed data. For a preliminary comparison, time series plots for observed and simulated flows were generated for visual assessment of the superposition of rising or falling limbs with under- and over-prediction of base and peak flow. Further, to evaluate the accuracy of the model to simulate streamflow three statistical indicators (NSE, r^2, PBIAS) were used. Nash-Sutcliffe Efficiency (NSE) was used as the objective function to measure the fit between the observed and simulated flow. Coefficient of determination (r^2) and Percent Bias (PBIAS) were also used to check the goodness of fit. The NSE ranges from $-\infty$ to 1.0 and provides a relative comparison of the variance of simulated and observed data. PBIAS index represents the under- or over-estimation of simulated data than the observed data. A PBIAS value of 0 for simulated data indicates a perfect fit. As suggested by previous hydrological model studies (Moriasi et al. 2007; Engel et al. 2007), a value higher than 0.5 for NSE and r^2 with PBIAS value within -15% to 15% can be considered as a good fit and satisfactory model performance.

4.2.5. Scenarios Definition

The SWAT model for Skunk Creek watershed was established for baseline scenario (1976-2005) in monthly time steps with a 5-year warm-up period (1971-1975) and used to simulate 66 scenarios considering all future climate and ICL system scenarios

(Table 1A). The study was divided into three phases. The first phase covered simulating the effect of ICL systems implemented over the watershed without considering climate change effects. We considered a conventional cropping system (corn[*Zea mays* L.]-soybean[*Glycine* max (L.) Merr.]; 2-year rotation) integrated with light grazing of corn residues (one cow per hectare grazing corn residues for 55 days), with the assumption of no change in soil physical properties (Singh et al., 2020). Additional information for the crop and grazing management operations are described in Table 4.1. The second phase includes projected climate changes while considering current agricultural practices over the entire period. Although the SWAT model allows using the dynamic LULC during the simulations, the projected LULC maps were not considered in this study due to the following two reasons: 1.) projected LULC maps were covering a part of the study region (~80%) and 2.) projected LULC maps have not shown any major changes in the agricultural area, which covers around 90% of the SK watershed. The third phase considered the combined effect of ICL systems and projected climate changes, where all corn and soybean agricultural practices were replaced with ICL practices. All future scenarios were constructed using two periods *i.e.* near future (2021-2050) and far future (2070-2099) with 16 unique climate datasets from four GCMs. The periods of near future (NF) and far future (FF) were selected based on radiative forces variation within the RCPs over 2021 to 2099. SWAT considers several management practices to simulate water quantity and quality. However, only crop operation and cycle management practices like crop rotation, planting, fertilizer applications, killing and harvesting with grazing operations were considered for the representation of the considered ICL system in SWAT (Table 4.1).

4.2.6. Climate Data and Bias Correction Method

Bias-corrected and downscaled (spatial resolution: 12km) climate data for precipitation and temperature for many GCM climate models can be obtained from the CMIP5-BCCA archive (Maurer et al. 2007; Brekke et al. 2013). The GCM models simulation tools are based on oceanic circulation models coupled with atmospheric circulation models. In this study, 16 projected climate datasets from the four GCMs for four emission scenarios were used (Table 4.2).

The climate projections available in the CMIP5-BCCA archive are bias-corrected and downscaled. However, the downloaded data was still associated with biases for the Skunk Creek watershed region. Therefore, these data were further bias corrected using modified quantile mapping techniques for precipitation data and delta method for temperature data as recommended by Gautam et al. (2018) and Shrestha et al. (2019). In the delta method, monthly means of observed temperature data were used to match and correct the simulated temperature data by developing a correction factor from historic observed and simulated temperature data (Ramírez Villegas and Jarvis 2010). The equation used to develop the correction factor for each month is:

$$T_c = \frac{\sum_{C=1}^{C_i} T_{ij} - \sum_{C=1}^{C_i} \widehat{T_{ij}}}{C_{ij}} \tag{2}$$

where T_c is the correction factor (°C), T_{ij} is the daily-observed temperature data (°C), $\widehat{T_{ij}}$ is daily-simulated temperature data (°C) on day i in month j, C_{ij} and C_i are the total number of days in month j. The calculated correction factor is an additive term, which can be used for linear shifting of simulated data toward more realistic temperature scenarios, as represented in equation 3.

$$T_{ij} = \widehat{T_{ij}} + T_c \tag{3}$$

The precipitation data biases were corrected in two steps using the quantile mapping (Maraun 2013; Grillakis et al. 2017; Grillakis et al. 2013). The CMIP5-BCCA simulated precipitation data contains two major limitations: numerous drizzle days and underestimated extreme events. In the first step, the number of precipitation days in simulated data was reduced using a precipitation threshold value developed from the relative comparison of observed and simulated precipitation data on a monthly basis. Precipitation days below the threshold values were removed and categorized as no precipitation. A scaling factor (developed using the quantile mapping method) was estimated to limit the extreme precipitation events based on observed historical data. This scaling factor was calculated for each month by dividing the maximum precipitation within that month over observed data with the maximum precipitation over simulated data for the same month.

The RCPs were established at different levels of GHGs and their increasing and decreasing rates in the environment. The increased CO_2 concentrations can affect plant growth and evapotranspiration. Considering this fact, different CO_2 concentrations were considered while simulating the scenarios for future and historical scenarios. The CO_2 concentration values were obtained from RCP database 2.0 (http://tntcat.iiasa.ac.at/RcpDb/), which provides the related information about each emission scenario, its development process, and considered assumptions. From this database, CO_2 concentrations at the end of the decade over the Skunk Creek watershed region for the years 1971-2099 were acquired and an average value of CO_2 concentration for the simulation period was used. Table 4.3 shows the details of used CO_2 concentration levels for each RCP. SWAT limits the maximum CO_2 concentrations to 800 ppm,

therefore for the far future scenarios (2070-2099) under RCP 8.5, 800 ppm concentration level was used instead of 804 ppm.

4.3. Results

4.3.1. Calibration and Validation of SWAT Model for Skunk Creek Watershed

The model was calibrated and validated for the monthly streamflow at the outlet of Skunk Creek watershed (USGS-06481500). These two steps ascertain the performance of the model to represent the hydrological responses of the watershed. The performance of the model was judged based on model evaluation criteria suggested in previous hydrological model studies (*e.g.,* Engel et al., 2007; Moriasi et al., 2007). A total of 23 soil and hydrological parameters were used to achieve satisfactory calibration and validation. The optimum values with the considered initial ranges of these calibration parameters are in Table 2A. The hydrographs for observed and simulated streamflow for calibration and validation periods with the statistics (R^2, NSE, and PBIAS) are shown in Figure 4.2. The statistics values suggest that the SWAT model for the calibrated and validated Skunk Creek watershed simulated the streamflow very well.

4.3.2. Future Climate Projections

Projected minimum and maximum temperatures were associated with biases. The CCSM-GCM simulated temperatures were over-predicted during January through September and under-predicted during the remaining months. The temperature during February was associated with maximum biases. An additive temperature correction factor was calculated for each month, as explained in the previous section, and used to remove associated biases. Figure 4.3 shows the monthly mean of simulated maximum and

minimum temperature before and after temperature corrections with the observed

temperature over the historical period (1976-2005) for RCP 4.5 of CCSM 4.1 GCM.

The ensemble means temperature for the near future and the far future revealed an

increasing trend. For the NF period, RCP 6.0 resulted in a minimum temperature

increment of 1.24°C, while RCP 8.5 caused a maximum temperature increment of

1.66°C. Similarly, for the FF period, the minimum temperature increment would be for

RCP 2.6 (1.25°C) and the maximum temperature increment would be for RCP 8.5

(4.44°C). The results for temperature increment are consistent with the GHG

concentration variations over the period. Most significant changes were observed in RCP

8.5 which consider a rapid increment in GHG concentration in the environment and

represents a failure to prevent global warming (Riahi et al. 2011). The RCP 6.0

considered the lowest radiative forces in the near future and resulted in the lowest

temperature change for the same period (Masui et al. 2011). However, the GHGs

concentrations increase rapidly under this scenario and only stabilize after the 21st

century. Under RCP 4.5, radiative forces are considered to be stabilized (peaked in 2080)

before the end of the century (Thomson et al. 2011) and showed less temperature

increment as compared to the RCP 6.0. The RCP 2.6 is considered as a peak and decline

climate scenario, as it touches its peak of radiative forces in the NF period and then

shows a continuous decrement in radiative forces and GHGs concentrations in the

environment (Van Vuuren et al. 2011). Subsequently, a decrease in temperature in the far

future over the study watershed was observed for RCP 2.6 (1.34°C in NF and 1.25°C in

FF). Maximum temperature increment was observed for January month for both NF and

FF periods under all four RCPs.

Similarly, simulated precipitation was also associated with two types of biases.
First, the simulated precipitation from CMIP5-BCCA GCMs was under-predicted for
extreme events. Second, it had a large number of drizzle days. In a review paper,
Gutmann et al. (2014) discussed similar limitations associated with the CMIP5-BCCA
downscaled climate data. Using the threshold values of precipitation developed from the
quantile mapping approach, the number of precipitation days were reduced by removing
the precipitation days with the precipitation records below the threshold values. The
under-predicted extreme events were also adjusted using the scaling factor. Figure 4.3
represents the monthly mean of observed precipitation data and bias-corrected
precipitation data for RCP 4.5 of the CCSM 4.1 model.

Winter, spring, and fall precipitation showed an increasing trend under the four
RCPs, whereas in the summer season, projected changes are small but have presented a
drying trend (Table 3A). However, annual mean precipitation is projected for the higher
precipitation amount (Figure 4.4). According to the Fourth National Climate Assessment
report (USGCRP, 2018), the northern states of the Great Plains region of the USA will
face higher precipitation in the winter and spring season with small projected changes in
summer and fall season with drying summers in central Great Plains. Maximum
precipitation changes were observed under ensembled RCP 8.5 (around 6% for NF and
8% for FF). In summer, a decrease in precipitation during July and August may increase
water stress days in the region.

4.3.3. Phase I: Water Yield Response under Long-Term ICL System

A nonparametric statistical hypothesis test (Wilcoxon signed-rank test) was used to
compare the ICL system hydrological responses with the base scenario. Projected long-

term ICL system of corn-soybean rotation with livestock grazing of corn residues has shown a significant decrement in contributing water to streams for all the HRUs scheduled under the ICL system. Results from streamflow simulations along with its hydrological components contributing to streamflow (surface runoff and lateral flow) and ET under the ICL system and baseline scenarios are shown in Figure 4.5. Results show that the long-term ICL system implementation to the cropland would result in a significant reduction in surface runoff (15%) with a little decrement in lateral flow from all associated HRUs. Subsequently, we observed a significant decline (7%) in streamflow. While streamflow and its components showed a decline under the implemented long-term ICL system, the ET was found to increase, which might result from removed soil cover by grazing operation.

4.3.4. Phase II: Water Yield and Surface Runoff Response due to Climate Changes

An additional verification of simulated hydrological responses under projected climate data with the simulated hydrological responses under the baseline scenario (S01) was carried out before comparing the phase II responses with the baseline scenario. A close resemblance in the average-monthly and 30-year average simulated hydrological responses was observed. The ensemble 30-year average annual water yield and surface runoff with climate changes were found likely to be increased under both future scenarios for all four RCPs (Table 3a and 4a). The RCP 8.5 would induce maximum changes, whereas RCP 2.6 would result in the least changes. Results indicated that the water yield may increase by 7-37% during the NF period (2021-2050) and 15-66% by the end of the century. A shift in the peak of monthly water yield from June to May was also observed under RCP 6.0 and RCP 8.5. The increase in water yield for NF and FF periods might be

the result of the combined effect of projected increased temperature and precipitation over the Skunk Creek watershed for both periods.

Similarly, for surface runoff RCP 8.5 would induce maximum increments of around 19% and 12% for NF and FF, respectively. The RCP 4.5 is projected to have more precipitation for FF than RCP 6.0, but the water yield and surface runoff responses for RCP 6.0 were observed to be higher than the RCP 4.5, which might be enhanced by the higher temperatures and higher snowmelt rates in the spring season under RCP 6.0 for the FF period. RCP 2.6 would also induce higher water yield changes than RCP 4.5 for the FF period which might be resulted due to the decreased precipitation in summer under RCP 4.5 FF period. Increased surface runoff for February and decreased surface runoff for March and April indicates early snowmelts in the spring season under all the RCPs (Table 3a and 4a).

Unlike the surface runoff and water yield responses, ET over the region is likely to show very small changes for the NF period. RCP 2.6 was found to be associated with a minimal increase of 0.3% in annual evapotranspiration for both NF and FF periods while RCP 4.5 would not introduce any changes in ET for the NF period and ET in the FF period might face a slight increment. The RCP 6.0 and RCP 8.5 would cause a reduction of 5 and 7%, respectively, for the FF period. This decrement in ET maybe because of earlier plantation considered by SWAT as this hydrological model considers a base temperature for the plantation. The increased temperature under these two RCPs caused an earlier emergence of plants and decreased projected precipitation amounts for the summer season could result in lower ET for the summer and fall seasons. Gautam et al.

(2018) observed similar ET responses to climate change over the Goodwater Creek watershed in Missouri.

4.3.5. Phase III: Water Yield and Surface Runoff Responses due to the Combined Effects of Long Term ICL System Implementation and Future Climate Changes

The combined effect of long-term ICL system and climate changes would result in 4-34% increase in water yield for NF and 16-63% for FF (Table 5a and 6a). For the NF period under the long-term ICL system, RCP 2.6, RCP 4.5, and RCP 6.0 showed little changes in surface runoff and water yield, whereas RCP 8.5 would a significant increase in both. For the FF period, the surface runoff will remain unaffected under all the considered RCPs, but water yield might face increments under all RCPs except RCP 2.6. While surface runoff and water yield are projected to increase from near future to far future, evapotranspiration appears to be increased in NF for all RCPs and decreased in FF for RCP 4.5, RCP 6.0, and RCP 8.5, although these changes were not significant except for RCP 8.5 FF period scenario. The RCP 8.5 would introduce maximum changes in water yield, surface runoff, and evapotranspiration.

Similar to phase I, integrating grazing with crop rotation reduced the surface runoff and water yield under all future climate scenarios (phase III) as compared to the changes only because of climate changes (phase II). The water yield changes for RCP 2.6 under climate scenarios shifted from significant to nonsignificant by introducing grazing to the cropping system. For RCP 6.0 also, a significant reduction in water yield was observed. Grazing did not reduce the water yield impacts for both future scenarios under RCP 8.5, which might be a consequence of high precipitation. The relative impact of

climate and ICL system would cause an increase in ET, which might be explained by the removal of soil cover and increased soil evapotranspiration.

4.4. Discussion

The objective of the study was to assess the impact of long term ICL system implementation and future climate changes on water yield and its hydrological components (i.e. surface runoff and lateral flow) in an agricultural dominated watershed. To achieve this objective, the outputs from the calibrated SWAT model for water yield and its hydrological components along with evapotranspiration were analyzed. Results show a significant reduction in water yield and surface runoff with little decrease in lateral flow under long-term ICL system while ET is subjected to increase. The reduction in surface runoff and water yields from fields is always targeted by producers and agricultural drainage managers to prevent nutrient and soil losses to receiving waters resulting in degraded aquatic ecosystems. Keeping the assumption of no significant change in soil physical properties under light grazing operation over dry and frozen soil, reduction in water yield and surface runoff might be explained by the improved topsoil health characteristics which in turn affect the soil hydrological properties. Sulc and Tracy (2007) discussed the potential positive effect of a well-managed ICL system on soil functioning and profitability. SWAT uses the SCS-CN method to simulate surface runoff volumes. The CN values for the scenarios under long-term grazing implementation of crop residues were lower than the scenarios with crop rations without grazing operations. The curve number value decreases with better soil hydrological conditions. Lower CN values indicate better soil conditions consideration by SWAT under the ICL system.

Increased evapotranspiration effect might be due to the removal of soil cover by grazing operations, resulting in an increase in soil evaporation.

Future climate projections suggest high annual precipitation and temperature over the Skunk Creek watershed, which would induce noticeable changes in the surface and subsurface water budget. The agricultural systems in the Skunk Creek watershed are mostly rainfed, and the watershed is prone to water-logging and high soil moisture during the spring period. Increased future precipitation during the spring period would intensify these water-logging situations, which can result in an adverse impact on agricultural production by delay in plantations and reducing the agricultural land. This increased soil moisture during the plantation period could be viewed as an intensification of subsurface drainage systems in the area. The increase in water yield and surface runoff also reveal higher agricultural nutrients (e.g. nitrate, phosphorous, and sediments) transportation from fields to downstream waters and impairment of water resources. Additionally, the projected decrease in precipitation during the summer months can increase the number of water stress days. The shift in peak monthly water yields, increased precipitation during spring, decreased precipitation for summer, and early snowmelts compared to the baseline period make the Skunk Creek watershed more susceptible to extreme events such as floods during spring and droughts during the summer seasons. Therefore, water management efforts and strategies should be developed at a watershed scale to secure a future with sustainable agricultural production able to achieve food security goals.

Long - term implementation of the ICL system may mitigate the impact introduced by future climate changes on water yield and surface runoff. The positive hydrological

influences of long term ICL system adoption suggest further exploration of the impact of other more complex ICL systems with future climate scenarios to aggrandize the impacts.

4.5.   Limitations of the Study

Although this study shows useful insights into potential changes in hydrological cycle components introduced by future climate changes and long-term ICL system of corn-soybean rotation with the grazing of corn residues, it has a few limitations. This study is solely based on the long-term implementation of a single ICL system, while the impacts of other more complex ICL systems are still needed to be explored. The study also used one LULC map for the entire study period due to the non-availability of projected LULC maps for the entire study region. The used hydrological model SWAT does not simulate changes in soil physical properties. Therefore, the study assumes no significant changes in soil physical properties due to light grazing of corn residues in the dry and frozen period. The downscaled GCMs outputs tend to have uncertainty in data, which can be overcome by using ensemble results of multiple GCMs outputs. Because of the high computational demand, we used only four GCMs for the study. The streamflow data for the Skunk Creek watershed is only available for its outlet, so only one streamflow dataset is used to calibrate and validate the model. This may lead to spatial uncertainties in the results. Future efforts should consider a multi-site and multi-parameter approach for calibration and validation of the model.

4.6.   Conclusions

The study evaluated the potential impacts of long-term ICL system implementation and future climate scenarios on water yield and its hydrological components in the Skunk Creek watershed, South Dakota. The study was conducted in three phases covering the

impact of individual ICL systems and climate changes with the combined impact of both on water yield. The climate scenarios considered in this study involve the future climate data from four CMIP5-BCCA GCMs with four RCP (RCP 2.6, RCP 4.5, RCP 6.0, and RCP 8.5) under NF (2021-2050) and FF (2069-2099) periods. The simulated ICL system considers two-year corn-soybean rotation with light-grazing of corn residues. In the first phase, when grazing was introduced with crop rotation, water yield (~7%) and surface runoff (~15%) were reduced with a lower CN value. The results from phase-I suggest improved soil hydrologic conditions by incorporating light corn residue grazing. According to the projected climate data from GCMs, the study watershed is projected to receive higher annual precipitations, which may result in 15-66% increase in annual water yield by the end of the century. Changing the current agricultural practices to ICL systems might shrink these impacts of climate changes.

The monthly analysis of future climate data and its impact suggests the possible hydrologic alteration such as a shift in the peak streamflow (June to May), reduced precipitation in summer (-0.4%-8%), and early snowmelt and increased precipitation in spring (5%-26%). These alterations make the study watershed vulnerable to extreme events like floods during springs and drought during summers. The Skunk Creek watershed is prone to water-logging problems. Increased precipitation and increased snowmelt in spring would cause higher soil moisture and may result in higher waterlogged areas in the watershed. These situations may lead to reduced agricultural production area and the intensification of subsurface drainage.

According to the study results, the ICL systems have the potential to reduce the water yield and surface runoff by improving soil hydrologic conditions. The improved

soil hydrologic conditions might have induced other agricultural benefits (crop production, pesticide, and nutrient movement) as well. These positive hydrological outcomes by the ICL system invite researchers to explore the impact of other more complex ICL systems on soil hydrology and agricultural responses. The study can be beneficial for the model developers to incorporate the impact of grazing operation on soil physical properties into the models. In addition, the negative impacts of future climate change signal to the practitioners, watershed managers, and policymakers to be cautious and well prepared to minimize the impacts.

APPENDIX A- Additional Information about simulation scenarios, calibration parameters, and month-wise percentage variation in different hydrological components under different scenarios can be found in Table 1A- 6A.

References

Abbaspour, K. C. (2013). SWAT-CUP 2012. In: *SWAT Calibration Uncertainty Program—A User Manual*.

Ahiablame, L., Sinha, T., Paul, M., Ji, J.-H., & Rajib, A. (2017). Streamflow response to potential land use and climate changes in the James River watershed, Upper Midwest United States. Journal of Hydrology: Regional Studies, 14, 150-166.

Archuleta, C., Constance, E., Arundel, S., Lowe, A., Mantey, K., & Phillips, L. (2017). The National Map seamless digital elevation model specifications (No. 11-B9). US Geological Survey.

Arnold, J.G., Moriasi, D.N., Gassman, P.W., Abbaspour, K.C., White, M.J., Srinivasan, R., Santhi, C., Harmel, R.D., Van Griensven, A., Van Liew, M.W., and Kannan, N. (2012). SWAT: Model use, calibration, and validation. Transactions of the ASABE, 55(4), 1491-1508.

Arnold, J.G., Kiniry, J.R., Srinivasan, R., Williams, J.R., Haney, E.B., and Neitsch, S.L. (2013). SWAT 2012 input/output documentation. Texas Water Resources Institute.

Bawa, A., Senay, G.B. and Kumar, S. (2021). Regional crop water use assessment using Landsat-derived evapotranspiration. Hydrological Processes. e14015. https://doi.org/10.1002/hyp.14015

Bilotta, G. S., Brazier, R. E., & Haygarth, P. M. (2007). The impacts of grazing animals on the quality of soils, vegetation, and surface waters in intensively managed grasslands. Advances in Agronomy, Vol 94, 94, 237-280. doi:10.1016/S0065-2113(06)94006-1

Brekke, L., Thrasher, B., Maurer, E., & Pruitt, T. (2013). Downscaled CMIP3 and CMIP5 climate and hydrology projections: Release of downscaled CMIP5 climate projections, comparison with preceding information, and summary of user needs. US Dept. of the Interior, Bureau of Reclamation, Technical Services Center, Denver.

Changnon, S. A., & Kunkel, K. E. (1995). Climate-related fluctuations in Midwestern floods during 1921–1985. Journal of Water Resources Planning Management, 121(4), 326-334.

Chien, H. C., Yeh, P. J. F., & Knouft, J. H. (2013). Modeling the potential impacts of climate change on streamflow in agricultural watersheds of the Midwestern United States. Journal of Hydrology, 491, 73-88.

Collins, M., Knutti, R., Arblaster, J., Dufresne, J.L., Fichefet, T., Friedlingstein, P., Gao, X., Gutowski, W.J., Johns, T., Krinner, G. and Shongwe, M. (2013). Long-term climate change: projections, commitments and irreversibility. In Climate Change 2013-The Physical Science Basis: Contribution of Working Group I to the Fifth Assessment Report of the Intergovernmental Panel on Climate Change (1029-1136). Cambridge University Press.

Cronshey, R.G., Roberts, R.T. and Miller, N. (1985). Urban hydrology for small watersheds (TR-55 Rev.). In Hydraulics and hydrology in the small computer age (pp. 1268-1273). ASCE.

de Wit, M., & Stankiewicz, J. (2006). Changes in surface water supply across Africa with predicted climate change. Science, 311(5769), 1917-1921. doi:10.1126/science.1119929

Drewry, J., Cameron, K., & Buchan, G. (2008). Pasture yield and soil physical property responses to soil compaction from treading and grazing—a review. Soil Research, 46(3), 237-256.

Dunne, J. P., John, J. G., Adcroft, A. J., Griffies, S. M., Hallberg, R. W., Shevliakova, E., . . . Harrison, M. J. (2012). GFDL's ESM2 global coupled climate–carbon earth system models. Part I: Physical formulation and baseline simulation characteristics. Journal of Climate, 25(19), 6646-6665.

Dunne, J. P., John, J. G., Shevliakova, E., Stouffer, R. J., Krasting, J. P., Malyshev, S. L., . . . Cooke, W. (2013). GFDL's ESM2 global coupled climate–carbon earth system models. Part II: carbon system formulation and baseline simulation characteristics. Journal of Climate, 26(7), 2247-2267.

El-Khoury, A., Seidou, O., Lapen, D. R., Que, Z., Mohammadian, M., Sunohara, M., & Bahram, D. (2015). Combined impacts of future climate and land use changes on

discharge, nitrogen and phosphorus loads for a Canadian river basin. Journal of Environmental Management, 151, 76-86. doi:10.1016/j.jenvman.2014.12.012

Engel, B., Storm, D., White, M., Arnold, J., & Arabi, M. (2007). A Hydrologic/Water Quality Model Applicati1 1. Journal of the American Water Resources Association, 43(5), 1223-1236.

Ficklin, D. L., Luo, Y. Z., Luedeling, E., & Zhang, M. H. (2009). Climate change sensitivity assessment of a highly agricultural watershed using SWAT. Journal of Hydrology, 374(1-2), 16-29. doi:10.1016/j.jhydrol.2009.05.016

Field, C. B. (2014). Climate change 2014–Impacts, adaptation and vulnerability: Regional aspects: Cambridge University Press.

Fisher, B., Nakicenovic, N., Alfsen, K., Corfee-Morlot, J. and Riahi, K. (2007). Issues related to mitigation in the long-term context (Chapter 3). In: Climate Change 2007: Mitigation. Contribution of WG III to the Fourth Assessment Report of the IPCC. Eds. Metz, B., Davidson, O.R., Bosch, P.R., Dave, R. & Meyer, L.A., Cambridge: Cambridge University Press.

Gautam, S., Costello, C., Baffaut, C., Thompson, A., Svoma, B. M., Phung, Q. A., & Sadler, E. J. (2018). Assessing Long-Term Hydrological Impact of Climate Change Using an Ensemble Approach and Comparison with Global Gridded Model-A Case Study on Goodwater Creek Experimental Watershed. Water, 10(5), 564. doi:UNSP 56410.3390/w10050564

Gent, P. R., Danabasoglu, G., Donner, L. J., Holland, M. M., Hunke, E. C., Jayne, S. R., . . . Zhang, M. H. (2011). The Community Climate System Model Version 4. Journal of Climate, 24(19), 4973-4991. doi:10.1175/2011jcli4083.1

Grillakis, M. G., Koutroulis, A. G., Daliakopoulos, I. N., & Tsanis, I. K. (2017). A method to preserve trends in quantile mapping bias correction of climate modeled temperature. Earth System Dynamics, 8(3), 889-900. doi:10.5194/esd-8-889-2017

Grillakis, M. G., Koutroulis, A. G., & Tsanis, I. K. (2013). Multisegment statistical bias correction of daily GCM precipitation output. Journal of Geophysical Research-Atmospheres, 118(8), 3150-3162. doi:10.1002/jgrd.50323

Groisman, P. Y., Knight, R. W., & Karl, T. R. (2001). Heavy precipitation and high streamflow in the contiguous United States: Trends in the twentieth century. Bulletin of the American Meteorological Society, 82(2), 219-246. doi:Doi 10.1175/1520-0477(2001)082<0219:Hpahsi>2.3.Co;2

Gutmann, E., Pruitt, T., Clark, M. P., Brekke, L., Arnold, J. R., Raff, D. A., & Rasmussen, R. M. (2014). An intercomparison of statistical downscaling methods used for water resource assessments in the U nited S tates. Water Resources Research, 50(9), 7167-7186.

Kumar, S., Anderson, S. H., Udawatta, R. P., & Gantzer, C. J. (2010). CT-measured macropores as affected by agroforestry and grass buffers for grazed pasture systems. Agroforestry Systems, 79(1), 59-65. doi:10.1007/s10457-009-9264-4.

Liebig, M. A., Kronberg, S. L., Hendrickson, J. R., & Gross, J. R. (2014). Grazing Management, Season, and Drought Contributions to Near-Surface Soil Property Dynamics in Semiarid Rangeland. Rangeland Ecology & Management, 67(3), 266-274. doi:10.2111/Rem-D-13-00145.1

Liebig, M. A., Tanaka, D. L., & Wienhold, B. J. (2004). Tillage and cropping effects on soil quality indicators in the northern Great Plains. Soil & Tillage Research, 78(2), 131-141. doi:10.1016/j.still.2004.02.002

Livneh, B., Rosenberg, E. A., Lin, C., Nijssen, B., Mishra, V., Andreadis, K. M., . . . Lettenmaier, D. P. (2013). A long-term hydrologically based dataset of land surface fluxes and states for the conterminous United States: Update and extensions. Journal of Climate, 26(23), 9384-9392.

Maraun, D. (2013). Bias Correction, Quantile Mapping, and Downscaling: Revisiting the Inflation Issue. Journal of Climate, 26(6), 2137-2143. doi:10.1175/Jcli-D-12-00821.1

Masui, T., Matsumoto, K., Hijioka, Y., Kinoshita, T., Nozawa, T., Ishiwatari, S., . . . Kainuma, M. (2011). An emission pathway for stabilization at 6 Wm− 2 radiative forcing. Climatic change, 109(1-2), 59.

Maurer, E. P., Brekke, L., Pruitt, T., & Duffy, P. B. (2007). Fine-resolution climate projections enhance regional climate change impact studies. Transactions American Geophysical Union, 88(47), 504-504.

McNeill, K., Macdonald, K., Singh, A., & Binns, A. D. (2017). Food and water security: Analysis of integrated modeling platforms. Agricultural Water Management, 194, 100-112. doi:10.1016/j.agwat.2017.09.001

Mehan, S., Kannan, N., Neupane, R. P., McDaniel, R., & Kumar, S. (2016). Climate Change Impacts on the Hydrological Processes of a Small Agricultural Watershed. Climate, 4(4), 56. doi:ARTN 5610.3390/cli4040056

Moriasi, D. N., Arnold, J. G., Van Liew, M. W., Bingner, R. L., Harmel, R. D., & Veith, T. L. (2007). Model evaluation guidelines for systematic quantification of accuracy in watershed simulations. Transactions of the Asabe, 50(3), 885-900. Retrieved from <Go to ISI>://WOS:000248036800021.

Neitsch, S.L., Arnold, J.G., Kiniry, J.R. and Williams, J.R. (2011). Soil and water assessment tool theoretical documentation version 2009. Texas Water Resources Institute.

Neupane, R.P. and Kumar, S. (2015). Estimating the effects of potential climate and land use changes on hydrologic processes of a large agriculture dominated watershed. Journal of Hydrology, 529, 418-429.

Pachauri, R.K., Allen, M.R., Barros, V.R., Broome, J., Cramer, W., Christ, R., Church, J.A., Clarke, L., Dahe, Q., Dasgupta, P. and Dubash, N.K. (2014). Climate change 2014: synthesis report. Contribution of Working Groups I, II and III to the fifth

assessment report of the Intergovernmental Panel on Climate Change (p. 151). IPCC.

Paul, M., Rajib, M.A. and Ahiablame, L. (2017). Spatial and temporal evaluation of hydrological response to climate and land use change in three South Dakota watersheds. JAWRA Journal of the American Water Resources Association, 53(1), 69-88.

Pérez-Gutiérrez, J.D. and Kumar, S. (2019). Simulating the influence of integrated crop-livestock systems on water yield at watershed scale. Journal of environmental management, 239, 385-394.

Pulido, M., Schnabel, S., Lavado Contador, J.F., Lozano-Parra, J. and González, F. (2018). The impact of heavy grazing on soil quality and pasture production in rangelands of SW Spain. Land Degradation & Development, 29(2), 219-230.

Ramirez, J. and Jarvis, A. (2010). Downscaling global circulation model outputs: the delta method. Decision and policy analysis working paper, 1, 1-18.

Riahi, K., Rao, S., Krey, V., Cho, C., Chirkov, V., Fischer, G., Kindermann, G., Nakicenovic, N. and Rafaj, P. (2011). RCP 8.5—A scenario of comparatively high greenhouse gas emissions. Climatic Change, 109(1-2), p.33.

Ruane, A.C. and McDermid, S.P. (2017). Selection of a representative subset of global climate models that captures the profile of regional changes for integrated climate impacts assessment. Earth Perspectives, 4(1), p.1.

Shrestha, S., Sharma, S., Gupta, R. and Bhattarai, R. (2019). Impact of global climate change on stream low flows: A case study of the great Miami river watershed, Ohio, USA. International Journal of Agricultural and Biological Engineering, 12(1), 84-95.

Singh, N., Abagandura, G.O. and Kumar, S. (2020). Short-term grazing of cover crops and maize residue impacts on soil greenhouse gas fluxes in two Mollisols. Journal of Environmental Quality, 49, 628–639.

Solomon, S., Qin, D., Manning, M., Chen, Z., Marquis, M., Averyt, K., Tignor, M. and Miller, H. (2007). IPCC fourth assessment report (AR4). Climate change, 374.

South Dakota Mesonet. (2020). From South Dakota State University. South Dakota Mesonet Database.

Stagl, J., Mayr, E., Koch, H., Hattermann, F.F. and Huang, S. (2014). Effects of climate change on the hydrological cycle in Central and Eastern Europe. In Managing protected areas in Central and Eastern Europe under climate change (31-43). Springer, Dordrecht.

Sulc, R.M. and Tracy, B.F. (2007). Integrated crop–livestock systems in the US Corn Belt. Agronomy Journal, 99(2), 335-345.

Taghizadeh-Mehrjardi, R., Bawa, A., Kumar, S., Zeraatpisheh, M., Amirian-Chakan, A. and Akbarzadeh, A. (2019). Soil Erosion Spatial Prediction using Digital Soil

Mapping and RUSLE methods for Big Sioux River Watershed. Soil Systems, 3(3), 43.

The 2018 South Dakota integrated report for surface water quality assessment. (2020). Prepared by South Dakota Department of Environment and Natural Resources.

Thomson, A.M., Calvin, K.V., Smith, S.J., Kyle, G.P., Volke, A., Patel, P., Delgado-Arias, S., Bond-Lamberty, B., Wise, M.A., Clarke, L.E. and Edmonds, J.A. (2011). RCP4. 5: a pathway for stabilization of radiative forcing by 2100. Climatic change, 109(1-2), p.77.

USDA National Agricultural Statistics Service Cropland Data Layer. (2018). Retrieved from https://nassgeodata.gmu.edu/CropScape/. Retrieved December 10, 2018, from USDA-NASS, Washington, DC https://nassgeodata.gmu.edu/CropScape

USGCRP (2018). In D. R. Reidmiller, C. W. Avery, D. R. Easterling, K. E. Kunkel, K. L. M. Lewis, T. K. Maycock, & B. C. Stewart (Eds.), Impacts, risks, and adaptation in the United States: Fourth national climate assessment, volume II: Report-in-Brief (p. 186). U.S. Global Change Research Program. 10.7930/NCA4.2018.

Van Vliet, M.T.H. and Zwolsman, J.J.G. (2008). Impact of summer droughts on the water quality of the Meuse river. Journal of Hydrology, 353(1-2), 1-17.

Van Vuuren, D.P., Edmonds, J., Kainuma, M., Riahi, K., Thomson, A., Hibbard, K., Hurtt, G.C., Kram, T., Krey, V., Lamarque, J.F. and Masui, T. (2011). The representative concentration pathways: an overview. Climatic change, 109(1-2), 5.

Van Vuuren, D.P., Stehfest, E., den Elzen, M.G., Kram, T., van Vliet, J., Deetman, S., Isaac, M., Goldewijk, K.K., Hof, A., Beltran, A.M. and Oostenrijk, R. (2011). RCP2. 6: exploring the possibility to keep global mean temperature increase below 2 C. Climatic Change, 109(1-2), 95.

Table 4.1. Crop and grazing management operations

Agricultural practice	Management practice	Management scheduled
Growing corn	Fertilizer	Urea (46-0-0) - 168 kg ha^{-1}
		Di-ammonium phosphate (16-46-0) - 168 kg ha^{-1}
		Mono-ammonium phosphate (11-52-0) - 56 kg ha^{-1}
	Tillage	No till
	Planting	May 5th
	Harvest and kill	October 5th (Harvest) and December 30th (kill after grazing)
Growing soybean	Tillage	No till
	Planting	May 15th
	Harvest and kill	October 15th
Grazing	Initiation	November 1st
	Duration	55 days
	Plant biomass consumed	34.8 kg ha^{-1} day^{-1}
	Amount of manure applied	9.0 kg ha^{-1} day^{-1}
	Plant biomass trampled	24.2 kg ha^{-1} day^{-2}

Table 4.2. List of CMIP5 models used in this study

Model	CMIP5- Climate Modeling Group	Reference
CCSM 4.1	National Centre of Atmospheric	Gent et al. (2011)
CCSM 4.2	Research (NCAR)	
gfdl-esm-2g	Geophysical Fluid Dynamics	Dunne et al. (2012)
gfdl-esm-2m	Laboratory- NOAA (gfdl-NOAA)	Dunne et al. (2013)

Table 4.3. CO_2 concentration levels for each RCP under different simulation periods

RCPs	CO_2 concentration (ppm)		
	1976-2005	2021-2050	2070-2099
RCP 2.6	360	431	429
RCP 4.5	360	448	532
RCP 6.0	360	442	612
RCP 8.5	360	474	800
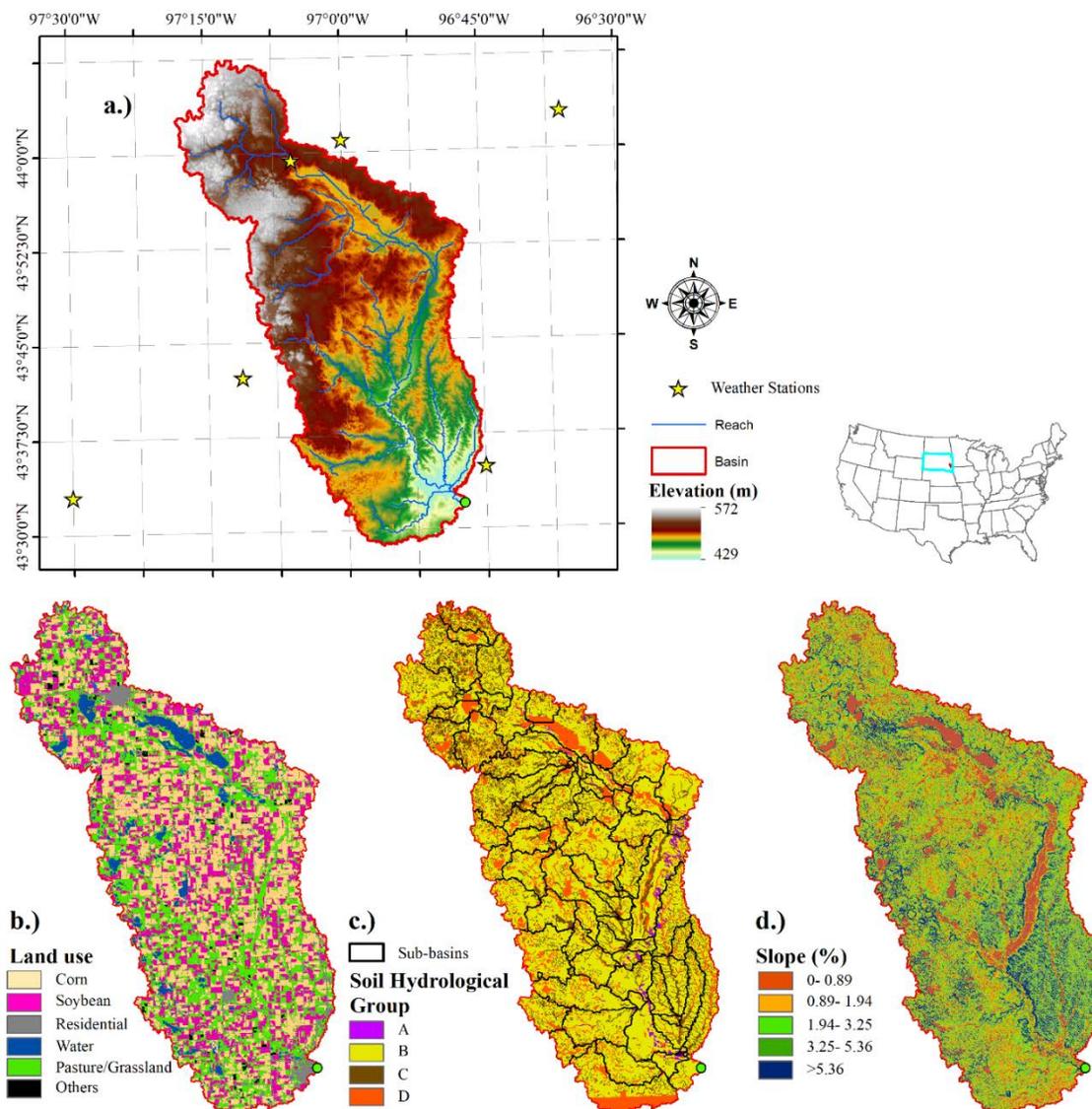
Fig. 4.1. The Skunk Creek watershed location with its main characteristics: a) elevation map with projected climate data grid and stream network, b) land use map (NASS CDL 2008), c) soil hydrological group map with sub-basin boundaries, and d) slope distribution map across the watershed.
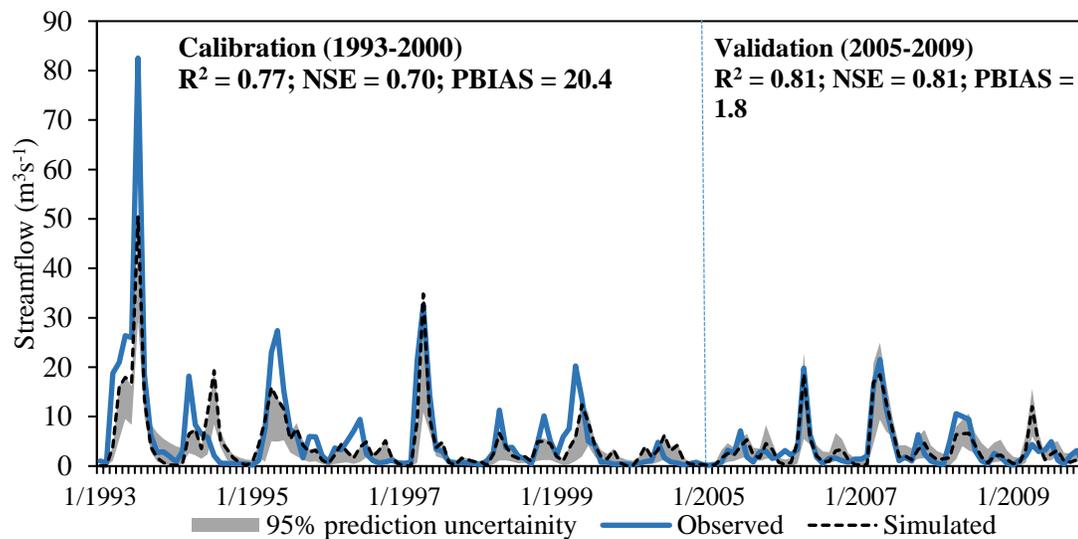
Fig. 4.2. Streamflow comparison of simulated and observed monthly streamflow at the outlet of the Skunk Creek watershed
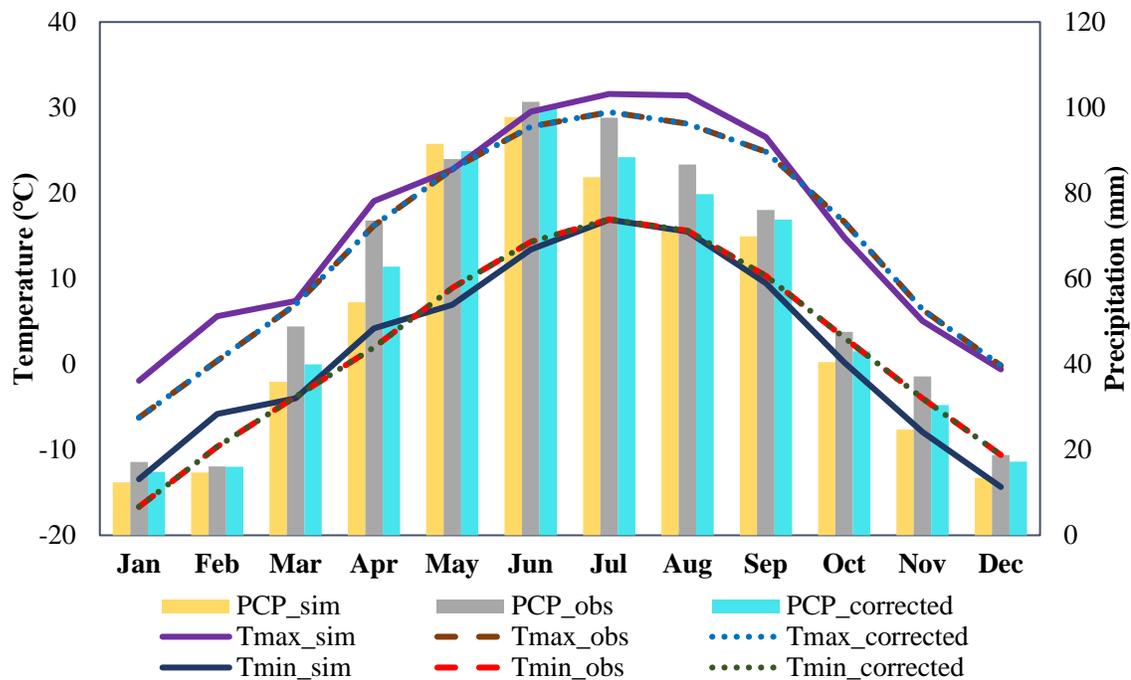
Fig. 4.3.Monthly mean temperature and precipitation data for simulated CCSM 4.1 under RCP 4.5 before (sim) and after (corrected) correction and observed (obs) data for Skunk Creek watershed during the period of 1976-2005. (PCP indicates precipitation; Tmax indicates maximum temperature and Tmin indicates minimum temperature)
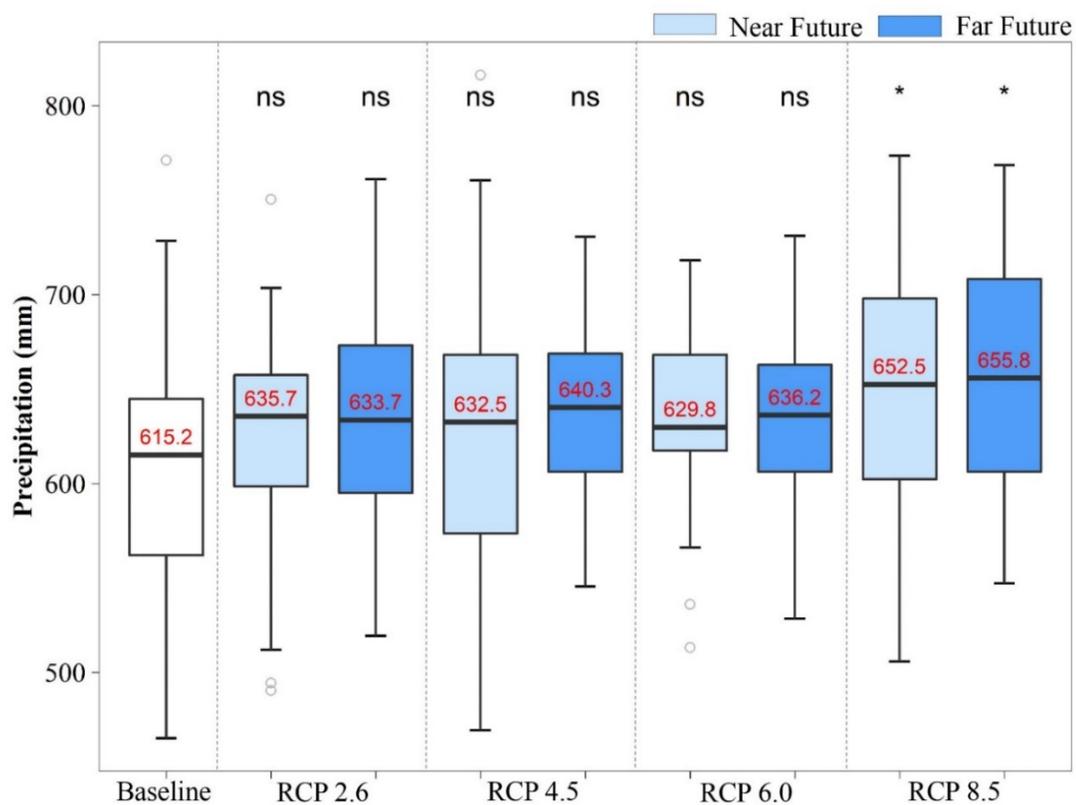
Fig. 4.4. Annual precipitation for near future and far future under RCP 2.6, RCP 4.5, RCP 6.0, and RCP 8.5 scenarios. (*ns* indicates *p*-value greater than 0.05; * indicates significance at $p = 0.05$; ** indicates significance at $p = 0.01$)
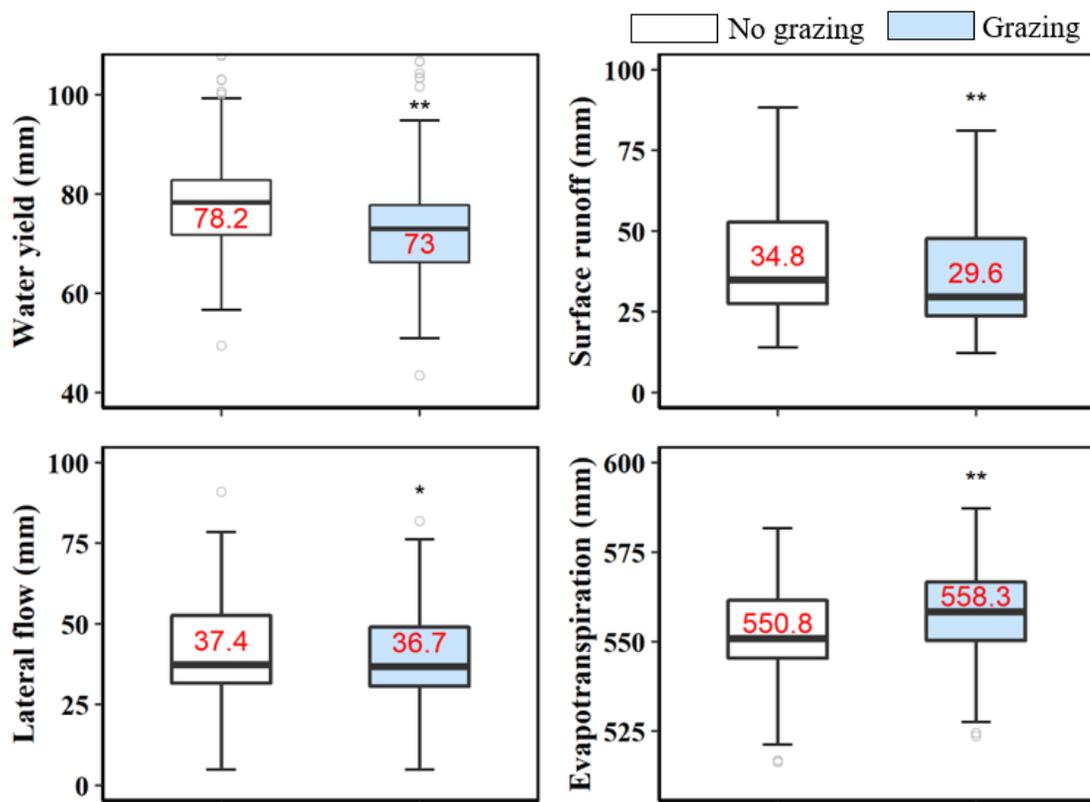
Fig. 4.5. Water yield and hydrological component comparison between baseline and ICL system. (* indicates significance at $p = 0.05$; ** indicates significance at $p = 0.01$)

a)
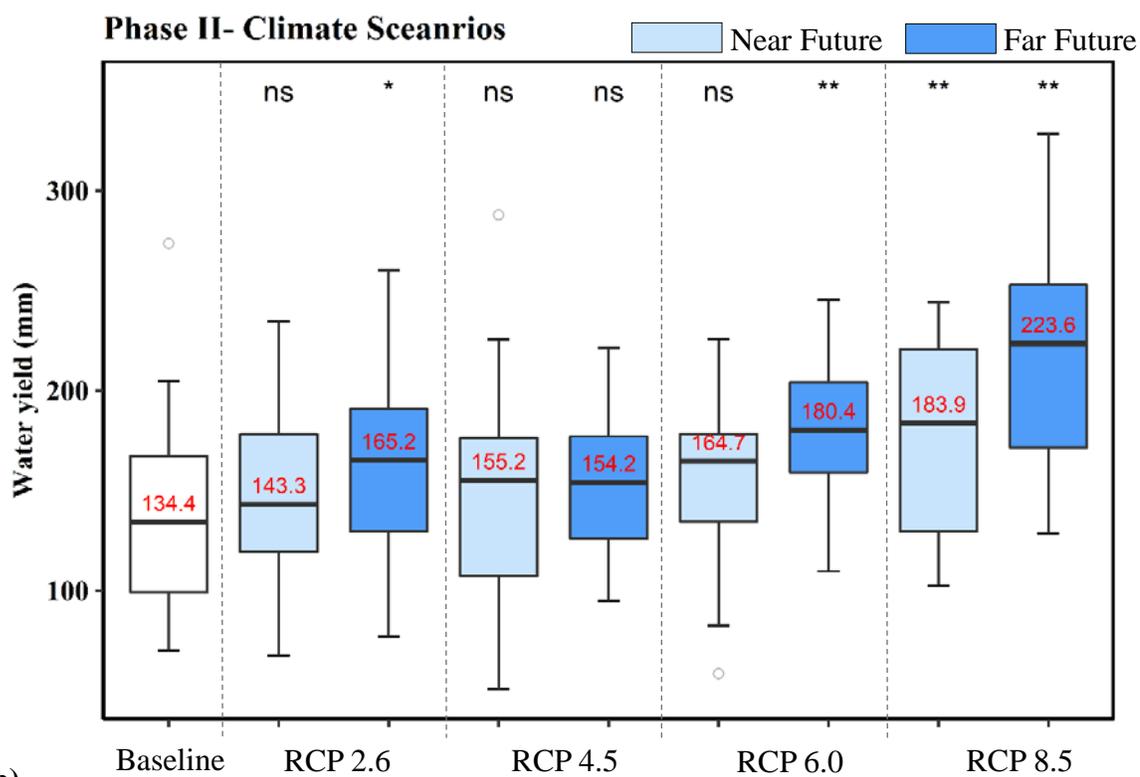
b)
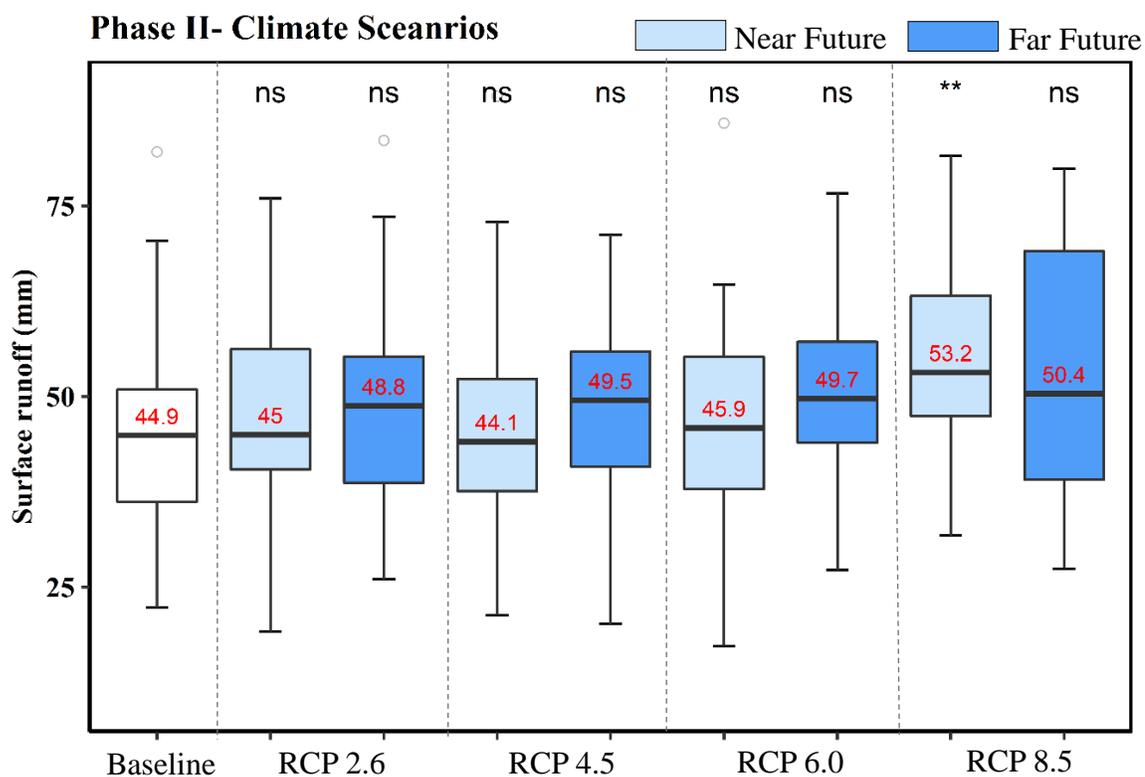
c)
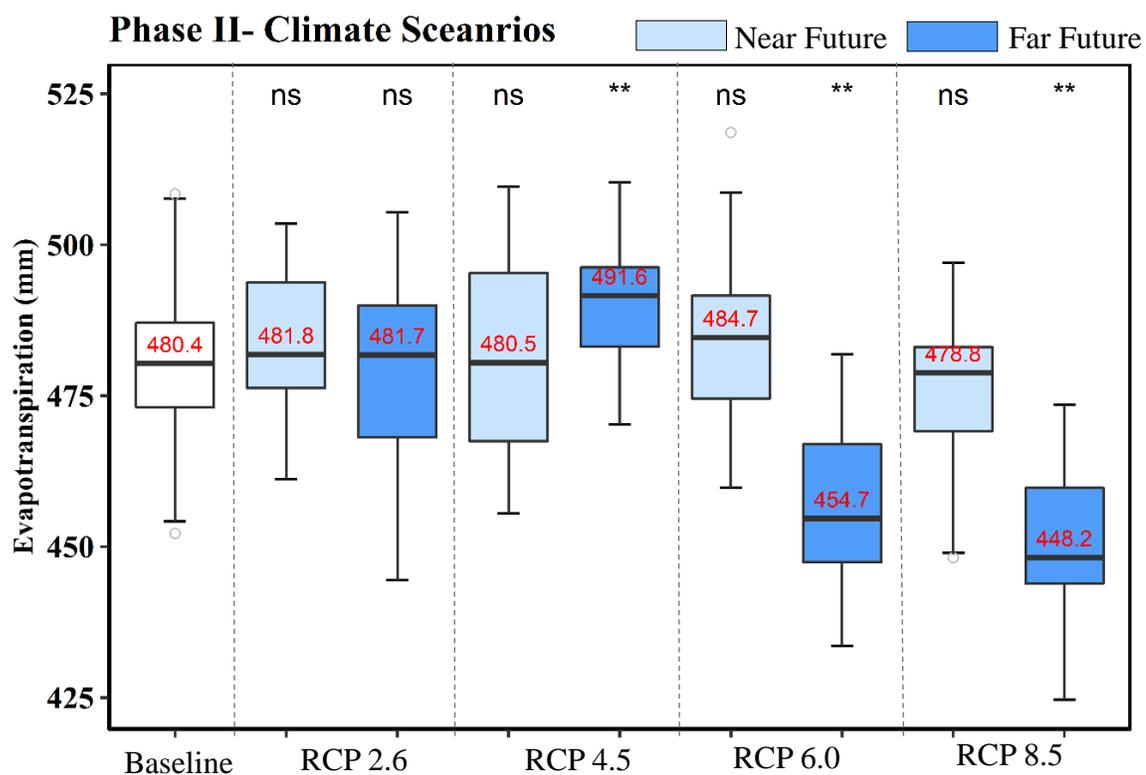
Fig. 4.6. Comparison of precipitation and different hydrological components (water yield, surface runoff, and evapotranspiration) compared to baseline (1976-2005) in response to ensembled future projection of climate change scenarios for near-future (2021-2050) and far future (2070-2099) over Skunk Creek watershed. (*ns* indicates *p*-value greater than 0.05; * indicates significance at $p = 0.05$; ** indicates significance at $p = 0.01$)

a)
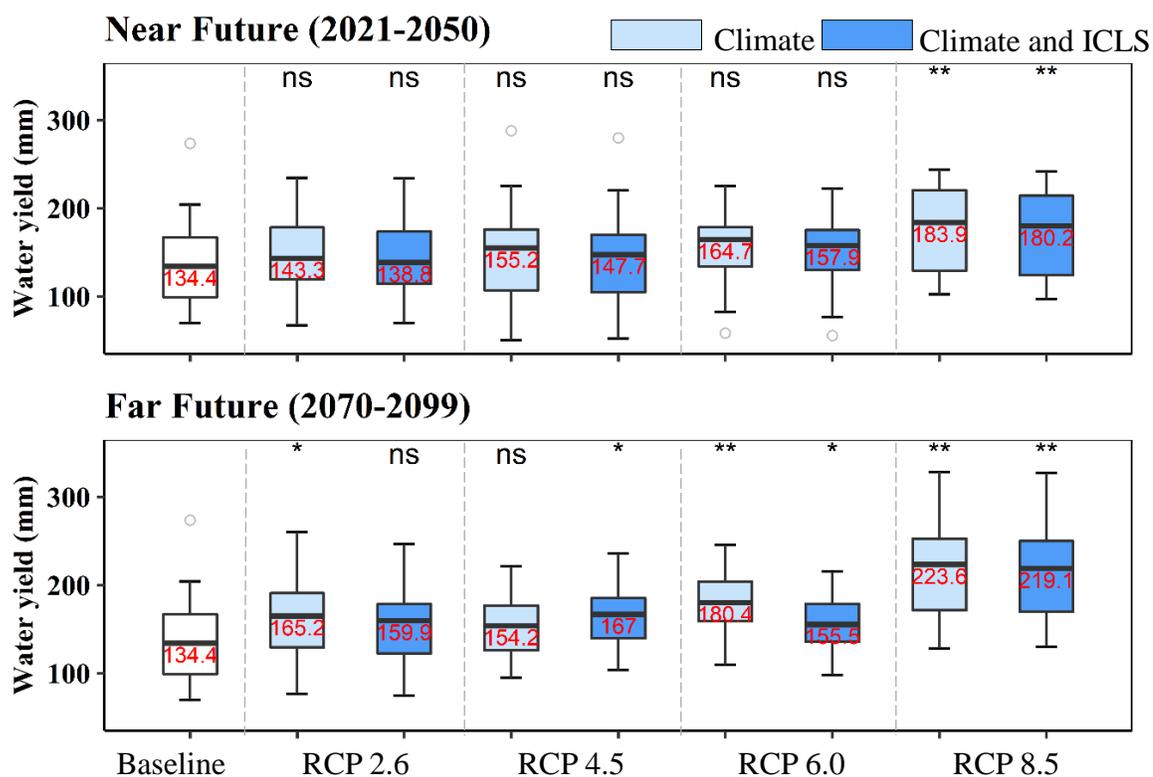
b)
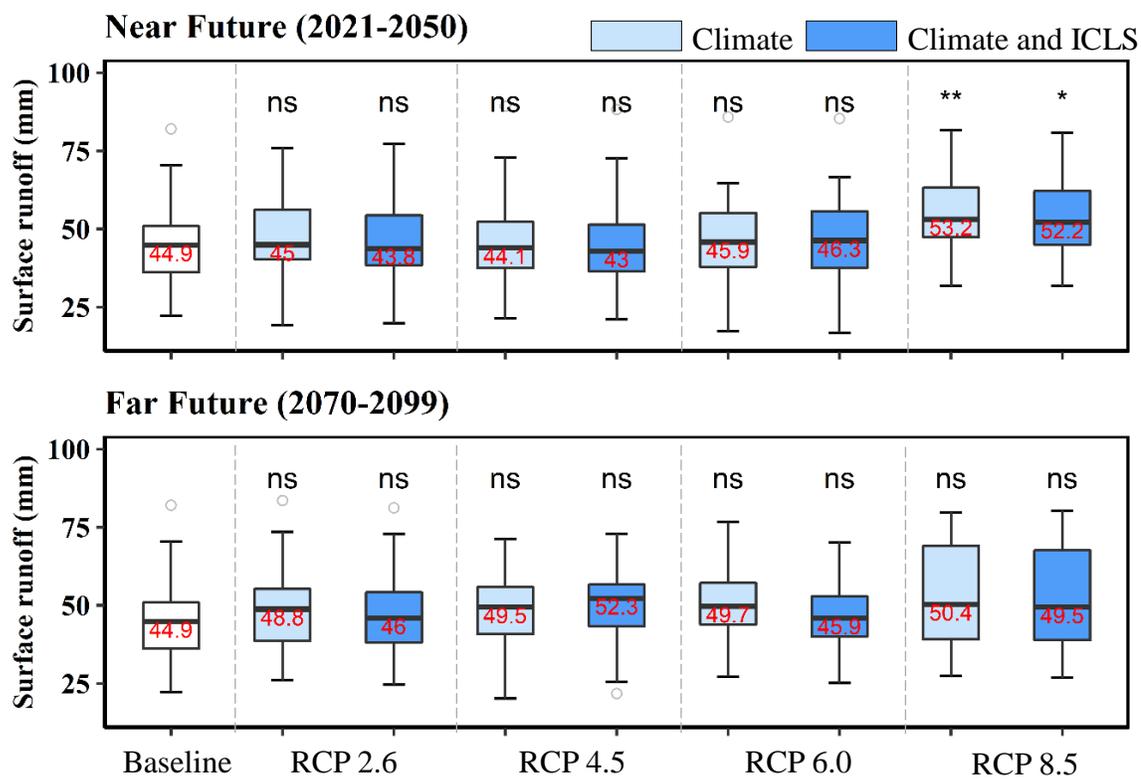
c)
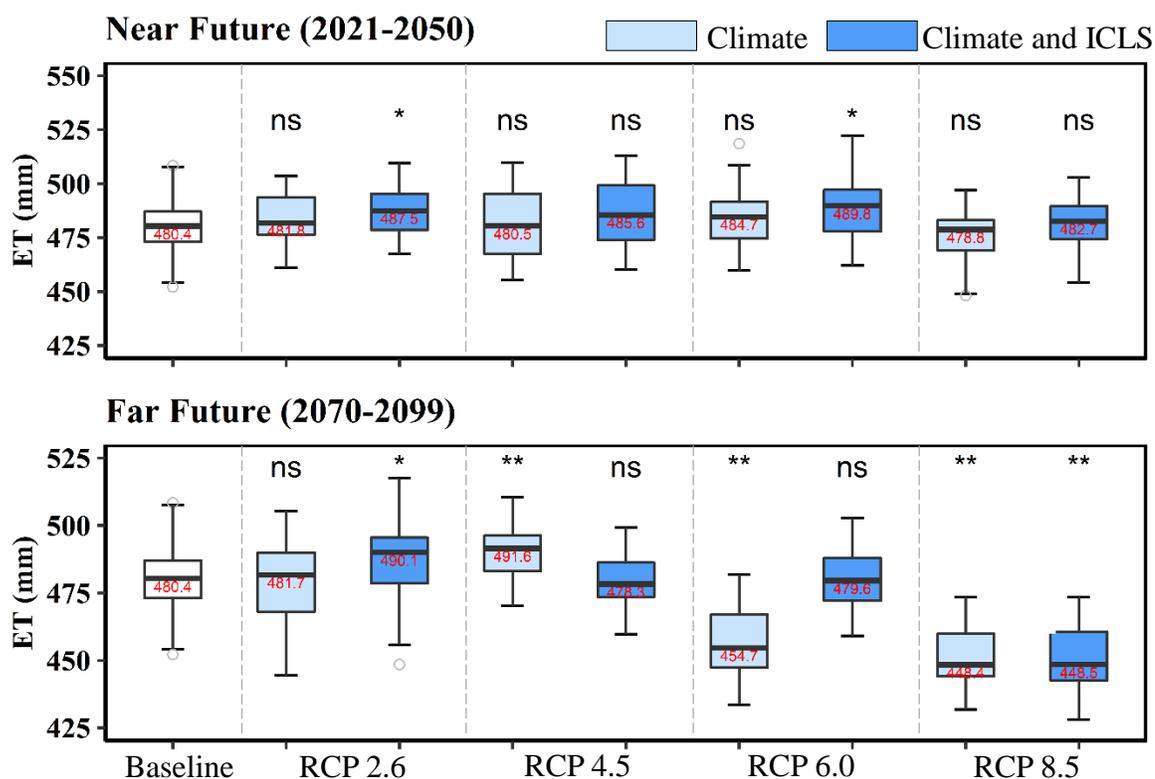
Fig. 4. 7. Comparison of different hydrological components [water yield, surface runoff, and evapotranspiration (ET)] compared to baseline (1976-2005) in response to combined effect of long term ICL system implementation and ensembled future projection of climate change scenarios for near-future (2021-2050) and far future (2069-2099) over Skunk Creek watershed. (*ns* indicates *p*-value greater than 0.05; * indicates significance at *p* = 0.05; ** indicates significance at *p* = 0.01)

CHAPTER 5

REGIONAL CROP WATER USE ASSESSMENT USING LANDSAT-DERIVED

EVAPOTRANSPIRATION ACROSS SOUTH DAKOTA

ABSTRACT

Reliable information on water use and availability at basin and field scales are important to ensure the optimized constructive uses of available water resources. This study was conducted with the specific objective to estimate Landsat-based actual evapotranspiration (ETa) using the Operational Simplified Surface Energy Balance (SSEBop) model across the state of South Dakota (SD), USA for the 1986-2018 (33-year) period. Validated ETa estimations ($r^2 = 0.91$, PBIAS= -4%, and %RMSE = 11.8%) were further used to understand the crop water-use characteristics and existing historic mono-directional (increasing/decreasing) trends over the eastern (ESD) and western (WSD) regions of SD. The crop water-use characteristics indicated that the annual cropland water uses across the ESD and WSD were more or less met by the precipitation amounts in the area. The ample water supply and distribution have led to high rainfed and low percentage of irrigated cropland (~2.5%) in the state. The WSD faced greater crop-water use reductions than the ESD during drought periods. The landscape ETa responses across the state were found to be more sensitive than precipitation for the drought impact assessments. The Mann Kendall trend analysis revealed the absence of a significant trend ($p > 0.05$) in annual ETa at a regional scale due to the varying weather conditions in the state. However, about 12% and 9% cropland areas in the ESD and WSD, respectively, revealed a significant mono-directional trend at pixel scale ETa. Most of the pixels under significant trend showed an increasing trend that can be explained by the shift in

agricultural practices, increased irrigated cropland area, higher productions, moisture regime shifts, and decreased risk of farming in the dry areas. The decreasing trend pixels were clustered in mid-eastern SD and could be the result of dynamic conversion of wetlands to croplands and decreased irrigation practices in the region. This study also demonstrates the tremendous potential and robustness of the SSEBop model, Landsat imagery, and remote sensing-based ETa modeling approaches in estimating consistent spatially distributed evapotranspiration.

5.1.   Introduction

Historical spatial and temporal crop water use trends provide important insights of managing the water resources across the field and watershed scales. Additionally, it can also play a critical role in future water management policies to ensure optimized and constructive uses of available water resources (Senay, Friedrichs, Singh, & Velpuri, 2016; Senay, Schauer, Friedrichs, Velpuri, & Singh, 2017; Vadeboncoeur et al., 2018; Zhang et al., 2016). The knowledge of demand and supply is the basis of water rights management and water regulations. In agriculturally dominant basins, the precipitation, surface water, and groundwater can provide the major part of water supply, whereas, quantifying the actual evapotranspiration (ETa) from the area provides the information of the water demand. The ETa is the major component of the water budget and accounts for 60-75% of the total precipitation across an agricultural basin (Brutsaert, 2005; Vörösmarty, Federer, & Schloss, 1998). The high variability of ETa is due to its dependency on environmental and climatic drivers, which makes it an important indicator to study the landscape response in association with temperature, soil moisture, vegetation

health, and atmospheric demands (Rajib, Evenson, Golden, & Lane, 2018; Senay et al., 2019a; Senay et al., 2019b; Yang et al., 2020).

Direct evapotranspiration (ET) measurements using plot-scale water balance and water vapor transfer methods are time-consuming, labor-intensive, and limited only to field-scales. Satellite remote sensing has enabled the development of effective ET estimation methods and is becoming popular for basin-wide/region-wide ET applications. Due to spatiotemporal coverage of satellite data, the remote sensing techniques for ET modeling are widely adopted by the scientific community across the world. The majority of remote sensing ET estimation methods are based on solving the energy balance (Allen, Pereira, Raes, & Smith, 1998). However, accurate ET estimations using satellite remote sensing techniques is still a challenge as a result of the numerous assumptions and complex factors such as radiations, temperature, vapor-pressure deficit, sensible heat, and ground heat fluxes those must be considered (Ji, Senay, Velpuri, & Kagone, 2019; Velpuri, Senay, Singh, Bohms, & Verdin, 2013). Visible, infrared, and thermal infrared wavelength satellite data with remote sensing and energy balance based ET estimation models [e.g., Surface Energy Balance Index (SEBI), Two-Source Energy Balance (TSEB), Surface Energy Balance Algorithm for Land (SEBAL), Simplified Surface Energy Balance Index (S-SEBI), Surface Energy Balance System (SEBS), Mapping Evapotranspiration at high Resolution with Internalized Calibration (METRIC), Atmosphere-Land Exchange Inverse (ALEXI), and Operational Simplified Surface Energy Balance (SSEBop)] have solved the ET estimation complexity to some degree (Allen, Tasumi, & Trezza, 2007; Anderson, Norman, Mecikalski, Otkin, & Kustas, 2007; Bastiaanssen, Menenti, Feddes, & Holtslag, 1998; Kustas & Norman, 2000; Mu, Zhao, &

Running, 2011; Roerink, Su, & Menenti, 2000; Senay et al., 2013; Senay, Budde, Verdin, & Melesse, 2007; Su, 2002). The accuracy of ET estimations depends upon the model complexity with the number of input variables and assumptions considered by the model. Generally, more complex models are designed to account for sub-processes and approximate the ET more accurately. However, involving large number of input variables might result in a high error as the error and assumptions might be associated with the input variables. The less complex models, on the other hand, compromise accuracy by eliminating less important processes but are more operational over large areas (Chen, Senay, Singh, & Verdin, 2016; Ji et al., 2019; Singh & Senay, 2016).

In this study, we used the Operational Simplified Surface Energy Balance (SSEBop) model to estimate the ETa over the state of South Dakota (SD). The model is a re-parameterized and operational version of the Simplified Surface Energy Balance (SSEB) method developed by Senay et al. (2007). The model uses a location- and time-based pre-defined hot and cold reference boundary limit and the principle of satellite psychrometry to estimate the psychrometric surface equivalents of dry-bulb and wet-bulb air temperatures, those are further used to calculate an evapotranspiration factor (ET_f) and ETa for each pixel. Here, the SSEBop model utilizes the thermal band from the Landsat imagery to obtain the land surface temperature (T_s) for ET_f estimations. Due to the field-scale spatial resolution (30 m), Landsat data are quite beneficial for field-level management practices. The ETa estimation at the field-scale spatial resolution allows for field characterizations such as the distribution of irrigated fields, relating ETa to cropland data layers, and crop water use for specific crops.

Several studies have reported identifying the crop water use at field scales or regional scales based on ETa estimations derived from field-based and remote sensing-based techniques for various parts of the state (Hankerson, Kjaersgaard, & Hay, 2012; Khand, Kjaersgaard, Hay, & Jia, 2017; Reyes-González, Kjaersgaard, Trooien, Hay, & Ahiablame, 2017; Yang et al., 2017). However, no study has developed so far the state-wide ETa estimations to characterize the spatiotemporal dynamics of crop water use in SD. Therefore, the overall objective of this study was to characterize crop water-use dynamics and trends across the eastern and western regions of SD using Landsat imagery and SSEBop model-derived ETa estimations from 1986-2018 (33 years). Additionally, the annual evapotranspiration values calculated using the water balance approach at the 8-digit hydrologic unit code (HUC8) sub-basin level were compared to the modeled ETa estimates to evaluate the model performance and validate the results.

5.2.   Materials and Methods

5.2.1. Study Area

The present study was conducted in the state of SD (Figure 5.1), which is located in the north-central region of the USA and is part of the Great Plains. The state has a continental climate with hot, semi-humid summers and cold, dry winters. The state represents a transition in climate from wet climate conditions on the eastern side of the state to semi-arid to arid conditions on the western side. The average rainfall (South Dakota Mesonet, 2020) in the area ranges from 370 mm/year (semi-arid) in the northwestern part of the state to 660 mm/year (semi-humid) in the southeastern part. Total annual snowfall across the state varies from 63.5 to 254 mm snow water equivalents. Despite heavy rainfall and snowfall, the state is vulnerable to recurring

droughts. The average daily temperature across the state varies between -12°C (minimum temperature observed in January) and 32°C (maximum temperature observed in July) (South Dakota Mesonet, 2020; Taghizadeh-Mehrjardi et al., 2019).

The Missouri River Basin (MRB) drains most of the state except a small portion in the northeast and the Missouri River divides the state into two parts i.e. eastern SD (46%; ESD) and western SD (54%; WSD). Cropland covers about 37% of the total area and contributes substantially to the state's economy. The ESD is dominated by agricultural land (~70% of the total eastern SD area), whereas, the WSD is mainly occupied by shrub/barren land. Most of the state's agricultural area is rain-fed. A major percentage of cropland is in the ESD (80% of the total cropland) and is dominated by corn (*Zea mays* L.)-soybean (*Glycine max* (L.) Merr.) rotation. In an average year, more than 3.24 million ha area in SD has been used under corn and soybean productions. Other major crops in the area include wheat (*Triticum aestivum*) and sunflower (*Helianthus annuus*) (SD agriculture: https://cdn.agclassroom.org/nat/data/stats/southdakota.pdf). Most of the agricultural area is rain-fed, located primarily east of the Missouri River. About 2.5% of the agricultural land is under irrigation (71% irrigated by sprinklers and 29% by surface applications). According to the U.S. Geological Survey (USGS) water use reports of 2005, 2010, and 2015, the primary categories for water use for the state were irrigation (~58%) and domestic water supplies (~20%). Of the total withdrawals from surface and groundwater (1.89 Mm^3/day), about 1.1 Mm^3/day (292 Mgal/d; 51% from groundwater and 49% from surface water) is for irrigation (Carter & Neitzert, 2008; Dieter et al., 2018; Maupin et al., 2017).

5.2.2. Input Data

To estimate the ETa, the thermal band of the Landsat satellite was used to obtain T_s. Landsat imagery for 18 path-row combinations (Paths 29-34 and Rows 28-30) was acquired from Landsat imagery (Landsat 5/7/8) pre-collection 1 using the Google Earth Engine (GEE). In total, 12,016 Landsat images with ≤70% cloud cover were collected for the 1986-2018 time period. The Landsat satellite has a temporal resolution of 16 days, which becomes 8 days with dataset availability from two satellites. The maximum number of acquired images was for 2016 (534 images; Landsat 7 and Landsat 8) and the minimum was for 1990 (139 images; Landsat 5).

An Fmask algorithm (Zhu, Wang, & Woodcock, 2015) with a combination of a cloud buffer (temperature difference threshold of 15K; air temperature - T_s = 15K) was applied to remove the cloud-contaminated pixels (clouds and cloud shadows) from the Landsat images. After pre-processing of images, acquired Landsat images were used to calculate T_s (using the thermal band 10 and emissivity) and Normalized Difference Vegetation Index (NDVI; using red and near-infrared bands). The SSEBop model uses gridded reference evapotranspiration (ET_r) datasets, those are bias-corrected using station-based meteorological datasets. The ET_r data were obtained from Climatology Lab gridMET datasets (Abatzoglou, 2013; available at http://www.climatologylab.org/gridmet.html) at ~4km spatial resolution and daily temporal resolution. A reference ET bias-correction coefficient (k) of 0.85 was used to adjust the potential overestimation of ET_r (Blankenau, Kilic, & Allen, 2020; Justin Huntington, 2020, pers communication).

Gridded air temperature was obtained from TopoWx ("Topography Weather") at 800-m spatial resolution. TopoWx (Oyler, Ballantyne, Jencso, Sweet, & Running, 2015) provides gridded estimates of daily minimum and maximum temperature generated by interpolation and extrapolation of historical daily station observations. A Digital Elevation Model map with 30m spatial resolution for 2008 was obtained from the USGS-Shuttle Radar Topographic Mission (SRTM) (Farr & Kobrick, 2000). Considering the assumptions listed in Senay et al. (2013) and using net radiations, the temperature differential parameter (dT) was computed for each day of the year for each pixel by the SSEBop model.

The cropland data layer and crop mask layer for 2018 (USDA NASS Cropland Data Layer, 2018), obtained from the U.S. Department of Agriculture, National Agricultural Statistics Service (USDA-NASS), was used to extract the cropland extent at a 30m spatial resolution for the state. The crop mask layer provides the pixels under cultivated cropland for at least 2 years out of the last 5 years.

5.2.3. SSEBop Model

The SSEBop modeling approach is based on the surface energy balance, but it does not solve all the energy balance terms like the other energy balance models. SSEBop uses the satellite psychrometric approach to calculate ET_f for all the pixels of the image and use it in the combination of ET_r to calculate actual ET.

$$ETa = ET_f * k * ET_r \tag{1}$$

where, ETa is the actual evapotranspiration, ET_f is the ET fraction ranging from 0 to 1, k (0.85) is the reference ET bias-correction coefficient and ET_r is the alfalfa (*Medicago sativa*) reference ET. The SSEBop model uses a pre-defined dT parameter (Senay et al.,

2013) to define the "wet" and "dry" conditions for each pixel. Wet conditions refer to the cold temperature (T_c; in case of no sensible heat flux) and dry conditions refer to the hot temperature (T_h; in case of no latent heat flux). This innovative parameterization procedure for limiting extreme surface temperature conditions helps the model to eliminate all complex calculations to solve energy balance terms and provides a simple energy balance approach to obtain the ET_f (equation 2). Also, the predefined dT approach overcomes the limitation of the original SSEB formulation or similar models (e.g., SEBAL, METRIC) that need a set of reference hot and cold pixel pairs derived from the image to calculate dT (Senay et al., 2013). Sometimes, it is difficult to find reference hot/cold points, for example, determining a hot reference point during the mid-growing season in the ESD is almost impossible. Also, the predefined, pixel-specific dT from SSEBop overcomes the requirements for a uniform hydro-climatic region and can be applied over complex terrain (Senay et al., 2013).

The variables T_h and T_c define the temperature under dry and wet extreme conditions, respectively. The dry extreme condition refers to zero latent heat flux. As there is no available water for evaporative cooling at dry limiting condition, T_s will increase to maximum (T_h) and ET_f will decrease to zero. However, under wet extreme conditions, surface temperature and air temperature are assumed equal and no energy is transferred in the form of sensible heat ($H = 0$). Energy is transferred in the form of latent heat flux at the maximum rate ($ET_f = 1.0$). This energy transfer phenomenon is based on the assumption that on a clear sky day, as T_s approaches near-surface air temperature ($T_s = T_c$; $dT = T_h - T_c$), ET will become equal to the maximum crop ET rate (i.e., $ET_f = 1.0$). Equation 2 represents the formulation to calculate ET_f for any T_s.

$$ET_f = \frac{T_h - T_s}{dT} \tag{2}$$

where, T_h is the hot temperature limiting condition for the pixel on a particular day, T_s is the satellite-observed land surface temperature, and dT is the pre-defined temperature difference of extreme conditions for the same pixel $(T_h - T_c)$ on the same day. To avoid the negative and high values of ET_f, the results of equation 2 were capped to 0 as a minimum value and 1.05 as the maximum value.

To calculate the dT, the model assumes a pre-defined difference in extreme temperature limiting conditions for each pixel using the albedo, location, and elevation data for each pixel. The values of dT parameter are assumed to be unique for each day of year and location, and do not change year to year. The model considers T_c for any pixel approximately equals to the corresponding air temperature assuming that on a clear sky day, there will be no or very little sensible heat fluxes under well-watered conditions (i.e. T_s = air temperature). So, in the approach to calculate spatially dynamic cold reference limit (T_c), a new parameter i.e., c-factor was determined to calibrate the cold temperature for the region using constraints listed in Table 5.1. The c-factor was multiplied to the daily median air temperature (considering study period; 1986-2018) to obtain T_c for each pixel. Further to estimate T_h, the dT is added to T_c. A detailed description of the model and model parameters can be found in Senay et al. (2013) and Senay (2018).

The SSEBop model calculates the daily ET_f values for the overpass and uses the ET_r to estimate ET_a. Considering the temporal nature of the Landsat satellite, a linear interpolation was used to estimate the daily ET_f values in between the nearest overpass ET_f values (Senay et al., 2016; Singh, Liu, Tieszen, Suyker, & Verma, 2012). This

method allowed us to incorporate the general ET_r trend over the course of the study

period in order to estimate more accurate ET_a estimations. Singh et al. (2014) suggested a

minimum requirement of 10-12 images per year for reasonable ET estimates. A monthly

ET_a for each pixel was obtained as the final product of the model. A simple summation of

monthly estimations was used to obtain the annual ET_a.

5.2.4. Model Validation

To validate the Landsat-based ETa estimations from the SSEBop model, a water

balance approach (equation 3) was used at the basin scale to estimate water balance

evapotranspiration (WBET) and use it to compare with the model results.

$$WBET = P - Q - \Delta S \qquad (3)$$

where, P, Q, and ΔS are the annual basin precipitation, basin runoff, and change in water

storage, respectively. The annual (water year) runoff and precipitation from HUC8 sub-

basins across the MRB were obtained from the National Hydrography Dataset Plus

(NHDplus; available at https://www.epa.gov/waterdata/nhdplus-national-hydrography-

dataset-plus) and gridMET (Abatzoglou, 2013), respectively. The WBET has been

widely adopted to validate the hydrological model and remote sensing estimated ET at a

watershed or regional scale(Jin, Zhu, & Xue, 2019; Senay et al., 2016; Singh et al., 2014;

Zhang, Kimball, Nemani, & Running, 2010). In this approach, an annual water storage

change across the basin is assumed to be zero (i.e., $\Delta S = 0$).

For greater confidence in the SSEBop ETa estimations, estimated ETa results

were validated over the HUC8 sub-basins across the whole MRB (307 sub-basins)

instead of HUC8 sub-basins across SD (46 sub-basins). The channels in the MRB,

especially the Missouri River, are highly regulated for flood control, water supply,

irrigation, and hydropower. The six big dams over the river generate unnatural flow conditions in the river that could lead to additional errors in validation due to the assumption of zero annual change in storage. Also, the application of the WBET approach is limited over the problematic sub-basins where the water balance is not expected to close ($i.e., WBET \neq P - Q - \Delta S$). So, before proceeding further with the evaluation of estimated ETa results at the HUC8 sub-basin scale, four criteria were considered to exclude the problematic HUC8 sub-basins. This included sub-basins with high baseflow, dominant groundwater flow, and those heavily irrigated or those with large irrigation districts. First, the sub-basins with a runoff-rainfall ratio (Q/P; average Q and P over 1986-2018) greater than 0.33 (Velpuri et al., 2013) and with the negative WBET values (i.e. Q+ ΔS > P) were removed to avoid the validation uncertainties introduced by high groundwater flow or base flow to the runoff. The threshold for the Q/P ratio varies from basin to basin. Senay et al. (2016) considered 0.55 value as the threshold Q/P ratio for the Colorado River Basin. Velpuri et al., (2013) also considered 0.55 as the Q/P coefficient for the conterminous United States and reported less than about 0.3 Q/P in general for most of the basins. For the MRB, we observed low Q/P ratios (less than 0.3) for most of the HUC8 sub-basins (with a maximum value of 0.5). The threshold for the Q/P ratio (0.33) was arbitrarily selected considering the sub-basins with an exceptionally higher Q/P ratio than other sub-basins. About 95% of the sub-basins had a lower Q/P ratio than the threshold. The sub-basins with a SSEBop model-estimated ET higher than precipitation were also excluded to avoid sub-basins with heavy irrigation, especially from groundwater resources. It also helped to remove sub-basins with large permanent water bodies or those having large irrigation districts (Senay et al.,

2016; Singh et al., 2014). Lastly, ET estimations using the GEE version of the SSEBop model were limited to the USA only. Sub-basins sharing the boundary with Canada were not considered for validation purposes. After considering these four criteria to exclude problematic sub-basins, 252 sub-basins (out of 307) across the MRB were finalized for validating the modeled ETa results. Additionally, for better water balance closure and to remove the additional uncertainties related to the assumption of zero change in the annual basin water storage, a 10-year mean WBET (1986-1995, 1996-2005, and 2006-2018) was compared with the 10-year mean of modeled ETa results for 252 HUC8 sub-basins.

To evaluate the accuracy of modeled ETa estimation, three statistical indicators (r^2, %RMSE, PBIAS) were used. The coefficient of determination (r^2) ranges from 0 to 1 and provides the measures of goodness of fit of the data to the fitted regression line. Root mean square error (RMSE) was used to check the prediction errors. The Percent Bias (PBIAS) index represents the under or over estimations of the simulated/predicted data. Previous model studies (e.g., Choi et al., 2009; Jin, Zhu, & Xue, 2019; Senay et al., 2019) have suggested that a value higher than 0.7 for r^2 with reasonable percentage RMSE (%RMSE; depending upon the objective of the study) and a PBIAS value within -15% to 15% can be considered as a good fit and satisfactory model performance.

5.2.5. Mann-Kendall (MK) Trend Analysis

The study utilized Mann Kendall (MK) trend analysis to examine the presence or absence of a trend in the time-series of ETa over the extracted cropland areas using the USDA-NASS crop mask layer for 2018. The MK trend analysis was performed for cropland ETa at two spatial scales: (1) region-wide scale and (2) pixel scale. The MK trend test is a non-parametric rank-based method to analyze time-series data for a

consistent mono-directional (increasing or decreasing) trend (Gilbert, 1987; Kendall, 1975; Mann, 1945). This method considers the assumption of independence, which means that the collected time-series data are not serially correlated over time. The autocorrelation functions of a univariate time series were estimated to check time-series data for the assumption of independence. The method initially subtracts each time-step value from other values in the data (i.e., $x_j - x_k$, where j>k) making n(n-1)/2 combinations. The method assigns a value of -1, 0, or 1 to each calculated difference based on the resulting sign of subtraction and calculates the sum of assigned values (S). A positive S indicates the observations made later in time are larger than the observations made earlier in time and indicates an upward/increasing trend. A negative S indicates a downward/decreasing trend. For the significance of the trend, the method uses the value of S and the number of observations in the time-series data to calculate the probability for the existence of a trend. The study considered a 95% confidence level for a statistically significant trend.

5.3. Results

5.3.1. Validation of ETa Estimations

Landsat-based ETa estimations showed strong agreement with the selected 252 sub-basins WBET results with a coefficient of determination (R^2) of 0.91, 59 mm/year RMSE (11.8%), and average bias of -4% (Figure 5.2). The minimum and maximum values of mean ETa estimated by the SSEBop model were 183 mm/year [HUC8 10080004; Muskrat watershed, Wyoming (WY)] and 978 mm/year [HUC8 10290109; Lake of the Ozarks watershed, Missouri (MO)], respectively, while the minimum and maximum mean WBET was 160 mm/year (HUC8 10080004; Muskrat watershed, WY)

and 990 mm/year (HUC810300102; Lower Missouri- Moreau watershed, MO), respectively. The minimum mean annual WBET and SSEBop ETa were in an identical HUC8 sub-basin, whereas the maximum mean annual WBET and SSEBop ETa were observed in different HUC8 sub-basins that are in close proximity.

5.3.2. Mann-Kendall (MK) Trend Analysis

5.3.2.1 Regional-scale Trend Analysis

The main goal of the study was to utilize the Landsat data in combination with the SSEBop model to estimate the crop water use at field scale (spatial resolution 30 m) over the selected period (1986-2018) and to evaluate the existing trends. First, the region-wide trend analysis was performed to understand the existing cropland ETa and precipitation trends over ESD, WSD, and the entire SD (Figure 5.3). Both parameters have shown a statistically non-significant ($p>0.05$) positive trend in annual ETa for all three considered regions. However, an increasing trend can be observed for normal and wet years. The ESD showed an increasing trend in cropland ETa and precipitation before the drought period of 2002-2006. Precipitation seems to continue the increasing trend after the drought period whereas cropland ETa showed a flat curve in figure 5.3. Similar behavior was observed for both parameters for the entire SD region. The WSD cropland ETa seems to be more sensitive to the drought. Higher ET reduction and a major decline in the ETa trend in figure 5.3 were observed during the drought period of 2002-2006 for the region.

5.3.2.2 Pixel-scale Trend Analysis

A pixel-scale analysis was performed to extract the field-level information about spatial and temporal variability of crop water use across the areas with significant trends.

127

About 12% and 9% of the cropland pixels revealed a mono-directional significant trend

in crop water use in the ESD and WSD, respectively (Figure 5.4). Most of the cropland

pixels under significant trends on either side of the state were associated with a positive

trend. A small part of the cropland in the mid-eastern part of the state indicated a negative

significant trend of crop water use. A close inspection of pixels under significant trends

showed that the majority of these pixels belong to corn and soybean, whereas, only a

small portion of the pixels under winter wheat showed a significant trend.

5.3.3. Crop Water Use

An increasing cropland ETa pattern from the northeast to southwest part of the

state was observed. The average annual ETa over cropland area in the ESD for the 33-

year study period (1986-2018) was 527 mm, which seems to be supplied by the

precipitation amounts (594 mm) in the area. Similar observations were found for the

WSD cropland area, where average annual cropland ETa and average annual

precipitations were 427 mm and 490 mm, respectively. In addition, a 10-year shift in the

mean annual SSEBop ETa over HUC8 sub-basins in the entire state was examined

(Figure 5.5). An increment in the number of HUC8 sub-basins with higher ETa was

observed during the 2006-2018 period as compared to the1986-1995 and 1996-2005

periods. This shift signifies increasing crop water use in the state.

Crop water use in the state was found to be sensitive to varying weather

conditions. During the drought period of 2002-2006, the average annual cropland ETa for

the state was reduced to 428 mm, which was 12% less than the 33-year average cropland

ETa. The western side of the state was impacted severely during this drought period

where average annual ETa and average annual precipitation declined to 319 mm (25%

reduction) and 399 mm (18% reduction), respectively. During the drought period, the most severe year for the WSD was 2002, where the WSD received a minimum annual precipitation of 305 mm (38% less than average), which dropped the annual cropland ETa to 251mm (41% less than the average). The eastern part of the state faced a 10% reduction in annual cropland ETa due to a 7% reduction in precipitation during this same drought period. The ESD also received the lowest precipitation in 2002 (469 mm; 21% less than average), but the maximum reduction in cropland ETa occurred in 2006 (22% reduction; 10% lower precipitation than average). The next meteorological drought faced by the state was in 2012, where the state received 30% less precipitation than the 33-year average precipitation. Surprisingly, however, the annual cropland ETa estimations showed contradictory results (an increment of 12% in cropland ETa) in the ESD.

Figure 5.6 represents the annual ETa anomalies and precipitation under varying weather conditions of SD. The ETa was found to be higher over the ESD under the normal year conditions compared to the other two extreme weather conditions (Figure 5.6b). Both the extreme weather conditions (dry and wet years) seem to be decreasing the annual ETa in the ESD.

5.4. Discussion

The availability of remotely sensed data and emerging satellite-based energy balance techniques show substantial promise to update historical crop water use records along with routine monitoring of seasonal crop water uses. Furthermore, capturing the spatial and seasonal ETa dynamics is the other merit of remotely sensed data and approaches. Remote sensing approaches have become an important component of the toolkits for water managers and planners around the world to compile and monitor water

use components at a watershed scale. ETa trends are also being widely studied and attributed to drought (Jung et al., 2010) and climatic changes (Douville et al., 2013; Zhang et al., 2016). The majority of crop water use trend studies are based on the crop coefficient (K_c) approach where K_c is derived using NDVI for a specific crop. The K_c approach assumes optimal agricultural practices and consistent NDVI for different Landsat sensors (Rocha, Perdigão, Melo, & Henriques, 2012). The energy balance ET models such as the SSEBop model overcome the limitations of the K_c approach and eliminate the uncertainties associated with crop type classification and the assumptions of optimal crop growth and consistent NDVI (Senay et al., 2019).

Satellite-based crop water use estimation approaches are prone to the uncertainties introduced by input data quality, cloud contamination, and an unequal number of images over different years. The SSEBop model requires low input model drivers and parameters, hence limits complexity and uncertainties introduced by input data quality and model parameterization. However, sometimes less complex models may compromise the accuracy of results on specific local conditions but remain more operational and consistent than the complex models over large areas and historical analysis. Model evaluation statistics ($r^2 = 0.91$, PBIAS= -4%, and %RMSE = 11.8%) of this study and previous studies across the world that include, for instance, USA (Senay et al., 2016, 2017, 2019), Brazil (Dias Lopes et al, 2019), China (Yin et al., 2020; Jin et al., 2019), India (Sharma et al., 2018), West Africa (Dembélé et al., 2020), and others, support the reliability of the SSEBop ET estimations. Other challenges for crop water use trend analysis using remote sensing approaches are due to the changes in satellite sensors over time (Senay et al., 2019). The innovative approach of scene-based c-factor in the SSEBop

modeling approach minimizes the potential difference in T_s calibration among Landsat

sensors (5, 7, and 8). In addition, the predefined dT parameter approach of the SSEBop

model provides a simplified and consistent model parameter over the study period. The

well-validated SSEBop ETa estimations of this study reflect the robustness of the

SSEBop model to quantify ETa over a wide range of vegetation types, climate, and water

availability. The spatial distribution of estimated ETa shows the potential of Landsat

imagery for water management. This study demonstrates a scalable and simplified ET

modeling approach that requires only freely available online datasets that include weather

information and Landsat imagery.

This study presents the spatiotemporal ETa dynamics and its governing factors

across the arid to humid continental climate regions of SD. Land cover and weather are

the two main driving factors for ETa. To understand the causes of exhibited ETa trends,

land cover changes across SD were first explored. Although the regional-scale trend

analysis did not show significant mono-directional (increasing or decreasing) trends for

precipitation and cropland ETa on either side of the state, an increasing trend was

observed for the rest of the period except the 2002-2006 drought period. This increasing

trend could be related to the increasing corn and soybean crop area and yields in the state

(USDA-NASS crop survey reports). The USDA-NASS crop survey data for SD

(available at https://quickstats.nass.usda.gov/) revealed a rapid change in crops used in

the rotations during the study period. According to the crop survey reports and SD

Census of Agriculture report (2017), the state faced a major change in agricultural

practices and agricultural production over the period from 1987-2017 (30 years) with a

26% increase in total cropland area. The state changed its major cultivation crop from

wheat to corn and soybean. The wheat production area was reduced by 60%, whereas, corn and soybean production areas were increased by 100% and 300%, respectively, during the 1987-2017 period. These shifts in crop practices and increased corn-soybean production area might have governed the increment in the number of HUC8 sub-basins with higher ETa for the last 13-year period (Figure 5.5). Also, the 2006-2018 period had fewer dry years than the other two periods (Figure 5.5), which could be another potential reason for the higher ETa over HUC8 sub-basins during this period.

The ET is an important hydro-meteorological variable to study climate change because it involves mass and energy exchanges between the land surface and atmosphere. The annual cropland ETa in SD is mainly driven by growing season climate changes. The chapter on Northern Great Plains in the Fourth National Climate Assessment report (USGCRP, 2018) and Hay and Todey (2011) suggest that an increasing trend of annual precipitation for the study region is likely being driven by increased precipitation during the non-growing seasons. Hay and Todey (2011) also discussed the increased average temperature in the Northwestern Corn Belt (including SD) being driven by the increase in minimum instead of maximum temperatures. The increased non-growing season precipitation and the increased minimum temperature seem to have minimal impact on cropland ETa. Considering the above reasons, the study has not explored the impact of climate factors on the cropland ETa. However, a moisture regime shift due to increased precipitation and increased mean temperature could be an additional factor for increasing cropland ETa trends.

Many regions of cropland over the north-central part of the ESD showed significant positive trends at the 0.05 significance level (Figure 5.4). The adoption of

higher biomass crops (corn-soybean) over lower biomass crops (wheat) might have led to these increasing crop water use trends. Additionally, the soils near the Missouri River were found to be quite productive under effective irrigation. Although the state has a small portion of irrigated cropland, an increase from 2 to 2.5% was observed in total irrigated land (i.e., 36% increase with respect to irrigated land). The state also experienced a significant increasing trend in crop productions (corn: 179 kg/ha in 2018 compared to 92 kg/ha in 1986 and soybean: 50.5 kg/ha in 2018 compared to 34 kg/ha in 1986) during the study period (USDA-NASS crop survey reports). The shift in agricultural practices, increased irrigated cropland, increased crop productions, and moisture regime shifts might have governed the crop water use in the area.

The ESD is located within the Northern Glaciated Plains (NGP) ecoregion. Taylor, Acevedo, Auch, and Drummond (2015) discussed two major changes in the NGP ecoregion during 1986-2000: (i) agricultural to grassland changes under the USDA Farm Service Agency Conservation Reverse Program (CRP), and (ii) dynamic changes in agricultural land to wetland and wetland to water as a result of a series of wet years and cyclic climatic conditions during this period. A major part of area A1 (Figure 5.4) belongs to the wetlands and permanent water bodies. The expansion of the wetland areas with increasing precipitation trends in area A1 might have resulted in the increasing crop water use trends. Areas A2 and A3 (Figure 5.4) located in the Northwestern Glaciated Plains (NWGLP) ecoregion and the Northwestern Great Plains (NWGP) ecoregion, respectively. Both areas are dominated by spring/winter wheat and sunflower. The pixels with a significant trend in area A2 were found to be associated with corn, soybean, spring wheat, and sunflower whereas the winter wheat pixels have not shown any significant

trend. Additionally, the availability of genetically modified crops with a decreased risk of farming in dry areas increased cropland areas and water demands in the SD part of the NWGLP and the eastern part of the NWGP ecoregions (Taylor et al., 2015).

The negative cropland ETa trend pixels were found to be clustered in the mid-eastern part of SD. This part of the state is in the Big Sioux River Basin and wetlands cover a substantial part of this area. Most of the pixels under negative significant trends are near to or across the boundaries of permanent water bodies. The decreasing trend across these pixels indicates either the loss of wetlands covered area or the conversion of wetlands to cropland. A subsurface drainage permit map (available in USGS data release by Finocchiaro (2014)) revealed clustered subsurface drainage practices in the region (counties: Moody, Minnehaha, Lake, McCook, and Kingsbury). The loss of wetland area due to the increased adoption of subsurface drainage practices in the last two decades could have influenced the annual ET values. Other reasons for this existing trend might be the dynamic change of a major crop from oats to soybean and decreased irrigation practices in this region (Dumke & Dobbs, 1999).

The exhibited ETa pattern across the state is the combined result of landuse and climate conditions. The northwest cropland area of the state is dominated by low biomass crops, has arid climate conditions, and exhibits low ETa. Whereas the cropland in the southeast part of the state is dominated by high biomass crops such as corn and soybean and has semi-humid to humid climate conditions. The higher biomass productions in the area can be related to the higher ETa.

The state of SD is vulnerable to recurring droughts. The higher reductions in ETa as compare to precipitation during a drought year indicates that the landscape response

(ETa) is more sensitive to drought as not all the precipitation amount is usable for the crops. It also suggests that ETa is a better variable for drought monitoring/drought studies than precipitation and precipitation-based indices because ET captures the temporal distribution of precipitation and provides more direct observations of drought patterns.

The rainfall amounts during the growing season are critical to the cropland ETa. The growing period of 2002 started with abnormally dry (D0) conditions across the entire state. A drought pattern of extreme drought conditions (D3) in the southwest to abnormally dry (D0) conditions in the northeast part of the state developed during the high crop water demand period (US Drought Monitor map archive, available at https://droughtmonitor.unl.edu/). Extreme drought conditions over the WSD resulted in high reduction in cropland ETa (41% less than average), whereas, abnormally dry conditions reduced 13% cropland ETa in the ESD. During the drought year of 2006, the drought started developing in the central part of the state at the beginning of the growing season. Conditions developed to exceptional drought (D4) in central SD with severe drought (D2) on the western side and moderate drought (D1) conditions on the eastern side of the state by the end of July (US Drought Monitor map archive). Even after receiving higher annual precipitation in 2006 than 2002, the 2006 drought impact was more intensive for the ESD cropland ETa (22% less than the average) than the 2002 drought impact. Higher annual cropland ETa than average in ESD during the drought year 2012 might be the result of high atmospheric demand with high ET. An inspection of the reference ET gridMET product revealed a higher annual reference ET (20%-30%) than the normal years, which could have exaggerated the modeled ETa.

The ESD is vulnerable to excess soil moisture during the spring and planting periods. The increased soil moisture conditions during the wet year result in a delay in planting crops, shortening the growing period, yield reductions, and reduction in cropland, which subsequently results in lower ETa in the region. During the 2010 wet year, the state's crop productions were 19% lower for corn, 11% lower for soybean, 28% less for sorghum, and 23% lower for sunflower than the 2009 normal year crop productions (USDA NASS crop survey reports). The other potential reason for the lower ETa during a wet year might be the reduced atmospheric demands (low ET_r).

5.5. Conclusions

This study aimed to understand the crop water-use characteristics and existing historic mono-directional crop water-use trends across eastern and western South Dakota (ESD & WSD) over the 1986-2018 (33-years) period. This study also evaluated the performance of the SSEBop model to estimate actual evapotranspiration (ETa) in a combination with the Landsat imagery. The Landsat-based ETa estimations were validated at the HUC8 sub-basin scale using water balance ETa (WBET) estimations. The validation statistics indicated a strong agreement ($r^2 = 0.91$, PBIAS= -4%, and %RMSE = 11.8%) between the SSEBop ETa and the WBET on annual basis.

The spatial average values of crop water use (demand: 527 mm/year and 427 mm/year) was found to be lower than the average rainfall amounts (supply: 594 mm/year and 490 mm/year) over the ESD and WSD regions. This difference could be related to the low percentage of irrigated cropland (~2.5%) in the state. Furthermore, the state observed severe reductions in crop water-uses under recurring droughts. The WSD was found to be more vulnerable to the varying weather conditions than the ESD.

Additionally, landscape responses for ET were found to be more sensitive than the precipitation deficit during the drought years, which suggests more severe drought impacts than expected. The high sensitivity of ETa to drought conditions suggests that the ETa responses are a better variable for monitoring and assessing droughts impacts across agricultural croplands than the precipitation-based meteorological drought indices.

In addition to crop water-use characteristics, Mann Kendall trend analysis was applied to test the presence or absence of a mono-directional trend in the time-series of annual ETa over the cropland areas at region-wide and pixel-level scale. At the regional scale, no statistically significant trend was observed in annual ETa and precipitation due to the varying weather conditions, although an increasing trend in ETa was observed among the normal and wet years. Also, an increase in the average ETa of HUC8 sub-basins was observed in the last 13 years (2006-2018) compared to the 1986-1995 and 1996-2005 periods. At the pixel-scale trend analysis, most of the pixels under statistically significant trends revealed an increasing trend. These increasing trends might be induced by the shift in agricultural practices, increased irrigated cropland, increased production, moisture regime shifts, and the decreased risk of farming in dry areas. The pixels under the significant decreasing trend might be influenced either by the dynamic conversion of wetlands to croplands or by the decreased irrigation practices in mid-eastern SD. Additionally, an inter-comparison of the annual ET anomalies during dry, normal, and wet years revealed lower ETa in the ESD during the dry and wet years.

This study demonstrates the tremendous potential and robustness of the SSEBop model in estimating spatially distributed evapotranspiration. This study also highlights the usefulness of the rich Landsat archive for conducting pixel-based crop water-use

analysis and for characterizing its spatiotemporal dynamics. In addition, these results

emphasize the importance and practicality of ET-based drought monitoring. This scalable

approach can be extended to any regional/nationwide/global level, depending upon data

availability, computing resources and efficiencies. This approach could become a

powerful tool for the water resources planners and policymakers, especially in the

planning and management of scarce water resources.

References

Abatzoglou, J. T. (2013). Development of gridded surface meteorological data for ecological applications and modelling. International Journal of Climatology, 33(1), 121-131.

Allen, R. G., Pereira, L. S., Raes, D., & Smith, M. (1998). Crop evapotranspiration-Guidelines for computing crop water requirements-FAO Irrigation and drainage paper 56. Fao, Rome, 300(9), D05109.

Allen, R. G., Tasumi, M., & Trezza, R. (2007). Satellite-based energy balance for mapping evapotranspiration with internalized calibration (METRIC)—Model. Journal of irrigation and drainage engineering, 133(4), 380-394.

Anderson, M. C., Norman, J. M., Mecikalski, J. R., Otkin, J. A., & Kustas, W. P. (2007). A climatological study of evapotranspiration and moisture stress across the continental United States based on thermal remote sensing: 1. Model formulation. Journal of Geophysical Research: Atmospheres, 112(D10).

Bastiaanssen, W. G., Menenti, M., Feddes, R., & Holtslag, A. (1998). A remote sensing surface energy balance algorithm for land (SEBAL). 1. Formulation. Journal of Hydrology, 212, 198-212.

Blankenau, P. A., Kilic, A., & Allen, R. (2020). An evaluation of gridded weather data sets for the purpose of estimating reference evapotranspiration in the United States. Agricultural Water Management, 242, 106376.

Brutsaert, W. (2005). Hydrology: an introduction: Cambridge University Press.

Carter, J. M., & Neitzert, K. M. (2008). Estimated use of water in South Dakota, 2005. Retrieved from World Wide Web, 605, 394-3200.

Chen, M., Senay, G. B., Singh, R. K., & Verdin, J. P. (2016). Uncertainty analysis of the Operational Simplified Surface Energy Balance (SSEBop) model at multiple flux tower sites. Journal of Hydrology, 536, 384-399.

Choi, M., Kustas, W. P., Anderson, M. C., Allen, R. G., Li, F., & Kjaersgaard, J. H. (2009). An intercomparison of three remote sensing-based surface energy balance

algorithms over a corn and soybean production region (Iowa, US) during SMACEX. Agricultural and Forest Meteorology, 149(12), 2082-2097.

Dembélé, M., Ceperley, N., Zwart, S. J., Salvadore, E., Mariethoz, G., & Schaefli, B. (2020). Potential of satellite and reanalysis evaporation datasets for hydrological modelling under various model calibration strategies. Advances in Water Resources, 143, 103667.

Dias Lopes, J., Neiva Rodrigues, L., Acioli Imbuzeiro, H. M., & Falco Pruski, F. (2019). Performance of SSEBop model for estimating wheat actual evapotranspiration in the Brazilian Savannah region. International Journal of Remote Sensing, 40(18), 6930-6947.

Dieter, C. A., Maupin, M. A., Caldwell, R. R., Harris, M. A., Ivahnenko, T. I., Lovelace, J. K., . . . Linsey, K. S. (2018). Estimated use of water in the United States in 2015: US Geological Survey.

Douville, H., Ribes, A., Decharme, B., Alkama, R., & Sheffield, J. (2013). Anthropogenic influence on multidecadal changes in reconstructed global evapotranspiration. Nature Climate Change, 3(1), 59-62.

Dumke, L., & Dobbs, T. L. (1999). Historical evolution of crop systems in eastern South Dakota: Economic influences. Department of Economics Research Reports. . Paper 63. http://openprairie.sdstate.edu/econ_research/63.

Farr, T. G., & Kobrick, M. (2000). Shuttle Radar Topography Mission produces a wealth of data. Eos, Transactions American Geophysical Union, 81(48), 583-585.

Finocchiaro, R. (2014). Agricultural subsurface drainage tile locations by permits in South Dakota. U.S. Geological Survey Data Release.[Online]. Available: http://dx. doi. org/10.5066/F7KS6PNW.

Gilbert, R. O. (1987). Statistical Methods for Environmental Pollution Monitoring. United Kingdom: Wiley.

Hankerson, B., Kjaersgaard, J., & Hay, C. (2012). Estimation of evapotranspiration from fields with and without cover crops using remote sensing and in situ methods. Remote Sensing, 4(12), 3796-3812.

Hay, C. H., & Todey, D. P. (2011). Precipitation and Evapotranspiration Patterns in the Northwestern Corn Belt and Impacts on Agricultural Water Management. Paper presented at the American Society of Agricultural and Biological Engineers, Louisville, Kentucky, August 7-10, 2011.

Ji, L., Senay, G. B., Velpuri, N. M., & Kagone, S. (2019). Evaluating the Temperature Difference Parameter in the SSEBop Model with Satellite-Observed Land Surface Temperature Data. Remote Sensing, 11(16), 1947.

Jin, X., Zhu, X., & Xue, Y. (2019). Satellite-based analysis of regional evapotranspiration trends in a semi-arid area. International Journal of Remote Sensing, 40(9), 3267-3288.

Jung, M., Reichstein, M., Ciais, P., Seneviratne, S. I., Sheffield, J., Goulden, M. L., ... & Dolman, A. J. (2010). Recent decline in the global land evapotranspiration trend due to limited moisture supply. Nature, 467(7318), 951-954.

Kendall, M. (1975). Rank correlation methods (4th edn.) charles griffin. San Francisco, CA, 8.

Khand, K., Kjaersgaard, J., Hay, C., & Jia, X. (2017). Estimating impacts of agricultural subsurface drainage on evapotranspiration using the Landsat imagery-based METRIC model. Hydrology, 4(4), 49.

Kustas, W. P., & Norman, J. M. (2000). A two-source energy balance approach using directional radiometric temperature observations for sparse canopy covered surfaces. Agronomy Journal, 92(5), 847-854.

Mann, H. B. (1945). Nonparametric tests against trend. Econometrica: Journal of the econometric society, 245-259.

Maupin, M. A., Kenny, J. F., Hutson, S. S., Lovelace, J. K., Barber, N. L., & Linsey, K. S. (2017). Estimated use of water in the United States in 2010.

Mu, Q., Zhao, M., & Running, S. W. (2011). Improvements to a MODIS global terrestrial evapotranspiration algorithm. Remote Sensing of Environment, 115(8), 1781-1800.

Oyler, J. W., Ballantyne, A., Jencso, K., Sweet, M., & Running, S. W. (2015). Creating a topoclimatic daily air temperature dataset for the conterminous United States using homogenized station data and remotely sensed land skin temperature. International Journal of Climatology, 35(9), 2258-2279.

Rajib, A., Evenson, G. R., Golden, H. E., & Lane, C. R. (2018). Hydrologic model predictability improves with spatially explicit calibration using remotely sensed evapotranspiration and biophysical parameters. Journal of hydrology, 567, 668-683.

Reyes-González, A., Kjaersgaard, J., Trooien, T., Hay, C., & Ahiablame, L. (2017). Comparative analysis of METRIC model and atmometer methods for estimating actual evapotranspiration. International Journal of Agronomy, 2017.

Rocha, J., Perdigão, A., Melo, R., & Henriques, C. (2012). Remote sensing based crop coefficients for water management in agriculture. Sustainable Development-Authoritative and Leading Edge Content for Environmental Management, 167-192.

Roerink, G., Su, Z., & Menenti, M. (2000). S-SEBI: A simple remote sensing algorithm to estimate the surface energy balance. Physics and Chemistry of the Earth, Part B: Hydrology, Oceans and Atmosphere, 25(2), 147-157.

Senay, G. B. (2018). Satellite psychrometric formulation of the Operational Simplified Surface Energy Balance (SSEBop) model for quantifying and mapping evapotranspiration. Applied engineering in agriculture, 34(3), 555-566.

Senay, G. B., Bohms, S., Singh, R. K., Gowda, P. H., Velpuri, N. M., Alemu, H., & Verdin, J. P. (2013). Operational evapotranspiration mapping using remote sensing and weather datasets: A new parameterization for the SSEB approach. JAWRA Journal of the American Water Resources Association, 49(3), 577-591.

Senay, G. B., Budde, M., Verdin, J. P., & Melesse, A. M. (2007). A coupled remote sensing and simplified surface energy balance approach to estimate actual evapotranspiration from irrigated fields. Sensors, 7(6), 979-1000.

Senay, G. B., Friedrichs, M., Singh, R. K., & Velpuri, N. M. (2016). Evaluating Landsat 8 evapotranspiration for water use mapping in the Colorado River Basin. Remote Sensing of Environment, 185, 171-185. doi:10.1016/j.rse.2015.12.043

Senay, G. B., Schauer, M., Friedrichs, M., Velpuri, N. M., & Singh, R. K. (2017). Satellite-based water use dynamics using historical Landsat data (1984–2014) in the southwestern United States. Remote Sensing of Environment, 202, 98-112.

Senay, G. B., Schauer, M., Velpuri, N. M., Singh, R. K., Kagone, S., Friedrichs, M., . . . Douglas-Mankin, K. R. (2019a). Field Scale Crop Water Use Trends and Spatial Variability over the Upper Rio Grande Basin of United States and Mexico using Landsat-Based Evapotranspiration. AGU Fall Meeting, 2019, H31L-1885.

Senay, G. B., Schauer, M., Velpuri, N. M., Singh, R. K., Kagone, S., Friedrichs, M., . . . Douglas-Mankin, K. R. (2019b). Long-term (1986–2015) crop water use characterization over the Upper Rio Grande Basin of United States and Mexico using Landsat-based evapotranspiration. Remote Sensing, 11(13), 1587.

Sharma, D. N., & Tare, V. (2018). Evapotranspiration Estimation Using SSEBop Method with Sentinel-2 and LANDSAT-8 Data Set. International Archives of the Photogrammetry, Remote Sensing and Spatial Information Sciences, 42, 5.

Singh, R. K., Liu, S., Tieszen, L. L., Suyker, A. E., & Verma, S. B. (2012). Estimating seasonal evapotranspiration from temporal satellite images. Irrigation Science, 30(4), 303-313.

Singh, R. K., & Senay, G. B. (2016). Comparison of four different energy balance models for estimating evapotranspiration in the Midwestern United States. Water, 8(1), 9.

Singh, R. K., Senay, G. B., Velpuri, N. M., Bohms, S., Scott, R. L., & Verdin, J. P. (2014). Actual evapotranspiration (water use) assessment of the Colorado River Basin at the Landsat resolution using the Operational Simplified Surface Energy Balance Model. Remote Sensing, 6(1), 233-256.

South Dakota Mesonet. (2020). from South Dakota State University. South Dakota Mesonet Database.

Su, Z. (2002). The Surface Energy Balance System (SEBS) for estimation of turbulent heat fluxes. Hydrology and earth system sciences, 6(1), 85-99.

Taghizadeh-Mehrjardi, R., Bawa, A., Kumar, S., Zeraatpisheh, M., Amirian-Chakan, A., & Akbarzadeh, A. (2019). Soil Erosion Spatial Prediction using Digital Soil

Mapping and RUSLE methods for Big Sioux River Watershed. Soil Systems, 3(3), 43.

Taylor, J. L., Acevedo, W., Auch, R. F., & Drummond, M. A. (2015). Status and Trends of Land Change in the Great Plains of the United States: 1973 to 2000: US Department of the Interior, US Geological Survey.

USDA National Agricultural Statistics Service Cropland Data Layer. (2018). Retrieved from https://nassgeodata.gmu.edu/CropScape/. Retrieved December 21, 2019, from USDA-NASS, Washington, DC https://nassgeodata.gmu.edu/CropScape/

USGCRP, (2018): Impacts, risks, and adaptation in the United States: Fourth national climate assessment, volume II: Report-in-Brief [Reidmiller, D.R., C.W. Avery, D.R. Easterling, K.E. Kunkel, K.L.M. Lewis, T.K. Maycock, and B.C. Stewart (eds.)]. U.S. Global Change Research Program, Washington, DC, USA, 186 pp. doi: 10.7930/NCA4.2018.

Vadeboncoeur, M. A., Green, M. B., Asbjornsen, H., Campbell, J. L., Adams, M. B., Boyer, E. W., . . . Shanley, J. B. (2018). Systematic variation in evapotranspiration trends and drivers across the Northeastern United States. Hydrological Processes, 32(23), 3547-3560.

Velpuri, N. M., Senay, G. B., Singh, R. K., Bohms, S., & Verdin, J. P. (2013). A comprehensive evaluation of two MODIS evapotranspiration products over the conterminous United States: Using point and gridded FLUXNET and water balance ET. Remote Sensing of Environment, 139, 35-49.

Vörösmarty, C. J., Federer, C. A., & Schloss, A. L. (1998). Potential evaporation functions compared on US watersheds: Possible implications for global-scale water balance and terrestrial ecosystem modeling. Journal of Hydrology, 207(3-4), 147-169.

Yang, Y., Anderson, M., Gao, F., Hain, C., Kustas, W., Meyers, T., . . . Sun, L. (2017). Impact of tile drainage on evapotranspiration in South Dakota, USA, based on high spatiotemporal resolution evapotranspiration time series from a multisatellite data fusion system. IEEE Journal of Selected Topics in Applied Earth Observations and Remote Sensing, 10(6), 2550-2564.

Yang, Y., Anderson, M., Gao, F., Hain, C., Noormets, A., Sun, G., . . . Sun, L. (2020). Investigating impacts of drought and disturbance on evapotranspiration over a forested landscape in North Carolina, USA using high spatiotemporal resolution remotely sensed data. Remote Sensing of Environment, 238, 111018.

Yin, L., Wang, X., Feng, X., Fu, B., & Chen, Y. (2020). A Comparison of SSEBop-Model-Based Evapotranspiration with Eight Evapotranspiration Products in the Yellow River Basin, China. Remote Sensing, 12(16), 2528.

Zhang, K., Kimball, J. S., Nemani, R. R., & Running, S. W. (2010). A continuous satellite-derived global record of land surface evapotranspiration from 1983 to 2006. Water Resources Research, 46(9).

Zhang, Y., Peña-Arancibia, J. L., McVicar, T. R., Chiew, F. H., Vaze, J., Liu, C., . . . Liu, Y. Y. (2016). Multi-decadal trends in global terrestrial evapotranspiration and its components. Scientific reports, 6, 19124.

Zhu, Z., Wang, S., & Woodcock, C. E. (2015). Improvement and expansion of the Fmask algorithm: Cloud, cloud shadow, and snow detection for Landsats 4–7, 8, and Sentinel 2 images. Remote Sensing of Environment, 159, 269-277.

Table 5.1. Constraint limits for c-factor determination

Parameter	Constrain Limits
NDVI	>0.7
Land Surface Temperature (T_s)	$T_s > 270K$
Temperature difference	$0 <=$ maximum air temperature $(T_a) - T_s <= 15$
c-factor	Mean of $(T_s/ T_a) - 2$ STD (for selected pixels)

NDVI = Normalized Difference Vegetation Index and STD = standard deviation of (T_s/ T_a)
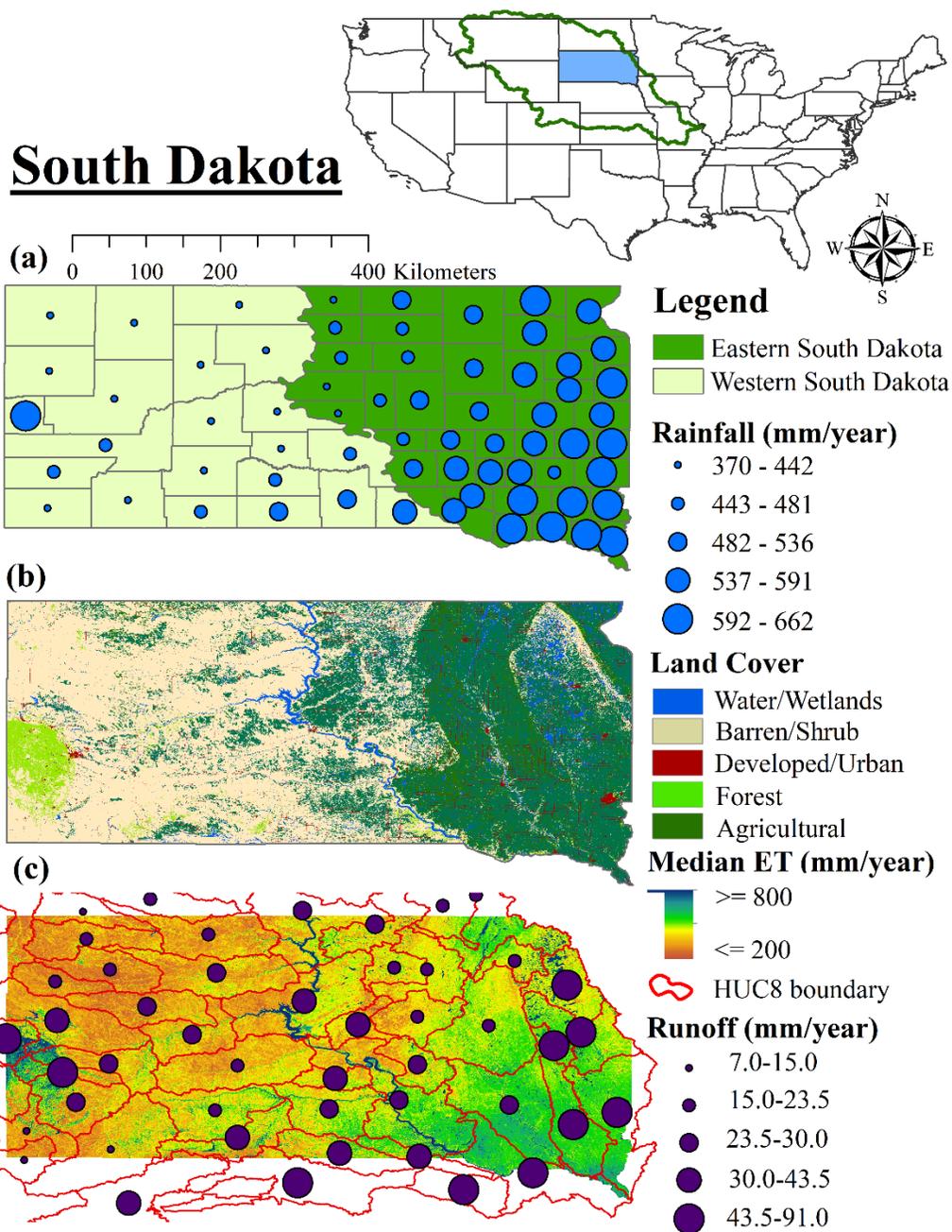
Fig. 5.1. Distribution of (a) rainfall, (b) land cover, and (c) median actual evapotranspiration with annual runoff from HUC8 sub-basins across the state of South Dakota, USA.
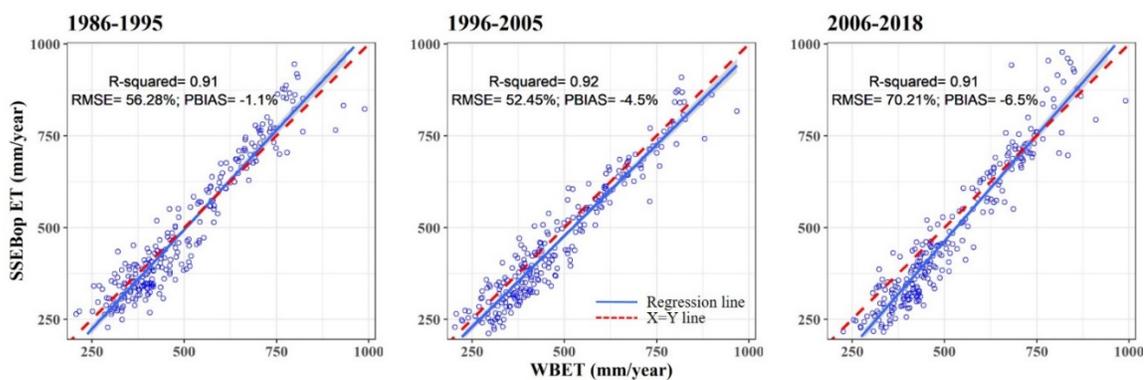
Fig. 5.2. Validation statistics for basin-scale validation of Landsat-based ETa estimations using the water balance evapotranspiration (WBET) approach.
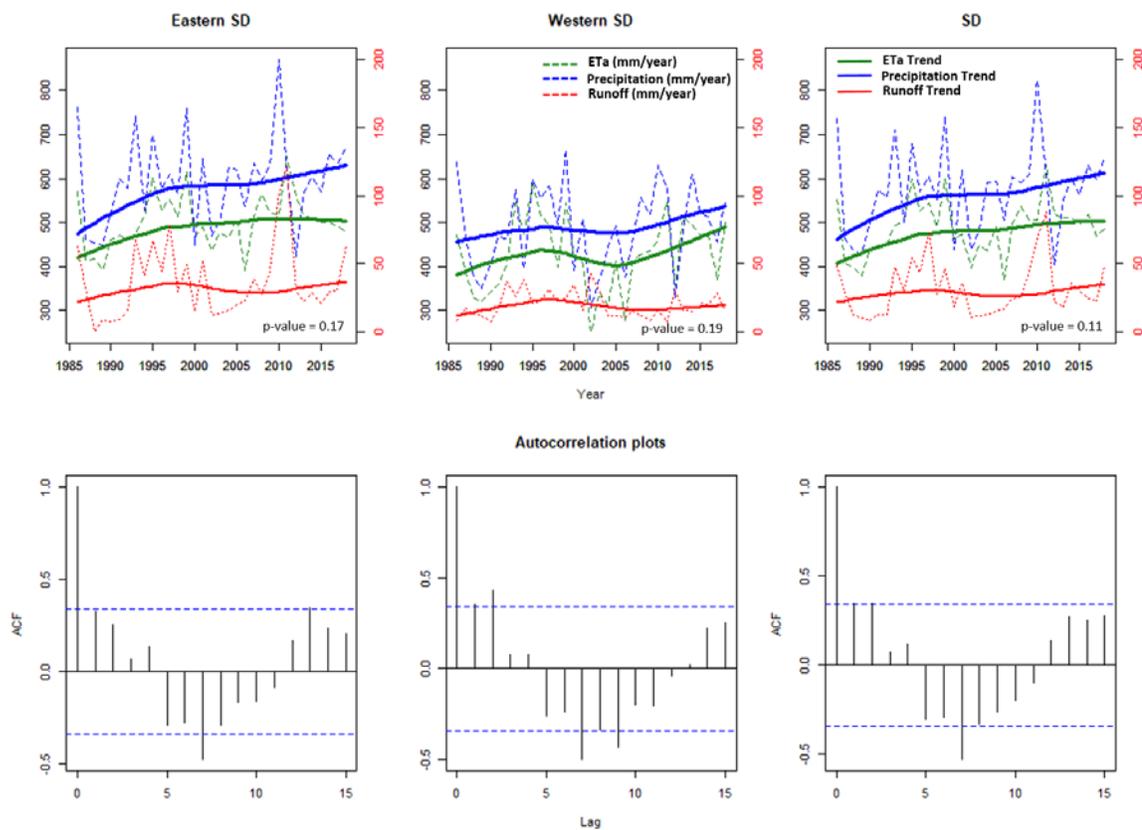
Fig. 5.3. Mann-Kendall regional-scale trend analysis with autocorrelation plots for actual crop water-uses (ETa), precipitation, and runoff across eastern, western, and the entire state of South Dakota, USA.
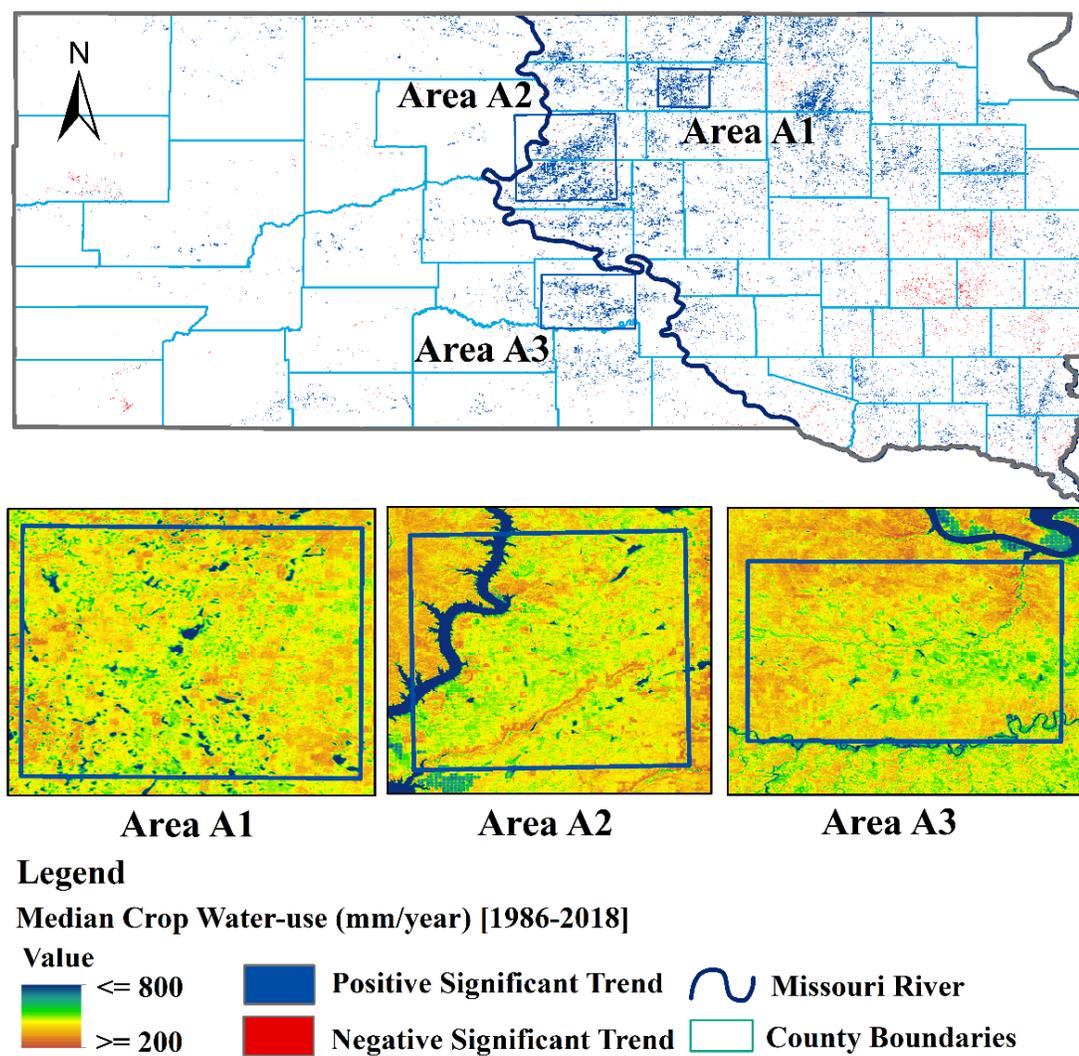
Fig. 5. 4. Mann-Kendall pixel-scale trend analysis over cropland extent across South Dakota.
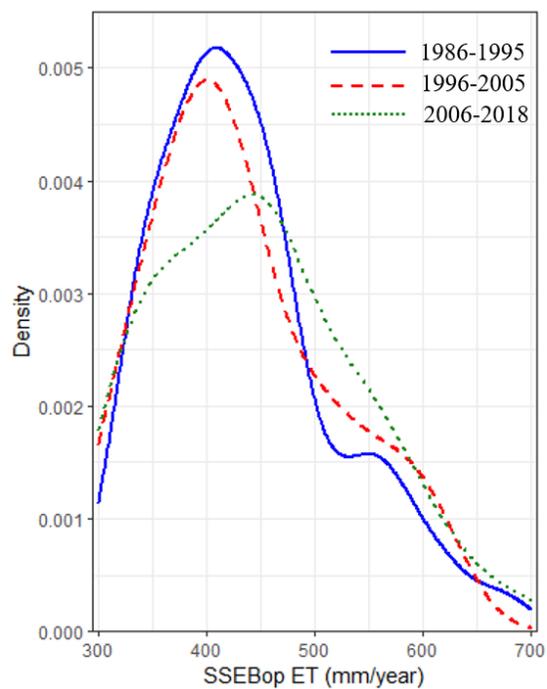
Fig. 5.5. Density plot of HUC8 sub-basins in the South Dakota region considering mean annual actual evapotranspiration.
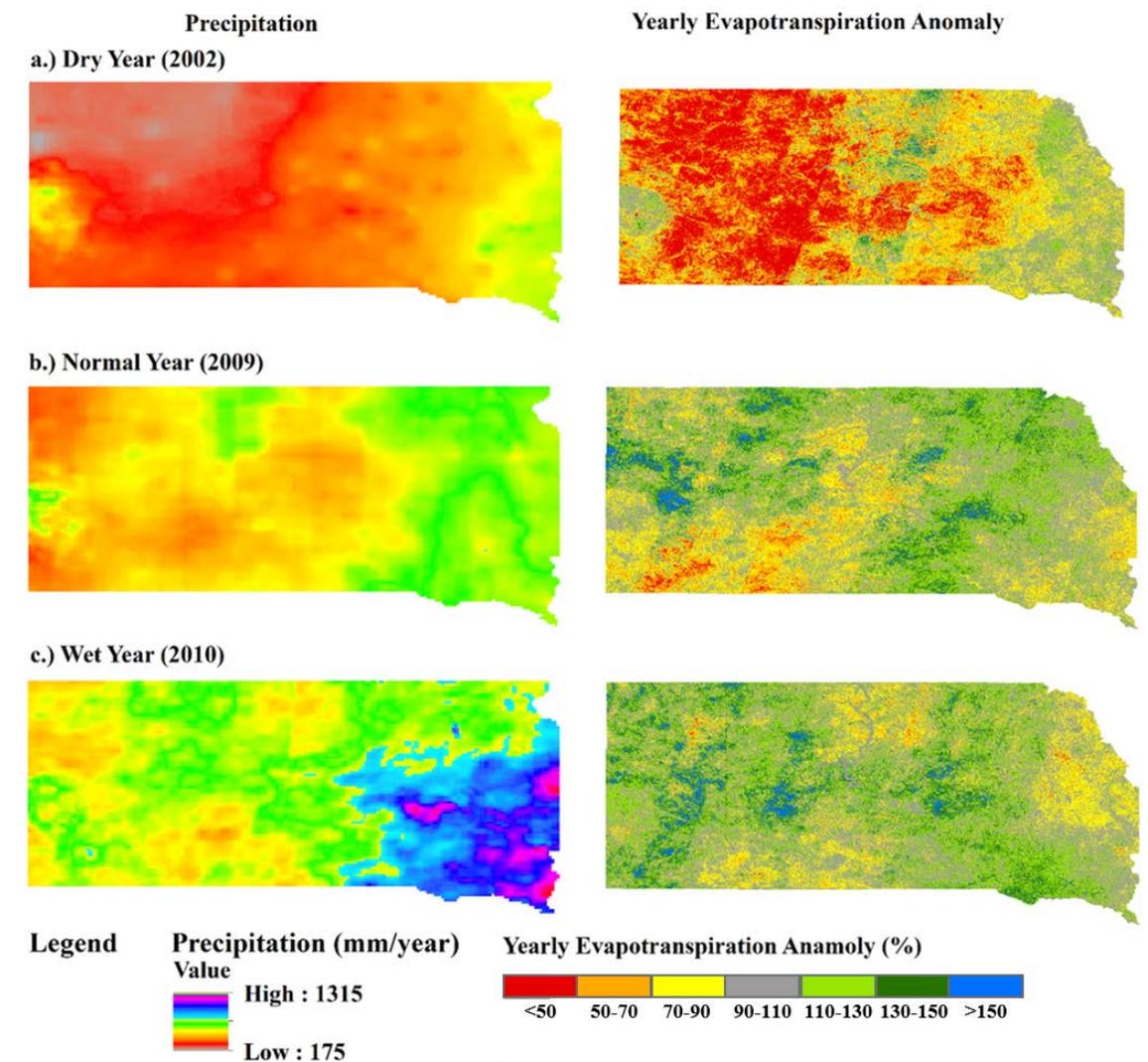
Fig. 5.6. Precipitation and annual evapotranspiration anomaly across South Dakota during a.) dry year (2002), b.) normal year (2009), and c.) wet year (2010).

CHAPTER 6

LANDSAT-DERIVED EVAPOTRANSPIRATION FOR LONG-TERM (1986-2018) CROP WATER USE ASSESSMENT ACROSS THE MISSOURI RIVER BASIN

ABSTRACT

Understanding historical crop water use (CWU) dynamics is critical to improve land and water management. In this study, well-validated ($r^2 = 0.91$, PBIAS= -4%, and %RMSE = 11.8%) actual evapotranspiration (ETa) time-series estimations were used to 1) assess summer season CWU (CWU-Su) dynamics, 2) investigate CWU-Su trends over the study period (1986-2018; 33 years) at regional- and pixel-scales, and 3) attribute CWU-Su driving factors across Missouri River Basin (MRB). Spatial variability of the Landsat-based ETa estimations were found to show strong correspondence with land cover and climate across the basin. The drier foothill regions in northwestern MRB, dominated by grassland/shrubland, showed lower ETa (< 400 mm/year), whereas, cropland dominated regions in lower semi-humid MRB and forested headwater exhibited higher ETa (> 500 mm/year). The CWU-Su anomalies revealed the vulnerability of basin to year-to-year weather conditions. The CWU-Su trend analysis revealed a significant increasing trend (p <0.1) at the regional-scale with 30% and 5% MRB cropland pixels under significant increasing and decreasing trend, respectively. A state-wide analysis of the MRB revealed a regional-scale increasing CWU-Su trend for Iowa, Missouri, Nebraska, North Dakota, and South Dakota, whereas, Colorado, Kansas, Minnesota, Montana, and Wyoming did not show a significant CWU-Su trend. The MRB cropland pixels under increasing CWU-Su trend were found to be clustered in the eastern- and mid-MRB as a result of the

combined effect of increased crop production area, increased crop yields, crop practices shifts to higher biomass crops, and increased irrigated land. Western MRB, having a constant major crop during the study period, revealed the impact of improved irrigation and water management practices with clustered decreasing CWU-Su trends. Overall, the study highlights the potential of Landsat imagery and remote sensing-based ETa modeling approaches in generating historical time-series ETa maps over a wide range of elevation, vegetation, and climate.

6.1. Introduction

The Missouri River is the longest river (~3700 km) of the United States (US) and the Missouri River Basin (MRB) is an important global food-producing region. The MRB covers about 28% of the US cropland area (USDA-NRCS 2012) and responsible for approximately half of the nation's wheat production (Wise et al. 2018; Mehta, Rosenberg, and Mendoza 2011). Gleick and Waggoner (1990) found the MRB to be vulnerable to climate variability and change for water demand (high consumptive demand or low supply), dependence on hydroelectricity, dependence on groundwater, and streamflow variability. The recurring droughts and floods fluctuate the vulnerability of the basin and are of concern for the MRB (Mehta, Rosenberg, and Mendoza 2011). The vulnerability of the basin and recurring long drought periods (1950s, 1980s, 2002-2006) in the MRB has caused tension between upstream and downstream users and between senior and junior water rights in the past (Mehta, Rosenberg, and Mendoza 2011). These tensions seem to be intensified under the projected climate scenarios. Qiao et al. (2014) studied the climate projections for the 2040-2069 period over the lower MRB and observed a decrease in precipitation for July and August and an increase in

precipitation for other months. Barnhart et al. (2016) suggested that the earlier snowmelt due to the increased temperature would reduce the streamflow during the summer months. The decreased precipitation and streamflow during the summer months (peak crop water demand period) will further escalate the tension between the MRB water users and would affect cropland negatively. In addition, the depletion of the groundwater resources such as Ogallala aquifer is threatening the water supplies for irrigation and drinking purposes in the MRB.

A review of historical crop water demands and supplies in the area is crucial for planning water management, water rights, and water resource allocation and minimizing the basin/watershed water supply vulnerability during extreme events (Senay et al. 2017). Quantifying actual evapotranspiration (ETa) is an effective way to study crop water use (CWU). Direct evapotranspiration (ET) measurements using vapor transfer or lysimeter water balance approaches are limited to field-scale. However, remotely sensed images and emerging energy balance techniques have enabled ETa estimations at various spatial- (field scale to global scale) and temporal-scales (daily/seasonal/annual) (Yang et al. 2020; Velpuri et al. 2020; Lurtz et al. 2020). The moderate spatial resolution (30 m) and available relatively long record of Landsat images provide an upper edge to study the CWU dynamics at field scale and to update the historical CWU records. Previously published studies (Velpuri et al. 2020; Senay 2019) suggest that Landsat images in combination with the Operational Simplified Surface Energy Balance (SSEBop) model can reliably quantify CWU at the field- and regional-scale.

Despite the importance of the MRB for agriculture and its vulnerability to demand and supply due to year-to-year varying weather conditions, relatively little is known

about the basin's historically varying water demands and supplies. Bawa et al. (2021) studied the CWU dynamics with a focus on the South Dakota state's region of the MRB and discussed the sensitivity of the landscape responses to the year-to-year varying weather conditions. Considering the findings of the study, the current study was expanded to the rest of the MRB focusing on the CWU (demands) dynamics for the peak crop water demand period (i.e., summer season). The main objective of this study was to quantify and characterize historical (1986-2018; 33 years) summer season CWU (CWU-Su) dynamics and CWU-Su trends across the MRB. In addition, the SSEBop model performance to quantify ETa was also evaluated at the 8-digit hydrologic unit code (HUC8) sub-basin level using the water balance ET (WBET) approach.

6.2. Materials and Methods

6.2.1. Study Area

The MRB drainage area is 1.37 million km^2 comprising all or part of 10 states of Conterminous United States (CONUS; Table 6.1) and two Canadian provinces (Mehta, Rosenberg, and Mendoza 2011). Cropland covers about 29% of the basin area, most of which is located in the southern and eastern MRB (USDA-NRCS 2012). Corn, wheat, and soybean are the major crops of the region. The basin is responsible for 22% of US corn, 34% of its cattle, and 46% of its wheat production (Mehta, Rosenberg, and Mendoza 2011). About 90% of the MRB cropland (total cropland ~38.45 million ha) is rain-fed and the rest 10% of cropland is under irrigation (Mehta et al., 2016). Most of the irrigated land extracts the water from the Ogallala aquifer. The large elevation range (120 m to 4399 m) and large extent (latitude: 90.1°N to 113.9°N, longitude: 90.1°W to 113.9°W) of the MRB induce a wide variation in climatic conditions across the basin.

The annual average precipitation ranges from less than 200 mm (east of Rocky mountains) to higher than 1000 mm (southeastern MRB and in parts of Rocky mountains; Figure 6.1) (USDA-NRCS 2012). Temperature extremes range from -51°C (during winter in Montana) to 49°C (during summer in Nebraska and Kansas) (USDA-NRCS 2012).

6.2.2. Model Input Datasets

This study utilized the Landsat imagery (Landsat 5/7/8) to estimate the ETa at a moderate spatial resolution (30 m). The thermal band of Landsat images was used to extract the land surface temperature (T_s) information. Normalized Difference Vegetation Index (NDVI) was computed using red and near-infrared bands of Landsat. Total 26,047 Landsat images (LT05: 12746 images; LE07: 9996 images; LC08: 3305 images) with ≤70% cloud cover were acquired covering the MRB (Paths 23-42 and Rows 25-35) for the summer season (June-August) over the study period. The repeat cycle of Landsat is 16 days, which reduces to 8 days with the availability of two satellites (Landsat 5 & 7: 1999-2011; Landsat 7 & 8: 2013-onwards) in the orbit. The number of images per year and the time gap between used Landsat images varied depending upon cloud cover and the number of satellites in the orbit. The cloud-contaminated pixels (clouds and cloud shadows) were removed using a combination of the Fmask (Function of Mask) algorithm (Zhu, Wang, and Woodcock 2015) and a cloud buffer (air temperature - T_s > 15K).

Other model inputs include reference evapotranspiration (ETr), Digital Elevation Model (DEM) map, and daily maximum air temperature (T_a). A daily gridded ETr data was acquired from Climatology Lab gridMET datasets (available freely at http://www.climatologylab.org/gridmet.html) at ~4km spatial resolution. These gridded

ETr datasets are validated and bias-corrected using station-based meteorological datasets (Abatzoglou 2013). Gridded maximum air temperature data were obtained from TopoWx ("Topography Weather") at 30 arc-second (~800 m) spatial resolution (Oyler et al. 2015). A DEM of 30 m spatial resolution was obtained from the U.S. Geological Survey (USGS)- Shuttle Radar Topographic Mission (SRTM) (Farr and Kobrick 2000).

6.2.3. Modeling Approach

The SSEBop model was used to estimate the ETa from Landsat images. The model does not solve all energy balance terms; rather it utilizes the satellite psychrometric approach and clear sky net radiation balance principles to define the limiting conditions (dry and wet extreme conditions) (Senay et al. 2013). Wet extreme conditions (T_c; cold temperature) refer to temperature over pixel with no sensible heat flux (H_0=0; $ET_f = 1.0$) and dry conditions (T_h; hot temperature) refer to temperature over pixel with no latent heat flux (LE = 0; $ET_f = 0$). The model estimate evapotranspiration fraction (ET_f) for each pixel using T_s and the limiting conditions (equation 2). The ETa is calculated as a product of ET_f and ET_r (equation 3).

$$ET_f = 1 - \gamma^s (T_s - T_c) \qquad\qquad (1)$$

$$ETa = ET_f * k * ET_r \qquad\qquad (2)$$

where ET_f is ET fraction ranging from 0 to 1, γ^s is the surface psychrometric constant over a dry bare surface, T_s is the land surface temperature obtained (dry bulb) from Landsat thermal band, T_c is the temperature under wet conditions (wet bulb), ETa is the actual evapotranspiration, k is the reference ET bias-correction coefficient (0.85), and ET_r is the alfalfa (*Medicago sativa*) reference ET. The γ^s is the inverse of the dT parameter which is defined as the temperature difference between limiting conditions

i.e., $T_h - T_c$ (Senay 2018). A detailed description of the SSEBop model and model parameters can be found in Senay et al. (2013).

The SSEBop model uses a linear interpolation in between nearest overpass ET_f values to estimate daily ET_f values. The inclusion of ET_r values to calculate ETa allows the model to incorporate the general ET_r trend in between the satellite overpass period to estimate more accurate ET_a. In this study, first, ETa was estimated at a monthly scale for each pixel and then the final summer season (June-August) ETa products were generated using a simple summation approach.

6.2.4. Cropland Extent

The study was focused on the CWU-Su dynamics and CWU-Su trend analysis across the MRB. The MRB cropland extent at 30 m spatial resolution was extracted using a crop mask layer for the year 2018. The U.S. Department of Agriculture-National Agricultural Statistics Service (USDA-NASS) produces the geo-referenced crop data layer and crop mask layer for each year at 30 m spatial resolution. The crop mask layer includes the pixels that were under cultivated cropland for at least 2 years out of the last 5 years. The crop mask layer for the year 2018 (representing cropland pixels under cultivation for at least 2 years during 2014-2018) was used to extract the maximum cropland extent for the MRB during the study period (1986-2018) assuming cropland increased throughout the study period.

6.2.5. Mann-Kendall (MK) Trend Analysis

The relatively long record of Landsat imagery (1984 onward) has provided an opportunity to generate and analyze the time series of the CWU. In this study, Mann-Kendall (MK) trend analysis approach (Mann 1945; Kendall 1975) was used to examine

the presence or absence of a mono-directional trend in the time-series of CWU-Su at two spatial scales: (1) region-wide scale and (2) pixel scale. The MK trend analysis assumes that the time-series values are not serially correlated over time. This non-parametric and rank-based trend analysis method initially generates n(n-1)/2 values by subtracting each time-step value from other values in the time-series (i.e., $x_j - x_k$, where j>k). Based on the resulting sign of subtraction, the method assigns a value of -1, 0, or 1 to each time step. The sum of assigned values (S) and the number of observations in the time-series are further used to evaluate the significance and direction of the trend. This study evaluated the direction of the CWU trend at a 90% significance level and examined the assumption of independence using autocorrelation functions of a univariate time series.

6.2.6. Validation of ET Estimates

A HUC8 sub-basin scale validation of SSEBop ETa was performed using a WBET approach (equation 6). WBET approach has been widely used by the hydrological scientific community to validate the remote sensing-based ETa estimations at a basin/watershed scale (Velpuri et al. 2013; Zhang et al. 2010; Senay et al. 2017). WBET approach assumes zero or negligible change in water storage (i.e. $\Delta S = 0$) for a basin at an annual scale. In this study, a multiple-year mean SSEBop ETa estimations (1986-1995, 1996-2005, and 2006-2018) for 252 HUC8 sub-basins across the MRB were compared with mean WBET of the same period for a better water balance closure and to remove uncertainties introduced by the assumption of zero change in annual water storage at HUC8 sub-basin scale.

$$WBET = P - Q - \Delta S \qquad (6)$$

where P, Q, and ΔS are the spatially averaged HUC8 sub-basin precipitation, basin runoff, and change in water storage at annual (water year) scale, respectively. Georeferenced rasters containing annual (water year) precipitation information (spatial resolution ~4 km) of the study region were obtained from gridMET (Abatzoglou 2013) and runoff information at HUC8 sub-basin scale was obtained from the National Hydrography Dataset Plus (NHDplus; available freely at https://www.epa.gov/waterdata/nhdplus-national-hydrography-dataset-plus).

The large extent of the MRB provides an advantage to validate the estimated ETa across a wide range of vegetation, elevation, and climate. Six big dams over the main channel and other highly regulated (for flood control, water supply, irrigation, and hydropower) channels across the MRB generate unnatural flow conditions in the channels. Application of the WBET validation approach is invalid for unnatural flow conditions and problematic sub-basins where water balance is not expected to close. So, to avoid validation uncertainties, the study considered four criteria to omit the problematic HUC8 sub-basins and the sub-basins with unnatural flow conditions. First, the problematic sub-basins with high groundwater flow and base flow were excluded using a runoff-rainfall ratio (Q/P; averaged Q and P over 1986-2018) threshold and negative WBET (i.e., P-Q-ΔS < 0) criteria. The Q/P threshold value of 0.33 was considered for the MRB (Velpuri et al. 2013). A detailed description of Q/P threshold selection can be found in Bawa et al. (2021). The presence of heavy irrigation (especially from groundwater resources), large permanent water bodies, and large irrigation districts in the sub-basin could lead to higher ETa than precipitation (i.e., ΔS< 0) for the sub-basin. To avoid validation uncertainties from the sub-basins with negative annual storage,

the sub-basins with the SSEBop modeled ET higher than precipitation were not considered for validation purposes. Additionally, twelve HUC8 sub-basins of the MRB sharing the boundary with Canada were also excluded as the study used the Google Earth Engine (GEE) version of the SSEBop model whose application is limited to the USA only. A total of 252 HUC8 sub-basins (out of 307) were finalized to validate the SSEBop ETa estimations.

The accuracy of the SSEBop ETa estimations was evaluated using three statistical indicators (r^2, %RMSE, PBIAS). The coefficient of determination (r^2) is a measure of goodness of fit of the data to the fitted regression line and reflects the percentage of the observed data variance that is explained by the modeled data. This coefficient varies from 0 to 1. The Percent Bias (PBIAS) is an index to quantify the under- or over-estimation of the modeled values relative to the observed values. Root mean square error (RMSE) provides the prediction errors. The $r^2 > 0.7$ and PBIAS value within -15% to 15% with reasonable percentage RMSE (depending upon the objective of the study) are desired for a good fit and satisfactory model performance (Singh and Senay 2016; Choi et al. 2009).

6.3.   Results and Discussion

6.3.1. Validation of ETa Estimations

The WBET approach, also known as mass balance or inflow-outflow approach, can be used over large integrated areas at any temporal scale (hours to years) to understand the water fluxes and storage changes, requiring other components of mass balance to be known at that temporal and spatial scale (Allen, Pereira, Howell, & Jensen, 2011). The study considered HUC8 sub-basins as individual units and a multi-year water balance closure for zero or negligible storage changes for validation purposes. The MRB

is a well-gaged basin for the runoff in the channels. The availability of well-monitored runoff and precipitation records for a long period, a relatively high number of sub-basins, and the considered assumption of zero water storage change over a multi-year period make the WBET approach very acceptable for ET validation for the study region.

Validation statistics indicated a strong agreement between SSEBop ETa and WBET for all three considered periods (Figure 6.2). A close alignment of regression lines to the 1:1 line indicates the accuracy of the annual spatial and temporal ET dynamics by the SSEBop model over a wide range of vegetation, climate, and elevation across the MRB. Additionally, the annual SSEBop ETa estimations were compared with the annual WBET, precipitation, and runoff for each individual sub-basin. The SSEBop ETa values largely track well the WBET, precipitation, and runoff pattern during the study period with a dip during the drought periods and an increment with the increase in precipitation amounts in the HUC8 sub-basin. The correspondence of regression lines to the 1:1 line (Figure 6.2) also indicated that the model underestimated ETa for the HUC8 sub-basins with low ETa and overestimated ETa for the sub-basins with high ETa. Overall, the SSEBop ETa was observed to be slightly overestimated by the model (PBIAS: -4%). However, the ETa over-estimations were well within the model satisfactory performance criteria (-15% < PBIAS < 15%) considering the study objectives. The close match between the SSEBop ET and WBET suggested the reliability of estimated CWU for the MRB and encouraged further assessment of CWU dynamics.

6.3.2. Spatial and Temporal ETa Variation

Mean ETa varies notably across the MRB (Figure 6.3). For the study period, mean ETa showed an increasing pattern from northwest to southeast across the MRB. A low spatially averaged annual ETa (< 400mm/year) was observed for the barren/shrub land-

dominated HUC8 sub-basins across Montana (MT) and Wyoming (WY) (Figure 6.3).

The minimum ETa was 212 mm/year for the Muskrat watershed in WY (HUC8

10080004). The annual ETa was higher toward the HUC8 sub-basins with the high-

irrigated lands in NE, KS, IW, and MO. The maximum ETa was 940 mm/year for the

Lake of the Ozarks watershed in MO (HUC8 10290109). Higher mean ETa in the

southeastern HUC8 sub-basins was likely because of the combination of land use and

high precipitation amounts. This part of the MRB is a part of the Midwest Corn Belt and

is dominated by cropland which fosters higher biomass and ETa. The spatial variability

of ETa was found to be associated with spatial land use and climate variation. The drier

foothill regions in the northwestern MRB, dominated by grassland/shrubland, showed

lower ETa (< 400 mm/year), whereas, cropland dominated regions in lower semi-humid

MRB and forested headwater exhibited higher ETa (> 500 mm/year). A few HUC8 sub-

basins of WY and MT (the western mountain regions) exhibits higher ETa (> 400

mm/year) compared to other nearby sub-basins, which may be explained by the presence

of permanent cover and higher precipitation at the Rocky Mountains. Similar kind of

higher ETa were also observed for Black Hill National Forest region in the western SD.

The probability density plot (Figure 6.4) revealed a shift in the number of HUC8

sub-basins from low mean ETa (250 mm/year- 500 mm/year) to medium or high mean

ETa (500 mm/year- 950 mm/year) for the 2006-2018 period than other two periods

(1986-1995, 1996-2005). The observed density plot pattern was found to coincide with

the observed increasing CWU trends at regional- and pixel-scale (discussed in section

6.3.4) across the MRB. A similar pattern was observed for the precipitation, whereas

runoff from sub-basins did not show much change for the considered three periods (Figure 6.4).

6.3.3. Summer Season Crop Water Use Dynamics

Figure 6.5 represents the year-to-year variation for the CWU-Su for the MRB. The MRB is vulnerable to recurring short- and long-term droughts. The deviation of CWU-Su from mean CWU-Su, presented in Figure 6.5-right panel, reflecting the sensitivity of the basin's CWU-Su to the year-to-year varying weather conditions. The observed mean CWU-Su for the MRB during the study period was 97 mm, which was decreased to 88 mm (~9% less than average) and 86 mm (~11% less than average) during the two major drought periods (1987-1989 and 2002-2006, respectively) of the basin. The lowest CWU-Su was during 1988 (82 mm; 15% less than average) when the basin received 35% less summer precipitation than average. The lower decrement in the CWU-Su than precipitation reflects the potential of groundwater resources within the basin. However, there are rising concerns for the health of the groundwater resources of the basin such as the depletion of the Ogallala aquifer.

6.3.4. Summer Season Crop Water Use Trends
6.3.4.1. Regional-scale Trend

The basin-wide CWU-Su showed a significant increasing trend (p-value = 0.054) whereas the summer season cropland precipitation did not show a significant trend (p-value = 0.65; Figure 6.6). Trend analysis with a 3-year moving average for ETa and precipitations (Figure 6.6) was also evaluated to neutralize the impact of dry and wet year periods. The 3-year moving average for cropland precipitation was still associated with a non-significant trend. A rapid increase in MRB CWU was observed for the 2003-2018 period. The long drought periods (1987-1989 and 2002-2006) seemed to be neutralizing

the increasing CWU trends (Figure 6.6). The observed CWU and precipitation trends

reflect the increasing stress on the ground and surface water resources for irrigation in the

basin.

6.3.4.2. Pixel-scale Trend

The CWU-Su trend analysis at pixel-scale showed a significant mono-directional

trend ($p<0.1$) for about 35% of the cropland area. About 30% of pixels revealed a

positive trend while the remaining 5% cropland pixels showed a decreasing trend. The

pixels under increasing trend were found to be clustered in the mid and eastern part of the

basin (i.e., North Dakota, ND; South Dakota, SD; Nebraska, NE; Iowa, IW; Minnesota,

MN; Kansas, KS; and Missouri, MO states), whereas decreasing trend pixels were

clustered in the western MRB [i.e., MT, WY, and Colorado (CO) states] (Figure 6.7).

Table 6.2 shows regional- and pixel-scale CWU-Su trends for each state in the MRB. A

detailed description of the regional- and pixel-scale CWU trends is discussed in the

following three MRB sections.

6.3.4.3. Western MRB

Western MRB includes about 23% of the MRB cropland. The majority of

croplands in the region are along water channels due to uneven terrain and semi-arid to

arid climate conditions. Wheat is the major crop of the region and mostly depends on

surface water for irrigation. Since the region has not experienced many crop practice

shifts during the study period, the improved water management and irrigation practices

(shifting from traditional flood irrigation to irrigation with sprinkler systems) could be the

driving factors for the observed decreasing CWU trends.

The CWU-Su (p-value: 0.34) and cropland precipitation (p-value: 0.61) in the

MRB part of MT state (MT-MRB) did not show any significant mono-directional trend at

the regional-scale. The pixel-level trend analysis revealed the presence of both increasing

and decreasing CWU-Su trends over a substantial portion (about 10% and 20% cropland

pixels under a significant increasing and decreasing trend; Table 6.2) of the MT-MRB

region which could be related to the non-significant CWU-Su trends at regional-scale.

The decreasing trend pixels were found to be clustered in the western MT-MRB and

increasing trend pixels were clustered in the northeast MT (Figure 6.7). About 16% of the

MRB cropland is in the MT state. The MT state has about 4 million ha of cropland (as

per the year 2017; USDA census of agriculture, 2017) and a major part of it is in MT-

MRB. The state's cropland increased by 21% during the 1992-2018 period (USDA

census of agriculture, 2017). The major crop of Montana is wheat for grain. The state

faced a decrease in spring wheat practices (1.62 million ha to 0.93 million ha) and an

increase in winter wheat practices (0.32 million ha to 0.65 million ha) during the 1997-

2017 period (USDA census of agriculture, 2017). Most of the pixels under spring wheat

and winter wheat in western MT-MRB were found to be associated with a negative trend.

The crop shift from spring wheat to winter wheat and other crops along with improved

surface irrigation and water management might be the leading factors for these clustered

decreasing trend cropland pixels in the western MT-MRB. Only, the pixels under pivot

irrigation (along Sun River) showed an increasing CWU trend in the western MT-MRB.

The adoption of pivot irrigation over non-irrigated fields could have resulted in

increasing cropland ETa trends. Similar increasing CWU trends were observed for the

pivot-irrigated fields along the Yellowstone River and its creeks (dominated by alfalfa

crop) in southern MT-MRB. The northeast part of MT is dominated by durum wheat and

winter wheat cropland pixels. The state also observed an increase in durum wheat acres

(117K ha to 318K ha) during 1997-2017 (USDA census of agriculture, 2017). The shift in cropping practices from sparsely planted winter wheat (226-248 plants per sq. m) to densely planted durum wheat (323-344 plants per sq. m) (Wiersma and Ransom 2005) in combination with moisture regime shift and increased crop productions in northeast MT could be driving factor for clustered increasing trend cropland pixels.

A very small part of the MRB cropland (Table 6.1) is in the MRB part of the WY state (WY-MRB). The CWU-Su (p-value: 0.78) and cropland precipitation (p-value: 0.72) in WY-MRB did not show any significant mono-directional trend at the regional-scale (Table 6.2). The presence of both increasing and decreasing trends over a substantial portion (18% and 11%, respectively) of the region (Figure 6.7) resulted in a non-significant regional scale trend. The decreasing trend cropland pixels might be the result of a large number of low precipitation years encountered during 1999-2013, whereas, increased irrigated cropland and increased crop productions could have induced an increasing trend.

The MRB part of CO state (CO-MRB) includes about 6% of the MRB cropland. The regional-scale CWU-Su and precipitation did not show a significant mono-directional trend (p>0.1) for the CO-MRB region. The varying landscape responses due to varying weather conditions and the existing both increasing and decreasing trends at the pixel-scale (Figure 6.7) appease to be governing the non-significant CWU trend at the regional-scale. About 11% and 11% cropland pixels in the region were found to be associated with significant increasing and decreasing CWU trends, respectively, at pixel-scale. The decreasing CWU trend pixels were found to be clustered in the mid-CO-MRB (Figure 6.7), whereas, eastern part showed the clustered increasing CWU trends. The CO-

MRB covers the major crop area of the state. The state faced an increase in the corn production area (376K ha to 526K ha) and a decrease in the wheat production area (1000K ha to 838K ha) with an increase in the total cropland area (~8%) during the 1987-2017 period (USDA census of agriculture, 2017). The corn production area of CO primarily increased in the CO-MRB region. The clustered increasing CWU trend pixels in eastern CO-MRB were found to be associated with corn fields under a pivot irrigation system. The increased corn production area, adoption of pivot irrigation, increased crop yields, and moisture regime shift due to increased temperature could be the potential reasons for the clustered increasing CWU trends at pixel-scale in the eastern CO-MRB. The mid-CO-MRB is dominated by wheat and have not experienced much crop shift. The irrigated cropland in CO was decreased (~8.3%; USDA census of agriculture, 2017) during the 1987-2017 period. The decreasing trend in the mid-CO-MRB might be the result of improved water management and irrigation practices and decreased irrigated cropland in the region.

6.3.4.4. Mid MRB

The majority of Mid MRB is part of the Great Plains and showed both increasing and decreasing CWU trends (Figure 6.7). Mid MRB experienced increased crop productions and a rapid shift of crop practices from low biomass crops (wheat-oats) to high biomass crops (corn-soybean) during the study period that might have governed the clustered increasing trend pixels in the area. In addition, the area also experienced an intensification of agricultural practices due to the reduction of fallow cropland practices and the adoption of conservation practices that improved soil moisture storage.

The MRB part of ND (ND-MRB) and SD (SD-MRB) states revealed a significant increasing trend for CWU-Su at a regional-scale, whereas, summer season precipitation

showed a non-significant trend but was still found to be sufficient to meet the crop water demands. This increasing regional scale CWU-Su trend was led by the 45% ND-MRB cropland pixels and 34% SD-MRB cropland pixels (Figure 6.7) under a significant increasing trend. The ND-MRB and SD-MRB faced the increased cropland (31% and 26%, respectively; USDA census of agriculture, 2017), increased corn and soybean production area (Corn: 519% and 100%; Soybean: 595% and 300%, respectively), and increased irrigated cropland (36% and 26%, respectively) during 1987-2017. The significant increasing CWU-Su trend in the regions seems to be mainly governed by the increased cropland areas and irrigated cropland along with the shift in agricultural practices (wheat to corn-soybean) and decreased risk of farming in the dry areas. The increased agricultural productions (USDA crop survey reports), reduced fallow cropland practices, and a moisture regime shift due to increased precipitation and increased temperature could be the other potential reasons for the increased cropland ETa at pixel- and regional-scale for both regions. In addition, regional CWU-Su trends and anomalies suggested the high sensitivity of landscape responses to the varying weather conditions for both regions. This high CWU sensitivity might be the result of high rain-fed and low irrigated cropland in the state. Only 1% of the SD-MRB cropland pixels, clustered in Mideast SD (Figure 6.7), were found to be associated with a significant decreasing CWU trend. The conversion of wetland to cropland and decreased irrigation practices in the mid-eastern SD region could have influenced the decreasing CWU-Su trend (Bawa et. al., 2021).

The MRB drains the whole area of the NE state. The state's cropland contributes the largest portion (~21%) to the MRB cropland. The regional scale CWU-Su showed a

significant increasing trend with 40% of cropland pixels under a significant increasing trend (Figure 6.7). The NE state was the only region that revealed a significant increasing trend for the summer season cropland precipitation also at the regional scale. The cropland in NE is highly dependent on irrigation and extract water from groundwater resources (Ogallala aquifer). The increased precipitation in the region has decreased the cropland dependency on surface and groundwater resources for irrigation purposes. As per the USGS water use reports for estimated water use in the United States (Dieter et al. 2018; Hutson 2004), the irrigated cropland in the state was increased during the 2000-2015 period (3.2 million ha in 2000 to 3.89 million ha in 2015), whereas, the water withdrawal for irrigation purposes was decreased sustainably (33.3 m^3/day to 23.1 m^3/day). In addition, the state has experienced about 27% increase in total cropland along with a 54% and 147% increase in corn and soybean production area, respectively, and a 44% decrease in the wheat production area during 1987-2017 period (USDA census of agriculture, 2017). Crop productions (USGS crop survey reports) have also rapidly increased during the study period. The combined impact of increased cropland productions, increased irrigated cropland, a shift from low biomass crops (wheat) to high biomass crops (corn-soybean), and moisture regime shift might have governed the regional- and pixel-scale significant increasing CWU-Su trend for the NE.

The MRB part of KS state (KS-MRB) covers about 12% of the MRB cropland. The region revealed a non-significant trend for CWU-Su and precipitation at the regional-scale. The varying weather conditions in the state and the presence of both increasing and decreasing CWU trends over substantial portions of the KS-MRB (about 15% and 4% cropland pixels under a significant increasing and decreasing trend, respectively)

governed the non-significant CWU trend at the regional-scale. Corn, soybean, wheat, and

Sorghum are the major crops of the state. The state faced a rapid increase in corn and

soybean production area (333% and 172%, respectively) with a decrease in wheat and

sorghum production area (19% and 29%, respectively) during the 1987-2017 period

(USDA census of agriculture, 2017). State's cropland under irrigation remained the same

whereas the water withdrawal amounts for irrigation purposes was decreased

substantially (14K m^3/day in 2000 to 10K m^3/day in 2015) (Dieter et al. 2018; Hutson

2004). The decreased water withdrawal for irrigation purposes indicates improved water

management and irrigation practices in the KS-MRB region which could be the potential

reason for the observed clustered decreasing trend pixels in the mid-KS-MRB (Figure

6.7).

The increasing CWU trend pixels were found to be clustered in the western KS-

MRB (Figure 6.7). Most of these pixels were associated with pivot irrigated corn

production fields. The pixels under winter wheat in the region did not show a significant

CWU trend. The observed trends suggest that the development of pivot irrigation systems

and crop shift from wheat to corn might have governed the clustered increasing CWU

trend pixels in the western KS-MRB. The eastern KS-MRB was also found to be

dominated by increasing trend pixels. Corn and soybean dominate the cropland in the

region. Increased corn-soybean production area and yields (USDA crop survey reports)

might be the main driving factors for the increasing CWU trend in the region.

6.3.4.5. Eastern MRB

Eastern MRB is a part of the Midwest and is entirely dominated by the increasing

trend pixels. The increasing CWU trends in this region could be the result of increased

crop yields and production area. A moisture regime shift due to the increased

precipitation and increased temperature during the study period could be the other potential reason for these observed increasing trends.

The MRB part of MO state (MO-MRB) includes about 5.9% of the MRB cropland. The cropland in the region revealed a significant increasing trend at the regional-scale for CWU-Su, whereas, the cropland summer precipitation did not show a significant trend for the study period. A rapid increase for the CWU-Su was observed for the region during 2005-2018. About 41.9% of cropland pixels revealed a significant increasing trend for CWU-Su, whereas, only 0.5% of pixels were found to be associated with a significant decreasing trend. The MO-MRB covers the major crop area of the state. The state faced an increase in cropland area (~16.5%) and irrigated cropland area (214K ha to 619K ha) during the 1987-2017 period (USDA census of agriculture, 2017). The state also experienced an increase in corn (838K ha to 1364K ha) and soybean (1951K ha to 2375K ha) production area with a decrease in wheat (306K ha to 223K ha) and sorghum (253K ha to 9K ha) production area during the same period (USDA census of agriculture, 2017). A major part of all the crop practice changes occurred in the region. The increased crop production area, crop practice shift from low biomass (wheat-sorghum) to higher biomass (corn-soybean), increased irrigated cropland area, increased crop productions (USDA crop survey reports), and moisture regime shift due to increased temperature could be the reasons for the observed increasing CWU trends at regional- and pixel-scale.

The MRB part of IW state (IW-MRB) covers about 31% of the state's area and about 8.4% of the MRB cropland. The CWU-Su showed a significant increasing trend whereas no trend was observed for the cropland precipitation at the regional-scale. About 41.6% of cropland pixels showed a significant CWU-Su trend, of which ~41.5 % of

cropland pixels were associated with increasing CWU trend and only 0.15% showed a negative CWU-Su trend. Corn and soybean dominate the state's cropland. The state's cropland (8.29 million ha to 9.85 million ha) and irrigated cropland area (37K ha to 90K ha) increased during the 1987-2017 period (USDA census of agriculture, 2017). The state also experienced a rapid increase in crop productions during the study period (USDA crop survey reports). The increased cropland, irrigated cropland, and crop productions with a moisture regime shift due to increased precipitation and temperature might have governed the significant increasing CWU trends at pixel- and regional-scale for the IW-MRB region.

The MN has a small portion in the MRB and covers the smallest part (0.98%) of the MRB cropland. The cropland in the region revealed the absence of a significant trend for CWU-Su and precipitation at the regional-scale whereas about 18.4% of cropland pixels showed a significant trend. About 17.4% of cropland pixels were associated with a significant increasing CWU trend and only 1% of cropland pixels were found to be associated with a negative trend. The increasing trend in the region could be the result of the combined impact of increased crop productions and moisture regime shift. Varying weather conditions, varying cropland ETa, and only a limited portion of the region under significant monodirectional trend could be the reason for the non-persistence mono-directional trend at the regional-scale.

6.4. Conclusions

This study utilized Landsat-derived ETa to generate the CWU-Su time-series (1986-2018; 33-year) for the MRB. The generated CWU-Su maps were further used to understand CWU-Su dynamics and present CWU-Su trends across the basin. The study

also evaluated the performance of the SSEBop model for ETa mapping using Landsat imagery. The Landsat-derived annual ETa estimations were validated using the WBET approach from 252 HUC8 sub-basins of the MRB. The observed close correspondence of SSEBop ETa and WBET reflects the capability of the SSEBop model for capturing spatial and temporal ETa variation over a large range of vegetation, climate, and elevation. Also, the observed validation statistics reinforce the usefulness of Landsat imagery to study the field-level CWU dynamics. This study also highlights the GEE-based simplified, innovative, and parameterized approach of the SSEBop model that requires only weather information and thermal sensor-based satellite datasets.

The spatial variability of ETa was found to be coinciding with spatial land cover and climate variation. The generated map showed a lower ETa (< 400 mm/year) coming from the drier foothill HUC8 sub-basins in the northwestern MRB that are dominated by grassland/shrubland. The forested headwater sub-basins having a permanent cover and the cropland-dominated sub-basins in the lower semi-humid MRB exhibited higher ETa (> 500 mm/year). The time-series information on CWU-Su reflected the impact of drought periods and revealed the vulnerability of the MRB for the CWU-Su to year-to-year varying weather conditions. The lower reductions in the CWU-Su than the reduction in precipitation amounts during the drought periods represent the potential of groundwater resources for irrigation.

The study also investigated the CWU drivers for the basin. The increasing CWU trend appears to be influenced by the increased crop production area, increased crop yields, crop practices shifts to higher biomass crops, and increased irrigated land. Reduced fallow land practices, adoption of conservation practices for soil moisture

storage improvement, and moisture regime shifts due to increased precipitation and increased temperature could be the other potential driving factors for the increasing CWU trend in the basin. The clustered decreasing CWU trend pixels could be influenced by the decreased wastage of water through ET due to the improved and more efficient irrigation and water management practices (e.g., shifting from flood irrigation to sprinkler irrigation systems) over the regions with the minimal crop practices shifts during the study period. Although the study may not have accounted for all underlying factors for CWU dynamics, this study provides useful insights for the distribution of ETa and a time-series overview of CWU-Su across the MRB. Such information is critical to understand land use-CWU interactions. The generated ETa time-series could be used by the watershed managers to understand water supplies and demand for the effective planning and management of water resources in the region. The study results also provide an opportunity for the individual farmer or the irrigation districts for the inter-comparison of crop productions, crop water demands, and the relationship between water allocation and use at the individual field level.

APPENDIX B- *Additional information about state-wise Mann Kendal trend analysis at regional and pixel scale along with existing crop production trends can be found in Figure 1B-29B.*

References

Abatzoglou, J. T. (2013). Development of gridded surface meteorological data for ecological applications and modelling. International Journal of Climatology, 33(1), 121-131.

Allen, R. G., Pereira, L. S., Howell, T. A., & Jensen, M. E. (2011). Evapotranspiration information reporting: I. Factors governing measurement accuracy. Agricultural Water Management, 98(6), 899-920.

Barnhart, T. B., Molotch, N. P., Livneh, B., Harpold, A. A., Knowles, J. F., & Schneider, D. (2016). Snowmelt rate dictates streamflow. Geophysical Research Letters, 43(15), 8006-8016.

Bawa, A., Senay, G. B., & Kumar, S. (2021). Regional crop water use assessment using Landsat-derived evapotranspiration. Hydrological Processes, 35(1), e14015. doi:10.1002/hyp.14015

Choi, M., Kustas, W. P., Anderson, M. C., Allen, R. G., Li, F., & Kjaersgaard, J. H. (2009). An intercomparison of three remote sensing-based surface energy balance algorithms over a corn and soybean production region (Iowa, US) during SMACEX. Agricultural and Forest Meteorology, 149(12), 2082-2097.

Dieter, C. A., Maupin, M. A., Caldwell, R. R., Harris, M. A., Ivahnenko, T. I., Lovelace, J. K., . . . Linsey, K. S. (2018). Estimated use of water in the United States in 2015: US Geological Survey.

Farr, T. G., & Kobrick, M. (2000). Shuttle Radar Topography Mission produces a wealth of data. Eos, Transactions American Geophysical Union, 81(48), 583-585.

Gleick, P. H., & Waggoner, P. E. (1990). Climate Change and US Water Resources. Vulnerability of Water Systems, PE Waggoner (Editor). Wiley Interscience, New York, 223-240.

Hutson, S. S. (2004). Estimated use of water in the United States in 2000: Geological Survey (USGS).

Kendall, M. (1975). Rank correlation methods (4th edn.) charles griffin. San Francisco, CA, 8.

Lurtz, M. R., Morrison, R. R., Gates, T. K., Senay, G. B., Bhaskar, A. S., & Ketchum, D. G. (2020). Relationships between riparian evapotranspiration and groundwater depth along a semiarid irrigated river valley. Hydrological Processes.

Mann, H. B. (1945). Nonparametric tests against trend. Econometrica: Journal of the econometric society, 245-259.

Mehta, V. M., Rosenberg, N. J., & Mendoza, K. (2011). Simulated Impacts of Three Decadal Climate Variability Phenomena on Water Yields in the Missouri River Basin 1. JAWRA Journal of the American Water Resources Association, 47(1), 126-135.

Oyler, J. W., Ballantyne, A., Jencso, K., Sweet, M., & Running, S. W. (2015). Creating a topoclimatic daily air temperature dataset for the conterminous United States using homogenized station data and remotely sensed land skin temperature. International Journal of Climatology, 35(9), 2258-2279.

Qiao, L., Pan, Z., Herrmann, R. B., & Hong, Y. (2014). Hydrological variability and uncertainty of lower Missouri River basin under changing climate. JAWRA Journal of the American Water Resources Association, 50(1), 246-260.

Senay, G. (2019). Characterizing crop water use dynamics in the Central Valley of California using landsat-derived evapotranspiration. Remote Sensing, 15(11).

Senay, G. B. (2018). Satellite psychrometric formulation of the Operational Simplified Surface Energy Balance (SSEBop) model for quantifying and mapping evapotranspiration. Applied engineering in agriculture, 34(3), 555-566.

Senay, G. B., Bohms, S., Singh, R. K., Gowda, P. H., Velpuri, N. M., Alemu, H., & Verdin, J. P. (2013). Operational evapotranspiration mapping using remote sensing and weather datasets: A new parameterization for the SSEB approach. JAWRA Journal of the American Water Resources Association, 49(3), 577-591.

Senay, G. B., Schauer, M., Friedrichs, M., Velpuri, N. M., & Singh, R. K. (2017). Satellite-based water use dynamics using historical Landsat data (1984–2014) in the southwestern United States. Remote Sensing of Environment, 202, 98-112.

Singh, R. K., & Senay, G. B. (2016). Comparison of four different energy balance models for estimating evapotranspiration in the Midwestern United States. Water, 8(1), 9.

USDA-NRCS. (2012). Assessment of the Effects of Conservation Practices on Cultivated Cropland in the Missouri River Basin. Washington, DC Retrieved from https://www.nrcs.usda.gov/wps/portal/nrcs/detail/national/technical/nra/ceap/pub/?cid=stelprdb1048705

Velpuri, N. M., Senay, G. B., Schauer, M., Garcia, C. A., Singh, R. K., Friedrichs, M., . . . Conlon, T. (2020). Evaluation of hydrologic impact of an irrigation curtailment program using Landsat satellite data. Hydrological Processes.

Velpuri, N. M., Senay, G. B., Singh, R. K., Bohms, S., & Verdin, J. P. (2013). A comprehensive evaluation of two MODIS evapotranspiration products over the

conterminous United States: Using point and gridded FLUXNET and water balance ET. Remote Sensing of Environment, 139, 35-49.

Wiersma, J. J., & Ransom, J. K. (2005). The small grains field guide. In: St. Paul, MN: University of Minnesota Extension Service.

Wise, E. K., Woodhouse, C. A., McCabe, G. J., Pederson, G. T., & St-Jacques, J.-M. (2018). Hydroclimatology of the Missouri river basin. Journal of Hydrometeorology, 19(1), 161-182.

Yang, Y., Anderson, M., Gao, F., Hain, C., Noormets, A., Sun, G., . . . Sun, L. (2020). Investigating impacts of drought and disturbance on evapotranspiration over a forested landscape in North Carolina, USA using high spatiotemporal resolution remotely sensed data. Remote Sensing of Environment, 238, 111018.

Zhang, K., Kimball, J. S., Nemani, R. R., & Running, S. W. (2010). A continuous satellite-derived global record of land surface evapotranspiration from 1983 to 2006. Water Resources Research, 46(9).

Zhu, Z., Wang, S., & Woodcock, C. E. (2015). Improvement and expansion of the Fmask algorithm: Cloud, cloud shadow, and snow detection for Landsats 4–7, 8, and Sentinel 2 images. Remote Sensing of Environment, 159, 269-277.

Table 6.1. State-wise division of the Missouri River Basin (US-MRB: US part of the Missouri River Basin)

State	% state area in the MRB	% of the US-MRB area	% of the US-MRB cropland
Colorado	28.55	5.82	6.06
Iowa	30.91	3.41	8.41
Kansas	49.01	7.89	12.35
Minnesota	2.13	0.35	0.98
Missouri	52.31	7.16	5.91
Montana	82.32	23.74	15.95
Nebraska	100	15.15	20.67
North Dakota	58.06	8.05	11.34
South Dakota	97.13	14.69	17
Wyoming	71.74	13.74	1.33

Table 6.2. State-wise regional- and pixel scale CWU and precipitation trend for the summer season

STATE[†]	Regional-Scale		Pixel-Scale		
	CWU trend	Precipitation trend	Cropland pixels under significant CWU trend	Cropland pixels under increasing CWU trend	Cropland pixels under decreasing CWU trend
Colorado	No-trend	No-trend	22%	11%	11%
Iowa	*Increasing*	No-trend	41.6%	41.5%	0.1%
Kansas	No-trend	No-trend	19%	15%	4%
Minnesota	No-trend	No-trend	18.4%	17.4%	1%
Missouri	Increasing	No-trend	42.4%	41.9%	0.5%
Montana	No-trend	No-trend	30%	10%	20%
Nebraska	*Increasing*	*Increasing*	41%	40%	1%
North Dakota	*Increasing*	No-trend	45.5%	45%	0.5%
South Dakota	*Increasing*	No-trend	35%	34%	1%
Wyoming	No-trend	No-trend	29%	18%	11%

[†]Only for the MRB part of the state
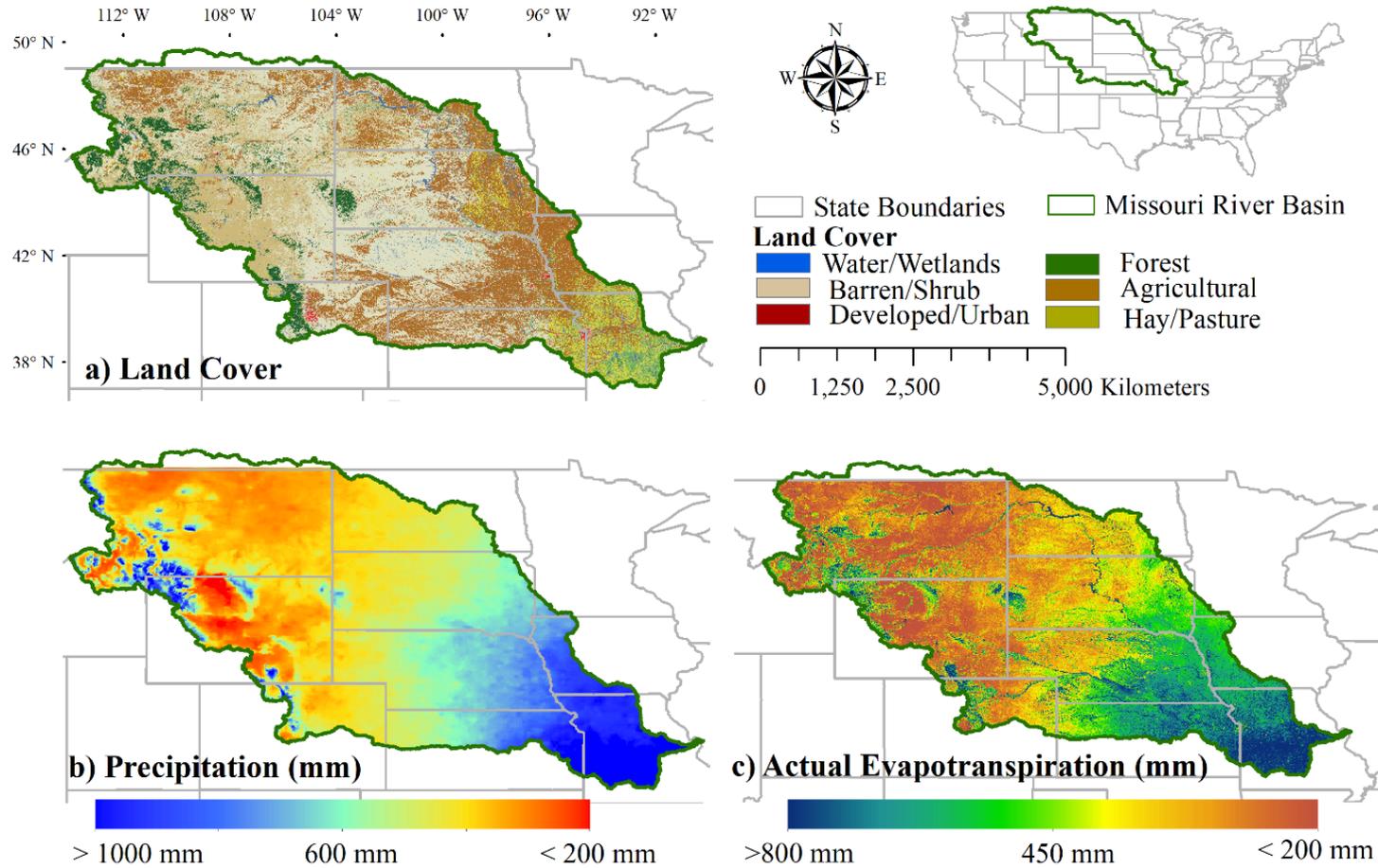
Fig. 6.1. The geographic location of the Missouri River Basin with the distribution of (a) land cover, (b) annual precipitation, and (c) annual actual evapotranspiration across the basin.
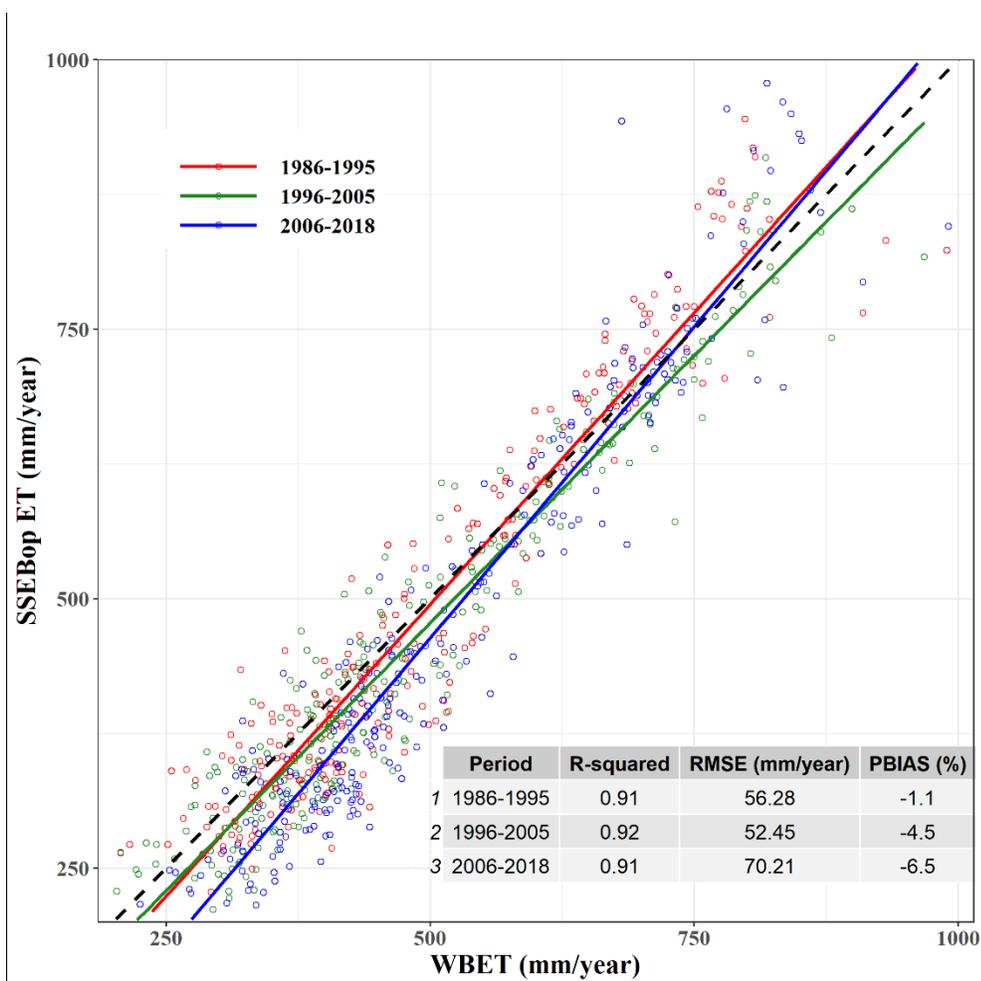
Fig. 6.2. Annual SSEBop ET estimations compared to the water balance evapotranspiration (WBET) at HUC8 sub-basin scale.
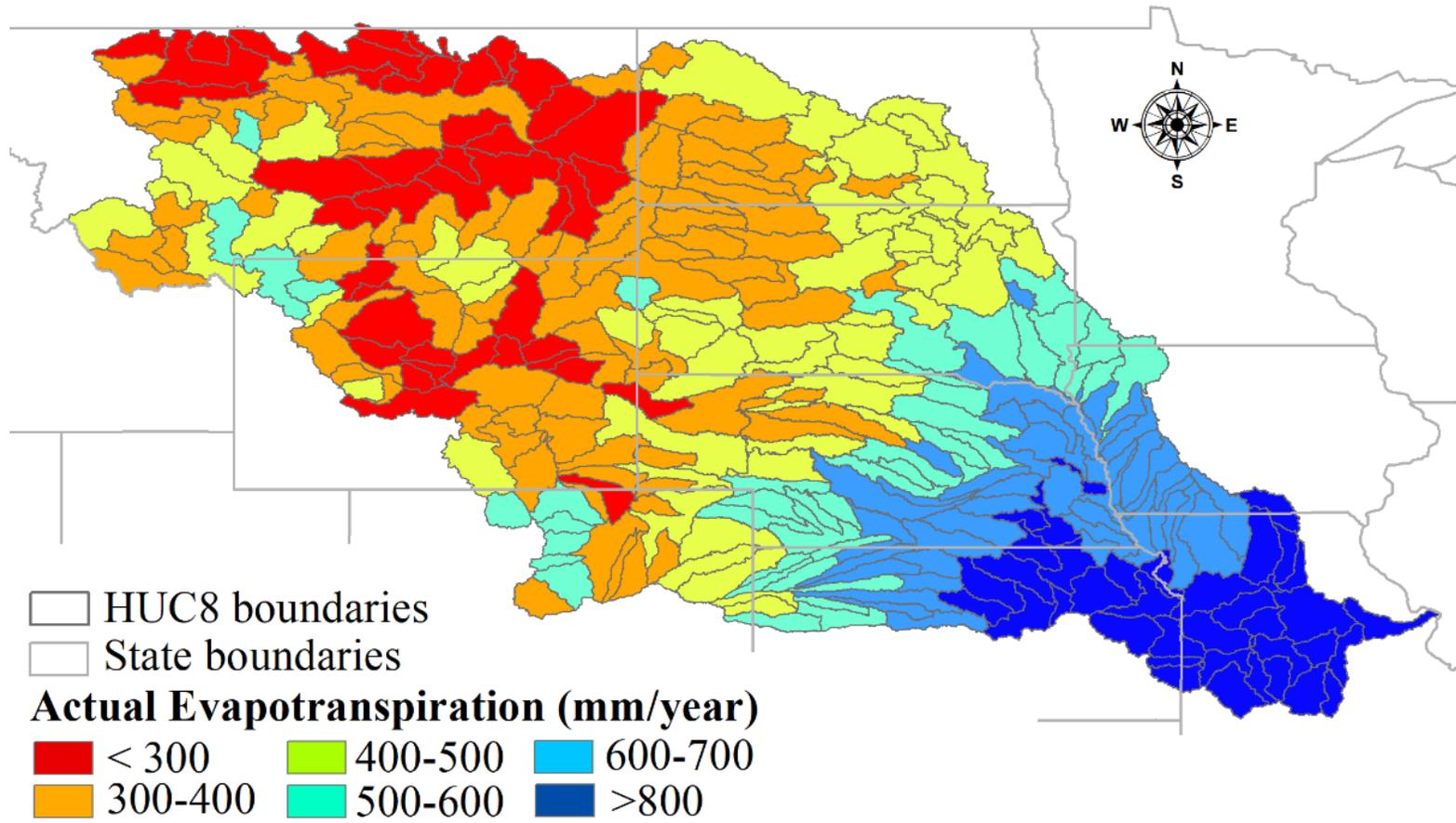
Fig. 6.3. Spatial distribution of annual actual evapotranspiration (ETa) at HUC8 sub-basin scale across the Missouri River Basin
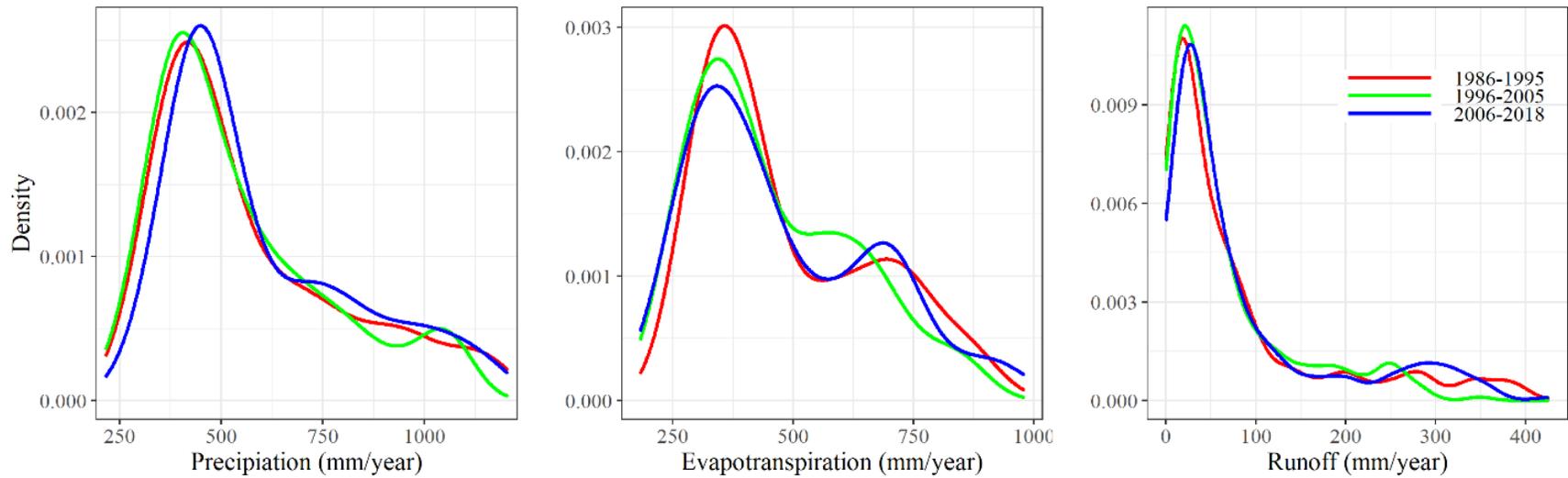
Fig. 6.4. Density plot for temporal variation considering average annual ETa (left), precipitation (middle), and runoff (right) at HUC8 sub-basin scale
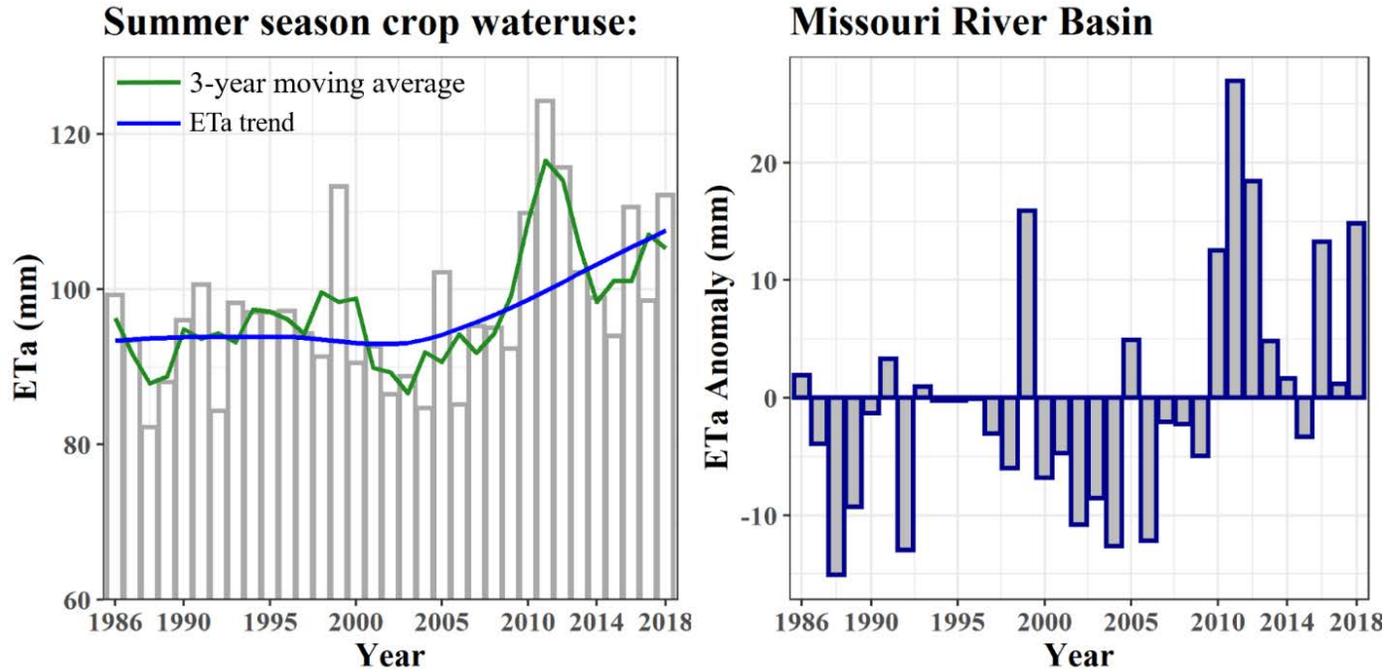
Fig. 6.5. Summer season cropland actual evapotranspiration (ETa, left) and ETa anomalies (right) for the Missouri River Basin
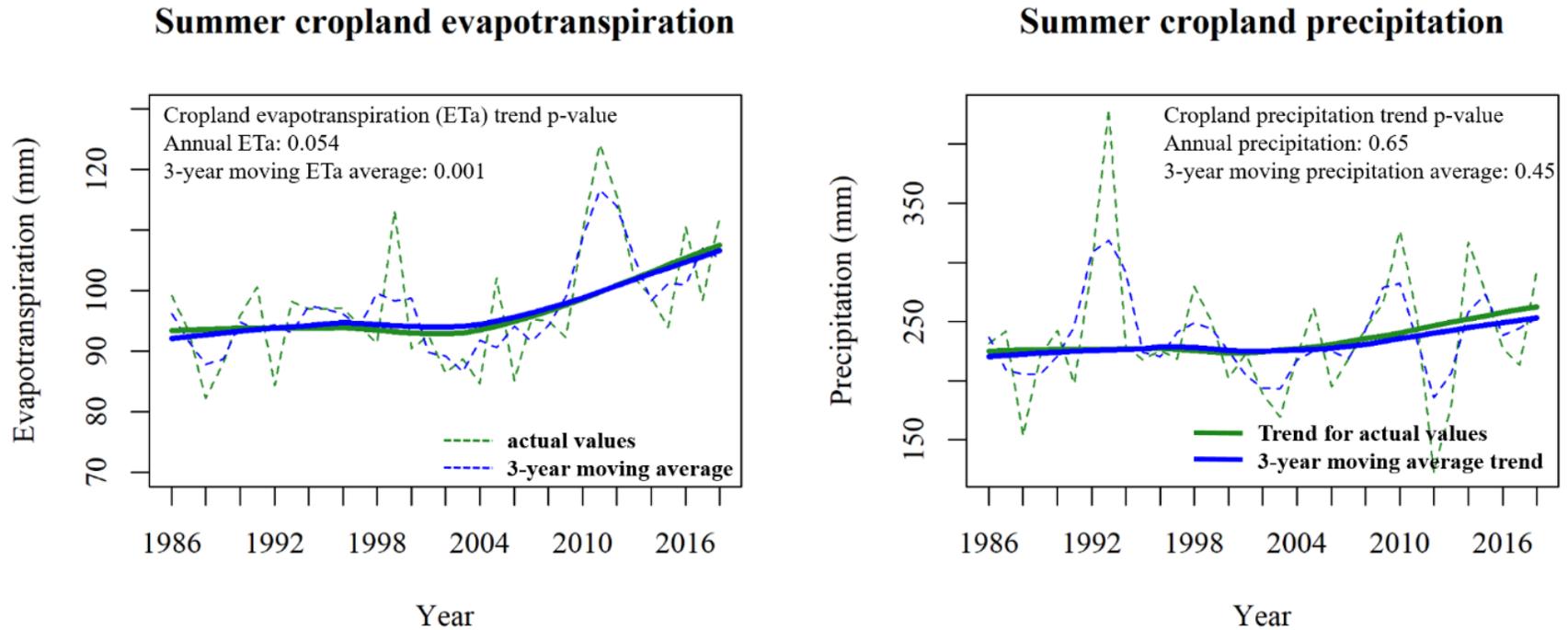
Fig. 6.6. Mann-Kendall regional-scale trend analysis for the summer season crop water use (left) and precipitation (right) [dashed and solid lines represents actual values and trend, respectively, for annual and 3-year average values]

Fig. 6.6. Mann-Kendall regional-scale trend analysis for the summer season crop water use (left) and precipitation (right) [dashed and solid lines represents actual values and trend, respectively, for annual and 3-year average values]
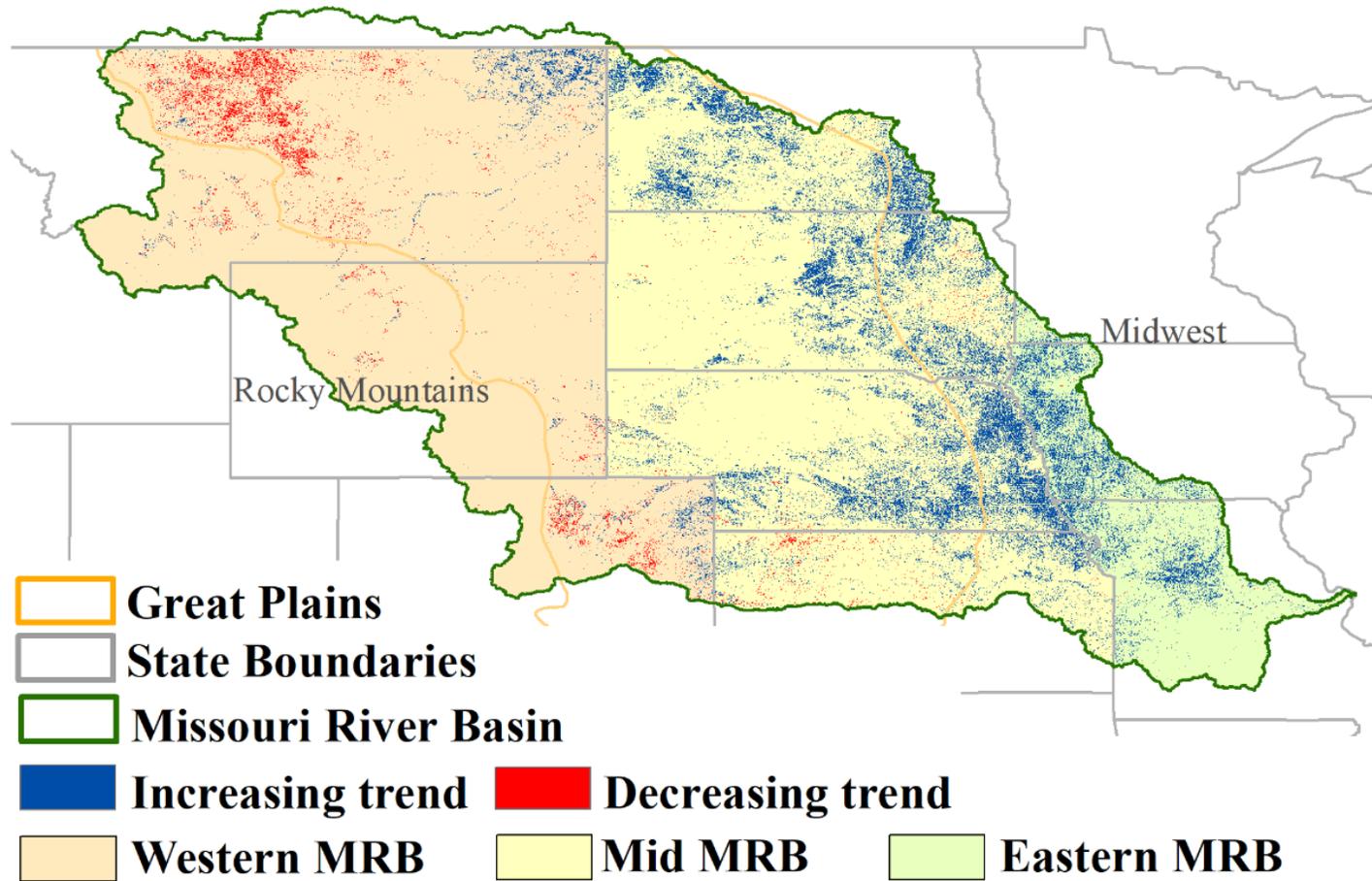
Fig. 6.7. Mann-Kendall pixel-scale trend analysis for the summer season crop water use across the Missouri River Basin.

CHAPTER 7

CONCLUSIONS

This dissertation focuses on understanding the impacts of land use land cover (LULC) and climate changes on water resources across the Missouri River Basin (MRB). Further, the impacts of cover crops and integrated crop-livestock (ICL) systems on water resources at field and watershed scales were also studied. The past influences of LULC and climate shifts were explored using Landsat-based evapotranspiration (ET) estimations, whereas, future impacts were explored using projected climate data from General Circulation Models (GCMs). This dissertation was divided into four different studies, and the following conclusions were determined from these studies:

Study 1. Winter Rye Cover Crop and Water Quality

- The present study was conducted to assess the impacts of winter rye as a cover crop (CC) on soil health and water quality parameters. This study was established in 2017 under a no-till corn (*Zea mays* L.)-soybean [*Glycine max* (L.) Merr.] rotation to assess the impacts of winter rye (*Secale cereale* L.) CC on soil health and water quality parameters.

- Cover cropping did not affect the water quality for the majority of the study period (2017-2020). However, a significant reduction in leached nitrate (~19-20%) and total nitrogen (~8.5-16%) concentrations were found only in 2019, pertaining to sequestered 18.8 kg-N ha^{-1}.

- A significant reduction in leached nitrate and total nitrogen concentrations were observed due to winter rye for one (2019) out of three study years, indicating that well-established rye CC (biomass = 1213 kg ha^{-1}; which was 4.8 and 8.3 times higher than that

in 2018 and 2020) has the potential of reducing nutrient leaching and enhancing soil health for the study region.

- Winter rye showed 13 and 11% significantly higher microbially active carbon and water-extractable organic nitrogen, respectively, than the no cover crop (control) treatment. However, the non-significant impacts on the majority of soil health indicators were due to the shorter (3 years) study duration.

- In terms of soil health parameters, observed higher MAC and WEON under rye CC than the NCC treatment indicates enhanced soil respiration and availability of easily decomposed and released N by soil microbes to growing plants resulting in the minimal possibility of loss. However, to observe the positive influence of a rye CC on soil health parameters, a study duration of greater than 3 years is required. Moreover, an insignificant increase in most of the soil parameters under rye CC than NCC suggests that the duration of study and conservation practices play a crucial role in understanding soil health benefits.

Study 2. Simulating Hydrological Responses to Integrated Crop-Livestock Systems

- This study assessed the hydrological responses of long-term implementation of the ICL system with the projected climate scenario using the Soil and Water Assessment Tool (SWAT) model over two time periods [i.e. Near Future (NF; 2021-2050) and Far Future (FF; 2070-2099)].

- Simulation results from well calibrated ($r^2 = 0.77$, NSE = 0.7, PBIAS = 20.4) and validated ($r^2 = 0.81$, NSE = 0.81, PBIAS = 1.8) SWAT model showed a significant decrease in water yield (7%) and surface runoff (15%) under the long-term (30 years)

implementation of ICL systems which indicate the improved soil hydrologic conditions by incorporating corn residue grazing.

• Projected climate data from GCMs suggested an increase in spring, fall, and winter precipitations with a decrease in summer precipitation in the NF and FF periods which in turn will alter other hydrological cycle components. The observed data for water yield and its hydrological components revealed the vulnerability of the study watershed to extreme events such as floods during spring, and drought during summer under projected climate changes.

• Simulated hydrological responses under the combined effects of long-term ICL system implementation and projected climate changes showed the reduction in water yield and surface runoff due to the ICL system and minimizing the induced detrimental impacts only due to climate change.

Study 3. Estimating Actual Evapotranspiration across South Dakota

• This study was conducted to understand the crop water-use (CWU) characteristics and existing historic mono-directional (increasing/decreasing) trends over the eastern (ESD) and western (WSD) regions of South Dakota (SD) for the 1986-2018 (33-years) period. Strong agreement ($r^2 = 0.91$, PBIAS= -4%, and %RMSE = 11.8%) between the Landsat-based actual evapotranspiration (ETa) estimations and water balance ET suggested the reliability of estimated ETa for the CWU assessment.

• The CWU characteristics indicated that the annual cropland water uses across the ESD (527 mm/year) and WSD (427 mm/year) were more or less met by the precipitation amounts (594 mm/year and 490 mm/year, respectively) in the area. The ample water

supply and distribution have led to a high rainfed and low percentage of irrigated cropland (~2.5%) in the state.

• The Mann Kendall trend analysis revealed the absence of a mono-directional significant trend in annual ETa and precipitation at the regional-scale due to the varying weather conditions of SD. About 12% and 9% cropland areas in the ESD and WSD, respectively, revealed a significant mono-directional trend at pixel-scale ETa. Most of the pixels under significant trend showed an increasing trend.

• The increasing trends across the state might be induced by the shift in agricultural practices, increased irrigated cropland, increased production, moisture regime shifts, and the decreased risk of farming in dry areas. Whereas, the pixels under the significant decreasing trend might be influenced either by the dynamic conversion of wetlands to croplands or by the decreased irrigation practices in mid-eastern SD.

Study 4. Estimating Actual Evapotranspiration across Missouri River Basin (MRB)

• This study used Landsat-based ETa time-series estimations to (i) assess summer season CWU (CWU-Su) dynamics, (ii) investigate CWU-Su trends over the study period (1986-2018; 33 years) at regional- and pixel-scale, and (iii) attribute CWU-Su driving factors across MRB.

• Spatial variability of the Landsat-based ETa estimations showed strong correspondence with land cover and climate across the basin. The drier foothill regions in northwestern MRB, dominated by grassland/shrubland, showed lower ETa (< 400 mm/year), whereas, cropland dominated regions in lower semi-humid MRB and forested headwater exhibited higher ETa (> 500 mm/year).

- At the basin scale, CWU-Su revealed a significant increasing trend, whereas, precipitation showed an absence of a monodirectional trend for the MRB. The Mann Kendall trend analysis revealed a significant increasing and decreasing CWU-Su trend for about 30% and 5% MRB cropland pixels, respectively.

- An assessment of CWU-Su driving factors suggested that the increasing CWU-Su trend across eastern- and mid-MRB appears to be driven by increased crop production area, increased crop yields, crop practices shifts to higher biomass crops, increased irrigated land, reduced fallow land practices, adoption of conservation practices for soil moisture storage improvement, and moisture regime shifts due to increased precipitation and increased temperature.

- The clustered decreasing CWU-Su trend pixels in the western MRB could be driven by the decreased wastage of water through ET due to the improved and more efficient irrigation and water management practices (e.g., shifting from flood irrigation to sprinkler irrigation systems) over the regions with the minimal crop practices shifts during the study period.

- Validation statistics of ETa estimations reinforce the capability of the SSEBop model and Landsat imagery for capturing spatial and temporal ETa variations over a large range of vegetation, climate, and elevation.

APPENDICES

APPENDIX A

Table 1A. Simulation scenarios to evaluate the impacts of the ICL system and future climate changes on streamflow of Skunk Creek watershed.

Phase	Scenario	Land use Data	Climate data	RCP	Simulation Period
Phase I ICL system	S01	NASS-2008/ corn-soybean rotation	NOAA data		1976-2005
	S02	ICL system	NOAA data		1976-2005
Phase II Climate Changes	S03	NASS-2008	CCSM_4.1	RCP_2.6	2021-2050
	S04				2070-2099
	S05			RCP_4.5	2021-2050
	S06				2070-2099
	S07			RCP_6.0	2021-2050
	S08				2070-2099
	S09			RCP_8.5	2021-2050
	S10				2070-2099
	S11		CCSM_4.2	RCP_2.6	2021-2050
	S12				2070-2099
	S13			RCP_4.5	2021-2050
	S14				2070-2099
	S15			RCP_6.0	2021-2050
	S16				2070-2099
	S17			RCP_8.5	2021-2050
	S18				2070-2099
	S19		NOAA-GFDL-ESM2G	RCP_2.6	2021-2050
	S20				2070-2099
	S21			RCP_4.5	2021-2050
	S22				2070-2099
	S23			RCP_6.0	2021-2050
	S24				2070-2099
	S25			RCP_8.5	2021-2050
	S26				2070-2099
	S27		NOAA-GFDL-ESM2M	RCP_2.6	2021-2050
	S28				2070-2099
	S29			RCP_4.5	2021-2050
	S30				2070-2099
	S31			RCP_6.0	2021-2050
	S32				2070-2099
	S33			RCP_8.5	2021-2050
	S34				2070-2099

Table 1A (*continued*). Simulation scenarios to evaluate the impacts of the ICL system and future climate changes on streamflow of Skunk Creek watershed.

Phase	Scenario	Land use Data	Climate data	RCP	Simulation Period
Phase III ICL systems and climate change	S35	ICL system	CCSM_4.1	RCP_2.6	2021-2050
	S36				2070-2099
	S37			RCP_4.5	2021-2050
	S38				2070-2099
	S39			RCP_6.0	2021-2050
	S40				2070-2099
	S41			RCP_8.5	2021-2050
	S42				2070-2099
	S43		CCSM_4.2	RCP_2.6	2021-2050
	S44				2070-2099
	S45			RCP_4.5	2021-2050
	S46				2070-2099
	S47			RCP_6.0	2021-2050
	S48				2070-2099
	S49			RCP_8.5	2021-2050
	S50				2070-2099
	S51		NOAA-GFDL-ESM2G	RCP_2.6	2021-2050
	S52				2070-2099
	S53			RCP_4.5	2021-2050
	S54				2070-2099
	S55			RCP_6.0	2021-2050
	S56				2070-2099
	S57			RCP_8.5	2021-2050
	S58				2070-2099
	S59		NOAA-GFDL-ESM2M	RCP_2.6	2021-2050
	S60				2070-2099
	S61			RCP_4.5	2021-2050
	S62				2070-2099
	S63			RCP_6.0	2021-2050
	S64				2070-2099
	S65			RCP_8.5	2021-2050
	S66				2070-2099

Table 2A. List of parameters selected for calibration of the Skunk Creek watershed model.

Parameter	Description	Type of change*	Calibration range	Best estimate
SOL_K	Saturated hydraulic conductivity	r	-15 - 15	-3.6
SLSUBBSN	Average slope length	v	10 - 100	51.8
HRU_SLP	Average slope steepness	v	0 - 1	0.07
SFTMP	Snowfall temperature (°C)	v	-5 - 5	-1.16
SMFMN	Minimum melt rate for snow during the year (occurs on winter solstice)	v	0 - 10	5.42
SMTMP	Snow melt base temperature (°C)	v	-5 - 5	3.16
CN2	SCS runoff curve number (Moisture condition II)	r	-0.4 – 0.6	-0.08
ALPHA_BNK	Baseflow alpha factor for bank storage	v	0.01 - 1.0	0.52
SOL_AWC	Available water capacity of the soil layer (mm mm^{-1})	r	-30 - 15	14.36
CANMX	Maximum canopy storage (mm)	v	0.01 - 25	11.8
GWQMN	Threshold depth of water in the shallow aquifer required for return flow to occur (mm)	v	10 - 100	105.32
ESCO	Soil evaporation compensation factor	v	0.001 - 1	0.83
EPCO	Plant uptake compensation factor	v	0.001 - 1	0.03
GW_DELAY	Groundwater delay (days)	v	0 - 450	177.5
ALPHA_BF	Baseflow alfa factor (days)	v	0 - 1	0.06
TIMP	Snow pack temperature lag factor	v	0.01 - 1	0.82
SURLAG	Surface runoff lag time (days)	v	0.05 - 24	16.63
CH_K2	Effective hydraulic conductivity in main channel alluvium (mm h^{-1})	v	0.0 - 150	158.3
CH_N2	Manning's *n* value for the main channel	v	0.01 - 0.3	0.18
GW_REVAP	Groundwater "revap" coefficient	v	0.08 - 0.2	0.45
REVAPMN	Threshold depth of water in the shallow aquifer for "revap" to occur (mm)	v	0 - 100	101.3
OV_N	Manning's *n* value for overland flow	r	0.01 - 0.9	0.49
SMFMX	Maximum melt rate for snow during year (occurs on summer solstice)	v	0 - 10	7.57

*v means the existing parameter value was replaced by a given value within the calibration range; r means an existing parameter value was multiplied by a factor defined by 1 + a given value within the calibration range.

Table 3A. Month-wise percentage variation in different hydrological components compared to baseline in response to the ensembled future projection of climate change scenarios for near-future over Skunk Creek watershed

RCP	Months											
	JAN	FEB	MAR	APR	MAY	JUN	JUL	AUG	SEP	OCT	NOV	DEC
Precipitation												
RCP 2.6	6.6	37.9	1.4	12.6	4.2	5.7	-10.1	-4.7	1.9	0.9	-6.8	3.5
RCP 4.5	3.4	29.3	6.4	7.5	1.7	6.3	-8.5	-8	6.9	17.3	-12.6	-2.2
RCP 6.0	-0.5	20.6	0.4	10.4	8.4	7.5	-6.9	-0.5	3.9	14.8	-13.2	-2.2
RCP 8.5	3	47.6	23.6	15	11.4	-2	-8.1	-2.6	1.1	18.3	11.1	10.5
Water Yield												
RCP 2.6	1.3	40	7	4.4	14.6	11.4	-5.4	-2	0.1	1.5	1.5	2.1
RCP 4.5	26.9	48	-12.4	-3.3	6.8	18.9	-2.7	11.6	10	36.7	8.7	18.7
RCP 6.0	24.6	14.1	2	1.7	25.2	20.4	9.6	26.1	18.8	20	3.6	0
RCP 8.5	44.7	72.2	15.6	34.1	44.9	19.2	4	31.2	18.8	29.6	49.8	32.7
Surface Runoff												
RCP 2.6	-7.5	51.5	2.7	-20.7	27	13.7	-18	5.8	-11.2	-14.2	5.7	4.4
RCP 4.5	42.5	57.4	-22.9	-35.1	14.7	21.1	-12.1	3	9.6	68.8	-4.5	29.9
RCP 6.0	39.6	11.9	-3.1	-25.4	36.3	6.3	17.2	48.2	27	27.4	-24.8	-45.1
RCP 8.5	70.3	84.5	1.4	-6.3	64.7	-1.2	-5.3	19.1	8.2	29.1	100.1	14.1
Evapotranspiration												
RCP 2.6	16.4	18.5	9.9	4.6	4	4.2	4.3	-5.5	-4.6	-8	-4.2	0.5
RCP 4.5	25.4	21.3	15.9	4.7	2.5	3.6	1.9	-6.2	-5.5	-6.1	-6.7	-1.2
RCP 6.0	15.5	14.5	7.1	2.8	1.9	3.8	3.4	-6.2	-2.9	-4.1	0.3	7.8
RCP 8.5	23.6	21.1	7.3	2.3	3.2	2.3	2	-6.7	-6.8	-9.8	-6.7	-3.2

Table 4A. Month-wise percentage variation in different hydrological components compared to baseline in response to the ensembled future projection of climate change scenarios for far-future over Skunk Creek watershed

RCP	Months											
	JAN	FEB	MAR	APR	MAY	JUN	JUL	AUG	SEP	OCT	NOV	DEC
	Precipitation											
RCP 2.6	-3.3	34.8	1.1	9.3	3.9	9.6	-7.8	-3	4	4.3	5.6	10
RCP 4.5	13.2	55.2	10.2	11.6	5.7	0.7	-13.3	-6.3	3	20.7	10.9	2.7
RCP 6.0	13.4	57.7	26.8	19.1	3.3	3.7	-17.5	-11.2	2.9	6.8	12.8	-2.5
RCP 8.5	24.4	71.1	27.3	26.3	24.5	-0.1	-14.5	-4.3	-11.9	9.4	11.9	23.2
	Water Yield											
RCP 2.6	59.4	29.3	-0.1	9.9	15.2	35.2	13.3	18.8	10.6	17.5	23.4	15.5
RCP 4.5	37.3	47.6	-1.6	5.9	8.4	13.4	-7.4	5.8	2.8	29.9	25.5	10.4
RCP 6.0	75	53.8	18.2	40.9	38.8	31.3	5	37.4	39.3	30.6	38.2	58.2
RCP 8.5	126.6	108.9	9.7	62.5	100.3	39.7	26	96	37.3	54.3	68.8	95.7
	Surface Runoff											
RCP 2.6	134.4	26.4	-10	-21.7	19.9	44.1	16.2	7.7	3.4	28.1	37.9	-5.3
RCP 4.5	96.9	57.6	-15.5	-36.1	12.1	25.1	-15.2	17.9	-0.7	56.3	39.8	-0.2
RCP 6.0	140.3	44.3	-7.4	-21.1	17.9	11.2	-31.2	62.8	36.8	21.7	37.7	81.6
RCP 8.5	199.8	77.1	-40.4	-24.9	103.3	14.4	6.9	94.4	8.3	78.4	41.4	91.1
	Evapotranspiration											
RCP 2.6	28.5	18.4	7.2	0.7	0.5	3.7	1.2	-6.2	-4.7	-3.4	-1.8	6.3
RCP 4.5	48.3	28.8	24.4	6.3	7.4	8.4	5	-9	-7.9	-13.5	-0.7	7.6
RCP 6.0	41.3	20.4	12.1	0.1	2.7	1.5	-1.6	-13.7	-15.7	-22.2	-17.2	0.1
RCP 8.5	49.4	49.1	14.6	3.2	3.7	4.7	-7.4	-19.1	-21.4	-22	-15	-13.7

Table 5A. Month-wise percentage variation in different hydrological components compared to baseline in response to the combined effect of long-term ICL system implementation and ensembled future projection of climate change scenarios for near future over Skunk Creek watershed.

RCP	Months											
	JAN	FEB	MAR	APR	MAY	JUN	JUL	AUG	SEP	OCT	NOV	DEC
Water Yield												
RCP 2.6	-3	37.1	5.4	2.6	12.3	10.7	-4.7	-5.5	-4.1	-4.9	-3.2	-4.1
RCP 4.5	20.2	42.8	-15.1	-7.5	3.7	18.4	-1.8	6.9	4.4	30.7	2.7	10
RCP 6.0	19.3	10.2	-0.2	-2.3	21.3	19.4	10.8	20.8	11.2	13.4	0.5	-2.3
RCP 8.5	36.8	68.3	12.7	30.9	41.6	17.9	3.1	22.8	12.9	23.4	41.1	25.6
Surface Runoff												
RCP 2.6	-10.6	49.5	1.6	-21.4	24.1	15	-17.2	-3.4	-14	-21.9	3.6	-5.7
RCP 4.5	34.7	52.6	-25	-37.2	11.7	20.9	-7.1	-2.1	3.4	63.1	-10.2	15.8
RCP 6.0	38.2	9.4	-4.3	-26.5	34.3	8.7	21.1	44.1	21.5	26.3	-24.3	-37.6
RCP 8.5	61.1	81.9	0	-6.6	61.7	0.7	-5.1	9.3	2.3	23.5	86.5	7.7
Evapotranspiration												
RCP 2.6	15	18.6	9.6	4.2	3.9	3.3	3.7	-3.2	-1.4	-6	-3	8.8
RCP 4.5	24.2	21.5	15.9	4.7	2.4	2.8	1.7	-3.3	-3.3	-3	-4.5	8.4
RCP 6.0	16.8	15.6	8.9	4.6	3	3.3	1.8	-4	-0.1	-1.5	0.6	9.7
RCP 8.5	22.9	22.2	8.1	3	3.7	1.8	1.7	-4.2	-3.6	-7.8	-6.2	4

Table 6A. Month-wise percentage variation in different hydrological components compared to baseline in response to the combined effect of long-term ICL system implementation and ensembled future projection of climate change scenarios for far future over Skunk Creek watershed.

RCP	Months											
	JAN	FEB	MAR	APR	MAY	JUN	JUL	AUG	SEP	OCT	NOV	DEC
Water Yield												
RCP 2.6	49.2	23.3	-3.2	4.2	9.6	31.2	12.2	13.5	2	8.8	15.8	5.3
RCP 4.5	48.1	55.3	3.5	13.8	16.6	21.6	3	13.2	8.9	41.3	35.7	23.4
RCP 6.0	46.5	34.8	5.5	20.2	21	18.7	-6	17.3	16.8	7.1	15.5	35
RCP 8.5	127.3	107.7	9.6	63.3	103.3	45.6	24.4	86	33.3	52.9	68.7	92.8
Surface Runoff												
RCP 2.6	124.1	22.5	-11.4	-23.2	15.9	43.4	16.2	0.9	-4.1	20.5	33.8	-16.2
RCP 4.5	101.2	61.5	-12.9	-33.7	18.5	29.1	-7.7	19.4	2.9	66.6	47.1	13.7
RCP 6.0	115.6	34.3	-12.9	-28.4	9.7	8.6	-33	45.2	21.4	0.9	23.7	73.9
RCP 8.5	203.1	76.7	-41.1	-24.7	107	22	1.6	78.9	3.3	73.8	36.1	77
Evapotranspiration												
RCP 2.6	32.6	21.3	10.3	2.8	2.2	3.6	0.7	-3.2	-1.3	-1.1	0.2	10.1
RCP 4.5	45.4	24.6	21	3.9	4.9	3.8	0.8	-9	-8	-13.3	-4.1	6.4
RCP 6.0	50.4	28.8	19.9	6.7	8.3	5.2	1.2	-8.5	-11	-17.4	-11.5	11.1
RCP 8.5	48.6	47.3	13.3	2.5	2.2	2.7	-5.5	-16.8	-21.2	-23.4	-16	-11.6

APPENDIX B
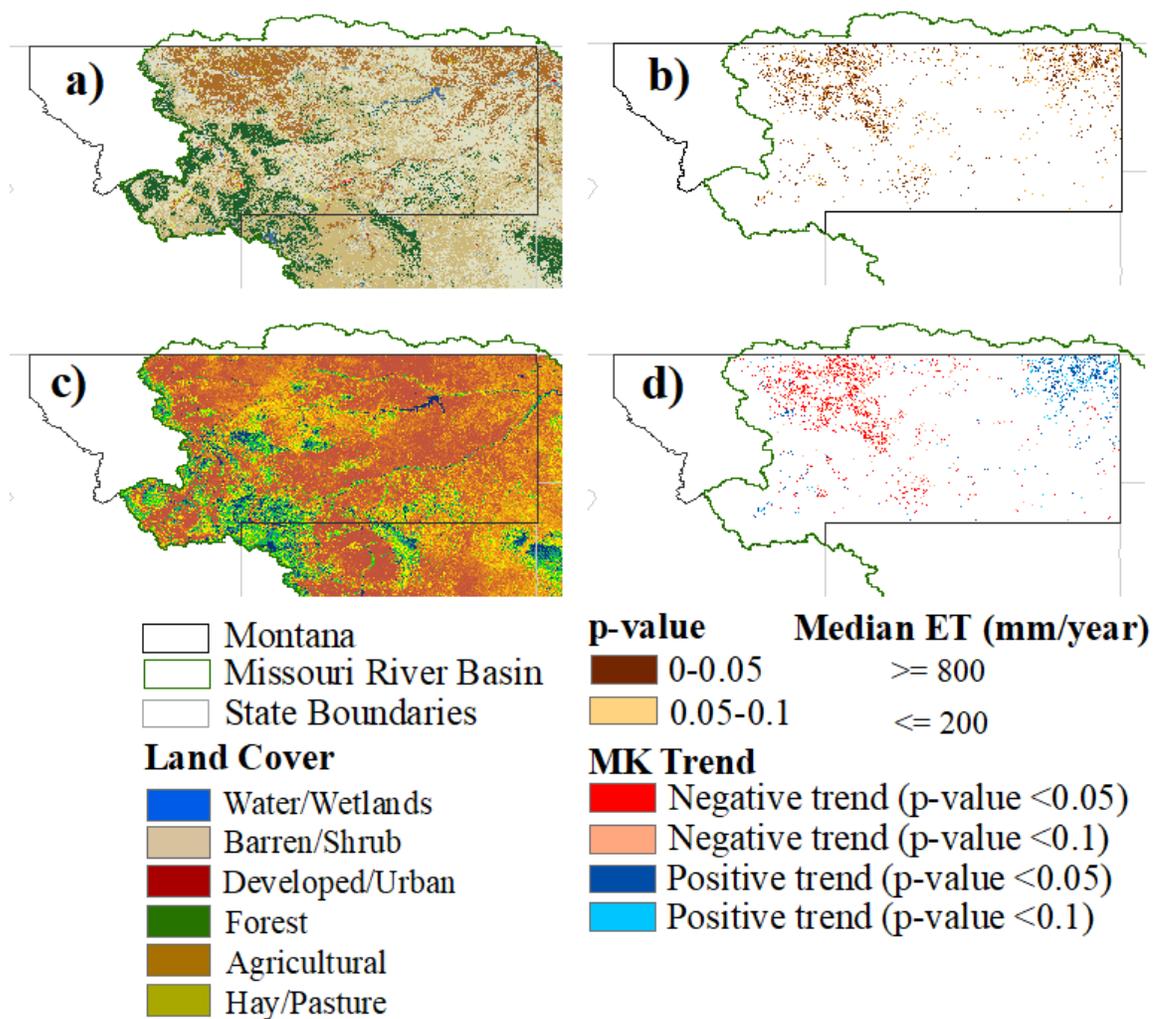
Fig. 1B. Distribution of (a) land cover, (b) p-values for summer season crop water use (CWU) trend, (c) median annual actual evapotranspiration, and (d) summer season CWU trend direction across the state of Montana, USA.
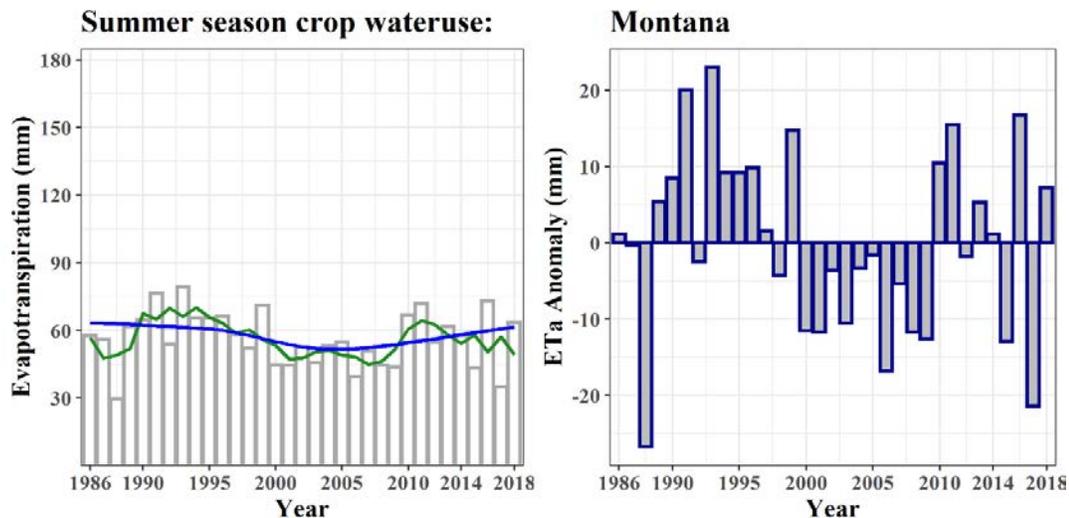
Fig. 2B. Mann-Kendall regional-scale trend for summer season ETa (left panel) and ETa anomalies (right panel) for Montana, USA.
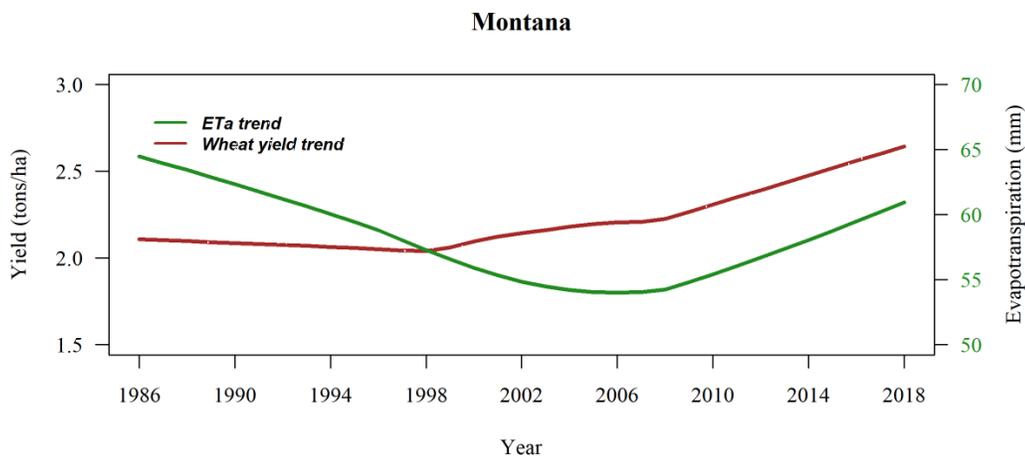

Fig. 3B. Crop production and summer season crop water use for the state of Montana, USA.
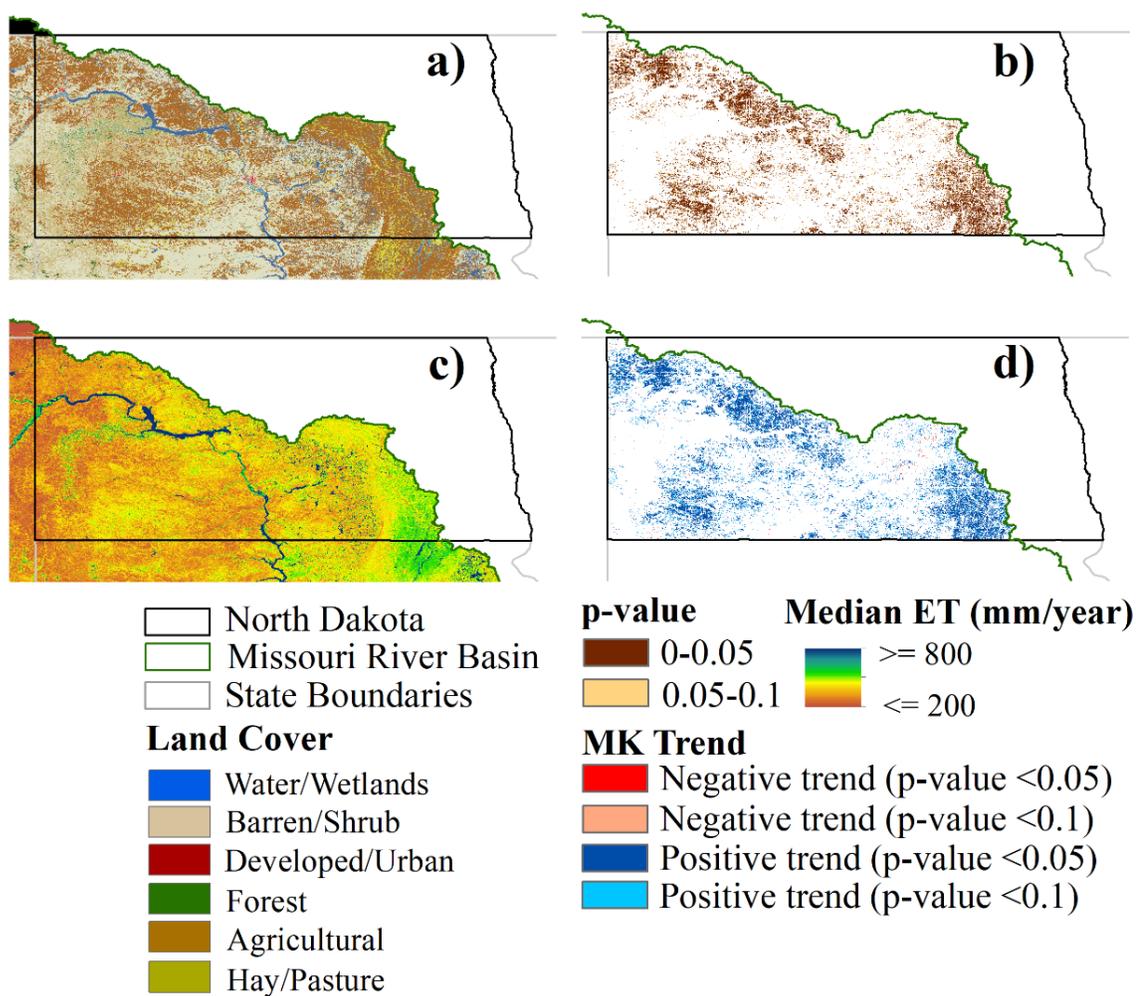
Fig. 4B. Distribution of (a) land cover, (b) p-values for summer season crop water use (CWU) trend, (c) median annual actual evapotranspiration, and (d) summer season CWU trend direction across the state of North Dakota, USA.
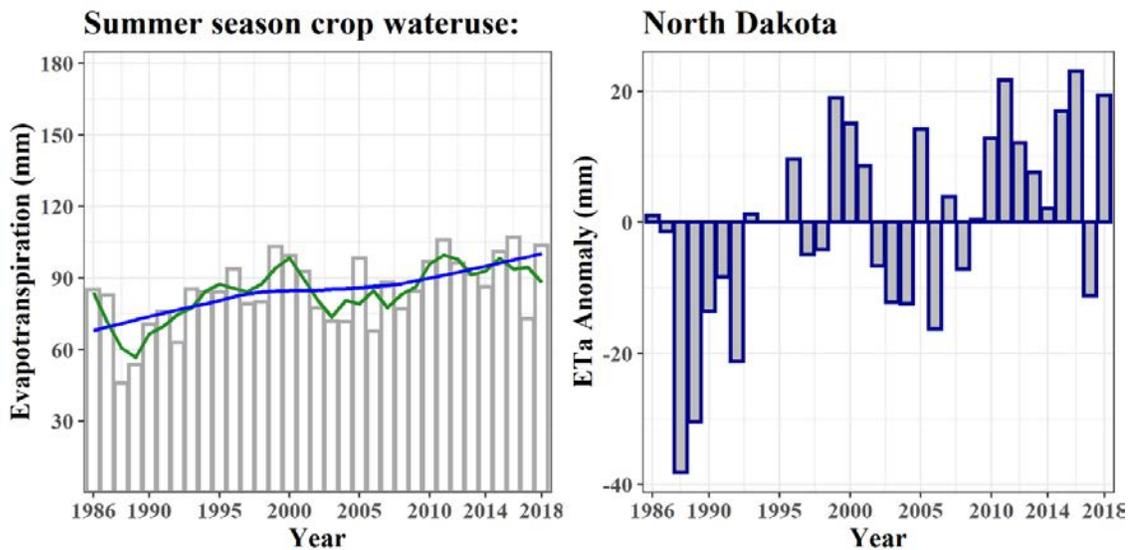
Fig. 5B. Mann-Kendall regional-scale trend for summer season ETa (left panel) and ETa anomalies (right panel) for North Dakota, USA.
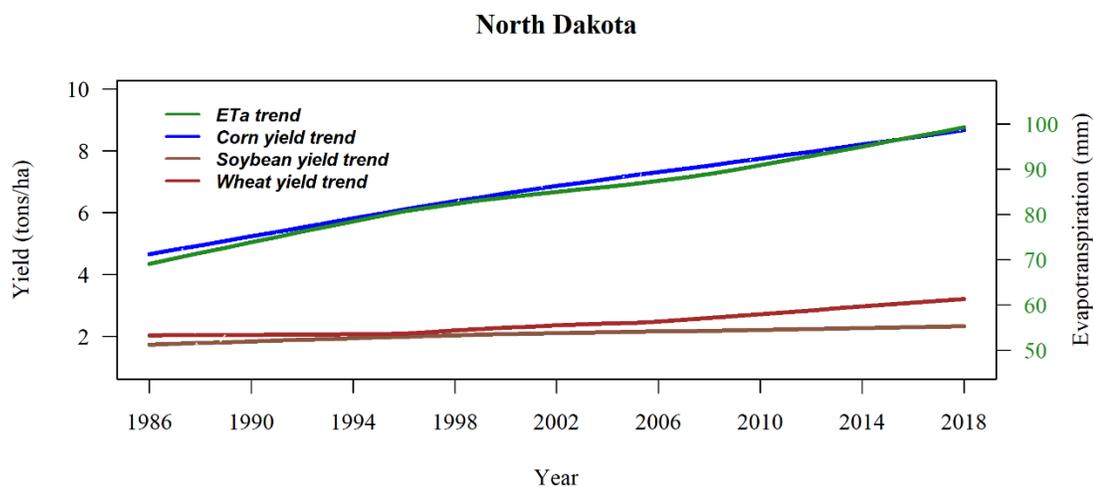

Fig. 6B. Crop production and summer season crop water uses for the state of North Dakota
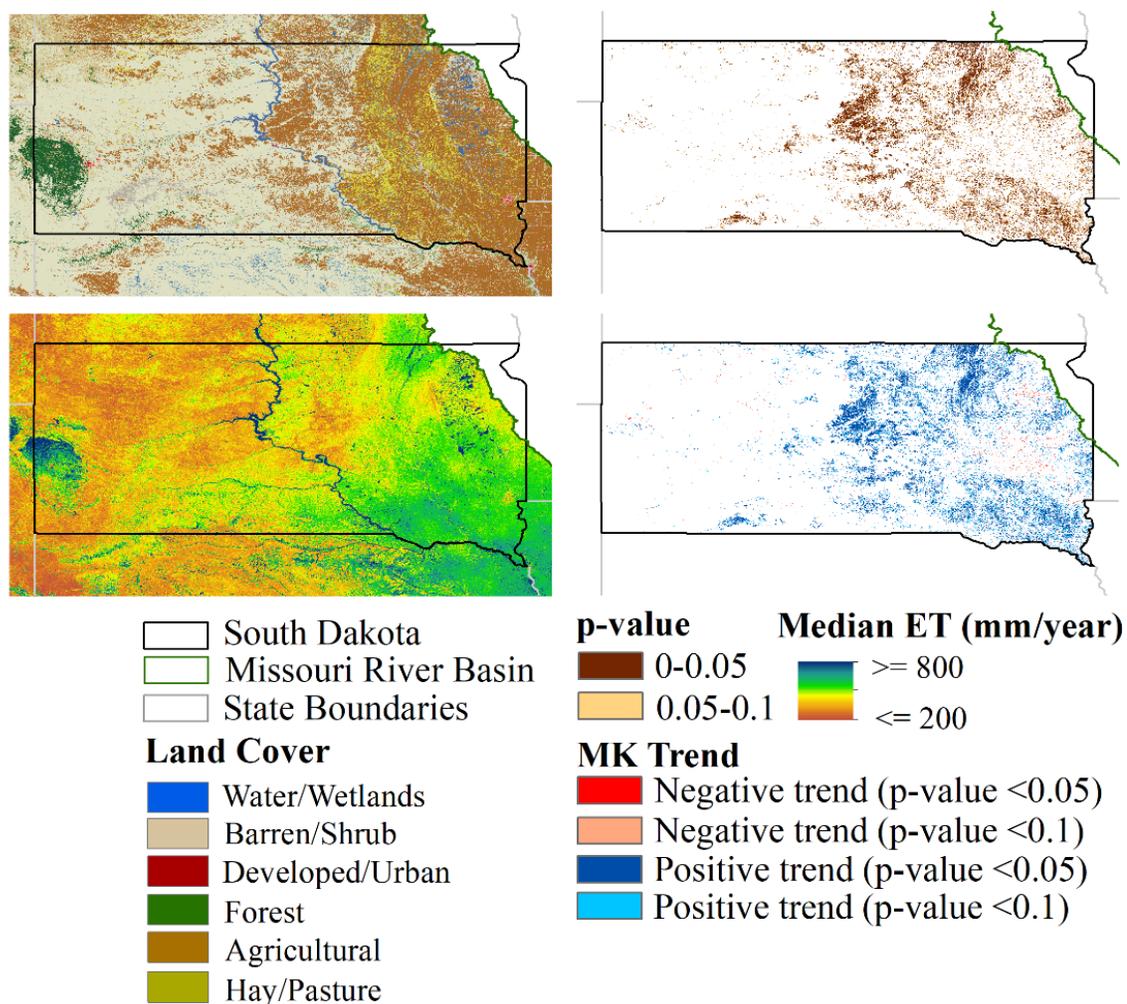
Fig. 7B. Distribution of (a) land cover, (b) p-values for summer season crop water use (CWU) trend, (c) median annual actual evapotranspiration, and (d) summer season CWU trend direction across the state of South Dakota, USA.
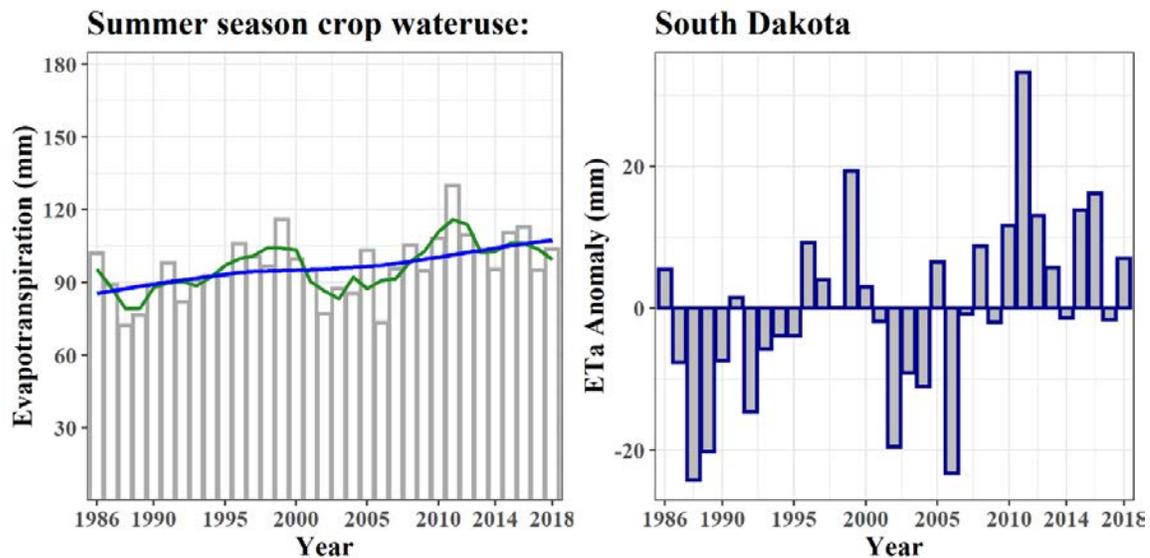
Fig. 8B. Mann-Kendall regional-scale trend for summer season ETa (left panel) and ETa anomalies (right panel) for South Dakota, USA.
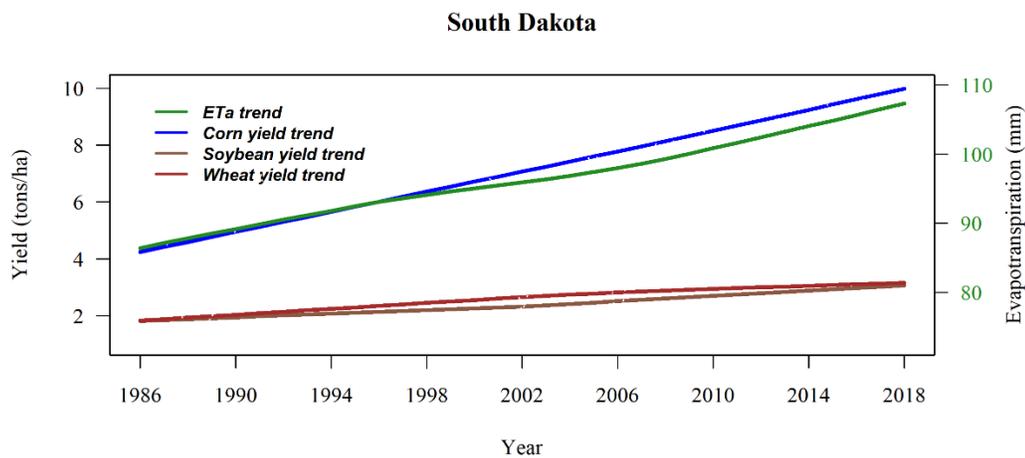
Fig. 9B. Crop production and summer season crop water uses for the state of South Dakota
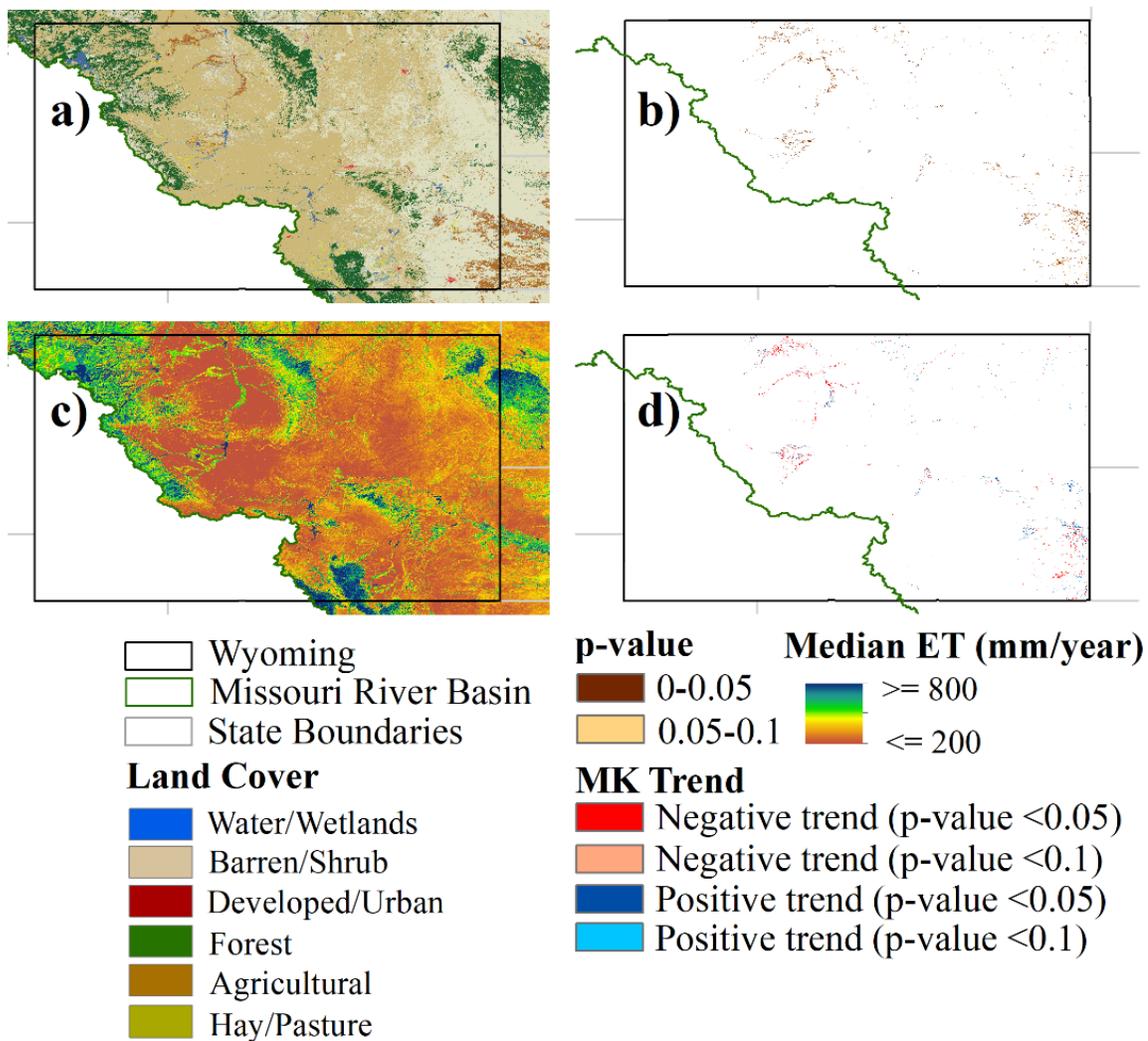
Fig. 10B. Distribution of (a) land cover, (b) p-values for summer season crop water use (CWU) trend, (c) median annual actual evapotranspiration, and (d) summer season CWU trend direction across the state of Wyoming, USA.
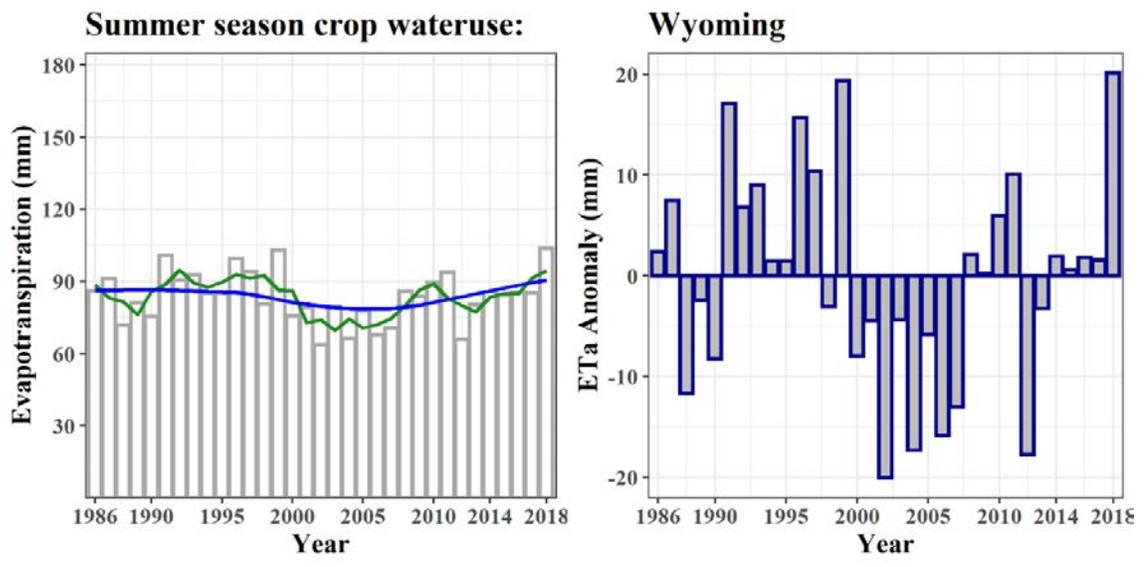
Fig. 11B. Mann-Kendall regional-scale trend for summer season ETa (left panel) and ETa anomalies (right panel) for Wyoming, USA.
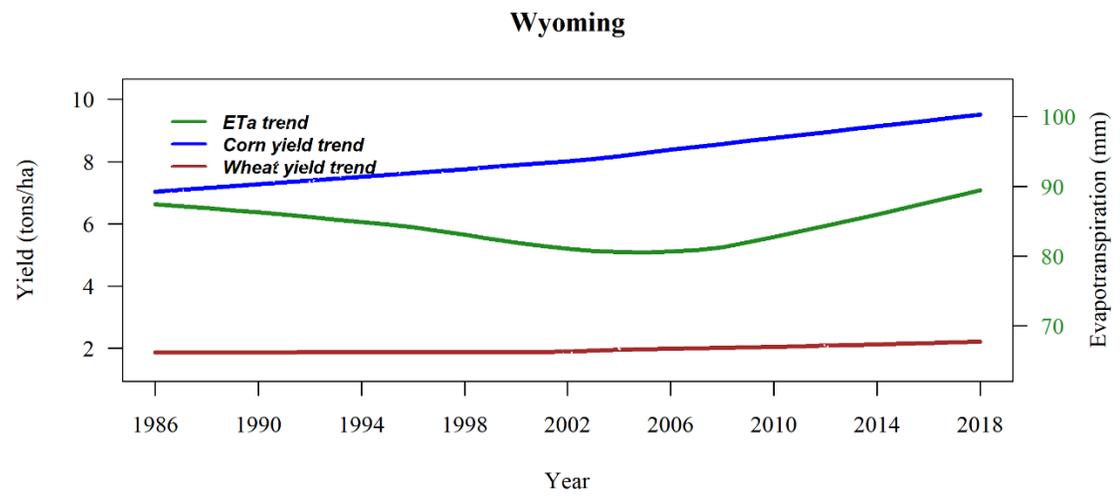

Fig. 12B. Crop production and summer season crop water uses for the state of Wyoming
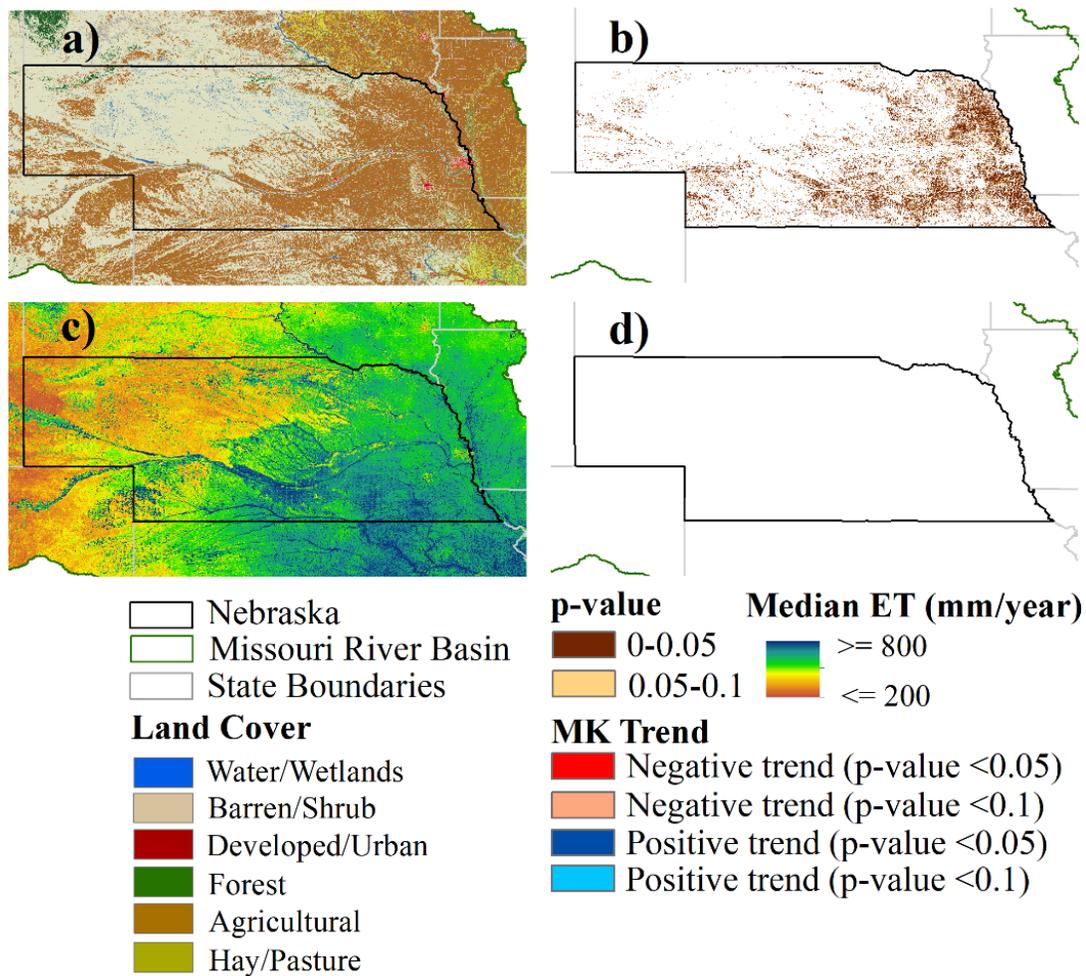
Fig. 13B. Distribution of (a) land cover, (b) p-values for summer season crop water use (CWU) trend, (c) median annual actual evapotranspiration, and (d) summer season CWU trend direction across the state of Nebraska, USA.
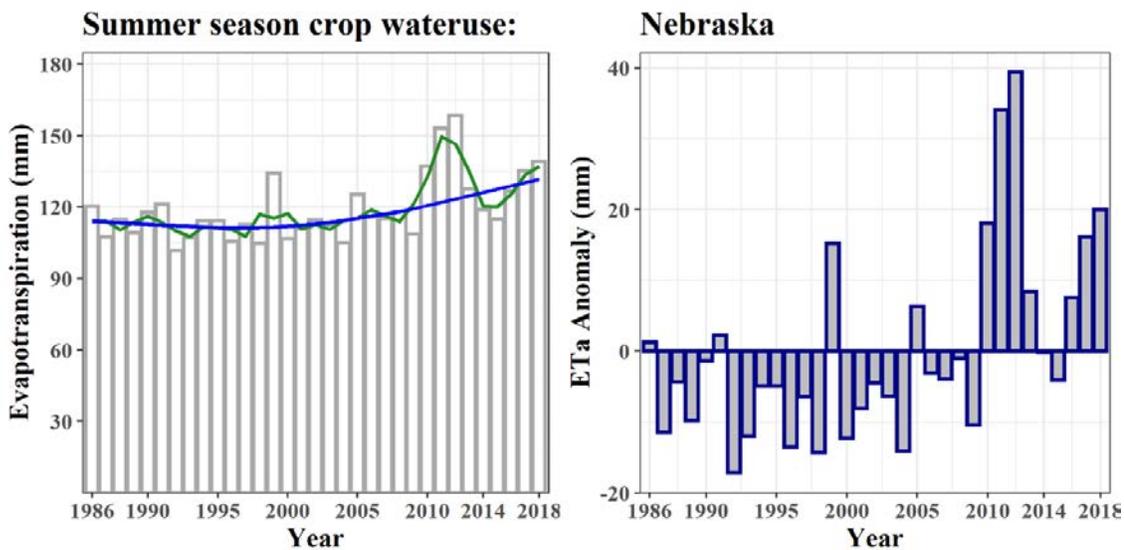
Fig. 14B. Mann-Kendall regional-scale trend for summer season ETa (left panel) and ETa anomalies (right panel) for Nebraska, USA.
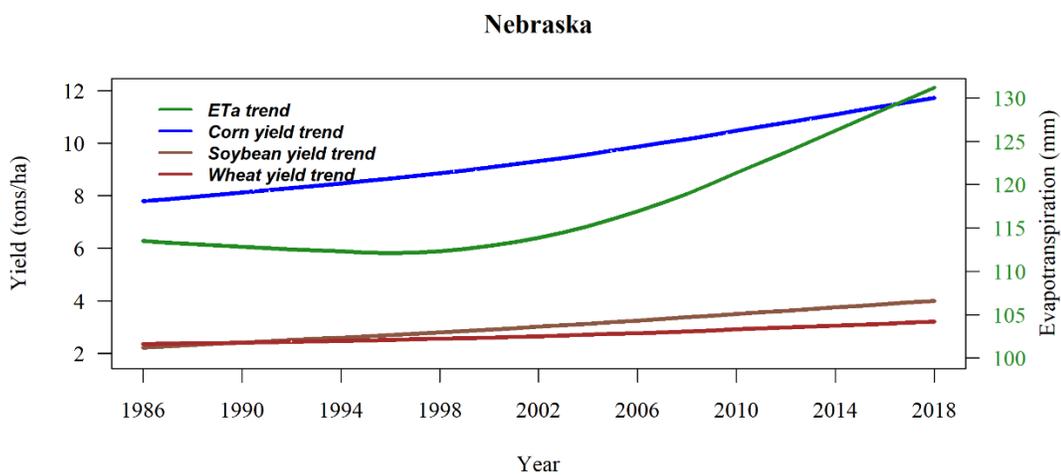
Fig. 15B. Crop production and summer season crop water uses for the state of Nebraska
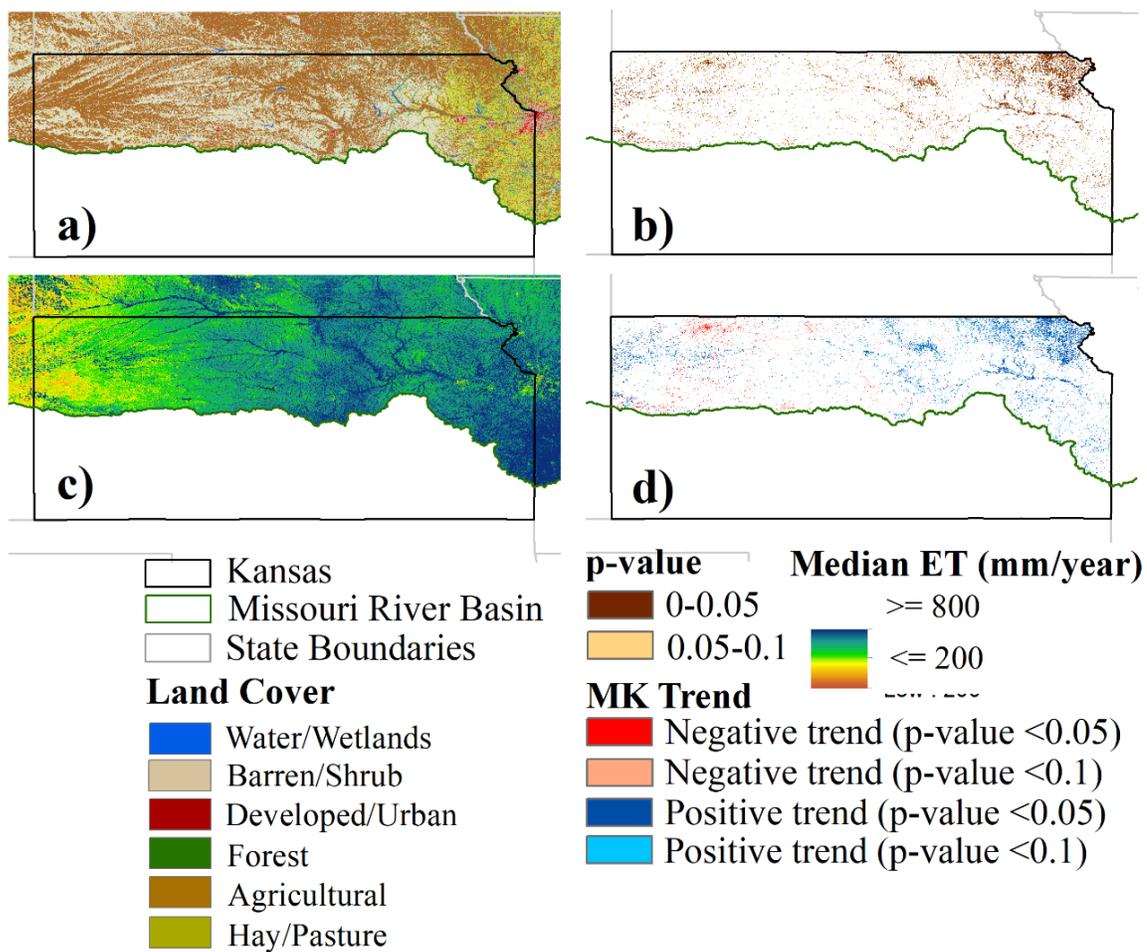
Fig. 16B. Distribution of (a) land cover, (b) p-values for summer season crop water use (CWU) trend, (c) median annual actual evapotranspiration, and (d) summer season CWU trend direction across the state of Kansas, USA.
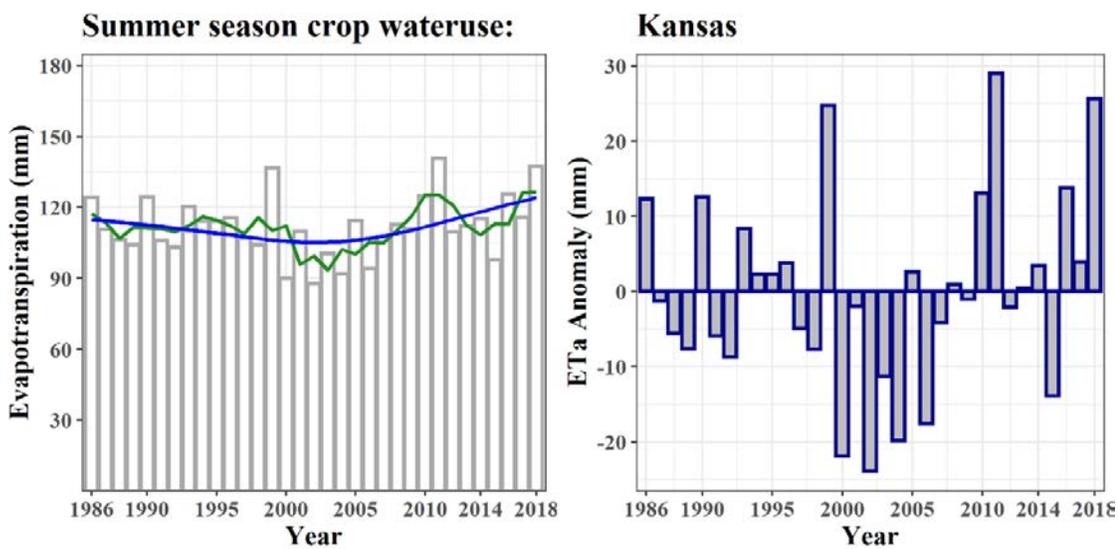
Fig. 17B. Mann-Kendall regional-scale trend for summer season ETa (left panel) and ETa anomalies (right panel) for Kansas, USA.
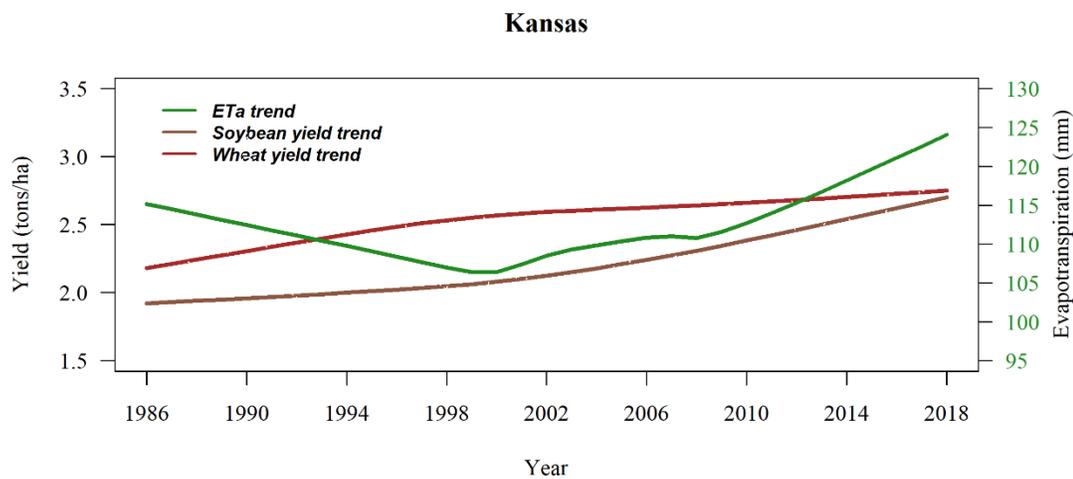

Fig. 18B. Crop production and summer season crop water uses for the state of Kansas
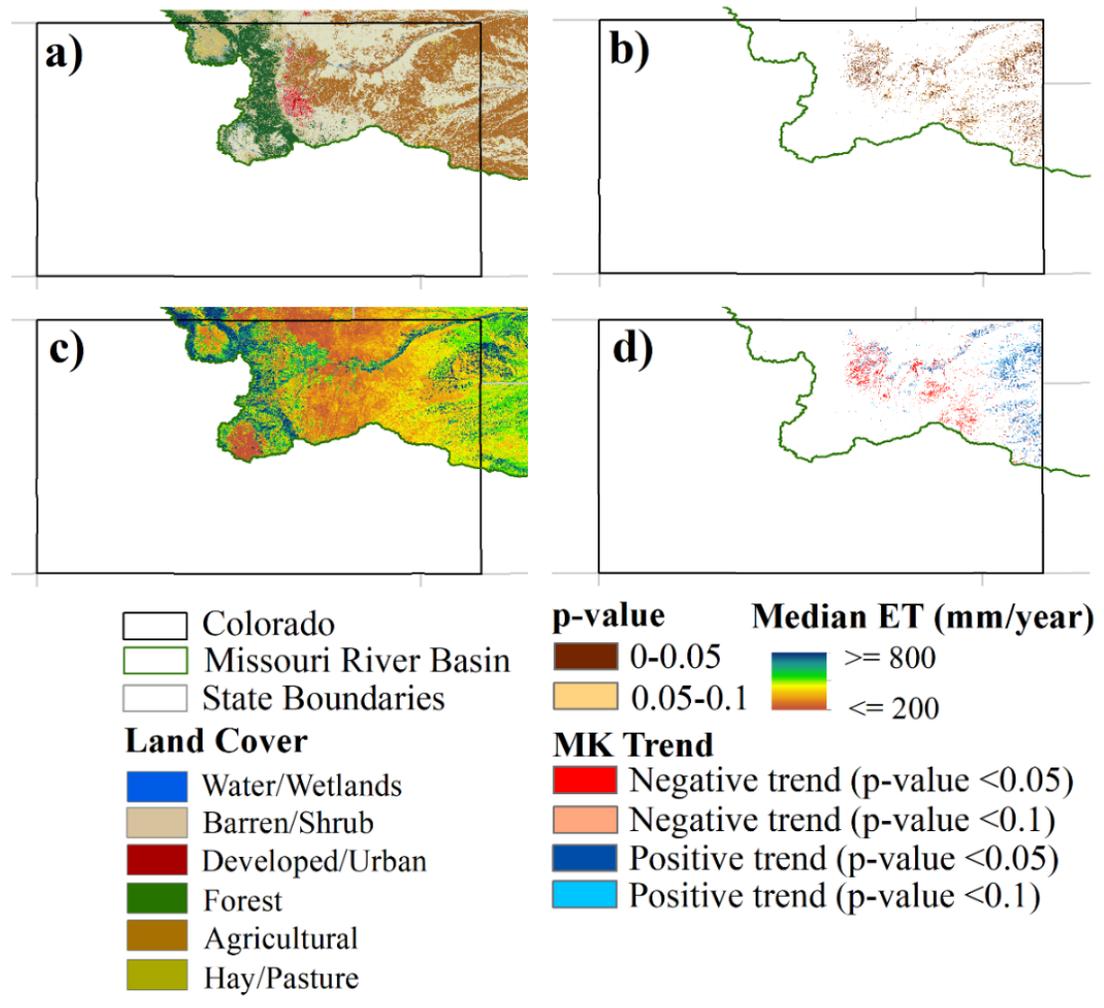
Fig. 19B. Distribution of (a) land cover, (b) p-values for summer season crop water use (CWU) trend, (c) median annual actual evapotranspiration, and (d) summer season CWU trend direction across the state of Colorado, USA.
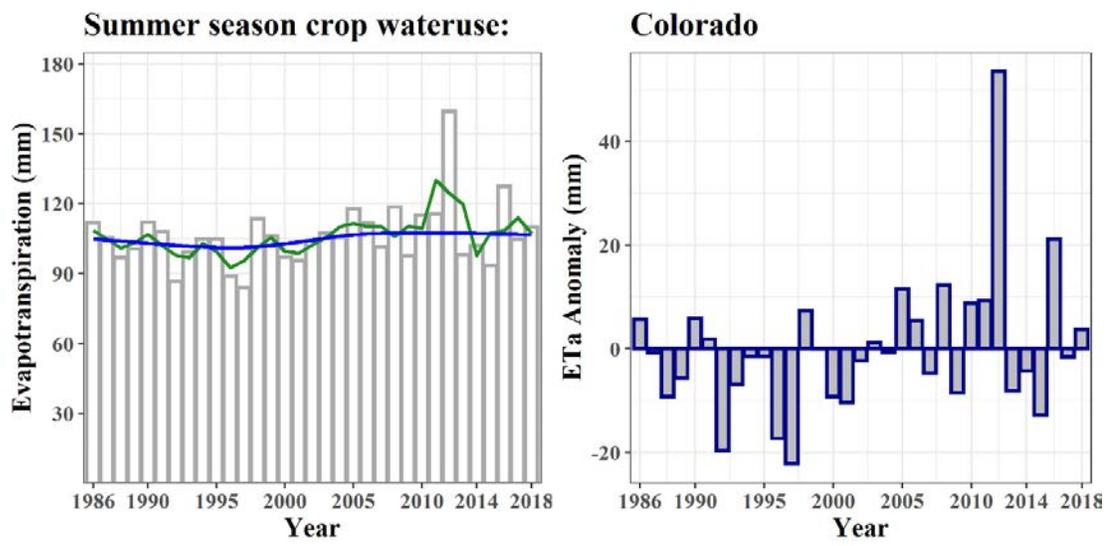
Fig. 20B. Mann-Kendall regional-scale trend for summer season ETa (left panel) and ETa anomalies (right panel) for Colorado, USA.
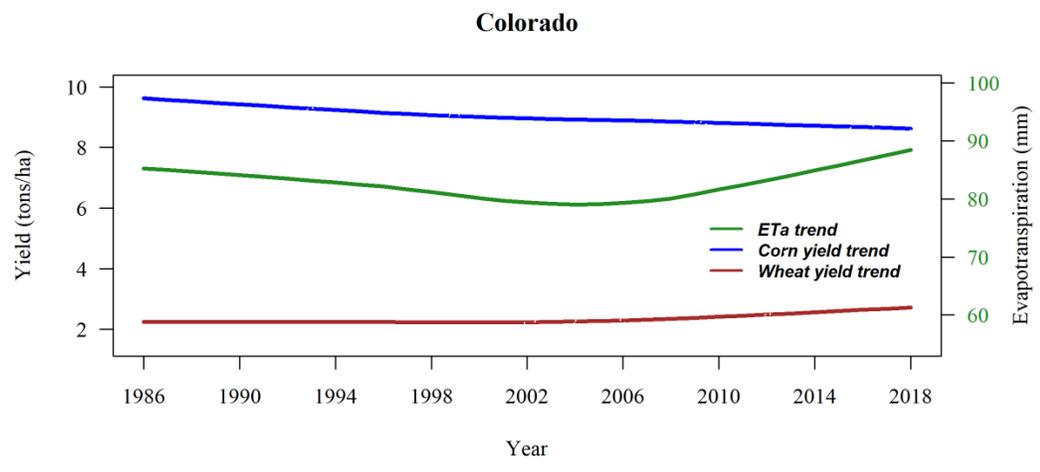
Fig. 21B. Crop production and summer season crop water uses for the state of Colorado
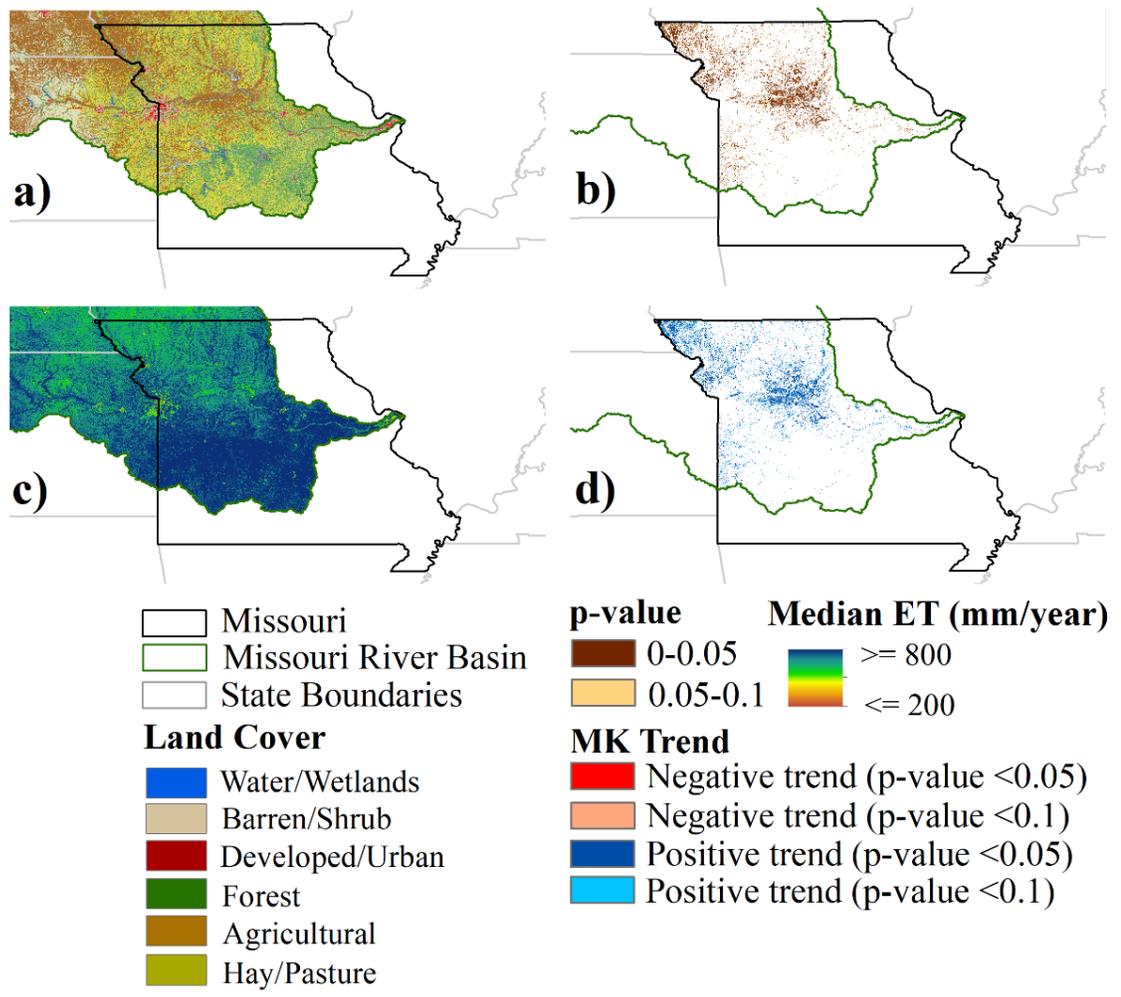
Fig. 22B. Distribution of (a) land cover, (b) p-values for summer season crop water use (CWU) trend, (c) median annual actual evapotranspiration, and (d) summer season CWU trend direction across the state of Missouri, USA.
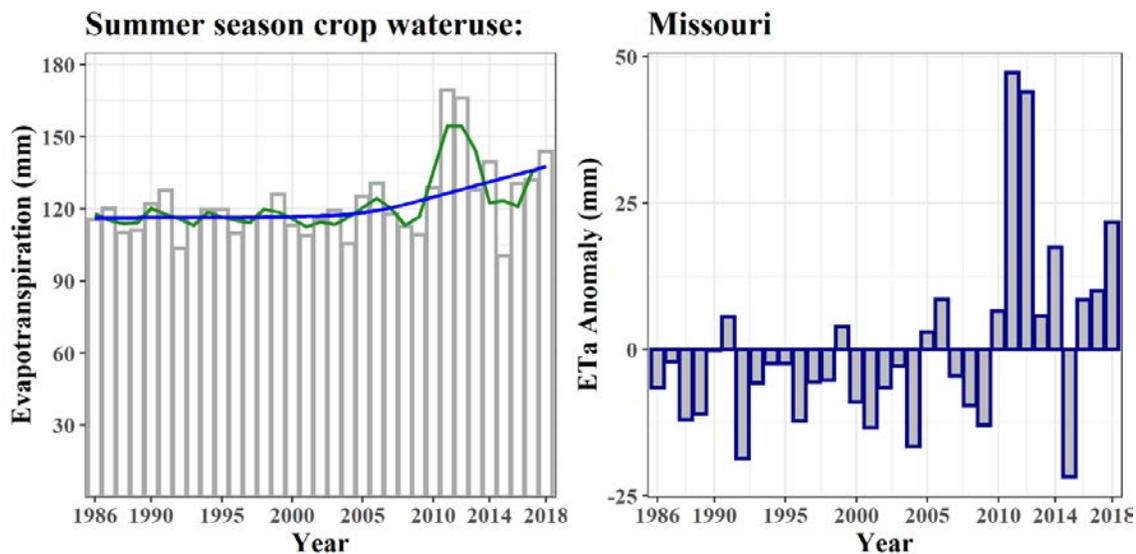
Fig. 23B. Mann-Kendall regional-scale trend for summer season ETa (left panel) and ETa anomalies (right panel) for Missouri, USA.
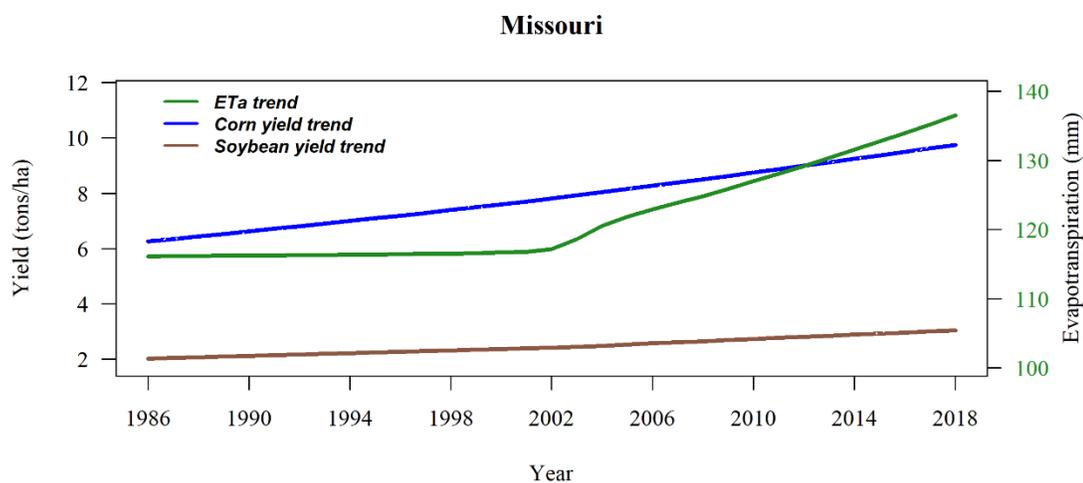
Fig. 24B. Crop production and summer season crop water uses for the state of Missouri
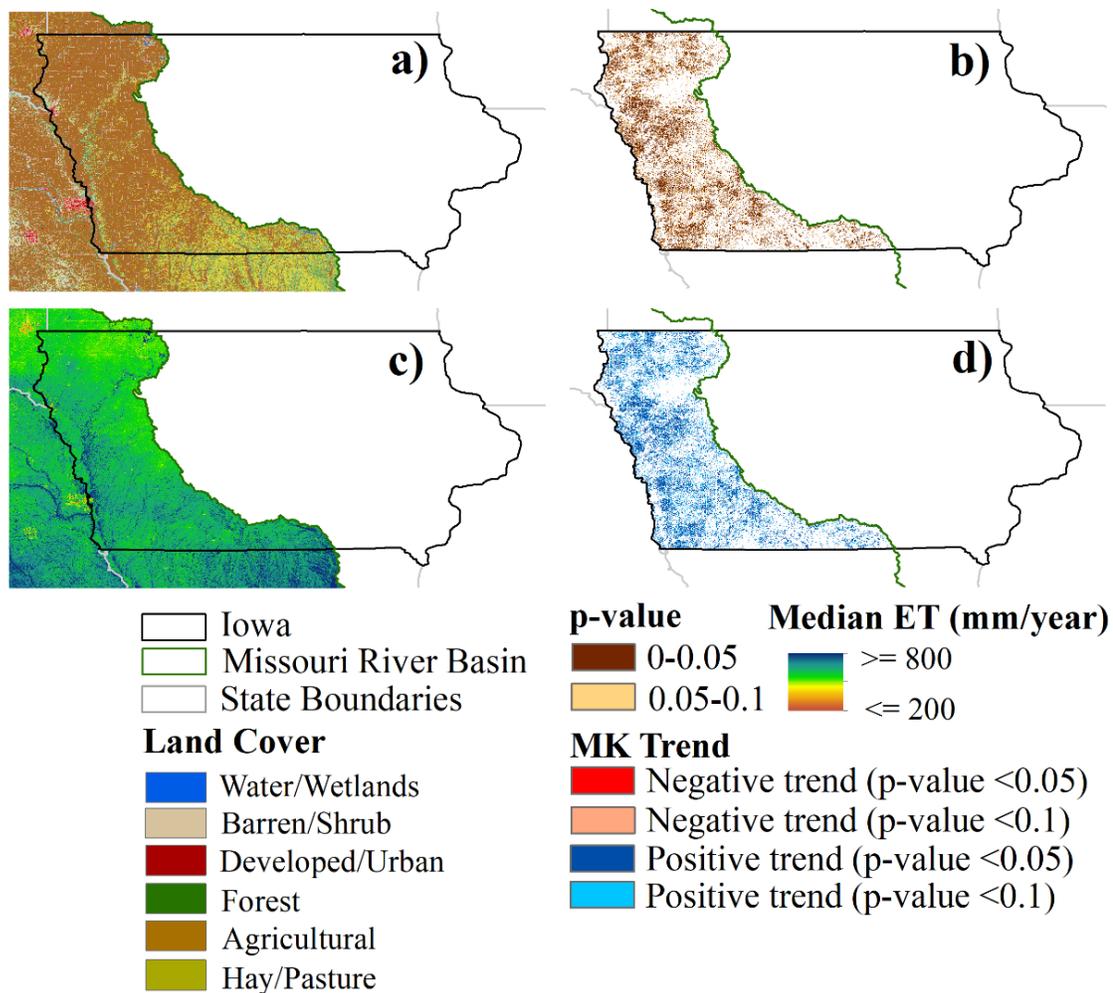
Fig. 25B. Distribution of (a) land cover, (b) p-values for summer season crop water use (CWU) trend, (c) median annual actual evapotranspiration, and (d) summer season CWU trend direction across the state of Iowa, USA.
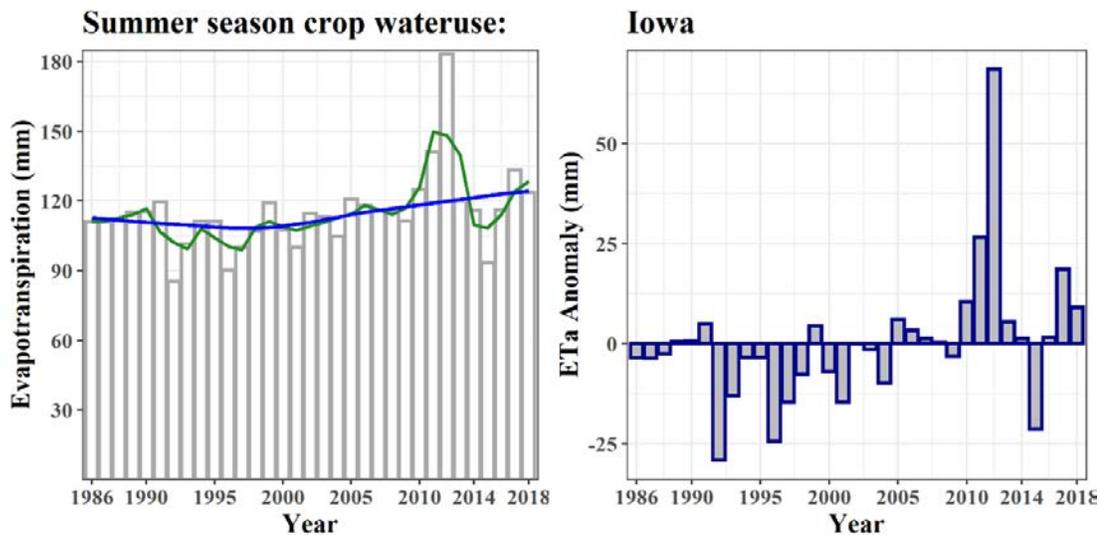
Fig. 26B. Mann-Kendall regional-scale trend for summer season ETa (left panel) and ETa anomalies (right panel) for Iowa, USA.
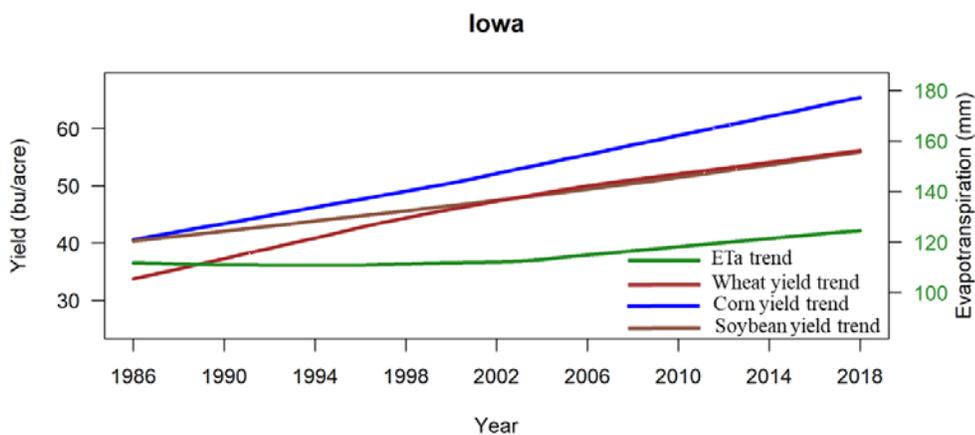

Fig. 27B. Crop production and summer season crop water uses for the state of Iowa
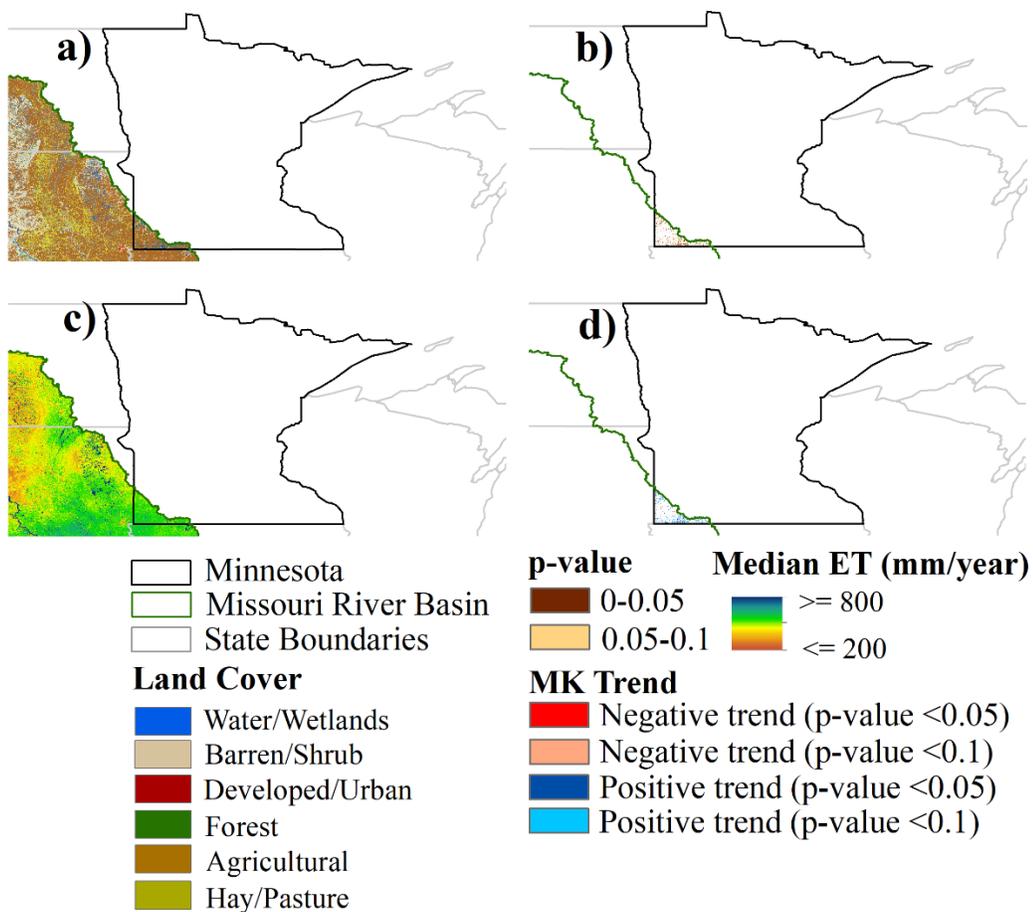
Fig. 28B. Distribution of (a) land cover, (b) p-values for summer season crop water use (CWU) trend, (c) median annual actual evapotranspiration, and (d) summer season CWU trend direction across the state of Minnesota, USA.
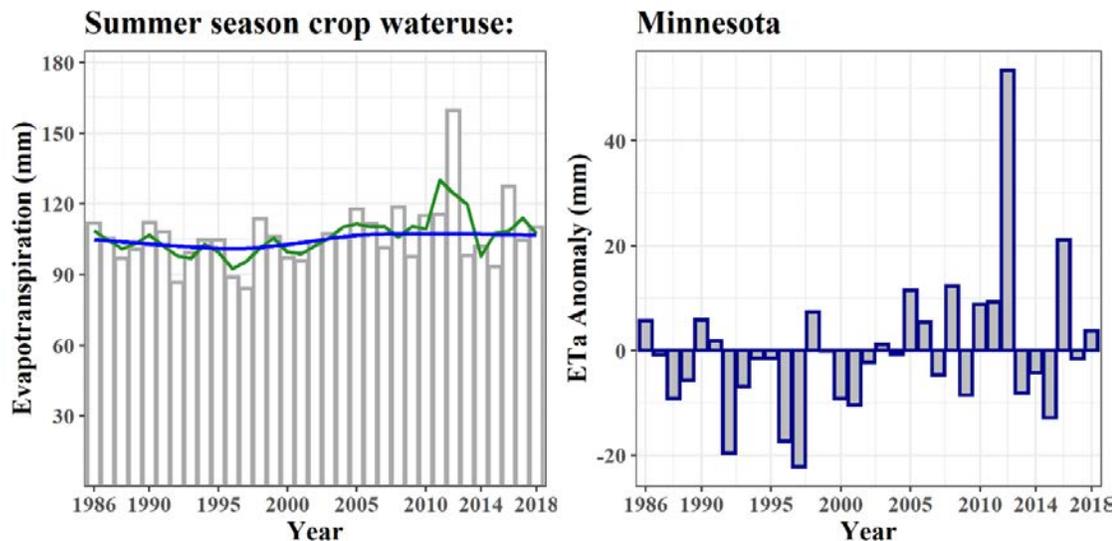

Fig. 29B. Mann-Kendall regional-scale trend for summer season ETa (left panel) and ETa anomalies (right panel) for Minnesota, USA.

VITA

Arun Bawa is a graduate research assistant in the Department of Agricultural, Biosystems, and Mechanical Engineering at South Dakota State University (SDSU), Brookings, SD, USA. He received his Bachelor in Technology (B. Tech) in Civil Engineering from Deen Bandhu Chhotu Ram University of Science and Technology, Murthal, Haryana, India in 2014. He received his Master of Engineering in Environmental Engineering from Punjab Engineering College (PEC), Chandigarh, India in 2016. In 2016, He became an Assistant Professor in the Department of Civil Engineering at Baddi University of Emerging Science and Technology, Baddi, India and later, in 2017, a Junior Engineer in the Department of Irrigation Engineering (Government of Haryana), Haryana, India. He joined the Department of Agricultural, Biosystems, and Mechanical Engineering at SDSU for PhD program in summer 2018 under the guidance of Dr. Sandeep Kumar. After completion of PhD program, he will be joining Dr. Srinivasulu Ale's lab as a Postdoctoral Research Associate in Texas A&M AgriLife Research at Vernon, TX.